Soil structure and moisture effects on biotic soil functions under different land use and climatic scenarios

Dissertation zur Erlangung des Doktorgrades der Naturwissenschaften (Dr. rer. nat.)

der

Naturwissenschaftlichen Fakultät III
Agrar- und Ernährungswissenschaften,
Geowissenschaften und Informatik

der Martin-Luther-Universität Halle-Wittenberg,

vorgelegt von

Frau Mengqi Wu

Gutachter :

PD. Dr. Steffen Schlüter

Prof. Dr. Doris Vetterlein

PD. Dr. Johannes Koestel

Datum der Verteidigung: 17.11.2025

Abstract

Soil structure and moisture interact to shape the microhabitat for microorganisms, soil fauna, and plant roots by forming the physical environment that governs spatial distribution and regulates access to air, water and nutrients. These two soil properties underpin essential soil functions, including carbon cycling, soil food web dynamics, plant-soil interactions, and yield production. However, both soil structure and moisture are highly dynamic and sensitive to external factors such as land-use change and climate variability. Long-term shifts in vegetation and management practices, as well as climate extremes, such as prolonged droughts or intense rainfall events, can significantly alter soil structural properties, modify water dynamic, and impact biological functioning. Despite their fundamental role in regulating ecosystem processes, the mechanisms by which soil structure and moisture respond to global change and mediate soil biotic functions remain insufficiently understood.

The overarching goal of this thesis is to advance the understanding of how soil structure and moisture regulate key soil biotic functions across different land-use systems and climatic scenarios. Utilizing data from the Global Change Experimental Facility (GCEF), a unique long-term field experiment designed to investigate the interactive effects of land use and climate change on terrestrial ecosystem, this research addresses four interlinked objectives that span micro-scale soil processes to ecosystem-scale functions. Specifically, this thesis aims to (1) examine whether and to what extent changes in soil carbon cycling induced by land use and climate change could be directly linked to alterations in soil microstructure, (2) investigate the extent to which variations in nematode community properties under contrasting land use be explained by differences in soil bulk properties and microstructural characteristics, (3) explore how climatic variability influences the soil structure-root interactions under different land-use systems, and (4) assess whether, and how legacy effects of land use and deep soil water storage shape plant productivity and water use efficiency (WUE) under climate extremes.

Using deep-learning-based X-ray Computed Tomography (CT) segmentation, this study quantified pore traits and particulate organic matter (POM) across croplands and grasslands over five years. Perennial grasslands promoted the formation of biopores and greater carbon inputs from

continuous root turnover. In contrast, croplands experienced higher mineralization rates due to tillage and seasonal root inputs. While heterotrophic respiration responded to future climate via soil moisture, the microstructure and organic carbon fractions remained largely unaffected. POM volumes, rather than pore structure, emerged as the primary driver of carbon mineralization, highlighting microbial accessibility over aeration as the main control on carbon turnover.

Soil structural and biochemical properties shaped by land use played critical role in determining the nematode community composition. Nematode communities responded strongly to land use and seasonality, with cropland nematodes closely linked to measurable microstructure properties such as POM volume, nematode-specific porosity, and pore connectivity. However, nematodes in grassland showed greater structural independence and more complex co-occurrence patterns. Climate effects were modest and not directly linked to measurable shifts in microhabitat. These results suggest that bottom-up regulation of nematodes is system-specific and predominantly shaped by land-use-driven physical and biochemical conditions.

Land-use differences strongly shaped root-soil structure interactions, with pronounced interannual variability. Grasslands exhibited higher root length density (RLD), bioporosity, and pore connectivity than croplands, reflecting the benefits of perennial vegetation and minimal disturbance. In croplands, RLD was more closely linked to soil moisture and bulk density than grasslands, suggesting that root proliferation in croplands was more sensitive to variations in the soil physical environment. Fine roots contributed more to structural development than thicker roots, particularly under dry conditions. Although future climate effects on root traits and microstructure were limited in the short-term, they interacted with land use to modify the strength of root-soil structure feedbacks.

Three-year of soil moisture monitoring, including two drought years and one year with extreme rainfall event, revealed persistent drought legacies in deep soil layers (30-110 cm), decoupling productivity from short-term climatic fluctuation. Croplands retained more deep water than grasslands due to reduced transpiration during fallow periods and efficient infiltration. In contrast, extensive grasslands exhibited higher water depletion due to continuous transpiration from perennial vegetation cover. WUE increased with land-use intensity, reflecting more optimized water use in croplands and frequent mowing in intensive grassland. Future climate scenario effects were most evident under extreme events and varied with vegetation traits and root strategies.

In summary, this thesis demonstrates that land use exerts a dominant and consistent influence on soil structure, biotic interactions, and water use dynamics, while the future climate scenario plays a subtler but context-dependent role, particularly during climatic extremes. These findings underscore the importance of integrating structural, biological, and hydrological processes to better predict ecosystem responses and guide sustainable land use management under changing environmental conditions.

Zusammenfassung

Bodenstruktur und Bodenfeuchtigkeit interagieren, um das Mikrohabitat für Mikroorganismen, Bodenfauna und Pflanzenwurzeln zu formen, indem sie die physikalische Umgebung schaffen, die die räumliche Verteilung bestimmt und den Zugang zu Luft, Wasser und Nährstoffen reguliert. Diese beiden Bodenigenschaften bilden die Grundlage zentraler Bodenfunktionen wie Kohlenstoffkreislauf, Dynamik des Boden-Nahrungsnetzes, Pflanzen-Boden-Interaktionen und Primärproduktivität. Allerdings sind sowohl die Bodenstruktur als auch die Bodenfeuchtigkeit hochdynamisch und reagieren empfindlich auf externe Einflussfaktoren wie Landnutzungsänderungen und klimatische Variabilität. Langfristige Veränderungen der Vegetation und der Bewirtschaftung sowie Klimaextreme, etwa langanhaltende Dürren oder intensive Niederschlagsereignisse, können die physikalischen Eigenschaften des Bodens erheblich verändern, Wasserflüsse im Boden umstrukturieren und biologische Prozesse beeinflussen. Trotz ihrer zentralen Rolle für die Steuerung von Ökosystemprozessen sind die Mechanismen, über die Bodenstruktur und -feuchte auf den globalen Wandel reagieren und biotische Bodenfunktionen steuern, bislang unzureichend verstanden.

Ziel dieser Dissertation ist es, ein vertieftes Verständnis darüber zu gewinnen, wie Bodenstruktur und Bodenfeuchtigkeit zentrale biotische Bodenfunktionen unter unterschiedlichen Landnutzungssystemen und Klimaszenarien regulieren. Die Untersuchungen basieren auf Daten der Global Change Experimental Facility (GCEF), einer einzigartigen Langzeit-Freilandplattform zur Analyse der Wechselwirkungen zwischen Landnutzung und Klimawandel auf terrestrische Ökosysteme. Die Arbeit verfolgt vier miteinander verbundene Zielstellungen, die von mikroskaligen Prozessen bis hin zu Funktionen auf Ökosystemebene reichen: (1) die Frage, inwieweit langfristige Veränderungen im Kohlenstoffkreislauf durch strukturelle Veränderungen des Bodens erklärt werden können, (2) die Analyse, ob Unterschiede in der Nematoden-Gemeinschaft durch bodenphysikalische Eigenschaften und Mikrostrukturmerkmale bedingt sind, (3) die Untersuchung der Wechselwirkungen zwischen Wurzeln und Bodenstruktur unter variierenden klimatischen Bedingungen, sowie (4) die Analyse von Langzeiteffekten der Bodenwasserspeicherung bzw. der Bodenwasserausschöpfung auf die Pflanzenproduktivität und

Wassernutzungseffizienz während Klimaextremen.

Mittels Deep-Learning-gestützter Segmentierung von Röntgen-Computer-Tomographie (CT)-Bildern wurden Porenmerkmale und Partikuläre Organische Substanz (POM) in Acker- und Grünlandsystemen über fünf Jahre hinweg quantifiziert. Perennierendes Grünländ förderte die Ausbildung stabiler Mikrostrukturen und Bioporen durch kontinuierlichen Wurzelumsatz, während Ackerflächen aufgrund von Bodenbearbeitung und saisonalen Wurzeleinträgen eine höhere Mineralisierungsrate aufwiesen. Während heterotrophe Atmung unter zukünftigen Klimabedingungen durch Bodenfeuchte beeinflusst wurde, blieben die Bodenmikrostruktur und organischen Kohlenstofffraktionen weitgehend unbeeinträchtigt. Die Ergebnisse zeigen, dass die Verfügbarkeit von POM, nicht jedoch die Porenstruktur, statistisch der Haupttreiber der Kohlenstoffmineralisierung ist, wobei mikrobielle Zugänglichkeit eine größere Rolle spielt als die Belüftung.

Die durch Landnutzung geprägten strukturellen und biochemischen Bodeneigenschaften spielten eine zentrale Rolle bei der Zusammensetzung der Nematoden-Gemeinschaften. Die Nematodengemeinschaften reagierten stark auf Landnutzung und Saisonalität. In Ackerflächen war die Nematodendichte eng mit strukturellen Eigenschaften wie Porosität im Nematodengrößenbereich, POM-Gehalt und Porenvernetzung verknüpft. In Grünlandsystemen zeigten die Gemeinschaften dagegen stärkere strukturelle Unabhängigkeit und komplexere Koexistenzmuster. Die Klimaeffekte waren gering und nicht direkt mit messbaren Mikrohabitaten verknüpft. Dies deutet darauf hin, dass die Regulation durch Ressourcenverfügbarkeit (Bottom-up-Kontrolle) system- und standortspezifisch ist und vor allem durch die Landnutzung und biochemische Bodeneigenschaften bestimmt wird.

Nutzungsbedingte Unterschiede prägten die Wechselwirkungen zwischen Wurzeln und Bodenstruktur deutlich und zeigten eine ausgeprägte interannuelle Variabilität. Im Grünländ wurde eine höhere Wurzellängendichte (RLD), Bioporosität und Porenvernetzung auf als Ackerflächen aufgezeigt, was die Vorteile von ausdauernder Vegetation und geringer Störung widerspiegelt. In Ackerflächen war die RLD stärker mit Bodenfeuchte und Bodendichte verknüpft als in Grasländern, was darauf hindeutet, dass die Wurzellängendichte dort empfindlicher auf physikalische Bodenbedingungen reagiert. Feine Wurzeln trugen stärker zur Entwicklung und Stabilisierung der Bodenstruktur bei als dickere Wurzeln, insbesondere unter trockenen Bedingungen. Obwohl die Auswirkungen des zukünftigen Klimas auf Wurzeleigenschaften und

Mikrostruktur kurzfristig begrenzt waren, beeinflussten sie in Wechselwirkung mit der Landnutzung die Stärke der Rückkopplung zwischen Wurzeln und Bodenstruktur.

Die dreijährige Bodenfeuchteüberwachung, einschließlich zweier Dürrejahre und eines mit extremen Niederschlagsereignissen, zeigte anhaltende Trockenheitseffekte in tieferen Bodenschichten (30-110 cm), die die kurzfristige Klimasensitivität der Produktivität entkoppelten. Bei Ackerflächen wurde mehr tiefes Bodenwasser gespeichert als im Grünländ, vor allem durch reduzierte Transpiration in Brachzeiten und effizientere Infiltration. Eine extensive Grünländbewirtschaftung zeigte eine stärkere Wasserverarmung durch permanente Transpiration. Die Wassernutzungseffizienz stieg mit der Landnutzungsintensität, bedingt durch kürzere Vegetationsperioden in Ackernutzung und häufigere Mahd im intensiv genutzten Grünland. Klimaeffekte waren insbesondere bei Extremereignissen relevant und variierten mit der Vegetationsstruktur und Wurzelarchitektur.

Zusammenfassend zeigt diese Dissertation, dass Landnutzung einen dominanten und stabilen Einfluss auf die Entwicklung der Bodenstruktur, biotische Wechselwirkungen und Wasserhaushaltsprozesse hat. Das zukünftige Klimaszenario wirkt subtiler, jedoch kontextabhängig, insbesondere bei Klimaextremen. Die Ergebnisse heben die Bedeutung eines integrierten Verständnisses physikalischer, biologischer und hydrologischer Prozesse zur besseren Vorhersage von Ökosystemreaktionen und zur Entwicklung nachhaltiger Landnutzungsstrategien unter sich wandelnden Umweltbedingungen hervor.

Contents

1 General introduction

1.1 Scope of the thesis

Soil, as the most complex biomaterial on Earth, functions as a dynamic interface linking atmospheric, hydrological, and biogeochemical processes (Banwart et al., 2019; Young & Crawford, 2004). It underpins a wide range of essential ecosystem functions and supports terrestrial life (Rahmati et al., 2023). Soil resources, despite their overall abundance, are often poorly available to organisms like microbes, fauna and plant roots. This is due to the strong binding capacity of the soil matrix for water and nutrients, as well as the constraints imposed by local physical microenvironment, which together limit biological activity and shape ecosystem productivity and resilience (Barrios, 2007; Erktan et al., 2020; Newcomb et al., 2017).

Soil structure refers to the three-dimensional arrangement of solid particles and pore spaces across different spatial scales (Rabot et al., 2018), serving as a foundation of key physical, chemical and biological functions in soils (Leuther et al., 2025; Or et al., 2021; Schlüter et al., 2020a). It forms the habitat for microorganisms, soil fauna, and plant roots, thereby influencing many key ecosystem processes such as carbon and energy cycling, water and nutrient uptake by plants, and biomass production (Kravchenko & Guber, 2017; Qi et al., 2024; Romero-Ruiz et al., 2018). X-ray computed tomography (CT) offers a powerful non-invasive tool to visualize and quantify the three-dimensional microhabitats of these organisms, enabling a more detailed understanding of how soil structure regulates their ecological functioning (Helliwell et al., 2013; Lucas et al., 2023; Schlüter et al., 2019).

Furthermore, soil structure exerts a strong influence on soil hydraulic properties (Basset et al., 2023; Schlüter et al., 2012). The size, connectivity, and distribution of pores determine water retention and movement within the soil matrix under varying matric potentials (Vogel, 2008). In particular, the abundance of macropores, rather than the total number of pores, plays a dominant role in water flow and solute transport, thus affecting soil water conductivity and soil moisture dynamics (Casali et al., 2024; Jarvis, 2007). Soil moisture is one of the most important environmental factors governing biogeochemical processes in soils (Kannenberg et al., 2024). It further regulates the mobility and accessibility of nutrients for plants, microbes and fauna, thereby

playing a critical role in sustaining soil functions and supporting plant productivity (Vereecken et al., 2022; Vicente-Serrano et al., 2025). For example, sufficient soil moisture promotes microbial decomposition of organic matter, thereby increasing the availability of plant-accessible nutrients and supporting biomass production (Bauke et al., 2022). In contrast, drought conditions suppress microbial processes and limit nutrient mobility, which can impair root growth, reduce plant productivity, and destabilize soil food web interactions (Schimel, 2018).

Thus, the interaction between soil structure and moisture creates the fundamental physical environment that governs biotic processes in soils. However, these interactions are highly dynamic and sensitive to external factors, especially land use and climate change, two major global change factors that can significantly modify soil physical properties and water dynamics through both gradual change and extreme events. Understanding how soil structure and moisture respond to global change factors is therefore essential for predicting soil functioning and ecosystem resilience under future environmental conditions.

1.1.1 Soil structure and moisture as the foundation of soil biotic functioning

This chapter introduces the foundational role of soil structure and moisture in shaping key biotic functions, including heterotrophic respiration and carbon (C) cycling, nematode abundance and community composition, and root growth and turnover.

(1) Heterotrophic respiration and C cycling: heterotrophic respiration, driven by microbial decomposition of soil organic matter, typically accounts for the majority of total soil carbon dioxide (CO_2) efflux as autotrophic respiration by living roots and represents a critical pathway in soil C cycling (Bond-Lamberty & Thomson, 2010; Kuzyakov, 2006). Even small increases in heterotrophic respiration can significantly elevate atmospheric CO_2 concentrations, thereby intensifying global warming (Lei et al., 2021; Liang et al., 2024). This process is strongly influenced by environmental factors, such as soil moisture and temperature (Liang et al., 2024; Liu et al., 2009), but the mechanisms underlying these responses are complex. For example, increased soil moisture may initially suppress microbial activity due to oxygen limitation but can later stimulate the mineralization of older C sources through redox processes such as iron reduction (Huang & Hall, 2017). Moreover, drying and warming can exacerbate soil C loss by accelerating the decomposition of previous protected organic matter, even though the general suppression of heterotrophic respiration under drying conditions due to restricted the mobility and microbial

accessibility of fresh C substrates (McFarlane et al., 2024). While the long-term role of physical protection for C persistence is well established, the role of soil microstructure in regulating short-term microbial C mineralization remains insufficient understood. Conflicting evidence on whether pore architecture constrains microbial communities and C turnover suggests that the microstructural control of C cycling is context-dependent (Li et al., 2024a; Nunan et al., 2017; Strong et al., 2004). Moreover, most previous studies employed disruptive sampling at the aggregate level or in simulated soil columns, which alters the natural soil structure and restricts our ability to complex mechanisms (Feng et al., 2025; Li et al., 2024a; Zhang et al., 2025).

Soil microstructure, the three-dimensional arrangement of particles, pores and organic matter, plays a critical role in C cycling by shaping the spatial distribution of labile C and associated microenvironmental conditions (Kravchenko & Guber, 2017; Leuther et al., 2025; Schlüter et al., 2022). Particulate organic matter (POM) and biopores associate soil C cycling by serving as microbial hotspots. The size, composition, and accessibility of organic inputs influence their decomposition and heterotrophic respiration rates (Cotrufo et al., 2022; Lucas et al., 2024). Labile POM, such as sugar- and starch-rich plant residues, decomposes rapidly, whereas recalcitrant materials like biochar and lignin-rich plant materials degrade more slowly, resulting in lower respiration rates (Dungait et al., 2012; Lyu et al., 2023; Wu et al., 2024). Biopores, formed by roots or fauna, enhance oxygen and nutrient flow and promote microbial colonization, particularly by concentrating labile C along their walls (Banfield et al., 2017; Wendel et al., 2022). The size and connectivity of these biopores further influence C turnover by modulating the microbial accessibility, particularly through physical protection in pores smaller than microorganisms or in disconnected pore networks with discontinuous water films (Ritz & Young, 2004; Schlüter et al., 2020a). Notably, biopores in the 30-150 μm range are closely associated with microbial habitats formation and soil C mineralization (Kravchenko et al., 2019; Li et al., 2024a). However, the effect of soil microstructure on heterotrophic respiration is highly context-dependent, dominating under wet conditions where pore connectivity limits oxygen supply, but diminishing in well-aerated soils where overall resource availability becomes more important (Schlüter et al., 2022b). The extent to which soil microstructure regulates C cycling likely varies with site-specific hydrological and climatic conditions, yet remains poorly understood under field conditions and warrants further in-depth investigation.

(2) Nematode abundance and community composition: nematodes, as the most diverse,

abundant, and widespread soil fauna taxon on Earth, occupying all major trophic levels of soil food webs, participating in many ecological processes, thereby regulating C and nutrient dynamics in terrestrial ecosystems (Jiang et al., 2017; van den Hoogen et al., 2019; Wan et al., 2022b). Numerous studies have identified soil physicochemical properties, like soil organic matter, pH, and soil texture as important drivers of nematode community composition (Bakonyi & Nagy, 2001; Treonis et al., 2019; Zhou et al., 2022). Nematode abundances, especially those of bacterivores and plant-parasite nematodes, were associated with soil properties like sand content, pH, and soil organic carbon content (Biswal, 2022; van den Hoogen et al., 2019). However, in agricultural ecosystems, the effects of soil physicochemical properties on nematode diversity may be diminished due to frequent anthropogenic disturbances like tillage, fertilization, and pesticide application, which alter habitat conditions and may shade natural environmental controls (Li et al., 2020; Vonk et al., 2013).

Soil moisture and pore space play a critical role in shaping nematode abundance and community composition due to their specific habitat requirements (Hassink et al., 1993; Martin & Sprunger, 2023). Elevated soil moisture has been shown to cause nematode community composition toward larger-bodied genera (Zheng et al., 2023). This is likely because of increased soil thermal buffering and reduced oxygen availability brought on by limited pore space, both of which can have a negative effect on nematode survival and activity (Chen et al., 2020; Kitazume et al., 2018). Moreover, although nematodes generally require water-filled pores for movement and survival, their trophic groups may differ in their responses to hydration due to the variations in the moisture dependence of their food resources (Xiong et al., 2019a). For example, bacterivores rely on bacterial populations that thrive in continuous water films, while fungivores can access fungi that bridge across air-filled pores through hyphal networks, making them less dependent on moisture conditions (Mulder et al., 2011; Neher, 2010).

Furthermore, pore geometry itself is a key physical constraint for nematodes. Nematodes movement and activity require water-filled pores larger than their body size (10-55 μm wide, 150-1500 μm long), as they cannot create their own pathways and depend on pore networks formed by roots or macrofauna (Erktan et al., 2020; Vonk et al., 2013). The optimal pore size range for nematode activity is typically 30-210 μm, though this varies by soil type (Otobe et al., 2004; Schlüter et al., 2022a). Pore geometry also affects nematode access to prey and predators by regulating gas and water transport and the spatial continuity of resources (Aochi & Farmer, 2005;

Soufan et al., 2018). Pore structure can thus influence resource accessibility and drive bottom-up effects on soil food webs (Wardle et al., 2004). Additionally, limited pore connectivity and high tortuosity constrain nematode movement and predator-prey interactions (Erktan et al., 2020; Hartmann & Six, 2022). These interactions highlight the critical role of soil microstructure and moisture in shaping nematode community assembly and function.

(3) Root-soil interactions: roots, as the primary interface between plants and soil environment, play a central role in resource acquisition and soil biotic interactions. Their proliferation and turnover are strongly regulated by both soil moisture and structural conditions, which together determine the biophysical environment in which roots grow, develop, and decay (Chapman et al., 2012; Freschet et al., 2021). To cope with spatial and temporal heterogeneity in soil resource availability, plants exhibit highly plastic root architectures, adjusting root depth and distribution in response to environmental cues such as water availability, nutrient gradients, and interactions with soil biota (Burr-Hersey et al., 2020; Colombi et al., 2024; Freschet et al., 2018; Shen et al., 2013).

Soil moisture directly regulates root-soil interactions by influencing both root growth and turnover processes (Chapman et al., 2012; Jin et al., 2013; Xiong et al., 2022b). Adequate moisture supports cell expansion, elongation, and nutrient uptake by maintaining turgor pressure and enabling optimal physiological function (Zuo et al., 2021). In contrast, both drought and waterlogged conditions impair root functioning: drought increases mechanical resistance and limits turgor, inhibiting root penetration, while excess water restricts oxygen availability, suppressing root respiration and metabolic activity (Bengough et al., 2011; Lozano et al., 2022). Similarly, root turnover is moisture-dependent: moderate moisture enhances microbial and enzymatic activity, promoting root decay, whereas excessively dry or saturated soils suppress microbial processes and slow decomposition (von Haden & Dornbush, 2014).

Soil structure modulates these interactions by governing mechanical impedance and shaping the spatial distribution and continuity of air- and water-filled pores (Bengough, 2003; Wang et al., 2025). Well-structured soils with stable aggregates and interconnected pore networks promote deeper and more extensive rooting, whereas compacted or degraded structures limit root growth and function (Pandey et al., 2021; Tracy et al., 2012). Additionally, soil structure affects the microhabitat conditions for microbial activity, thereby modulating root turnover rates and nutrient cycling (Kuzyakov, 2010; Negassa et al., 2015).

Roots, in turn, actively modify soil structure and hydrology through rhizodeposition, turnover

process, and biopore formation, enhancing aggregation and promoting microbial activity in the rhizosphere (Fan et al., 2016; Mueller et al., 2024). These feedbacks contribute to long-term soil functions, including organic matter stabilization, nutrient retention, and resilience to environmental change. Therefore, understanding root-soil interactions is essential for predicting plant performance and soil functional responses under land-use and climate change scenarios (Fan et al., 2017; Fatichi et al., 2020; Gould et al., 2016).

1.1.2 Effect of land use and climate change on soil structure and moisture

The structure of soils is constantly evolving, driven by changes in exogeneous factors (i.e. climate and land management) and mediated by various biological, chemical and physical/mechanical processes (Meurer et al., 2020; Phalempin et al., 2025b; Romero-Ruiz et al., 2018). However, soil structure is inherently fragile and highly sensitive to anthropogenic disturbance (Or et al., 2021). Intensive land management, especially the use of heavy machinery, can degrade structure through compaction, reducing porosity and pore connectivity (Shaheb et al., 2021). Although plowing loosens the soil and initially increases porosity, repeated application of tillage accelerates the loss of organic C, reduces structural stability, and eventually induces structural degradation (Guo et al., 2020a; Pires et al., 2017). These structural changes limit root growth, microbial activity, and overall soil function by reducing infiltration, increasing runoff, and inefficiently storing water (Kutílek, 2004; Robinson et al., 2019). In addition, they also affect the soil's ability to retain, transmit, and redistribute water (Gregory et al., 2015).

Land use and management strongly influence soil structure and moisture dynamics, particularly comparing grasslands and croplands (Budhathoki et al., 2022; Smith et al., 2016). Grasslands, characterized by minimal disturbance and the continuous input of organic matter through perennial root systems, promote the formation of stable soil aggregates and connected pore structure networks (Zhao et al., 2017a). These features enhance water retention and hydraulic conductivity (Dexter et al., 2008). Notable differences in the soil hydro-physical properties driven by soil pore structure may already arise just two years after conversion from croplands to grasslands (Ajayi et al., 2021). In contrast, frequent disturbance in croplands alters pore morphology and accelerates the breakdown of organic matter, weakening structural stability and reducing water-holding capacity (Desrochers et al., 2019; Kaur et al., 2024). Moreover, POM, comprising both readily decomposable and more persistent organic matter fractions, is especially

sensitive to land-use practices and serves as a reliable indicator of both structural stability and moisture retention under different agricultural systems (Gosling et al., 2013; Samson et al., 2020; Sequeira & Alley, 2011).

Climate change introduces additional complexity to soil structure and moisture dynamics. Alterations in temperature and precipitation patterns influence soil moisture regimes, microbial activity, and freeze-thaw or wetting-drying cycles, all of which can affect soil aggregation, pore formation, and overall structural stability (Cosentino et al., 2006; Hirmas et al., 2018; Meurer et al., 2020). Prolonged droughts can lead to aggregate breakdown, reduced pore connectivity, and increased soil shrinkage and cracking, while intense rainfall events can compact the surface, reduce infiltration, and promote surface crusting (Feng et al., 2024). These changes threaten soil quality, particularly in managed agricultural landscapes, by intensifying compaction, erosion, and carbon loss (Yang et al., 2024a). Therefore, understanding how land use and climate change jointly affect soil structure and moisture is key to predicting ecosystem resilience and informing sustainable land management strategies.

1.1.3 Ecosystem productivity responses to climate change across land-use systems

Climate change, especially the rise in climate extremes, poses a major threat to terrestrial ecosystems by disrupting temperature and precipitation regimes (Bei et al., 2023; Jones et al., 2009; Li et al., 2018). Extreme events such as multi-year droughts and intense rainfall are projected to increase in frequency, duration and intensity due to anthropogenic climate change (Chen et al., 2025; Spinoni et al., 2017), with direct consequences for ecosystem productivity. While some field experiments report substantial productivity declines under extreme conditions, others show limited effects, likely reflecting variations in baseline productivity and ecosystem resistance or resilience (Hoover et al., 2014; Li et al., 2023b; Nemecek et al., 2011; Wilcox et al., 2017). Enhancing the adaptive capacity of ecosystems is thus a central challenge for developing resilient and sustainable land-use systems (Nguyen et al., 2023; Yu et al., 2025).

Croplands and grasslands, two dominant land-use systems in temperate regions, differ fundamentally in both structure and function. Croplands are typically characterized by fast-growing annual species with initially shallow root systems (Asbjornsen et al., 2008; Thorup-Kristensen et al., 2020). Although some crops are capable of developing deep roots, their ability to access subsoil water depends on the timing of root growth relative to drought onset (Li et al.,

2022a; Lynch, 2018). This temporal mismatch makes croplands highly productive but vulnerable to prolonged droughts (Leakey et al., 2019; Pugh et al., 2016; Tracy et al., 2020). In contrast, perennial grasslands support deeper and more persistent root systems that enable continued water uptake during dry periods, potentially enhancing resilience to climate extremes (Korell et al., 2024; Swindon et al., 2019). Management practices such as tillage, fertilization, and mowing frequency further modulate both above- and belowground responses, although the underlying mechanisms remain insufficiently understood.

Understanding how ecosystem productivity responds to climate extremes across land-use systems is crucial for projecting future land performance, promoting sustainable resource use, and guiding adaptation strategies in agriculture. In particular, it is essential to account for the temporal legacy effects of climate events on plant growth, the buffering role of deep soil water storage (Bastos et al., 2020; Liu et al., 2025a), and the contribution of root system traits in mediating these interactions. However, these processes frequently take place over long periods of time, with cumulative and slow effects that are only detectable through multi-year monitoring. To capture delayed reactions and cumulative impacts, features that short-term research sometimes overlook, long-term field experiments that blend controlled climatic perturbations with realistic land-use patterns are crucial. However, because of their intricacy and logistical requirements, such studies are still uncommon.

This thesis draws on data from the Global Change Experimental Facility (GCEF), one of the few experimental platforms globally worldwide that integrates multiple land-use systems with simulated future climate scenarios under realistic field conditions. The GCEF offers a unique opportunity to systematic investigate both immediate and emergent ecosystem responses by facilitating the methodical research of long-term connections between land use and climate change (Schädler et al., 2019). Previous studies at the GCEF have shown that land use strongly mediates the resistance of grassland productivity to both future climate scenarios and interannual climatic variability (Korell et al., 2024). Additionally, this work is carried out under the framework of the GLIMPSE program (Global change impacts on microbiota-plant-soil processes relevant for water and matter cycling in agricultural ecosystems), which hypothesizes that climate change and increasing land-use intensity are affecting water and matter cycles through negative impacts on biodiversity and soil processes, which are influenced by physical properties at the soil-root interface. In this thesis, we analyze measurements collected five years after the establishment of

the GCEF, with most observations covering years eight to ten of the experiment. This perspective allows for the assessment of both immediate ecosystem responses and the gradual development of ecological changes. Such knowledge is essential to improve predictions of ecosystem responses under future climate scenarios and to design land-use strategies that enhance productivity and resilience in the face of increasing climate variability.

1.2 Study site

This study is conducted within the GCEF of the Helmholtz-Centre for Environmental Research (UFZ) in Bad Lauchstädt, Germany (51° 23′ N, 11° 53′ E, 118 m a.s.l.). The area is characterized by a sub-continental climate, with a mean annual precipitation of 525 mm (1993-2013) and a mean annual temperature of 9.7 °C (1993-2013) (Schädler et al., 2019). The soil type is a Haplic Chernozem, characterized by 0-45 cm depth medium-humous horizon with on average texture of 21 % clay, 69 % silt, and 10 % sand, and a mean dry bulk density of 1.3-1.45 g cm^{-3} (Altermann et al., 2005). The volumetric water content at field capacity (pF1.8 = -60 hPa) and permanent wilting point (pF4.2 = -15000 hPa) amount to 40.7 % and 14.9 % in the topsoil, respectively (**Chapter 5 Figure S5.1**). The upper soil (0-15 cm) pH ranges from 5.8 to 7.5, and contains 1.71-2.09 % total carbon and 0.15-0.18 % total nitrogen (Schädler et al., 2019).

The GCEF platform is established on previously agricultural land in 2013/2014 and consists of a split-plot design with two climate scenarios as the main plot factor and five land use types as the subplot factor (Figure 1.1). Ten (80 m × 24 m) main plots are randomly assigned to one of two climate treatments (ambient vs. future). Each main plot is divided into five (16 m × 24 m) subplots, which are randomly assigned to one of five land-use regimes: two annual croplands: conventional farming (CF) and organic farming (OF); three perennial grasslands: intensive meadow (IM), extensive meadow (EM,) and extensive pasture (EP).

The climate treatment is based on projections of the climate of Central Germany for the years 2070-2100 based on different dynamic regional climate models (Döscher, 2002; Jacob & Podzun, 1997; Rockel et al., 2008). The combined use of automated roofs, side panels, and irrigation systems in the future climate scenario is targeted to increase precipitation in spring (March-May) and autumn (September-November) by 10 % and reduces precipitation by 20 % in summer (June-August) as compared to the ambient climate. The use of automated roofs also passively increases the night temperatures, resulting in increased mean daily air temperature at 5 cm height by 0.55 °C,

and increases mean daily soil temperature at 1 and 15 cm depth by 0.62 and 0.50 °C, respectively (Schädler et al., 2019).

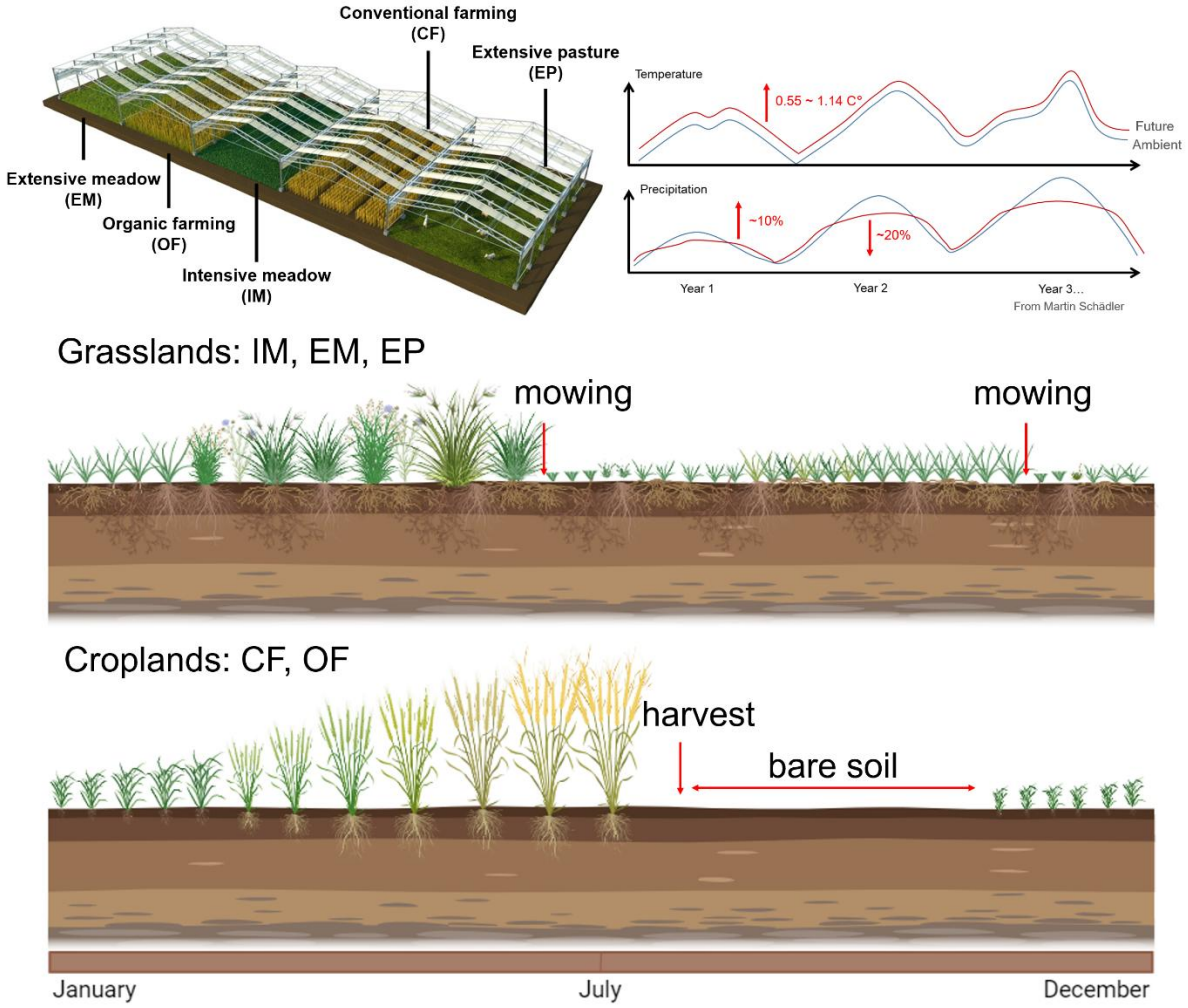

Figure 1.1 Conceptual overview of the experimental design and land management regimes at the Global Change Experimental Facility (GCEF) under ambient and future climate scenarios. The subfigures in the top left and top right are adapted from Tricklabor / Marc Hermann and Martin Schädler, respectively (source: https://www.ufz.de/index.php?en=42385).

CF is characterized by a three-year typical regional crop rotation of summer rape or triticale, winter wheat, and winter barley. The three-year crop rotation for OF includes alfalfa or white clover, winter wheat, and winter barley. Mineral fertilizers are applied according to crop-specific requirements, with annual rates ranging from 60 to 310 kg ha^{-1} $year^{-1}$, including approximately 60-160 kg N, 30-45 kg P, and 110-120 kg K ha^{-1}, along with additional sulfur and magnesium

compounds as needed. Pesticides are applied at least two to three times per year in CF, whereas only fertilization via biological N-fixation of legumes and rock phosphate and plant protection products based on natural compounds instead of chemically synthetic pesticides were applied in OF. Tillage on croplands is primarily conducted for plowing in late summer to autumn (August-October) following harvest, and for seedbed preparation in autumn prior to sowing winter wheat or barley. Seedbed preparation in early spring (March-April) is conducted in years with spring crops. Both CF and OF systems follow this seasonal pattern, with OF involving additional tillage for cover crop incorporation. Across both systems, tillage is predominantly concentrated within the top 5-15 cm of soil, with one deep plowing event reaching 28-30 cm typically conducted each year following harvest. IM is seeded with mixture of four forage grasses (20 % *Lolium perenne*, 50 % *Festucololium*, 20 % *Dactylis glomerata*, and 10 % *Poa pratensis*) and is frequently mown (2-3 times per year) and moderately fertilized. EM is established from a mixture of more than 50 plant species (legumes, grasses and forbs) from different regional populations and was moderately mown 1-2 times per year without the use of any agrochemicals. EP has the same species pool like EM and is managed by 1-3 grazing periods per year. Grasslands are generally not tilled. However, in the winter of 2020, the soil under IM treatment is plowed and reseeded due to problems with weed infestation. For further details on GCEF design, land-use management regime, and climatic conditions see **Chapter 2 Figure 2.1**, **Chapter 5 Figure 5.1**, and Schädler et al. (2019).

1.3 Objectives and Outline

The overall aim of this thesis is to investigate whether, and how, soil structure and moisture, shaped by land-use management and climate conditions, indirectly regulate key biological functions (Figure 1.2). These functions include the regulation of soil carbon cycling, structuring of nematode communities, and mediation of root-soil structural interactions. In addition, this thesis explores how plant-soil interactions across different land-use systems shape ecosystem productivity and water use efficiency under climate change. The central hypothesis of this thesis is that differences in soil structure and moisture among land-use systems partly explain changes in carbon dynamics, nematode community composition, and root proliferation. These belowground changes, in turn, affect the resistance and resilience of ecosystem productivity under climate extremes.

Chapter 2 focuses on five-year changes in soil structure and carbon cycling. In this study, I

collected a unique five-year dataset of soil microstructure using X-ray CT combined with a deep-learning-based image segmentation approach. I also monitored key soil biochemical properties, including organic carbon pools and microbial activity. The main objective is to track changes in soil structure under different land-use and climate scenarios, and to test whether observed shifts in carbon cycling could be linked to changes in soil microstructure.

The hypotheses are as follows:

(1) Topsoil microstructure dynamics are primarily governed by land-use practices, with only minor variability attributable to climate scenarios;

(2) Variations in C mineralization rates and organic C fractions under dry site conditions are more closely linked to POM inputs than to aeration-related macropore structure properties.

Chapter 3 examines nematode communities in relation to soil microstructure and biochemical properties under different land-use systems (cropland vs. grassland) and climate scenarios. This study aims to compare nematode abundance and community composition between croplands and grasslands, and to assess how these communities respond to seasonal changes and climate conditions. I also examined whether differences in nematode communities could be explained by soil properties and microstructure characteristics derived from X-ray CT.

The hypotheses are as follows:

(1) Perennial grasslands support higher nematode abundance and diversity than annual croplands;

(2) Climate and seasonal effects on nematode communities are mainly mediated by soil moisture;

(3) Soil microstructure plays a stronger role in shaping nematode communities in croplands than in grasslands.

Chapter 4 investigates root proliferation and its feedback to microstructure across different land-use types and climate scenarios. The main goal is to assess how climatic variations influence the root-soil structure interactions under different land-use systems and how these patterns are affected by the future climate scenario involving modified seasonal precipitation and higher temperature.

The hypotheses are as follows:

(1) Grasslands will show higher microstructural stability and more developed root systems than croplands due to perennial rooting systems and the absence of tillage;

(2) Under dry conditions, root proliferation in croplands becomes more dependent on existing pore networks than in grasslands, due to lower structural stability and the absence of perennial root systems;

(3) The feedback of root growth to soil microstructure is closely dependent on the root diameter, with finer roots more strongly contributing to the formation and stabilization of pore networks.

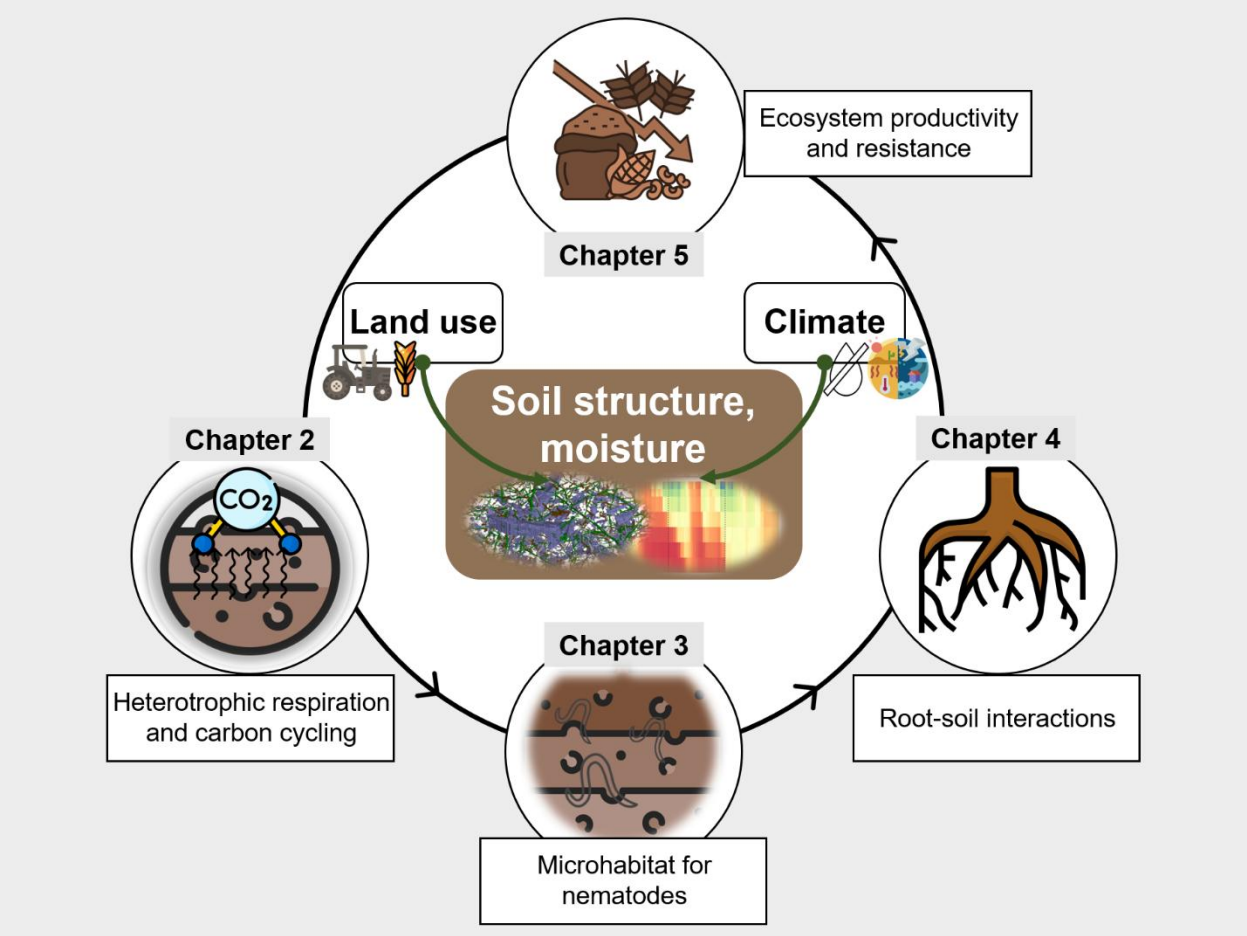

Figure 1.2 Conceptual framework of this thesis illustrating the central role of soil structure and moisture in regulating soil functions and ecosystem processes under varying land-use and climate conditions.

Chapter 5 focuses on soil water content profiles and their influence on plant productivity across five land-use systems under both ambient and future climate scenarios. This chapter examines how climate extremes affect soil water storage over time and how these changes are influenced by future climate conditions, which involve altered precipitation patterns and higher temperatures. I also investigated whether legacy effects of deep soil water storage influence plant

productivity and water use efficiency (WUE), based on a three-year monitoring period.

The hypotheses are as follows:

(1) Topsoil moisture is mainly controlled by atmospheric conditions, while deep soil moisture is influenced by root water uptake and past moisture conditions;

(2) Croplands maintain higher soil moisture than grasslands on an annual basis, due to their sparse root systems and shorter growing seasons. However, the effects of future climate on deep soil water storage are uncertain and addressed in this study;

(3) Croplands produce higher yields than grasslands due to breeding for rapid growth and high resource-use efficiency, whereas extensive grasslands, with greater plant diversity, are most resistant to climate extremes. Intensive grasslands, with lower diversity but permanent cover, are expected to be less resilient than extensive grasslands but more stable than croplands, owing to their perennial root systems and continuous ground cover;

(4) In response to drought and limited deep soil water supply, plants mainly adjust by increasing WUE rather than by altering rooting patterns or vegetation composition.

2 Links between soil microstructure dynamics and carbon cycling in response to land use and climate change

Abstract

Land-use systems differ in the balance between organic carbon inputs and microbial mineralization, affecting long-term soil carbon storage. Perennial grasslands maintain continuous root growth without tillage, promoting the accumulation of stable soil microstructure and biopores. In contrast, annual croplands experience fallow periods and periodic plowing, which disturb soil microstructure and accelerate the mineralization of physically protected carbon. However, the strength of soil microstructural regulation on carbon cycling and its responses to climate change remains unclear. Here, we studied five land-use types (two croplands and three grasslands) under ambient and future climate scenarios over five years, starting from the fifth year after establishment. The future climate scenario reflected regional projections of increased temperature and modified precipitation regimes. Using deep-learning-based X-ray CT image segmentation, we found that grasslands consistently contained higher volumes of biopores, particulate organic matter (POM), and decaying roots due to sustained root growth and turnover. In contrast, croplands exhibited a higher fraction of fresh roots in spring probably due to the rapid early-season growth of annual species, reduced microbial activity during fallow periods, and lack of year-round root inputs. A typical grassland microstructure fully developed in topsoil (5-10 cm) after 4-5 years. Land-use differences in deep soil (35-40 cm) remained small even after 10 years, based on historical site data. Microbial biomass carbon and extractable organic carbon were consistently greater in grasslands, whereas total organic carbon diverged more slowly. The future climate scenario primarily influenced heterotrophic respiration and labile carbon pools through soil moisture, but did not significantly alter topsoil microstructure or carbon pools. POM volume, rather than pore structure, was the key driver of carbon mineralization, as the aeration of these microbial hotspots was not limiting. These findings provide biophysical insights into how land-use and climate microstructure are drivers of carbon mineralization and long-term soil organic carbon storage.

Mengqi Wu [a] *, Maxime Phalempin [a], Thomas Reitz [b], Evgenia Blagodatskaya [b], Steffen Schlüter [a]

* corresponding authorship (mengqi.wu@ufz.de)

a Department of Soil System Science, Helmholtz-Centre for Environmental Research – UFZ, Halle, Germany

b Department of Soil Ecology, Helmholtz-Centre for Environmental Research – UFZ, Halle, Germany

This chapter is submitted to Soil Biology & Biochemistry: Mengqi Wu, Maxime Phalempin, Thomas Reitz, Evgenia Blagodatskaya, Steffen Schlüter. "Links between soil microstructure dynamics and carbon cycling in response to land use and climate change", submitted: 16.06.2025.

2.1 Introduction

Soils are the largest terrestrial carbon (C) pool, containing 3.3 times and 4.6 times as much C as the atmosphere and the biotic pool (Jackson et al., 2017; Lal, 2004). Global warming and land-use intensification have accelerated soil degradation and threaten soil C storage and stability (Smith et al., 2016). Carbon mineralization, that is, the breakdown of organic matter by soil microorganisms and the conversion into inorganic forms, influences the size and stability of soil C pools, thereby regulating the balance between soil C storage and emission (Matter et al., 2016; Paterson & Sim, 2013). Soil heterotrophic respiration, carbon dioxide (CO_2) release driven by microbial decomposition of organic matter, is the primary contributor of CO_2 efflux emitted by the soils to the atmosphere as autotrophic respiration by living roots and represents the second-largest terrestrial C flux (Bond-Lamberty & Thomson, 2010; Kuzyakov, 2006). Therefore, a small increase in soil heterotrophic respiration could substantially elevate the atmospheric CO_2 concentration, directly impacting global warming (Lei et al., 2021). Soil moisture, temperature, and other environmental factors are widely recognized as key drivers for soil heterotrophic respiration (Liu et al., 2009; McFarlane et al., 2024; Zheng et al., 2009). Additionally, heterotrophic respiration is modulated by the physical microenvironment that governs biological accessibility to oxygen and organic matter (Philippot et al., 2024; Schlüter et al., 2020a).

While the long-term role of physical protection for carbon persistence is well established (Lehmann & Kleber, 2015; Schmidt et al., 2011), the role of soil microstructure in regulating short-term microbial C mineralization remains insufficiently understood. In particular, studies have reported conflicting evidence on whether and how pore architecture constrains microbial communities and C decomposition rates. For example, connected pores under fluctuating moisture regimes facilitate gas exchange and prevent oxygen limitation, thereby supporting microbial respiration (Coucheney et al., 2025; Kim et al., 2024; Lucas et al., 2022). In contrast, in well-aerated soils, oxygen is non-limiting, and decomposition is more strongly controlled by C availability rather than pore structure (Curiel Yuste et al., 2007; Schlüter et al., 2022b). Furthermore, the spatial distribution of labile C, such as root exudates and particulate organic matter (POM), i.e., the primary fractions of readily decomposable organic matter, can create localized microbial hotspots that are not directly linked to bulk pore connectivity (Kim et al., 2020;

Schlüter et al., 2022b). These inconsistencies suggest that the influence of microstructure on C turnover is highly ecosystem-dependent and strongly shaped by biophysical conditions and resource distribution (Nunan et al., 2017; Ruamps et al., 2011; Strong et al., 2004). However, most previous investigations have relied on destructive sampling at the aggregate scale or in artificial soil column, which disturbs the native soil structure and limits mechanistic understanding (Feng et al., 2025; Li et al., 2024a; Zhang et al., 2025). These underscore the critical need for non-destructive, in situ approaches to better capture how soil microstructural regulates carbon dynamics under realistic field conditions.

Among microstructure features, POM and biopores, formed by plant roots and soil fauna, play a central role in shaping microbial microenvironment and regulating heterotrophic respiration dynamics (Banfield et al., 2017; Cotrufo et al., 2022; Lucas et al., 2024). POM serves as a key microbial energy source, with its decomposition depending on size, quality, biochemical composition (Lyu et al., 2023; Yoshimura et al., 2008). Easily degradable materials, such as sugar-rich residues, often lead to higher heterotrophic respiration due to rapid microbial activity, whereas more recalcitrant compounds like lignin or biochar decompose slowly and result in lower CO_2 release (Dungait et al., 2012; Wu et al., 2024). The turnover of POM further drives changes in soil pore morphology through the formation of biopores, which enhance aeration, water flow and microbial colonization (Ding et al., 2025; Haas & Horn, 2018; Mordhorst et al., 2014). Moreover, labile C enrichment along biopores walls can further stimulate microbial hotspots and promote C mineralization and stabilization (Banfield et al., 2017; Ganault et al., 2024; Wendel et al., 2022). Notably, biopores in the 30-150 μm range are recognized as key pathways for C input into the soil and as favorable microhabitats for microbial communities, thereby facilitating C stabilization through the formation of microbial necromass (Kravchenko et al., 2019; Li et al., 2024a).

Soil microstructure formation and development are continuously driven by changes in exogenous factors, mediated by various biological and physical processes (Leuther et al., 2023; Meurer et al., 2020; Ren et al., 2024b). It may subsequently alter microscale environment for microbial activity and thus influence soil C cycling over time. Soil microstructure varies drastically across land use, particularly between grasslands and croplands (Budhathoki et al., 2022; Jarvis et al., 2017; Smith et al., 2016). Grasslands, characterized by the absence of regular tillage and the presence of perennial vegetation cover and root growth, promote the formation of stable soil aggregates and pore structure (Zhao et al., 2017a). Long-term grassland has been shown to result

in higher macroporosity than arable soil, even under no-till management (Hyväluoma et al., 2024). In particular, grasslands tend to exhibit larger and more vertically oriented macropores, while croplands are typically associated with a greater abundance of horizontally or more isotropically distributed macropores in the surface layer (Budhathoki et al., 2022). Notable differences in the soil hydro-physical properties driven by soil pore structure may already arise just two years after conversion from croplands to grasslands (Ajayi et al., 2021). In croplands, intensive land use, especially tillage, alters pore morphology, disrupts soil pore structure, and accelerates the breakdown of organic matter (Desrochers et al., 2019; Kaur et al., 2024).

In addition to land use, climate change can exert profound effects on both soil C cycling and microstructure (Hirmas et al., 2018; Schimel & Carroll, 2024). While the direct impact of global warming on microbial activity and C turnover has been well documented (Crowther et al., 2016; McFarlane et al., 2024), the influence of warming and altered precipitation patterns on soil microstructure remains comparatively understudied. Changes in soil moisture, driven by altered precipitation patterns or irrigation, can reshape pore networks through frequent wetting-drying and freeze-thaw cycles that induce soil swelling and shrinkage (Pires et al., 2020; Shi et al., 2024). Elevated temperatures may further destabilize soil structure by accelerating organic matter decomposition and root turnover, thereby reducing structural stability and altering the formation and persistence of biopores (Guan et al., 2018). However, the extent to which climate-driven changes in soil microstructure influence C cycling remains poorly understood, largely due to the lack of integrated, long-term field studies that assess these dynamics across contrasting land-use systems under realistic climate scenarios.

The objectives of this study were to monitor land-use and climate-specific soil microstructure dynamics and assess whether observed changes in C cycling could directly be traced back to microstructure changes. To reach these objectives, we leveraged a unique long-term experimental platform to assess climate change effects across different land use types (Global Change Experimental Facility – GCEF, see Schädler et al. (2019)). An unprecedented, five-year record of soil microstructure data was collected and combined with the monitoring of several biochemical soil properties including organic C pools and soil microbial activity. Soil microstructure in our study was characterized with X-ray CT in combination with a novel deep-learning method to segment various POM and pore classes that allow for direct clues about their formation process and degradation history. We hypothesize that (1) soil microstructure evolution in the topsoil is

primarily driven by land use, with minimal fluctuations due to climatic conditions, and that (2) variations in C mineralization rates and organic C fractions under fairly dry site conditions are coupled with C input through POM volume rather than aeration-related macropore structure properties.

2.2 Material & Methods

2.2.1 Site description and field sampling

The study was conducted at the GCEF in Bad Lauchstädt, Germany, which combines two climate scenarios with five representative land-use types in a large-scale split-plot design. The site features a Haplic Chernozem under a sub-continental climate, and the future climate scenario simulates projected conditions for Central Germany by 2070–2100. The five land-use systems include two croplands (conventional farming (CF) and organic farming (OF)) and three grasslands (intensive meadow (IM), extensive meadow (EM), and extensive pasture (EP)). Detailed site characteristics, climate manipulation, and land-use management practices are described in **Chapter 1 Section 1.2**. The chapter is based on the data collected between 2019 and 2023.

During the growing seasons (April-October) of 2019, 2020 and 2022 (dry years), the precipitation amounts were 30-46 % lower than in 2021 and 2023 (normal years) (Figure 2.1a). In normal years, the accumulated amount of precipitation and irrigation during the growing season was decreased by about 10 % in future climate scenario compared to ambient climate, while no differences occurred in dry years, as the absolute effect of relative changes is small. The crops were summer rape and triticale under conventional farming in 2020 and 2023, while Persian clover and white clover were grown in organic farming (Figure 2.1b). In the winter of 2020, the soil under IM treatment was plowed and reseeded due to problems with weed infestation. The precipitation and irrigation patterns of each climate change scenario and the management history of each land use from 2019 to 2023 are summarized in Figure 2.1.

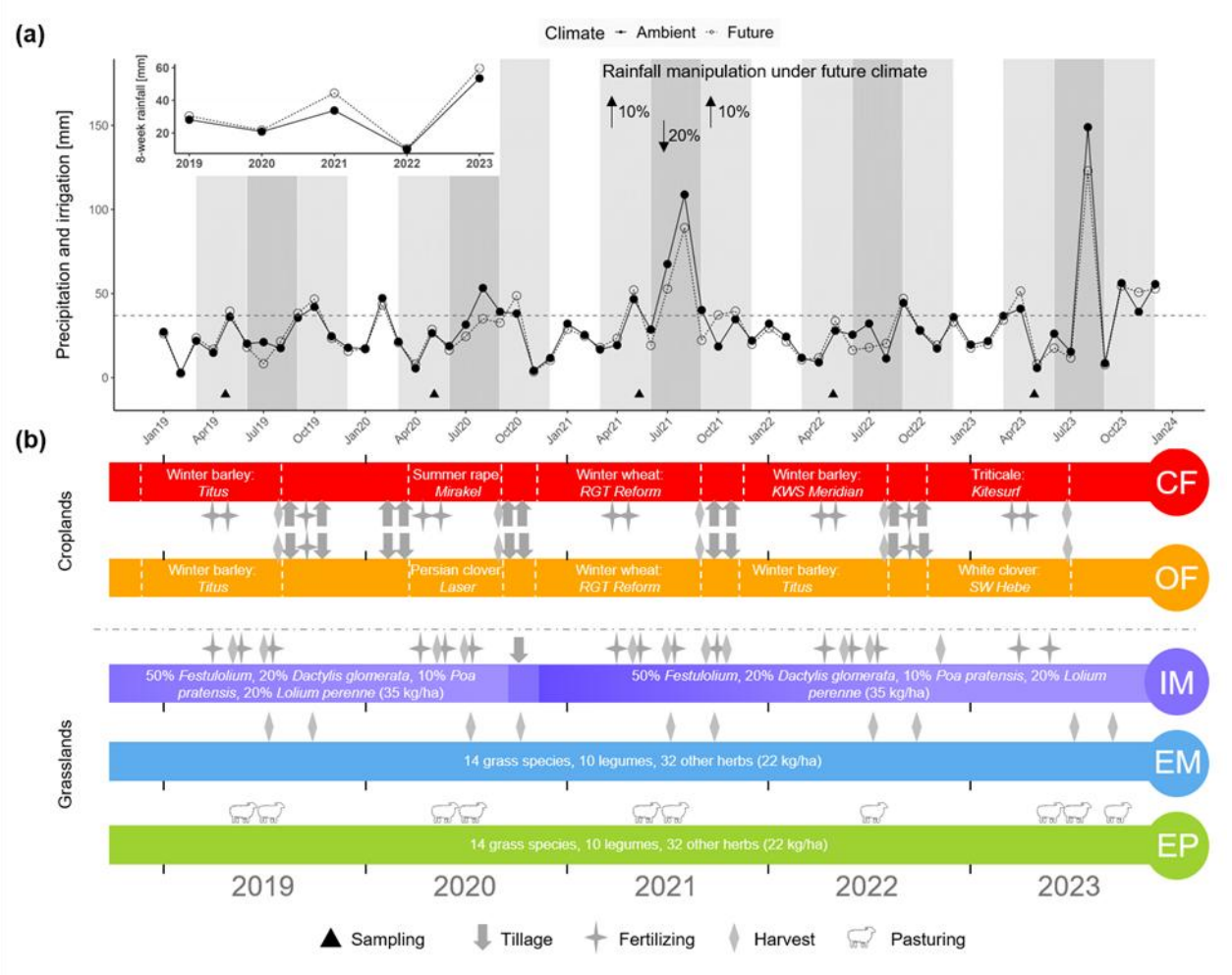

Figure 2.1 Precipitation and irrigation conditions (a), land use managements (b) at the Global Change Experimental Facility (GCEF) from 2019 to 2023. CF, OF, IM, EM and EP represent conventional farming, organic farming, intensive meadow, extensive meadow and extensive pasture, respectively. Gray dashed line represents the mean monthly precipitation over the past 30 years, providing a reference for identifying wetter or drier months. Light shaded area represents the increased rainfall during spring and autumn in future climatic scenario, dark shaded area represents the decreased rainfall during summer in the future climatic scenario. 8-week rainfall refers to the total rainfall accumulated over the 8 weeks preceding the sampling date (the days with temperature above 5 °C), with the irrigation amounts under future climate were included. Rainfall manipulation under future climate represents the future climate have increased 10 % rainfall in spring and autumn and reduced 20% rainfall in summer as compared to the ambient climate.

Soil sampling was carried out in late April or early May over five consecutive years (from 2019 to 2023) to explore the effect of land use on soil microstructure development and C cycling under ambient climate scenario (Figure 2.1a). Sampling in 2019 was limited to CF, OF and IM to establish baseline conditions for soil heterotrophic respiration measurements and initial assessment of soil microstructure. In croplands, crop phenology at the time of sampling varied across years.

Winter barley, grown in 2019 and 2022, had reached the heading to early grain-filling stages. Summer rape or clover in 2020 was in the early vegetative stage. Winter wheat in 2021 had typically progressed to stem elongation stages, while triticale or white clover in 2023 was in the vegetative to early reproductive stage. In addition, the future climate plots were sampled in 2022 and 2023 to further explore the impact of climate change. The detailed overview of soil core samples collected during the study period was presented in Table 2.1.

Table 2.1 Summary of disturbed and undisturbed soil sampling for soil basic soil properties, respiration and structure measurements. CF, OF, IM, EM and EP represent conventional farming, organic farming, intensive meadow, extensive meadow and extensive pasture, respectively.

Year	Climate scenarios	Land use	Treatment replication	Sampling replication	Depth	Sample number	Sample type
2019	Ambient	CF, OF, IM	5	2	5-10 cm	30	Undisturbed
2020	Ambient	CF, OF, IM, EM, EP	5	3	5-10 cm	75	Undisturbed
2020	Ambient	CF, OF, IM, EM, EP	5	Composite	0-15 cm	25	Disturbed
2021	Ambient	CF, OF, IM, EM, EP	5	3	5-10 cm	75	Undisturbed
2021	Ambient	CF, OF, IM, EM, EP	5	Composite	0-15 cm	25	Disturbed
2022	Ambient, Future	CF, OF, IM, EM, EP	5	3	5-10 cm	150	Undisturbed
2022	Ambient, Future	CF, OF, IM, EM, EP	5	Composite	0-15 cm	50	Disturbed
2023	Ambient, Future	CF, OF, IM, EM, EP	5	2	5-10 cm	100	Undisturbed
2023	Ambient, Future	CF, OF, IM, EM, EP	5	Composite	0-15 cm	50	Disturbed
2023	Ambient, Future	CF, OF, IM, EM, EP	5	2	35-40 cm	100	Undisturbed

Disturbed soil samples for each subplot were collected using a steel core sampler (2 cm diameter, 15 cm height) to measure basic soil properties, starting in 2020. In each plot, four soil cores were collected and combined to form a homogenized, composite sample. A total of 150 samples were collected across the study years, with 25 samples each in 2020 and 2021 (ambient climate only), and 50 samples each in 2022 and 2023 (ambient and future climate). The soil samples were stored at 4 °C after removing roots and litter and sieving to 2 mm.

Two or three undisturbed soil cores per subplot were taken from a depth of 5-10 cm with aluminum rings (5.6 cm diameter, 4 cm height) to characterize the microstructure and heterotrophic respiration. This sampling depth was selected to avoid the dense root mat in grasslands and surface disturbances in croplands, while targeting a biologically active zone with high microbial activity and root density. The soil core dimensions represented a compromise between sufficient sampling

volume and the resolution required for reliable visualization of macropores and POM relevant to microbial processes. In addition, soil cores were taken from beneath the current or historic plow layer (35-40 cm) in 2023 to explore the microstructure changes in deeper soil without the tillage effect based on site-specific plowing depth. Altogether, 430 and 100 undisturbed soil cores were sampled (a detailed overview of yearly sampling is provided in Table 2.1) from 5-10 cm and 35-40 cm, respectively, and stored at 4 °C in sealed plastic bags to avoid desiccation prior to X-ray CT scanning and respirometry.

2.2.2 Soil physical and chemical properties measurement

Volumetric soil moisture in the collected soil cores was determined by weight loss after oven drying at 105 °C for 48 hours. Bulk density was calculated with the final soil dry weight divided by the core volume (100 cm^3). Soil pH (air-dried soil in 0.01 M $CaCl_2$ (1: 2.5 (w/v))) was determined with a pH electrode (Mettler SevenEasy pH meter, Gießen, Germany). Soil available phosphorus (AP) was extracted with double lactate solution (1: 50 w/v, pH 3.6) and phosphate concentration was determined with molybdenum blue method (Murphy and Riley, 1962). Soil organic carbon (SOC) and total nitrogen (TN) content were measured using an elemental analyzer (Elementar Vario EL III), and C/N was calculated by SOC content dividing with TN content. Extractable organic carbon (EOC) and nitrogen (EN) were extracted form 5 g soil with 0.05 M K_2SO_4 in a 1:4 ratio and measured with Multi N/C 2100, analyzer (Analytik Jena, Germany). Microbial biomass carbon (MBC) and nitrogen (MBN) were measured by using the chloroform fumigation-extraction method with a conversion factor of 0.45 (Brookes et al., 1985; Wu et al., 1990).

2.2.3 X-ray tomography and structure analysis

Soil cores were scanned with an industrial X-ray microtomograph (X-tek XT H 225; Nikon Metrology, Herts, UK) set to 150 kV and 170 µA with 2500 projections. A 0.3 mm copper filter was used for reducing beam hardening artefacts. Tomograms were reconstructed in 8-bit grayscale and with 30 µm isotropic voxel size with the X-tek CT Pro software (Nikon Metrology). Grayscale contrast was stretched by setting the darkest and brightest 0.2 percentiles to 0 and 255, respectively.

The raw images were cut into the largest possible cylindrical region of interest that contained no disturbed regions along the core wall produced during sampling. Vertical and radial differences

in average gray value were determined within the soil matrix and removed from the image. All gray-scale images were segmented using nnUNet, a self-configuring deep-learning framework based on convolutional neural networks (CNNs) for biomedical image segmentation (Isensee et al., 2021). nnUNet is a powerful segmentation framework capable of distinguishing objects with similar gray values but differing in shape and texture. It also effectively addresses class imbalance through the use of weighted loss functions. These features make it particularly well-suited for segmenting complex soil CT images, where challenges such as overlapping structures, gradual gray-value transitions, and highly imbalanced component distributions are common. A training dataset for nnUNet has recently been curated based on X-ray CT data of soil microstructure in the GCEF, covering 20 sub-volumes equally distributed across grasslands and croplands (Phalempin et al., 2025). The manual annotations were contributed by two independent experts and comprised eight material classes: two mineral phases (porous soil matrix and solid particles), three pore phases, and three organic phases. The pore phase was classified into biotic pores that formed through physical processes such as tillage, wetting/drying, or freeze-thaw cycles and biotic pores created by biological activity such as root decay or bioturbation. They were further subdivided into root-induced channels and earthworm burrows, differentiated primarily by size, shape and internal texture. Earthworm burrows were typically larger, lacked lateral extensions, and were occasionally filled with casts. Within the organic phase, we separated fresh roots from decaying roots, the latter identified by their lower gray values and greater internal porosity, likely due to decay or desiccation. An additional class, non-root-derived POM (other POM), included materials such as biochar, seeds, straw fragments, and litter. Representative 2D segmentation results for cropland and grassland soils produced by nnUNet were shown in Figure S2.1. Training and segmentation with nnUNet were carried out on a high-performance computing cluster equipped with eight GPU nodes, each of them hosting one NVIDIA A100, which could be requested via a job scheduling system. The performance of the segmentation model during training was evaluated using the Dice score for individual class. Note that, this new deep-learning based segmentation method enabled to segment four more classes than the random forest classifier previously applied in the study of Schlüter et al. (2022) on the same dataset, while effectively reducing the amount of false positives and increasing segmentation accuracy (Phalempin et al., 2025). More detailed information regarding the segmentation procedure can be found in Phalempin et al. (2025).

After segmenting the images, the volume fraction of eight material classes and pore structure morphology were analyzed using Fiji/ImageJ (Schindelin et al., 2015). The pore structure was analyzed using the standardized protocol of the soil structure library (Weller et al., 2022) which is built on the functionality of the MorpholibJ plugin (Legland et al., 2016). Pore structure properties were analyzed by combining fresh roots, decaying roots, other POM, root channels, earthworm burrows, and other pores into a composite class. This combination would correspond to the visible pore space left after all POM was mineralized. The biopore structure properties were analyzed by excluding the other pore class that does not have a cylindrical shape. Pore structure properties of interest were visible porosity [mm^3 mm^{-3}], pore surface area density [mm^2 mm^{-3}], connection probability [-], pore distance [mm], pore diameter [mm], and critical pore diameter [mm]. For meaning and methodology, we refer to Weller et al. (2022). The fraction of bioporosity to total visible porosity was determined. In addition, root diameter, root length density and root volume were analyzed after combining fresh roots and decaying roots into a composite material class. The fraction of fresh roots to this composite class was also determined. Likewise, biopore features were analyzed after combining fresh roots, decaying roots, root channels and earthworm burrows to determine the biopore diameter, biopore length density and biopore volume.

2.2.4 Heterotrophic respiration measurement

Heterotrophic respiration measurements were carried out with intact soil cores (100 cm^3) at field water content using the automated heterotrophic respiration analyzer (Respicond V, Sweden) at 22 °C according to (Schlüter et al., 2022b). Emitted CO_2 was trapped in 10 mL of 0.6 M KOH solution and measured through the increase in electric impedance at a given voltage. Soil cores were incubated for more than two days, and the average heterotrophic respiration rate was determined for the period after some initial equilibration of more than one day. The measurement of heterotrophic respiration in undisturbed soil cores only started in 2020.

2.2.5 Statistical analysis

Linear mixed-effects models (LMMs) with random intercepts including split-plot design and repeated measures were implemented to evaluate the effects of land use, year, climate, and their interactions on soil microstructure, chemical and biological properties (Sünnemann et al., 2021). Land use, year, and climate were fixed factors, year (sampling time), block (main plot) and plot

(nested within main plot) served as random effects. Models were fitted with the maximum likelihood method and likelihood ratio tests were used to test for a statistically significant improvement of the models after step-wise addition of the fixed effects. The "*emmeans*" package was used to further analyze significant interactions, by running post hoc pairwise comparisons of estimated marginal means between treatment levels (Lenth et al., 2018). To find pairwise correlations among all 45 measured soil parameters and heterotrophic respiration as well as three organic C fractions (49 parameters in total), Spearman rank correlations were applied and correlated for multiple testing using the *Benjamini-Hochberg* method (Benjamini & Hochberg, 1995) (Table S2.1). To assess the most important predictors for heterotrophic respiration and organic C fractions, we applied both multiple linear regression analysis and random forest analysis (Lutz et al., 2023). Multiple linear regression allows for the evaluation of linear relationships between variables while random forest analysis captures complex interactions and non-linear relationships, offering complementary insights after the combination of two methods. To perform a stepwise reduction of parameters, firstly, strongly correlated parameters ($R < -0.8$, $R > 0.8$) were assessed, visualized in a heatmap (Figure S2.1), and subsequently reduced (Table S2.2). Random forest analysis, with the application of 1000 trees, was then performed to further identify key predictors of heterotrophic respiration from the reduced set of parameters. Finally, structural equation modeling (SEM) was established using the key predictors for heterotrophic respiration to assess how soil parameters directly and indirectly influence C cycling in response to land use, climate and year, using the dataset of 150 samples collected from 2020 to 2023. To address the absence of future climate scenario data in 2020 and 2021, the SEM was implemented using full information maximum likelihood (FIML) to handle missing data and bootstrapping to obtain robust standard errors. We employed the "*lmer*" function for LMMs in "*lme4*" package (Bolker et al., 2015), "*corr.test*" function for pairwise correlations in "*psych*" (v.2.4.6.26) package (Revelle, 2024), "*cor*" function for the stepwise reduction in stats package (R Core, 2013), "*randomForest*" function for random forest analysis in "*randomForest*" package (Liaw & Wiener, 2002), and "*sem*" function for SEM in "*lavaan*" package (Rosseel, 2012). All statistical analyses were conducted using R 4.1.3. Figures were produced with the package ggplot2 (Wickham, 2011). Statistically significant findings are reported at a level of $p < 0.05$, unless explicitly stated otherwise.

2.3 Results

2.3.1 Effect of land use on soil microstructure characteristics over five years

Visual assessment of the soil microstructure at the depth of 5-10 cm revealed significant differences in the morphology and formation process of pores and POM between grasslands and croplands (Figure 2.2). Croplands exhibited more incorporated plant litter and fresh roots, while grasslands showed a higher abundance of intact decaying roots and root channels. In contrast, these differences were much less pronounced at the 35-40 cm depth.

The IM treatment in 2021 was excluded in the following data analysis grouped by cropland and grassland due to its transitional microstructure characteristics after the plowing and reseeding in 2020.

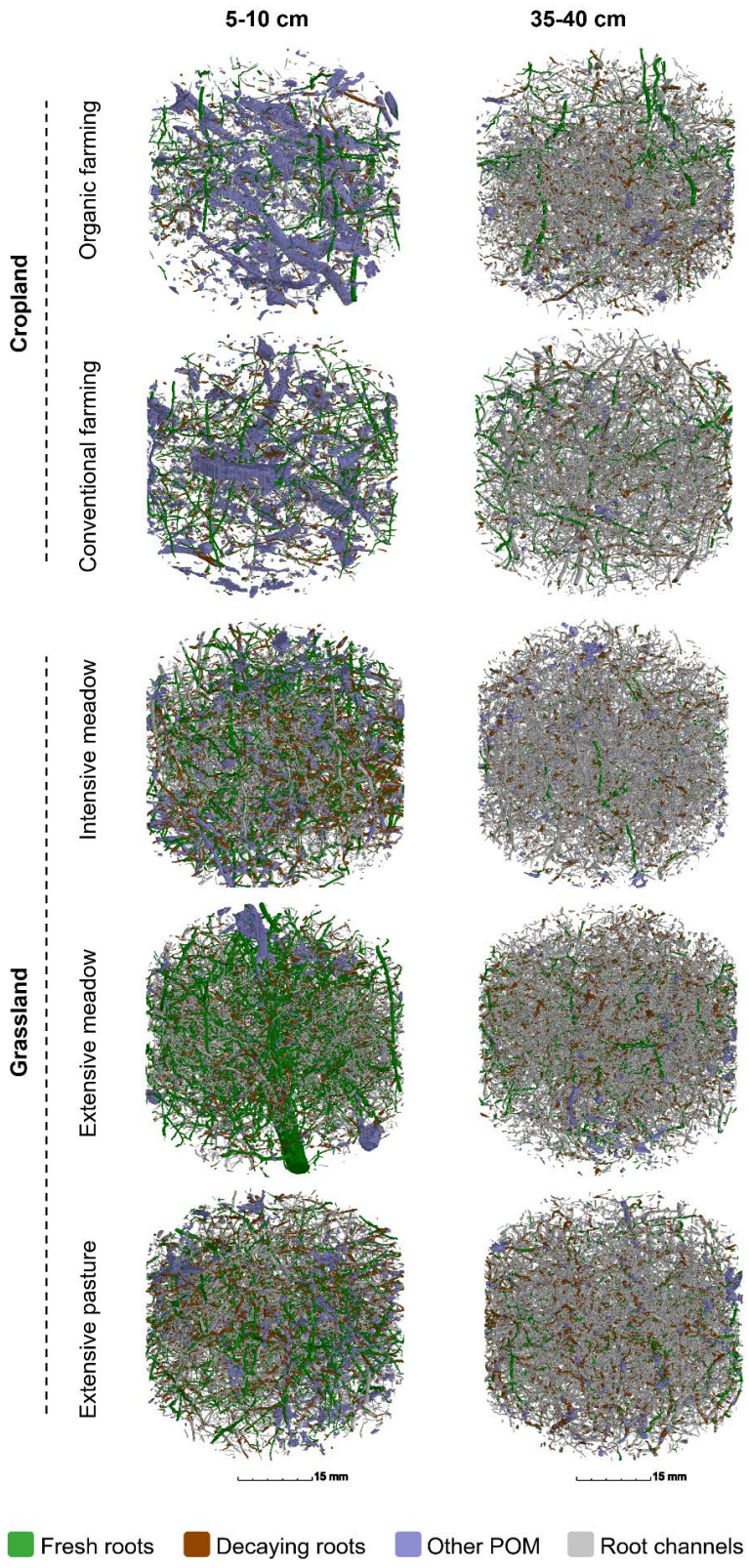

Figure 2.2 3D Microscale characterization of soil structure on the depth of 5-10 cm (shallow) and 35-40

cm (deep) among five land uses. The thin volumes have a dimension of 51 × 51 × 32.1 mm (height × width × depth) to reduce the amount of visible feature.

The volumetric POM content of grasslands was 10.0-87.5 % higher than that of croplands from 2019 to 2021, without a clear pattern in 2022 and 2023 (Figure 2.3a, Table S2.3). When separated into individual POM classes, croplands had a 33-62 % higher volumetric fresh roots than grasslands, while the volumetric decaying roots and other POM were only 19-36 % and 26-49 % of that in grasslands, respectively (Figure S2.3a-c, Table S2.3). As a result, the fraction of fresh roots (i.e. the contribution of fresh roots to all roots) in topsoil was always highest for croplands (> 0.8) and in a lower range for extensive grasslands (0.4-0.5) (Figure 2.3b). The IM treatment deviated from other grasslands in 2021-2022.

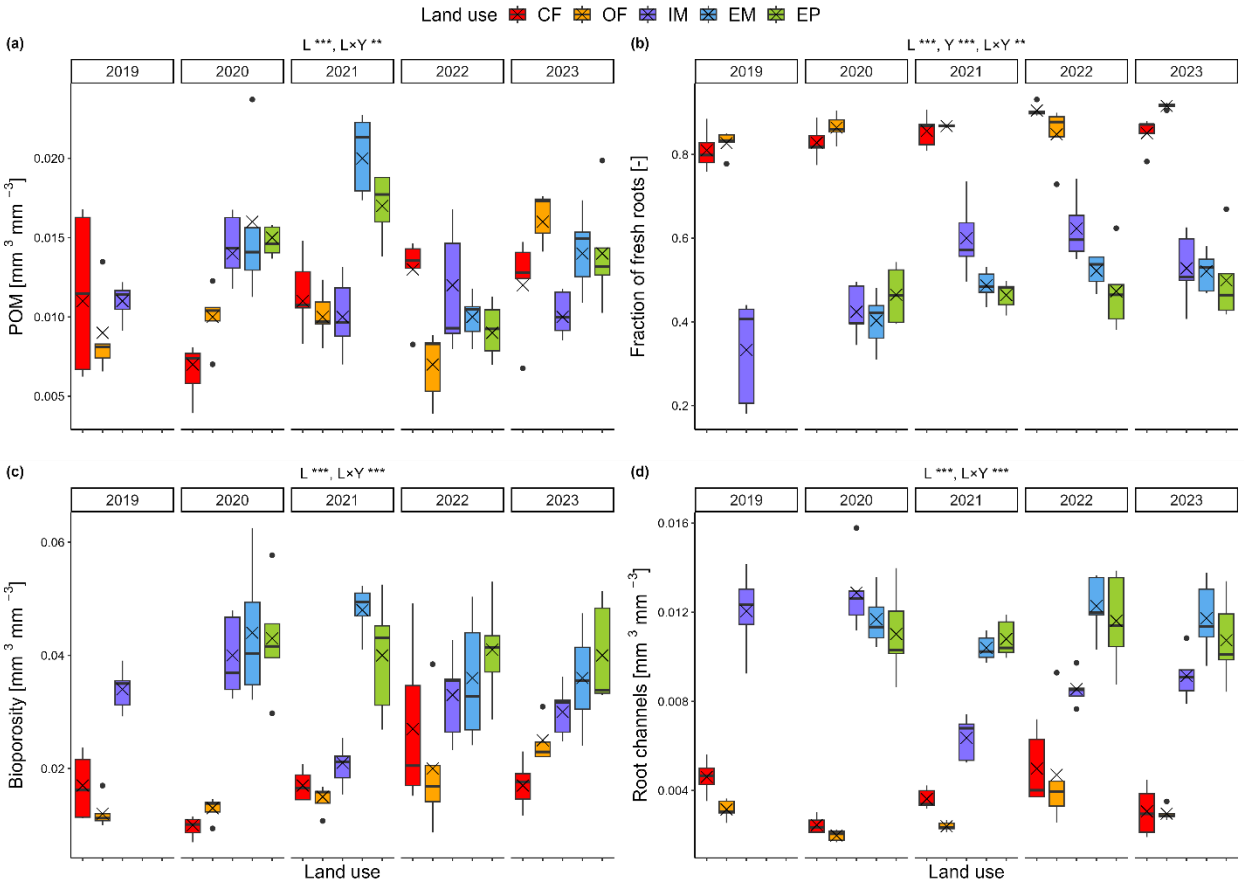

Figure 2.3 Effect of land use on soil microstructure characteristic over five years. (a) Particulate organic matter (POM), (b) Fraction of fresh roots, (c) Bioporosity, (d) Root channels. CF, OF, IM, EM and EP represent conventional farming, organic farming, intensive meadow, extensive meadow and extensive pasture, respectively. Significant differences between land use (L), year (Y), interaction of land use and year (L×Y) are indicated ** ($p < 0.01$) and *** ($p < 0.001$). Box plots represent the 0, 25, 50, 75, and 100 percentile and cross symbols the arithmetic mean (n = 5).

Total visible porosity showed no land-use effect, but the variability was consistently higher in croplands than in grasslands, with 115-367 % higher standard error (Figure S2.3f, Table S2.3). Since 2022, all system showed reduced porosity, driven by a decline in the volume fraction of pores with non-biological origin (37.2-57.0 % lower) (Figure S2.3e). In contrast, the volume fraction of root channels and composite bioporosity were consistently greater in grasslands, with root channels being 123-434 % higher than croplands (Figure 2.3c-d). Notably, the destruction of biopores after plowing of the IM treatment in autumn 2020 was evident, and root channel volumes had not fully recovered by 2023. In extensive grasslands, root-derived POM fractions were higher in normal years than in the last dry year, whereas biopore fractions and the fraction of fresh roots remained stable during the years (Figure 2.3, S2.3). Additionally, the connection probability of biopores was 67.0-486.8 % higher in grasslands than in croplands, while the connectivity of all pores was only 12.4-31.9 % greater (Table S2.3).

2.3.2 Climate effect on soil parameters in 2022 and 2023

The future climate scenario increased heterotrophic respiration by 21.7 % compared to the ambient climate, but only in the normal year of 2023 (Figure 2.4a-b). No significant effects of the future climate scenario on microstructure properties, nor nitrogen and carbon fractions were observed (Figure S2.4, Table S2.4).

2.3.3 Land use and climate effect on soil microstructure characteristics of the deep layer in 2023

Below the plow horizon (35-40 cm depth), land-use induced differences in microstructure properties were generally less distinct than in the shallow soil layer. POM showed no significant climate effect (Figure 2.5a). Croplands exhibited a higher fraction of fresh roots also at this depth than grasslands, but only evident under the ambient climate (Figure 2.5b). Root channels and bioporosity were lower in croplands than in grasslands, particularly under ambient climate scenario, but these patterns were less distinct under the future climate scenario, likely due to greater spatial variability and a more substantial increase in decaying roots observed in croplands (Figure 2.5c-d, S2.5b, Table S2.5).

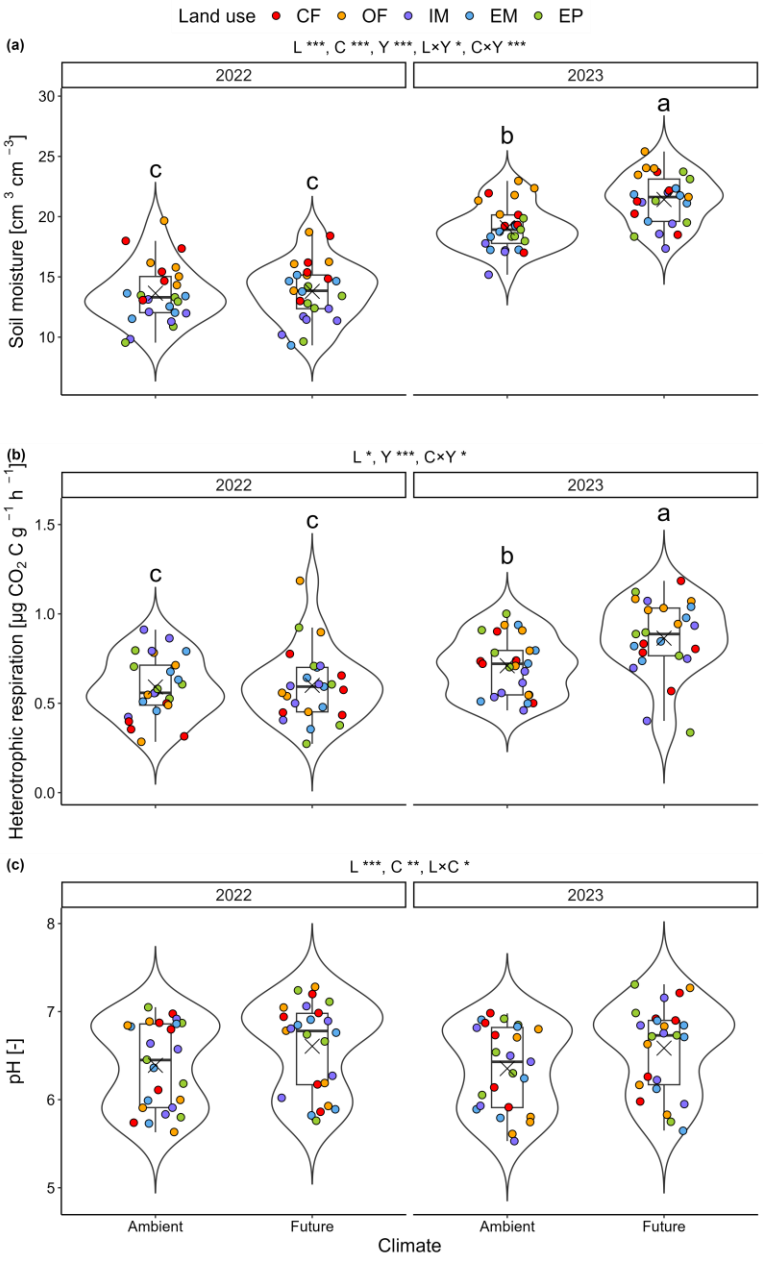

Figure 2.4 Effect of land use and climate change on soil moisture, heterotrophic respiration, and pH in year of 2022 and 2023. (a) Soil moisture, (b) Heterotrophic respiration, (c) pH. Significant differences between land use (L), climate (C), year (Y), interaction of land use and climate (L×C), land use and year (L×Y), and climate and year (C×Y) are indicated * ($p < 0.05$), ** ($p < 0.01$), and *** ($p < 0.001$). Box plots represent the 0, 25, 50, 75, and 100 percentile and cross symbols the arithmetic mean (n = 25). Jitter points represent individual sub-plots. Different letters indicate significant differences ($p < 0.05$) among treatments.

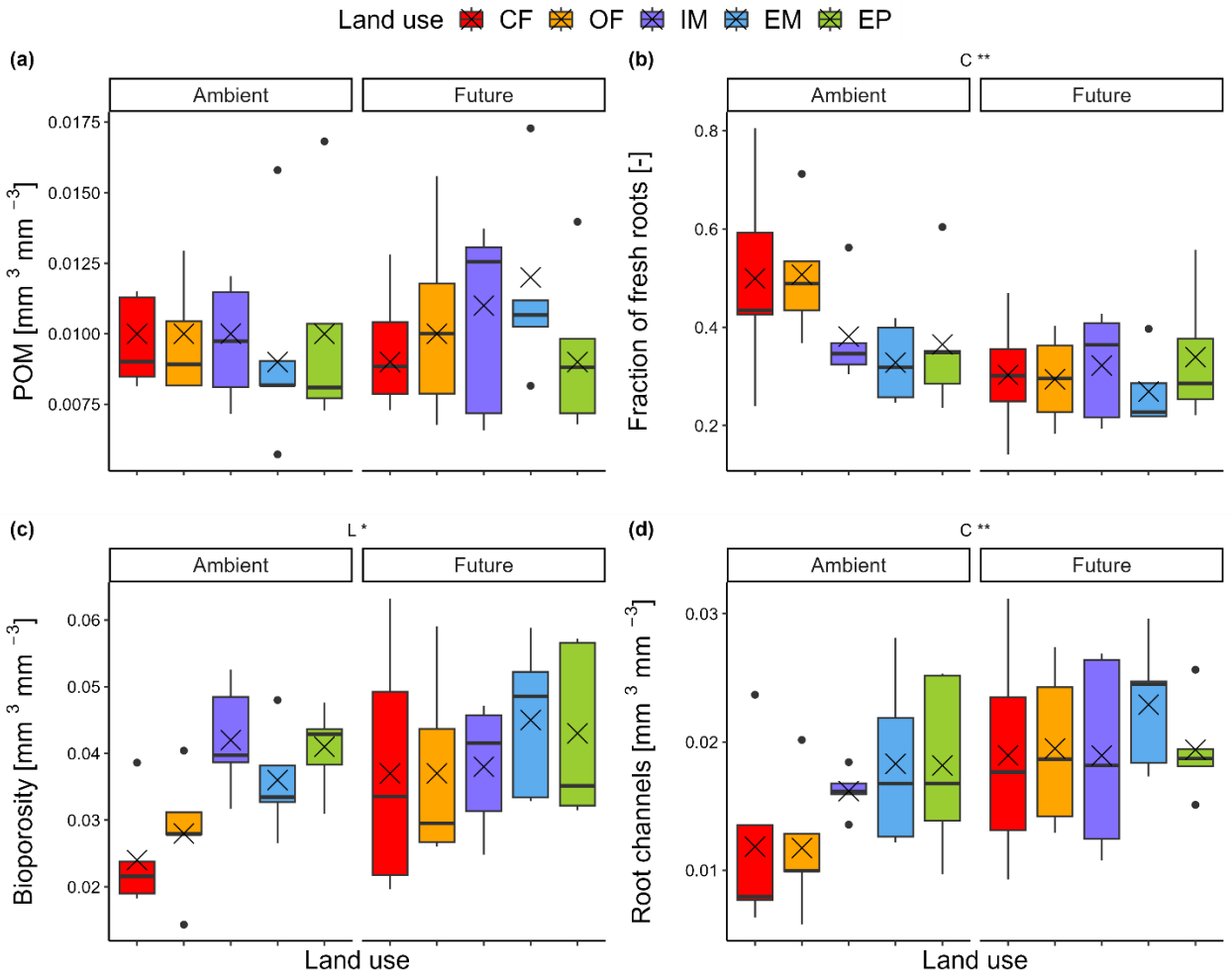

Figure 2.5 Effect of land use on soil microstructure characteristics of subsoil in year of 2023. (a) Particulate organic matter (POM), (b) fraction of fresh roots, (c) Bioporosity, (d) Root channels. CF, OF, IM, EM and EP represent conventional farming, organic farming, intensive meadow, extensive meadow and extensive pasture, respectively. Significant differences between land use (L) and climate (C) are indicated * ($p < 0.05$) and ** ($p < 0.01$). Box plots represent the 0, 25, 50, 75, and 100 percentile and cross symbols the arithmetic mean (n = 5).

2.3.4 Effect of land use on soil organic carbon fractions from 2020 to 2023

All organic C fractions and fluxes were elevated in grasslands compared to croplands, although magnitude of difference varied by fraction. Extractable organic carbon (EOC) ranged from 16.7 to 83.1 µg C g^{-1} across all treatments, with grasslands showing 51.3-128.9 % higher EOC than croplands (Figure 2.6a, Table S2.3). Microbial biomass carbon (MBC) ranged from 173.7 to 387.5 µg C g^{-1}, and was 29.3-66.8 % higher in the grasslands (Figure 2.6b, Table S2.3).

Furthermore, heterotrophic respiration was 32.6-53.9 % greater in grasslands than in croplands from 2020 to 2022, while no significant differences among land uses were observed in 2023 (Figure 2.7a, Table S2.3). The IM treatment had a heterotrophic respiration rate similar to croplands the year after plowing in 2021 but was more similar to the other grasslands in other years. Additionally, the total soil organic carbon (SOC) content was 5.6-15.8 % greater in grasslands than in croplands, with no significant differences in 2020 (Figure 2.6c, Table S2.3). The differences in SOC between grasslands and croplands were increasing over time.

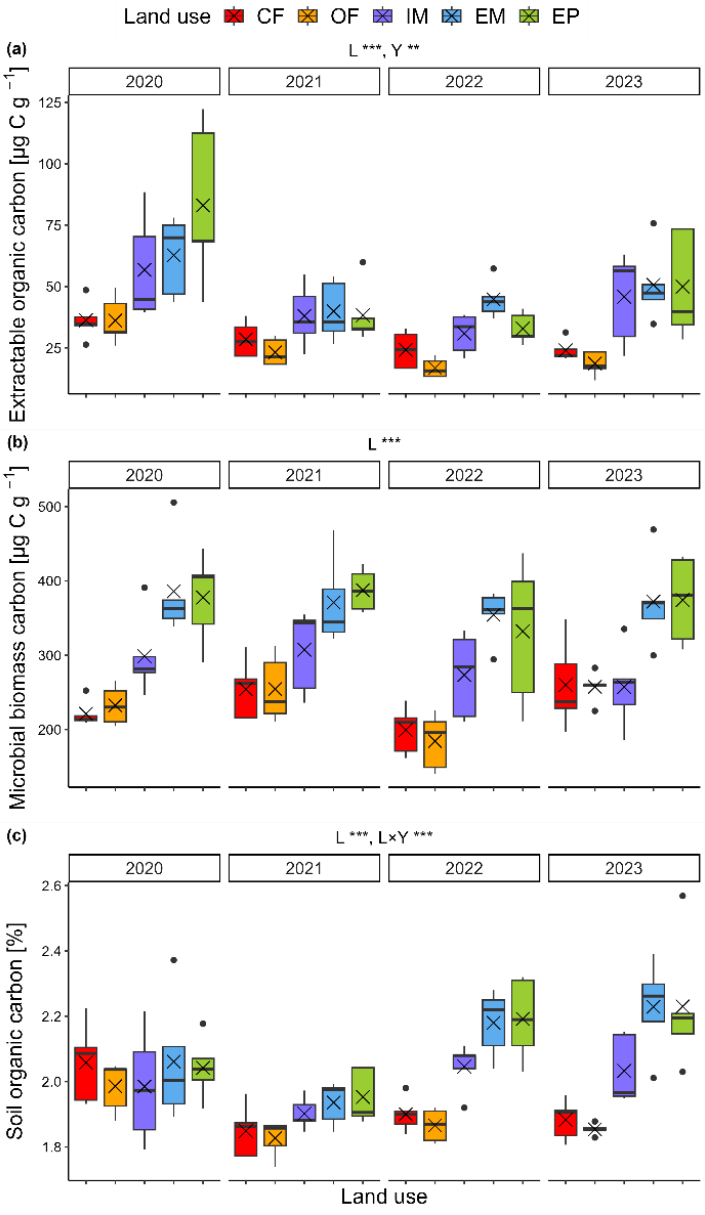

Figure 2.6 Effect of land use and climate change on soil carbon pools from 2020 to 2023. (a) Extractable

organic carbon, (b) Microbial biomass carbon, (c) Soil organic carbon. CF, OF, IM, EM and EP represent conventional farming, organic farming, intensive meadow, extensive meadow and extensive pasture, respectively. Significant differences between land use (L), climate (C), year (Y), interaction of land use and year (L×Y), and interaction of climate and year (C×Y) are indicated ** ($p < 0.01$) and *** ($p < 0.001$). Box plots represent the 0, 25, 50, 75, and 100 percentile and cross symbols the arithmetic mean (n = 5).

2.3.5 Most important soil properties for carbon cycling prediction

Random forest models identified volumetric POM content and soil moisture as the most important predictors of heterotrophic respiration (explained variance: 34.06 %; Figure 2.7b). Generally, biopore properties, pH, and available phosphorus (AP) also seemed to be of secondary importance, whereas bulk density, pore connectivity, and organic carbon contents had a negligible effect. When heterotrophic respiration was normalized by SOC or particulate organic carbon (POC) (the conversion from POM volume fraction to g POC is explained in Text S2.1), explained variance decreased to 31.9 % and 21.4 %, respectively, with pore and root-derived POM becoming more important (Figure S2.6). In contrast, the organic matter fractions EOC, MBC and SOC variability (41-59 % explained) was better predicted by decaying roots and root channels and biopore properties rather than soil moisture or POM (Figure S2.7).

Furthermore, the scoring of the best explanatory variables for heterotrophic respiration varied strongly with years. In dry years of 2020 and 2022, the explained variability was very low (2.89 %) and soil moisture failed as a suitable predictor. However, the explained variability in normal years of 2021 and 2023 increased to 45.06 %, with soil moisture, biopore diameter, fraction of bioporosity, and POM as the best predictors (Figure S2.8). In contrast, the clear grouping effect of normal and dry years was absent for MBC, EOC, and SOC.

Structural equation modeling confirmed that heterotrophic respiration was strongly influenced by soil moisture, pH and POM content, but showed a clear disconnection with SOC and labile carbon fractions (Figure 2.7c). In contrast, SOC and labile organic carbon fractions were strongly linked to the volume fraction of root channels (R = 0.45-0.66). The explained variation of heterotrophic respiration increased slightly from $R^2 = 0.35$ to $R^2 = 0.43$ and brought similar improvements for the considered carbon fractions when taking the main effects (land use, climate and year) into consideration (Figure S2.9). The extended model also confirmed that (1) differences in pH and available P are not due to management but a spatial gradient, that (2) root channel density is well explained ($R^2 = 0.73$) by main effects and reflects land-use-specific formation and

destruction of pores, and that (3) volumetric POM content is much less dependent on these main effects ($R^2 = 0.08$).

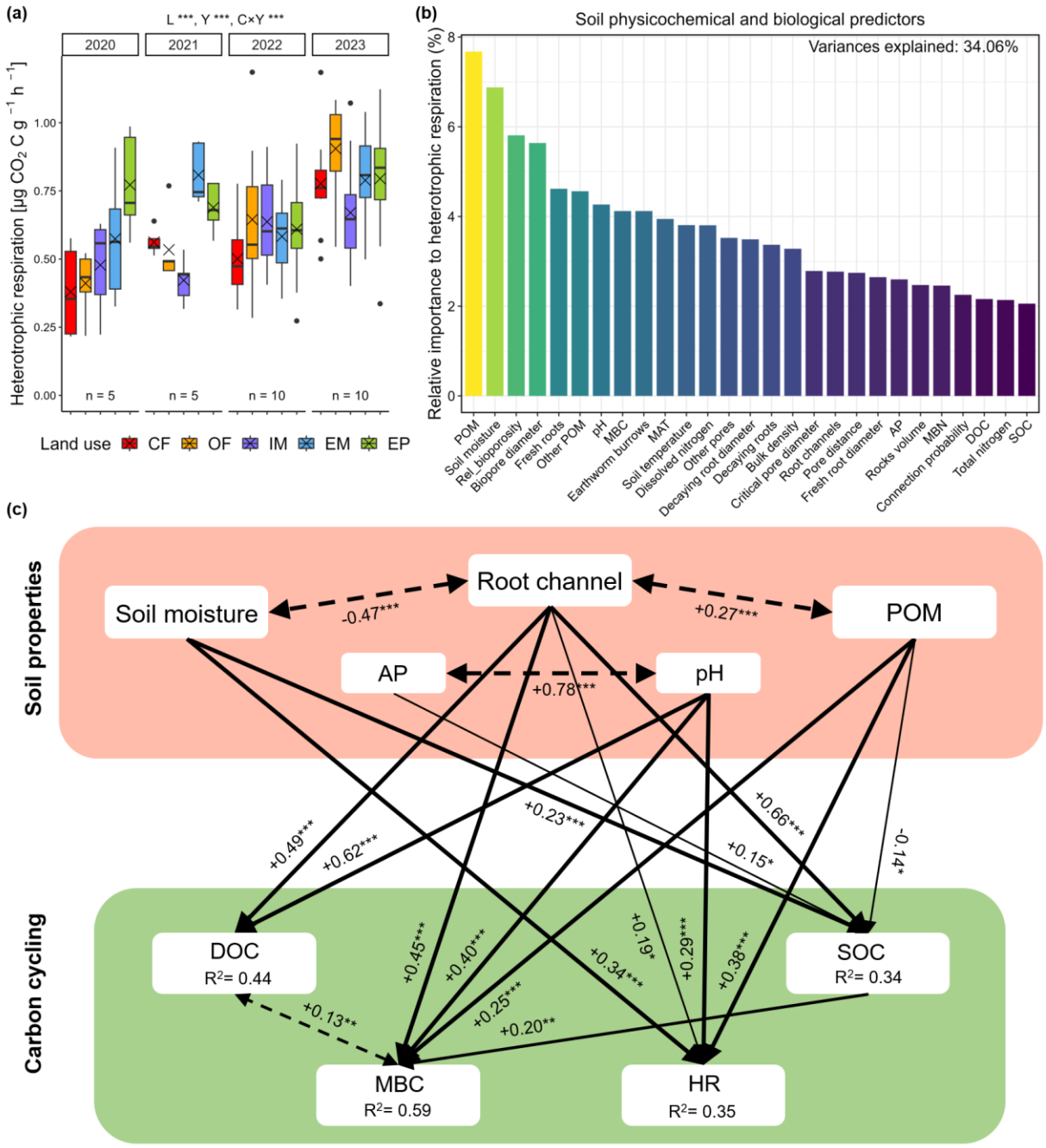

Figure 2.7 (a) Response of heterotrophic respiration to variations in land use and climate change. The data are presented as grouped box plots (the thick solid line represents the median, the lower and upper hinges correspond to the first and third quartiles), with cross symbol demotes mean value. (b) Relative importance of the most importance soil physicochemical and biological predictors of heterotrophic respiration. Predictors are displayed on the x-axis. Total variances explained of random forest model are shown in the top, right corner of figure. (c) Structure equation model depicting the role of soil properties driven by land

use, climate and year factors on carbon cycling. Numbers next to arrows indicate standardized path coefficients (robust standard errors of coefficients). Solid lines indicate significant relationships. Lines with double-sided arrows indicate potential relationship between covariances. POM: particulate organic matter, MBC: microbial biomass carbon, EOC: extractable organic carbon, SOC: soil organic carbon, MBC: microbial biomass nitrogen, HR: heterotrophic respiration, AP: available phosphorus, Rel_bioporosity: fraction of bioporosity, MAT: mean annual soil temperature. Line width reflects the level of statistical significance. *, **, *** indicate significant differences at 0.05, 0.01 and 0.001 levels, respectively. The parameters of model are χ^2/df = 0.994, GIF = 0.979, p = 0.458, RMSEA = 0.000, SRMR = 0.052 (n = 150, bootstrap = 1000).

2.4 Discussion

2.4.1 Soil microstructure development dynamics driven by land use, but not by climate change

With deep-learning-based image segmentation, it was possible to retrieve an unprecedented number of soil components from X-ray CT images, allowing the differentiation of three pore types and POM fractions with high accuracy (Phalempin et al., 2025b). This enabled a more comprehensive analysis of soil microstructure, capturing key indicators of land-use legacies and management interventions. Two structural indicators, root channels and the fraction of fresh roots, proved particularly effective for tracing soil structural changes. Root channel density indicated mechanical disturbance, with a marked decline after a single plowing event and a gradual recovery towards a grassland-specific dynamic equilibrium with time. The fraction of fresh roots distinguished between annual croplands and perennial grasslands, reflecting contrasting root growth and turnover patterns, and system continuity. Both indicators were less affected by spatial variability and more informative than bulk density or total visible porosity, which carried mixed information on tillage, wetting history, and sampling of random heterogeneity. More importantly, these new structure metrics calculated on a large dataset of 530 intact soils retrieved from a five-year chronosequence revealed new clues about typical soil microstructure dynamics under realistic field conditions.

In grasslands, root channels volume fraction amounted to 0.01-0.012 $mm^3\ mm^{-3}$ within 4-5 years after establishment, in line with previous studies suggesting a dynamic equilibrium of root channels to be reached within six years in the topsoil (Lucas et al., 2019). In contrast, croplands maintained consistently lower values (0.003-0.004 $mm^3\ mm^{-3}$), primarily due to recurrent tillage disrupting pore continuity. Notably, root channel volume in the intensive meadow treatment declined by about 50 % in 2021 following tillage in winter 2020, highlighting the sensitivity of

biopore structure to mechanical disturbance (Xiong et al., 2022a). Higher root channel density of grasslands was attributed to higher abundance of thick (tap-)roots, denser root system, lack of mechanical disturbance from tillage, and continuous root growth (Bacq‐Labreuil et al., 2020; DuPont et al., 2014; Kodešová et al., 2011; Yu et al., 2024a). Grasslands also showed consistently higher connectivity probability for both biopores and total pores than croplands, aligning with previous findings that sustained root activity and reduced disturbance under perennial vegetation promote pore connectivity, particularly in clay-rich soils (Bacq-Labreuil et al., 2018). Below the plow horizon (35-40 cm), differences in microstructure characteristics were much less among the five land uses, with only slightly higher bioporosity in grasslands. This aligns with previous studies, showing that establishing a dynamic equilibrium of soil microstructure takes longer in subsoil due to lower biological activity and limited root-induced pore formation (Banfield et al., 2018; Lucas et al., 2019; Peng et al., 2025). Moreover, it takes a long time to induce changes also since roots partly reuse the existing pore network once a stable microstructure is developed (White & Kirkegaard, 2010).

The fraction of fresh roots in the shallow soil layer of croplands was approximately 0.8, compared to just 0.4-0.5 in grasslands, further indicating lack of new root growth or faster decomposition of root residues after harvest in croplands, whereas continuous root turnover in perennial grasslands causes a steady formation of root residues (Linsler et al., 2013; Luo et al., 2021; Wander & Bidart, 2000; Wang et al., 2019e). Interestingly, the fraction of fresh roots in spring remained stable within five years, especially in croplands and extensive grasslands. This suggests that root degradation rates may be more influenced by intrinsic plant traits and general soil conditions than by short-term variations in belowground biomass production (Chen & Brassard, 2012; Wagai et al., 2013; Zhao et al., 2024). Furthermore, high variability in the absolute amounts of both fresh roots and decaying roots was observed due to their sensitivity to water supply. For example, elevated soil moisture in 2023 enhanced root growth in croplands, resulting in volumetric POM content comparable to grasslands. This indicates that factors such as root growth and soil moisture can significantly influence the composition and depth distribution of plant residues in soil (von Haden & Dornbush, 2014), potentially temporarily overcasting the effects of land use alone.

The future climate scenario had no effect on topsoil microstructure properties, suggesting a dominant influence of land use management and vegetation characteristics compared with the

relatively modest increase in temperatures and change in precipitation patterns in our study area. This finding aligns with previous studies showing that substantial alterations in soil microstructure generally require extreme climatic drivers such as wetting-drying/freezing-thaw cycles, longer timescales, or broader climatic gradients (Liu et al., 2024a; Peng et al., 2023; Rabbi et al., 2024; Xiong et al., 2019b). Furthermore, inherent soil properties, such as texture and mineralogy, along with resilient soil fauna like nematodes and earthworms, may also buffer against climatic variations and maintain microstructural stability (Józefowska et al., 2019; Li et al., 2022b; Siebert et al., 2020). However, climate effects were more apparent in the vertical distribution of root-derived POM and pore fractions. Under the future climate scenario, annual croplands accumulated more root channels and other biopores than ambient climate below the plow horizon, likely reflecting deeper rooting during dry periods (Fan et al., 2017; Thorup-Kristensen et al., 2020). These patterns were absent in grasslands, probably due to their more stable, multi-species root systems and limited disturbance, which buffer short-term climatic effects (Korell et al., 2024). Interestingly, in croplands, wetter spring conditions under the future climate scenario led to more intense shallow rooting and reduced fraction of fresh roots at depth, highlighting the root plasticity in response to moisture availability (Maurel & Nacry, 2020; Schmidt & Gaudin, 2017).

Thus, our study supports the first hypothesis that the evolution of soil biopores and POM content in topsoil is primarily driven by land use, with minimal fluctuations induced by climatic conditions that may arise from root system adaptations to water scarcity in croplands.

2.4.2 Carbon mineralization and carbon pools driven by land use and climate change

Continuous organic input of perennial vegetation, combined with reduced C loss due to less frequent disturbance from tillage, resulted in grasslands having 6-16 % higher SOC content than croplands after less than ten years of management. Notably, significant differences in SOC content only emerged after 7-8 years (after 2020) and continued to increase over time. This pattern aligns with previous reports that perennial grasslands accumulated 18-29 % more SOC than annual croplands after 29 years (Rui et al., 2022) and that conversion from cropland to grassland increases SOC by 25.7 ± 11 % after 21 ± 6 years (Don et al., 2011; Poeplau et al., 2011). Grasslands have greater potential for C sequestration than croplands, primarily due to long-term accumulation effects of higher C input and greater microbial activity, which converts fresh organic matter into more long-term stable necromass (Acharya et al., 2012; Bai & Cotrufo, 2022; Beillouin et al.,

2022).

Furthermore, our study found that MBC was consistently higher in grasslands than in croplands. This suggests that grasslands support a more active and abundant microbial community, which drives the decomposition of organic matter and subsequent C cycling (Baumann et al., 2012). Similarly, grasslands exhibited continuously elevated levels of EOC, indicating a higher availability of readily decomposable organic substrates, which directly contribute to accelerated C cycling (Liu et al., 2017). However, unlike SOC, the labile carbon pools (MBC and EOC) in our study were already fully developed in the 6^{th}-7^{th} year after establishment, showing no further increases during the chronosequence. This indicates that labile C pools stabilize more quickly than the slower-accumulating total SOC, which supports that labile C pools respond quickly to land-use change, while more persistent C fractions require longer-term buildup (Chen et al., 2017). These findings also align with previous studies suggesting that soil microstructure dynamics is synchronized with the turnover of fast cycling, labile C pools and decoupled from the slow turnover of total and mineral-associated organic matter (Leuther et al., 2023).

Heterotrophic respiration rates in grasslands were on average 33-54 % higher than in croplands, consistent with their elevated labile carbon availability. However, this difference disappeared in 2023, probably due to increased soil moisture that fostered greater growth of shallow roots and microbial activity in croplands, thereby narrowing the gap. Detailed interactions between soil moisture, structure and C availability are further explored in Section 2.4.3.

2.4.3 Importance of soil structure factors on soil carbon cycling

The huge variability in heterotrophic respiration rates and various organic C fractions across years, climate scenarios, and land uses provided a robust basis for identifying the independent variables most strongly associated with variation in carbon cycling processes. Our findings showed that heterotrophic respiration and organic C fractions were shaped by complex interactions among land use, soil structure and environmental conditions. Across land uses, POM content and soil moisture emerged as the strongest predictors of variations in heterotrophic respiration, supporting our second hypothesis that C input through POM closely coupled with C mineralization under fairly dry site conditions. Grasslands exhibited both higher heterotrophic respiration and POM contents compared to croplands, except in 2023. This finding aligns with a previous study conducted at the same site (Schlüter et al., 2022b), suggesting that POM acts as a primary source

of energy and nutrients fueling microbial metabolism, particularly under favorable moisture conditions (Angst et al., 2024; Lavallee et al., 2020; Xie et al., 2024b).

The strongest stimulation of respiration under the future climate scenario was observed in the relatively wet spring of 2023, when increased precipitation and irrigation likely increased the release of protected organic matter (Huang & Hall, 2017; Shen et al., 2008). Dissolved organic compounds under moist soil conditions was found to be more accessible to microbes, even in the compacted surface layers with limited physical structure (i.e. physical crust) (Feng et al., 2025). In contrast, no climate effect was observed under the dry spring of 2022, suggesting that moisture availability modulates the temperature sensitivity of microbial respiration (Hao et al., 2025).

Secondary predictors included soil pH and biopore properties, particularly root channels density. Both heterotrophic respiration and labile C pools (MBC and EOC) were significantly correlated with pH, likely reflecting microbial preferences for near-neutral conditions, which optimize microbial growth efficiency and enzyme activity (Malik et al., 2018; Neina, 2019). pH influences microbial carbon cycling processes through modulating mineral protection mechanisms involving iron-aluminum oxides and exchangeable cations (Jia et al., 2024; Ren et al., 2024a; Wang & Kuzyakov, 2024).

Our study found root channels positively correlated with the organic carbon fractions (R = 0.45-0.66) and heterotrophic respiration, suggesting that their role as key entry path for root-derived C inputs, including exudates, mucilage, and decaying root tissues (Bundt et al., 2001; Wendel et al., 2022). These inputs sustain microbial activity in both the rhizosphere and detritusphere, contributing to the formation of microbial necromass and enhancing nutrient cycling (Mueller et al., 2024; Nannipieri et al., 2023). Importantly, root channels typically fall within the 30-150 μm size range, which is highly favorable for microbial colonization and activity (Kravchenko et al., 2019). Pores in this range may offer an optimal balance of moisture and aeration, supporting C mineralization by enhancing substrate accessibility while promoting microbial C use efficiency (Kravchenko et al., 2019; Li et al., 2024a). In undisturbed grasslands, the persistence of root channels may support continuous C input and fosters microsites of high microbial turnover. Root proliferation within these channels can enhance nutrients uptake from decomposing tissues before nutrients are lost through leaching or immobilized in the surrounding soil matrix (McKee, 2002). Conversely, the loss of root channels through tillage in croplands may disrupt these processes and reduce physical protection of organic matter (Cooper et al., 2021;

McKee, 2002). Thus, root channels mark biologically active zones where rhizodeposition and microbial process converge, effectively linking plant-derived inputs with microbial transformation pathways that contribute to long-term C stabilization.

Interestingly, heterotrophic respiration did not show any direct correlations with labile carbon pools (EOC and MBC) or SOC across years, probably indicating that these C fractions are not the immediate drives of microbial CO_2 release under our study conditions. This disconnect may reflect differences in temporal dynamics: SOC and labile C pools represent medium- to long-term C accumulation, whereas heterotrophic respiration responds more rapidly to short-term fluctuations in environmental conditions and substrate availability, particularly due to the higher sensitivity of POM to land use and interannual climate variability (Kravchenko et al., 2015; Rocci et al., 2021). Moreover, root-derived respiration was not partitioned from total soil CO_2 fluxes in this study, which may confound the observed relationships between heterotrophic respiration and measured carbon fractions, particularly in systems with high root biomass where root respiration constitutes a substantial portion of total CO_2 emissions (Hopkins et al., 2013). The strong association between POM and heterotrophic respiration may be partly explained by the fact that both were measured on the same set of samples, where cut-off roots likely served as immediate substrates, similar to conditions shortly after mowing or harvest (Luo et al., 2021). The investigated soil properties explained a limited portion of heterotrophic respiration variability (R^2 = 0.35 in SEM; 34.06 % in random forest model), and adding the main effects only slightly improved the explanation (R^2 = 0.43). These results suggest that beyond organic C fractions and the analyzed physiochemical parameters, variables such as soil texture, POM quality, and heterogeneity in nutrient availability, and biological factors including enzyme activity, carbon use efficiency, and microbial or fungal colonization, may have a significant influence on heterotrophic respiration rates and carbon cycling processes (Adhikari et al., 2023; Balogh et al., 2011; Zheng et al., 2009). Moreover, spatial and temporal mismatches between undisturbed soil core sampling for microstructural analysis and respirometry and bulk soil measurements for basic physiochemical parameters may have contributed to the observed disconnect.

Strikingly, common used physical properties like bulk density, total visible porosity (as the proxy for air capacity), and overall pore connectivity, showed no significant relationship with heterotrophic respiration and organic C fractions, further supporting our second hypothesis. This contrasts with previous studies that reported a positive effect of pore connectivity on microbial

activity and carbon mineralization (Bhattacharyya et al., 2021; Smith et al., 2017), which may reflect differences in soil moisture regimes, soil texture, methodology, or non-limiting aeration in microbial hotspots under our study conditions (Schlüter et al., 2022b). Additionally, the physical microstructure across all land-use systems may have been sufficiently developed to permit microbial access to organic substrates, thereby minimizing the influence of structural variability on C mineralization (Patel et al., 2021). However, this finding does not negate potential structure-function relationships. Instead, the strong positive correlations between root channel and organic C fractions highlights the need for more detailed classification of pore types beyond commonly used bulk properties. Root-derived biopores may contribute to long-term C stabilization by serving as pathways through which labile C enter the soil, is rapidly processed by microbes, and subsequently transformed into microbial necromass that becomes stabilized within the soil matrix (Cotrufo et al., 2013; Kravchenko et al., 2019). Future studies should evaluate whether associations between pore metrics using X-ray CT and carbon fluxes represent independent structural effects, or whether they are confounded by co-variation with POM, which may be the more direct driver of microbial activity and carbon mineralization.

Overall, our findings indicate that short-term fluctuations in heterotrophic respiration are driven by changing environmental conditions, while long-term shifts in stable SOC pools are shaped by land use-induced changes in C inputs and mineralization processes. However, several methodological limitations should be acknowledged. First, the simulated climate change scenario involved only moderate alterations in precipitation and temperature, which may not fully capture the effects of more extreme or prolonged climatic events expected in the future. Second, soil sampling was conducted only in early spring, which may have missed seasonal variability in root growth and microbial interactions that influence soil structure. Finally, this study did not directly account for carbon use efficiency and how it is modulated by environmental factors (Domeignoz-Horta et al., 2020; Guo et al., 2020b). Future research should expand temporal sampling resolution and incorporate key biological and biochemical indicators, such as microbial activity, enzyme dynamics, and carbon use efficiency, to better link soil microstructure with underlying biogeochemical processes.

2.5 Conclusion

The conversion of annual croplands to perennial grasslands triggers changes in various

biochemical and physical topsoil properties at different rates. Differences in fast-cycling microbial biomass and dissolved organic carbon were already fully established after five years, whereas the soil organic carbon content diverged more slowly with clear differences only emerging after eight years and continuing to increase. The conversion into a typical grassland microstructure in terms of root channel density and fraction of fresh roots over all roots outpaced the soil organic carbon dynamics and was fully expressed after five years. These soil properties have in common that they change gradually and develop towards dynamic equilibria specific to cumulative carbon inputs and average carbon mineralization rates of grasslands. In this way, they differ from fluctuating soil properties like heterotrophic respiration which are more influenced by environmental conditions like soil moisture. In our study, the pore structure did not exhibit a long-lasting effect on carbon cycling, as it neither restricted root growth nor limited soil microbial aeration under any of the tested land uses and climate treatments. Resource availability, approximated by the volumetric water and POM content explained short-term carbon cycling much better. The future climate scenario induced at the experimental site influenced carbon cycling and soil microstructure primarily through shifts in the spatial and temporal patterns of soil moisture, as well as through adaptive changes in root system development.

3 Microhabitat properties explain variations in soil nematode communities across climate conditions in cropland, but not in grassland

Abstract

Soil nematodes are valuable bioindicators for the ecological status of soils. Nematode community properties are known to be altered by land-use intensity, to vary with seasonal dynamics, and to be affected by climate change. These external drivers also affect a range of structural, physical, and biochemical soil properties. However, it is unclear whether shifts in nematode community properties are the result of changing resource accessibility in the soil or whether these just co-occur. Here, we linked nematode community to microhabitat properties of intact soils and biochemical properties of bulk soils from a long-term field trial on land-use intensity (cropland vs. grassland) and simulated climate change (ambient vs. future climate). Soil samples were taken in two seasons (November vs. June) to capture a wide range of climatic conditions. The objective of the study was to investigate whether the resource accessibility imposed by microhabitat properties would regulate nematode communities and whether the strength of bottom-up regulation depended on climate change, land use intensification, seasonality and their interactions. Land-use and seasonality had clearly separable effects on nematode community composition. The coupling of physical microstructure properties with nematode community properties depended on land use. In cropland, nematode abundance was strongly associated with the features of the habitable pore space, such as nematode-specific porosity, pore connectivity, and particulate organic matter. Grassland nematode communities were independent of these measurable habitat properties and featured stronger co-occurrence networks. The effect of increased temperature and shifting precipitation patterns on nematode community properties were generally smaller, varied with land use and season, and were not linked to concomitant changes in microhabitat properties. Our findings indicate that characterizing microhabitat properties might be a promising approach to help explain the notorious variability in nematode community

composition. The strength of bottom-up regulation by resource accessibility could be a valuable indicator of the resilience of nematode communities to environmental stresses and perturbations.

Mengqi Wu * [a], Xiaoli Yang * [b], Thomas Reitz [c], Evgenia Blagodatskaya [c], Nico Eisenhauer [d,e], Martin Schädler [b, d], Steffen Schlüter [a]

* shared first and corresponding authorship (mengqi.wu@ufz.de, xiaoli.yang@ufz.de)

a Department of Soil System Science, Helmholtz-Centre for Environmental Research – UFZ, Halle, Germany

b Department of Community Ecology, Helmholtz-Centre for Environmental Research – UFZ, Halle, Germany

c Department of Soil Ecology, Helmholtz-Centre for Environmental Research – UFZ, Halle, Germany

c German Centre for Integrative Biodiversity Research (iDiv) Halle-Leipzig-Jena, Leipzig, Germany

e Institute of Biology, Leipzig University, Leipzig, Germany

This chapter is published in Soil Biology & Biochemistry: Wu, M., Yang, X., Reitz, T., Blagodatskaya, E., Eisenhauer, N., Schädler, M., & Schlüter, S. (2025). Microhabitat properties explain variations in soil nematode communities across climate conditions in cropland, but not in grassland. Soil Biology and Biochemistry, 201, 109657.

3.1 Introduction

Nematodes are the most diverse, abundant, and widespread soil fauna taxon on Earth (Li et al., 2020; van den Hoogen et al., 2019). They are featured in all major trophic levels of soil food webs and participate in many ecological processes (Neher, 2010; Sánchez-Moreno & Ferris, 2007; Wan et al., 2022a), thereby regulating carbon and nutrient dynamics in terrestrial ecosystems (Jiang et al., 2018; Porazinska et al., 1999; Quist et al., 2019). Thus, nematode-based indices are often considered to be valuable bioindicators of ecosystem health and functioning (Du Preez et al., 2022; Zuo et al., 2020), which is severely threatened by global change (Pecl et al., 2017). Moreover, land use intensification can threaten this ecosystem functioning and increase its vulnerability to climate extremes through annual cropping, soil tillage, pesticide, and mineral fertilizer application. These intensively managed ecosystems with low biodiversity, low functional redundancy, and lack of plant species asynchrony have fewer coping mechanisms to buffer or recover from extreme events like summer droughts (Blankinship et al., 2011; de Vries et al., 2012), cascading down to shifts in nematode communities (Cesarz et al., 2017; Lu et al., 2023; Yan et al., 2018; Zhou et al., 2022). The nematode community structure is known to be changed by land use through differences in disturbance intensity and food resource availability (Siebert et al., 2020).

Soil physicochemical properties, like pH, soil organic matter, soil texture, and soil moisture are known to be important drivers of nematode community properties (Treonis et al., 2019; van den Hoogen et al., 2019). Across various land uses at both global and local spatial scales, nematode abundances, especially those of bacterivores and plant-parasite nematodes, were associated with soil properties like sand content, pH, and soil organic carbon content (Biswal, 2022; van den Hoogen et al., 2019). However, weak effects of these soil properties were sometimes found on the diversity of soil nematodes communities in agricultural ecosystems (Li et al., 2020; Vonk et al., 2013). Potential links between soil properties and nematode communities can be disguised by the fact that both change in time but not at the same pace. Nematodes respond quickly to disturbances, environmental changes, and new resources (Bongers & Bongers, 1998; Bongers & Ferris, 1999; Neher, 2010; Zhou et al., 2022; Zuo et al., 2020), while many soil parameters change slowly. Furthermore, nematodes exhibited seasonal fluctuations resulting from changes in temperature and moisture (Papatheodorou et al., 2004; Vervoort et al., 2012). However, nematode communities can

also alter at much longer temporal scales due to climate change (Zhou et al., 2022). Climate change in Central Europe is projected to cause an increase in mean temperatures, a seasonal shift in precipitation patterns, and an increase in extreme events (Bastos et al., 2020; Lhotka et al., 2017; Madsen et al., 2014; Trenberth, 2011). The climate change effect on nematode communities does therefore not only depend on land use intensity but also on season and its interaction (Siebert et al., 2020). As a consequence, the effects of future climatic conditions and higher land use intensity on nematode abundances are either positive (Mueller et al., 2016; Siebert et al., 2020) or negative (Dong et al., 2013; Franco et al., 2022; Tsiafouli et al., 2015). It is, however, not well explored through which mechanisms these complex interactions may operate.

Clues to a better understanding of these inconclusive findings might arise from the environmental conditions experienced by the nematodes in their microhabitats. Nematode abundance and community composition are significantly influenced by features of the soil pore network because of their specific habitat requirements (Hassink et al., 1993; Jiang et al., 2017; Martin & Sprunger, 2023; Mulder & Vonk, 2011), as they rely on water-filled pores for movement (Griffiths & Caul, 1993; Jones et al., 1969) and pores of sufficient size. Nematodes, which range from 10-55 µm in diameter, with a length of 150-1500 µm (Vonk et al., 2013), can only access pores with diameters greater than their body diameter because they are unable to create pores themselves and essentially depend on existing pore space created by other larger soil organisms such as earthworms or plant roots forming their microhabitat (Erktan et al., 2020; Yvan et al., 2012). The optimal habitable pore diameter for nematode activity is in a range of 30-210 µm with some variation among soil types and textures (Erktan et al., 2020; Hassink et al., 1993; Otobe et al., 2004; Schlüter et al., 2022a). Soil pore structure regulates the sense of distance from predators to resources by affecting gas and water transport (Aochi & Farmer, 2005; Minnich, 1993), and controls the hunting of bacteria and fungi by spatial accessibility (Rutherford & Juma, 1992; Soufan et al., 2018), thereby influencing nematode resource accessibility and generating bottom-up effects on soil food webs (Neher, 2010; Wardle et al., 2004). Nematode trophic groups respond differently to the soil hydration state (Li et al., 2023c). The access of bacterivores to their prey mainly depends on the continuous water films across pores (Brussaard, 1998; Neher, 2010). Fungivores were found to be less impacted by soil water than bacterivores, since their preying efficiency is improved by fungal hyphae extending through air-filled pores (Mulder et al., 2011). Furthermore, the mobility and dispersal of nematodes in the soil are limited by pore connectivity

and tortuosity driven by pore geometry, which links to the nematode predator-prey encounter probabilities (Erktan et al., 2020; Hartmann & Six, 2022; Neher, 2010; Vargas & Hattori, 1986). However, there is thus far hardly any experimental evidence for the role of pore structure and distribution of accessible resources on nematode community composition due to technical challenges in characterizing microhabitats in intact soil. X-ray computed tomography (CT) is a well-suited technique to map the three-dimensional microhabitat of nematodes (Jiang et al., 2018; Schlüter et al., 2022a), which makes it possible to elucidate the role of soil microstructure on the nematode trophic level or community composition. However, its full potential to help explain observed shifts in nematode communities by land use intensification, climate change, seasonality and its interactions has barely been tapped.

Soil properties, climatic conditions, and land use can have a variety of effects on each other, making it difficult to study their interactions in-situ. We, therefore, made use of the combination of a unique experimental platform for the assessment of climate change effects in different land-use types (Global Change Experimental Facility – GCEF, see Schädler et al. (2019)) and the availability of X-ray CT to investigate if soil structural properties are mediators of climate and land-use induced changes in nematode communities. The objective of this study was to investigate the differences in nematode abundance and community composition between two contrasting land uses and how they are modulated by seasonality and climate change. We further aimed to explore to what extent observed differences in nematode community properties can be explained by differences in soil bulk properties and microstructure properties obtained via X-ray CT. We hypothesize that (1) perennial grassland would have higher nematode abundance and diversity than annual cropland system, that (2) the effect of climate, seasonality and their interaction on nematode community properties would be mainly mediated by soil water content, and finally that (3) soil microstructure should mediate effects of external drivers more tightly in perturbed cropland than in presumably more resilient grassland. These hypotheses were tested with topsoil from annual cropland (C) and perennial grassland (G) of the GCEF characterized by a huge variation in nematode community (Siebert et al., 2020) and microstructure properties (Schlüter et al., 2022b).

3.2 Material & Methods

3.2.1 Site description and field sampling

This study was conducted at the Global Change Experimental Facility (GCEF) in Bad Lauchstädt, Germany, a long-term field experiment with a split-plot design incorporating two climate scenarios and five land-use systems. The site features a sub-continental climate and Haplic Chernozem soils. Climate manipulation simulates projected conditions for Central Germany in 2070–2100 through adjustments in temperature and seasonal precipitation. Detailed site characteristics and experimental design are provided in **Chapter 1 Section 1.2**.

We focused on two land-use managements with the most contrasting land-use intensity in this experiment based on the GCEF: (1) conventional farming with annual crops (C) and (2) perennial grassland (G) managed as extensive meadow. Sampling was carried out in first week of November 2021 (ten weeks into the period of elevated precipitation in the future climate) and first week of June 2022 (directly after twelve weeks of elevated precipitation in the future climate) to explore the variability of potential changes in phases before and after the summer drought. Four intact soil cores per subplot were taken close to each other from a depth of 4-7 cm with aluminum rings (v = 15 cm^3, d = 2.7 cm, h = 2.7 cm). This resulted in 160 rings (20 subplots × 2 seasons × 4 replicates) which were scanned with X-ray CT and subsequently analyzed for nematode community properties. In November 2021, four additional rings were taken in each subplot and treated as unscanned controls to investigate the effect of X-ray exposure on nematodes.

3.2.2 X-ray tomography and microstructure analysis

All soil cores were scanned with an industrial X-ray microtomograph (X-tek XT H 225; Nikon Metrology, Herts, UK) set to 130 kV and 150 µA using a 0.1 mm filter for reducing beam hardening artefacts. 2500 projections with 1 frame per projection were acquired with an exposure time of 708 ms per frame. Tomograms were reconstructed in 8-bit grayscale and 15 µm voxel size using the X-tek CT Pro software (Nikon Metrology). Grayscale contrast was stretched by setting the darkest and brightest 0.2 percentiles to 0 and 255, respectively. Two out of 160 rings had to be discarded due to damage during transport.

All images were processed using the Fiji bundle for ImageJ and associated plugins according

to the methods described by Schlüter et al. (2022b). The raw data was cut into the largest possible cylindrical region of interest that contained no disturbed regions along the container wall that occurred during sampling. Vertical and radial differences in average gray value were determined within the matrix and removed from the image. The gray-scale data was segmented into pores, particulate organic matter (POM), matrix and large mineral particles using the Labkit plugin of ImageJ (Arzt et al., 2022). The classifier was trained with manual annotations on a few selected sub-volumes. The pore structure was analyzed after combining pores and POM into a single class using the standardized protocol of the soil structure library (Weller et al., 2022) that is built on the functionality of the MorpholibJ plugin (Legland et al., 2016). All above segmented images were further segmented with shape detection to obtain cylindrical biopores based on the Tubeness filter (Lucas et al., 2022; Phalempin et al., 2021). Soil material properties were POM [$mm^3\ mm^{-3}$] and POM surface area density [$mm^2\ mm^{-3}$]. Pore space features of interest were visible porosity [-], pore surface area density [$mm^2\ mm^{-3}$], the Euler characteristic (a topological number that counts isolated pore objects positively and redundant connections negatively) [mm^{-3}], connection probability [-], mean pore distance [mm], mean pore diameter [mm] and critical pore diameter [mm]. Biopore space properties were biopore diameter [mm], biopore length density [$mm\ mm^{-3}$], biopore volume [$mm^3\ mm^{-3}$]. For definitions and methodology, we refer to (Weller et al., 2022). In addition, we determined a nematode specific porosity which represents the porosity in the habitable pore size range of 30-210 µm (optimal correlation coefficient between nematode abundance and the porosity of different size range) (Schlüter et al., 2022a).

3.2.3 Nematode analysis

Soil nematode samples were extracted from approximately 30 g fresh soil per subplot using a modified Baermann method considering previous tests of the extraction efficiency at multiple field sites (including some sites in the same region; Cesarz et al. (2019)). It should be noted that the extraction efficiency of soil nematodes may depend on various environmental factors and that respective testing would be recommendable (Wiesel et al., 2015). The decision to use a 30 g soil sample in our study was based on the consideration of the cost and efficiency of the experimental conditions. The amount of soil used for nematode extraction often varies across studies, and the amount extracted in this study may be at the low end of the gradient, while it allows for repeated analyses on spatially restricted plots, optimizing both efficiency and resource use. The

morphological identification was performed by a Digital Microscope (KEYENCE VHX-2000, Japan) based on the key anatomical features such as size, stoma, esophagus, and tail shape. Additionally, we referred to the comprehensive nematode genus list published by Siebert et al. (2020) in their work on the GCEF experiment, which provided a reliable reference for identification. All extracted nematodes were identified to the genus level when the individuals were fewer than 100 in samples (in 4 out of 40 samples in total), whereas only the first 100 individuals were identified in the samples which had more than 100 individuals. The number of nematodes was transformed as individuals per 100 g of dry soil. Nematode taxa were classified into trophic groups: bacterivores, fungivores, plant-parasites, and omnivore-predators (Waldo et al., 2024; Yeates et al., 1993). Besides, nematodes were classified into c-p groups (colonizer-persister) from 1 to 5 on a linear scale according to their r and K characteristics (Bongers & Ferris, 1999). The nematode channel ratio (NCR) was calculated as NCR= B/(B+F), where B and F are the number of bacterivores and fungivores in the total soil nematode population (Yeates, 2003), that is, NCR is constrained to have values between 0 (totally fungal-mediated) and 1 (totally bacterial-mediated). The nematode maturity index (MI) was calculated as $MI=\sum v(i)f(i)$, where $v(i)$ is the c-p value of the taxon i, and $f(i)$ is the frequency of the taxon i in a sample (Bongers, 1990). MI gauges the soil ecosystem condition by the dominance of life strategies from quick responders to long generation times. The nematode channel index (CI) was calculated from the weighted proportions of fungivores of cp-2 and bacterivores of cp-1 (Sieriebriennikov et al., 2014). CI indicates whether the "fast" bacterial channel or "slow" fungal channel of energy transformation prevails in an ecosystem. The enrichment index (EI) is calculated as $EI=100*(e/e+b)$, where e is the weighted frequency of Ba_1 and Fu_2, and b is the weighted frequency of Ba_2 and Fu_2 nematodes (Ferris et al., 2001). EI is used to assess food web responses to available resources. The structure index (SI) is calculated as $SI=100*(s/s+b)$, where s is the weighted frequency of Ba_3-Ba_5, Fu_3-Fu_5, Ca_3-Ca_5, and Om_3-Om_5, and b is the weighted frequency of Ba_2 and Fu_2 nematodes (Ferris et al., 2001). The SI represents the soil food web's response to disturbance and remediation.

3.2.4 Bulk soil properties

Seasonal bulk soil properties were determined in November 2021 and June 2022 with a temporal shift from nematode sampling of only 1-2 weeks. Soil pH (air-dried soil in 0.01 M $CaCl_2$ (1:2.5 (w/v))) was determined with a pH electrode (Mettler SevenEasy pH meter, Gießen,

Germany) and total organic carbon (TOC) content was measured using an elemental analyzer (Elementar Vario EL III). Soil available phosphorus (AP) was extracted with double lactate solution (1:50 w/v, pH 3.6) and phosphate concentration was determined with molybdenum blue method (Murphy & Riley, 1962). Extractable organic carbon (EOC) was extracted from 5 g soil with 0.05 M K_2SO_4 in a 1:4 ratio and measured with Multi N/C 2100, analyzer (Analytik Jena, Germany). Microbial biomass carbon (MBC) was measured by using the chloroform fumigation-extraction method with a conversion factor of 0.45 (Brookes et al., 1985; Wu et al., 1990). Gravimetric water content was measured by weight loss upon oven drying (72 h at 40 °C) directly in the soil that was sampled for nematode analysis.

3.2.5 Statistical analysis

Linear mixed-effects models (LMMs) with random intercepts including split-plot design and repeated measures were performed to evaluate the effects of land use, climate, season, and their interactions on soil, microstructure, and nematode community properties (Sünnemann et al., 2021). Climate, land use, and season were fixed factors, season (sampling time), block (main plot) and plot (nested within main plot) served as random effects. Heatmaps between soil properties and nematode community properties as well as interaction networks among individual nematode taxa were constructed by calculating the pairwise Spearman's rank correlations. Principal coordinates analysis (PCoA) based on Bray-Curtis dissimilarity matrices was performed to visualize the effects of land use, climate, and season on the nematode community composition. Three-way permutational multivariate analysis of variance (PERMANOVA) was used to quantitatively evaluate the significance of the differences in nematode community composition and soil properties among treatments. Principal component analysis (PCA) was further performed to achieve a dimensionality reduction of soil bulk or microstructure properties driven by land use, climate, and season. The first two components of PCA based on the 11 selected soil bulk and microstructure properties were used to develop a structural equation modeling (SEM), uncovering the direct and indirect contributions of physical structural and biochemical properties to the total nematode abundance and community composition. PC1 and PC2 were considered as physical structure and biochemical property according to these factor loadings (Figure 3.3). We also completed SEM analysis to further test the role of direct and indirect contributions to the nematode abundance and community composition based on four individual feeding groups (Figure S3.4.).

The fit of the structural equation model was examined based on a nonsignificant chi-square test ($p > 0.05$), goodness of fit index, the root mean square error of approximation, and standardized root mean squared residual (Awang et al., 2015). We employed the "*lmer*" function for LMMs in "*lme4*" package (Bolker et al., 2015), the "*rda*" function for PCA, "*cmdscale*" function for PCoA and "*adonis2*" function in "*vegan*" package (Anderson, 2001) for PERMANOVA, and "*sem*" function in "*lavaan*" package (Rosseel, 2012) with application of bootstrapping for SEM. All statistical analyses were conducted using R 4.1.3. Figures were produced with the package ggplot2 (Wickham, 2011) except for the visualization of the interaction network which was produced with Gephi 0.10.1 (Bastian et al., 2009).

3.3 Results

3.3.1 Soil properties

The gravimetric water content featured a relative decrease by 32-54 % between November 2021 and June 2022 ($p < 0.001$, Table S3.2, Figure 3.1a). At the beginning of June 2022, the soil water content was higher by 15-20 % under the future climate treatment as compare to ambient climate treatment due to the additional irrigation in spring.

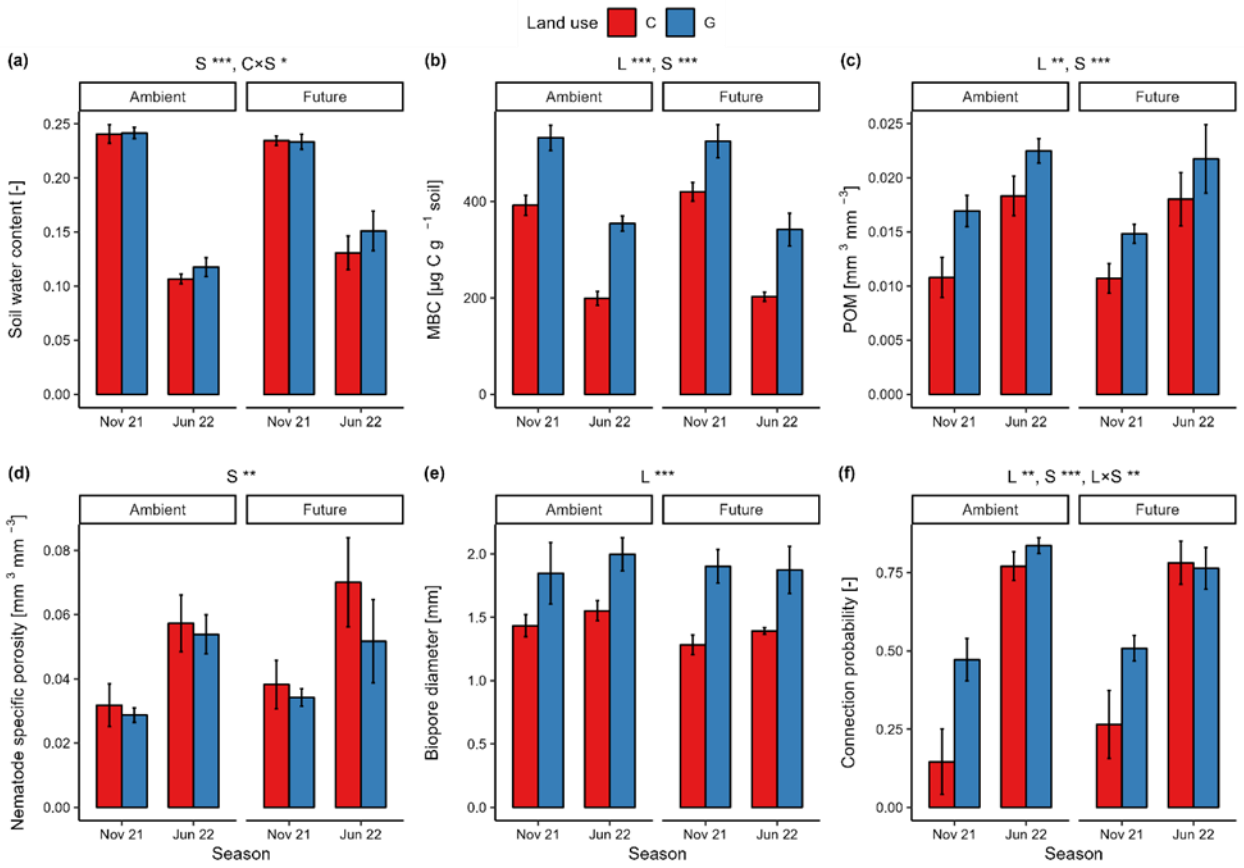

Figure 3.1 Effects of land use, climate, and season on the soil properties (a) soil water content, (b) microbial biomass carbon (MBC), (c) particulate organic matter (POM), (d) nematode specific porosity, (e) biopore diameter, and (f) connection probability. Values are arithmetic mean ± standard error (n = 5). C and G represent annual cropland and perennial grassland, respectively. Nov 21 and Jun 22 represent November 2021 and June 2022, respectively. Significant differences between land use (L), season (S), interaction of season and climate (C×S) are indicated by * ($p < 0.05$), ** ($p > 0.01$), and *** ($p < 0.001$).

Total organic carbon (TOC) content in the perennial grassland was 10-14 % greater than in annual cropland ($p < 0.001$, Table S3.1-3.2), but not affected by climatic conditions (climate and season). The difference in volumetric particulate organic matter (POM) content between land uses even amounted to 22-55 % ($p = 0.003$, Figure 3.1c), and in addition also increased by 29-64 % from November 2021 to June 2022 ($p < 0.001$) contributed by root growth. Microbial biomass carbon (MBC) was affected by land use ($p < 0.001$) and season ($p < 0.001$), with 25-78 % higher levels in the perennial grassland as compared to annual cropland and 51-108 % higher levels in November 2021 than in June 2022 regardless of climate (Table S3.2, Figure 3.1b). Extractable organic carbon (EOC) content was more complexly regulated due to the combined effect of

precipitation and irrigation, so that it was affected by land use ($p = 0.002$), season ($p = 0.024$), and the interaction of climate with land use and season and its combination (Table S3.2). More specifically, 85 % higher EOC contents in the perennial grassland as compared to annual cropland only occurred under the ambient climate treatment in June 2022 (Table S3.1).

3.3.2 Microstructure properties

The visual assessment of the soil microstructure revealed that the morphology and origin of pores and POM were very different between the perennial grassland and annual cropland treatments, with more incorporated plant litter in the annual cropland and more intact roots in the perennial grassland (Figure 3.2a, c). Microcracks seemed to have formed at lower soil moisture in June 2022, but not in November 2021 (Figure 3.2a, b). A climate treatment effect was not observed.

This visual impression was supported by quantitative microstructure analysis. The nematode-specific porosity in the habitable size range was 53-125 % higher in June 2022 as compared to November 2021 ($p = 0.002$), irrespective of land use and climate treatments (Figure 3.1d), and was to a large part contributed by microcracks.

The mean biopore diameter ranged between 1.28 and 2.00 mm and was 29-48 % higher in the perennial grassland as compared to annual cropland (Figure 3.1e, Table S3.2), mostly likely due to a higher abundance of large biopores.

The connection probability was affected by land use ($p = 0.003$), season ($p < 0.001$) and the interaction of land use and season ($P = 0.009$) (Figure 3.1f, Table S3.1), with 8-223 % higher levels in the perennial grassland as compared to annual cropland and 50-428 % higher levels in June 2022 than in November 2021 regardless of climate. For the same visible porosity, the pore structure formed under perennial grassland was more continuous. Moreover, the microcracks that were present in June 2022 induced a higher connection probability than in November 2021. The land-use effect was stronger in November 2021, when micro-cracks were absent.

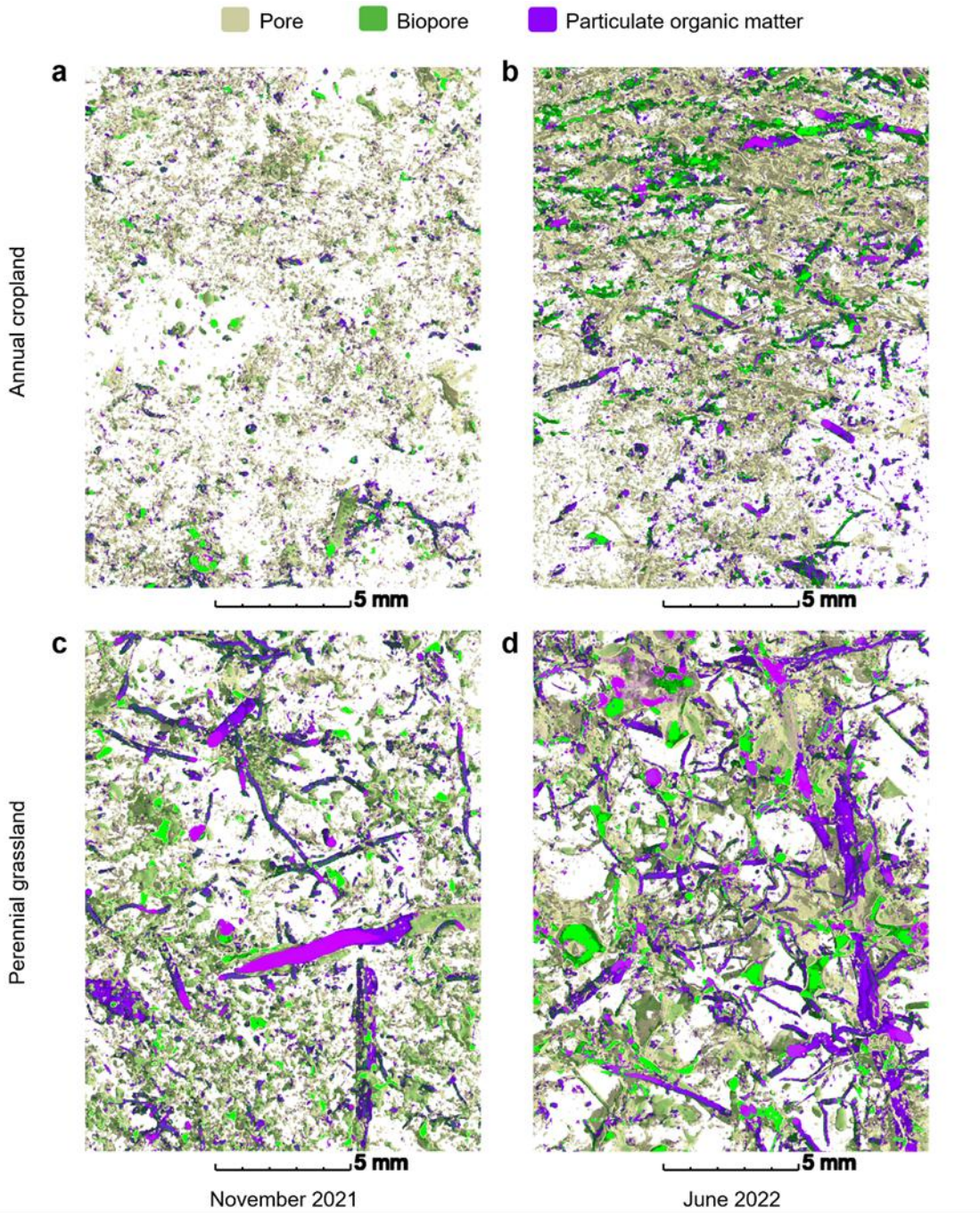

Figure 3.2 Representative segmented 3D soil microstructure images under different land uses and seasons. (a) annual cropland in November 2021, (b) annual cropland in June 2022, (c) perennial grassland in November 2021, (d) perennial grassland in June 2022. The thin volumes have a dimension of 19.4 × 14.7 × 1.5 mm (height × width × depth) to reduce the amount of visible feature.

Many of other microstructure properties (Table S3.1, S3.2) were somewhat redundant and highly correlated, e.g. nematode-specific porosity and visible porosity, mean biopore diameter and

mean pore diameter, biopore length density, and pore surface area density, etc. Critical pore diameter was more sensitive to climate than the properties in Figure 3.1, with on average larger values for the ambient treatment, but the climate effect was again much weaker than the land use and season effect.

A principal component analysis revealed a clear clustering of treatments mainly according to land use and season, and barely according to climate (Figure 3.3). The first principal component accounted for 52.2 % and the second for 23.2 % of the total variance. The highest loadings of the first component (PC1) were mainly but not exclusively related to the physical and structural properties, like connection probability (+1.74), nematode specific porosity (+1.66), biopore volume (+1.64), soil water content (−1.60), and pore surface area density (−1.57). In turn, the highest loadings of the second component (PC2) were mainly but not exclusively related to the biochemical properties, like biopore diameter (−2.27), TOC (−2.22), MBC (−1.74), critical pore diameter (−1.56), and Euler characteristic (+1.30). Average biopore diameter carries information about the spatial domain, but at the same time has a biological origin and is elevated in perennial grasslands. POM contents had similar loadings on both components as it serves both as a habitat and food resource. The land use effect and season effect were clearly separated from each other. The effect of season was mainly associated with PC1, and the land-use effect was mainly associated with PC2, i.e. they had diagonal orientation in the bi-plot and were orthogonal to each other (Figure 3.3).

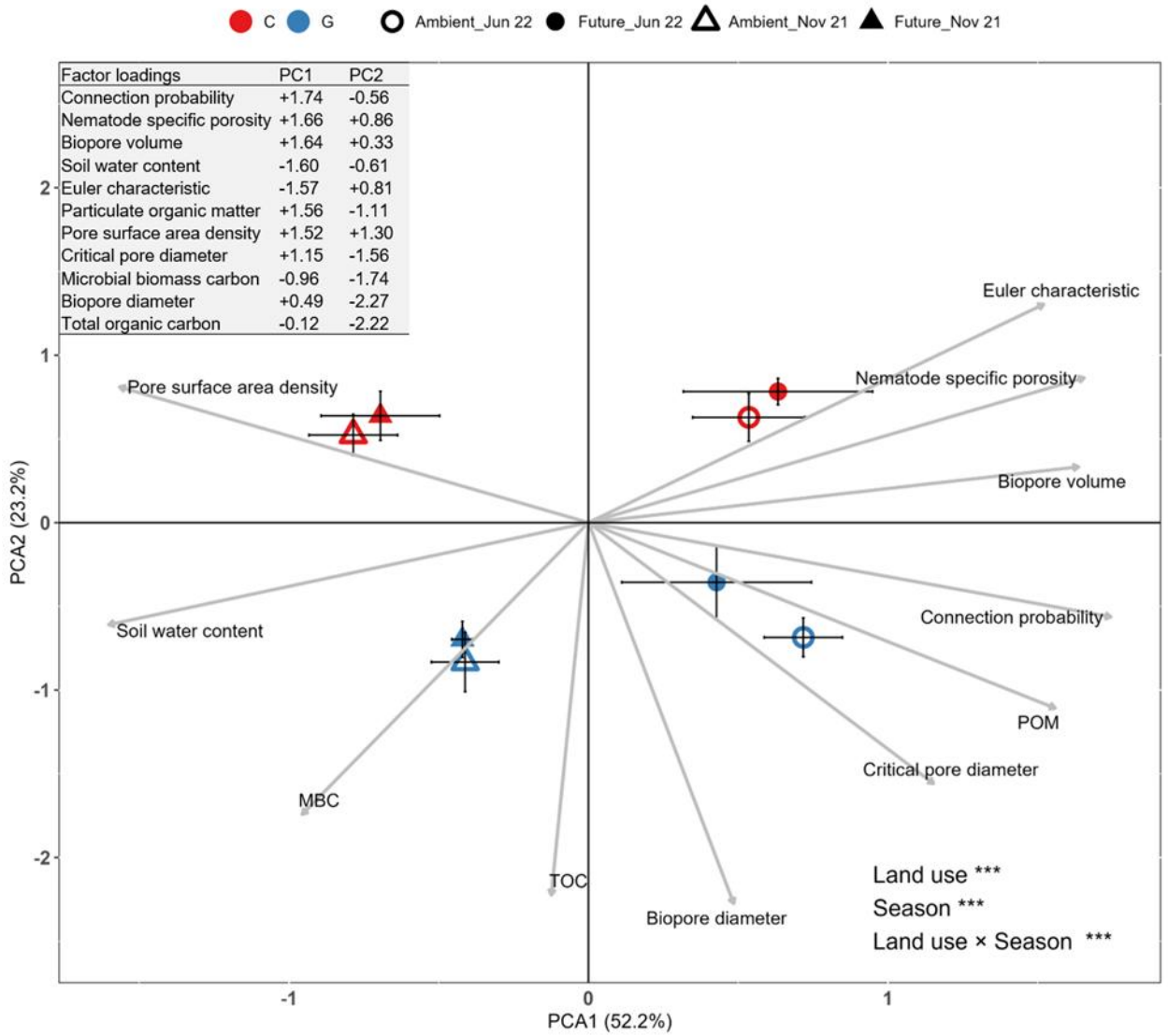

Figure 3.3 The first two principal components based on bulk soil variables, and soil microstructure properties as influenced by land use, climate, and season. C and G represent annual cropland and perennial grassland, respectively. Nov 21 and Jun 22 represent November 2021 and June 2022, respectively. A and F represent ambient and future climate treatments. POM, particulate organic matter; MBC, microbial biomass carbon; TOC, total organic carbon. Results of three-way PERMANOVA are shown in the bottom, right corner of figure. ***: $p < 0.001$.

3.3.3 Nematode community properties

There were hardly any differences in nematode community properties between samples with and without X-ray radiation (Figure S3.1), indicating that even if the dose of a single scan was harmful, it did not have an effect on nematode counts shortly after.

Land use and seasonality had clearly separable effects on nematode community properties. Seasonality mainly manifested itself in lower richness in June 2022 for most feeding groups and the same trend for total richness (p = 0.053) and similar tendencies for diversity (Table S3.3), but hardly affected abundances except for higher bacterivore abundance in June 2022. Land use, in turn, had a strong effect on abundances, feeding-group specific and total, but no effect on any other community properties (Table S3.4). Nematode abundance in perennial grassland was 10-147 % higher than in annual cropland (Figure 3.4a, $p < 0.001$). This increase was strongest for plant-parasites and bacterivores (Figure 3.5a) and thus also for the nematode channel ratio (NCR, Figure 3.4b), which balances bacterivores against fungivores. The land-use effect on NCR was highest under ambient climate in November 2021 and under future climate in June 2022.

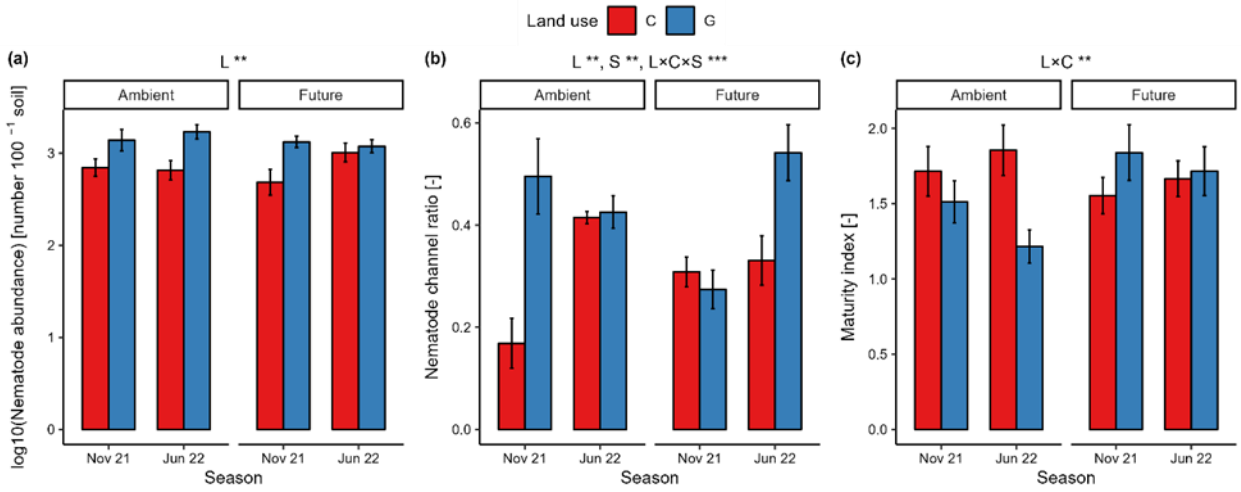

Figure 3.4 Effects of land use, climate, and season on the soil nematode properties (a) $\log_{10}$(nematode abundance), (b) nematode channel ratio, and (c) Maturity Index. Values are arithmetic mean ± standard error (n = 5). C and G represent annual cropland and perennial grassland, respectively. Nov 21 and Jun 22 represent November 2021 and June 2022, respectively. Significant differences between land-use (L), season (S), interaction of land-use and season (L×S), interaction of season and climate (C×S), interaction of land-use, climate and season (L×C×S) are indicated ** ($p > 0.01$) and *** ($p < 0.001$).

The nematode maturity index (MI) was higher in perennial grassland than in annual cropland but only under future climate (Figure 3.4c). Surprisingly, the order changed under ambient climate regardless of season. The interaction effects were more complex for the enrichment index (EI), as the EI was higher, indifferent, or lower in perennial grassland than in annual cropland depending on season and climate scenario (Table S3.3).

The composition of nematode community had a similar clustering (Figure 3.5b) to the bulk and microstructure properties of soil (Figure 3.3) with a clear separation of land use and season effects. In contrast to soil properties, a climate effect was evident in the nematode community composition in particular for the perennial grassland in June 2022, for which the difference in soil water content between ambient and future climate was highest.

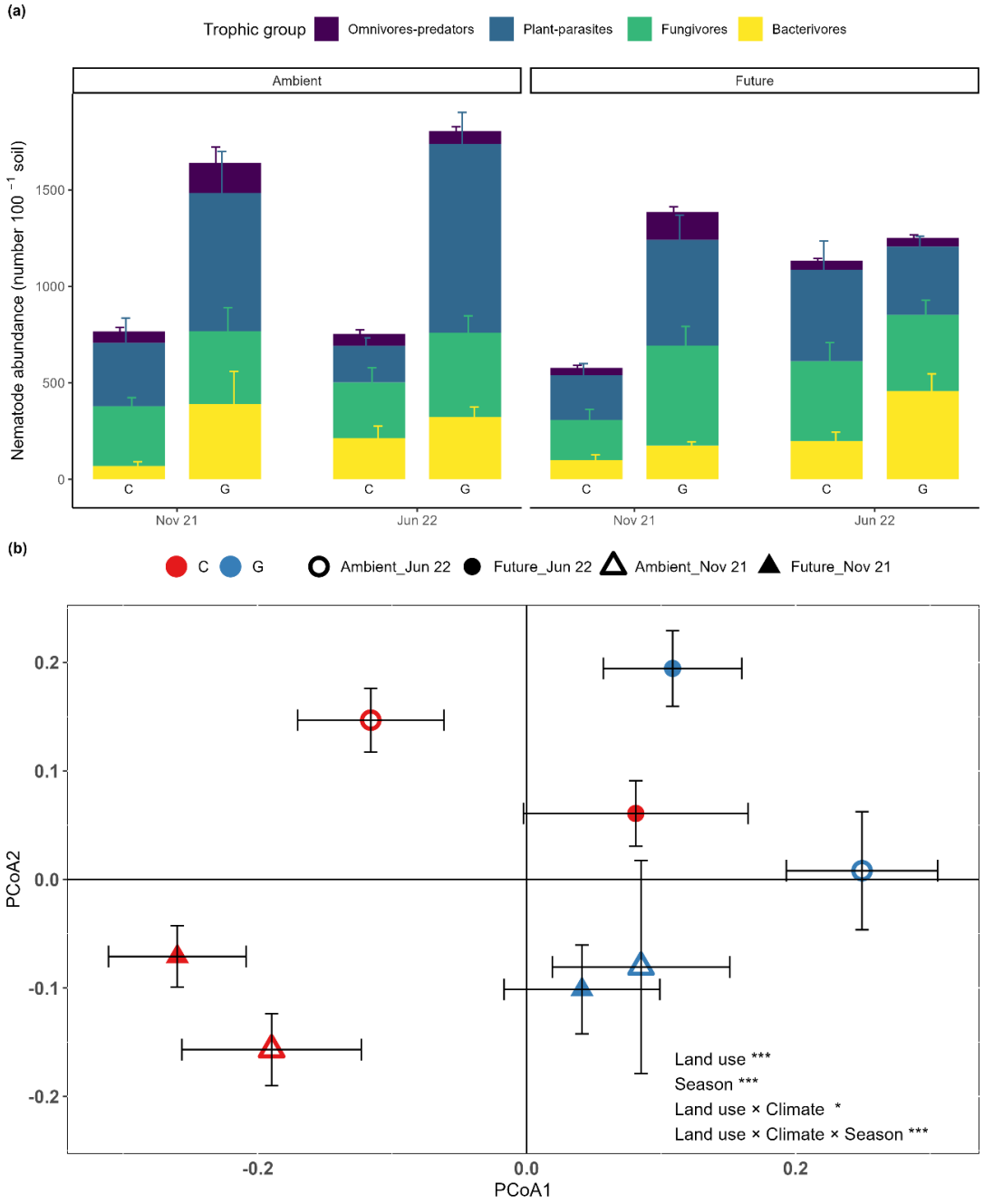

Figure 3.5 (a) Absolute nematode abundance in all combinations of land use, climate, and season

partitioned into different trophic groups. Nov 21 and Jun 22 represent November 2021 and June 2022, respectively; (b) Principal coordinates analysis (PCoA) of nematode community (taxa level). Nov 21 and Jun 22 represent November 2021 and June 2022, respectively. C and G represent annual cropland and perennial grassland, respectively. Significant differences between land, climate, season and their interactions are indicated by * ($p < 0.05$), and *** ($p < 0.001$).

3.3.4 Relationship between soil properties and nematode community traits

Pair-wise correlations indicated a tight association of nematode abundances with microstructure properties across land uses and climatic conditions (Figure S3.2a). In particular, bacterivore and total nematode abundance were positively associated with all pore connectivity metrics like connection probability, critical pore diameter, and Euler characteristic, whereas the associations of fungivore and plant-parasite abundance were weaker or minimal. Biochemical soil properties were poorly correlated with nematode abundances. Likewise, nematode community properties beyond abundances showed hardly any correlation with bulk soil and microstructure properties, when all land uses and seasons were considered. Within individual seasons, the patterns changed slightly, e.g. biochemical properties like MBC and POM became better predictors for plant-parasite and bacterivore abundances in both seasons (Figure S3.2b-c).

A structural equation model (SEM) for selected nematode community properties (initial model in Figure S3.3, final model in Figure 3.6) was built to address whether the effect of the external drivers (land use, season, climate) on nematode community properties would be direct or indirect and thus be manifested by links with the physical structure or biochemical soil properties. The SEM confirmed that land use had a significant effect on the principal component associated with biochemical properties (PC2) and season had a significant effect on the principal component associated with physical and structural properties (PC1), each with high correlation coefficients (0.80-0.89) (Figure 3.6), while climate had a negligible effect (path removed in the final model). Land use had a direct effect on total abundance and nematode community composition (Figure 3.6) that could only to a lesser degree be explained by the investigated soil properties, whereas the effect of season on total abundance and community composition was mainly indirect and brought about by the seasonal change in pore structure. The degree of explained variation in total nematode abundance ($R^2 = 0.32$) and community composition (first component of the principal coordination analysis, $R^2 = 0.58$) by the model was moderate and much lower than the explained variability of pore structure properties ($R^2 = 0.66$) and biochemical properties ($R^2 = 0.82$). A more diversified

pattern emerged when the SEM was conducted for individual feeding groups (Figure S3.4). The direct coupling with land use and indirect coupling with season through habitat properties was stronger for bacterivores and fungivores than for omnivore-predators.

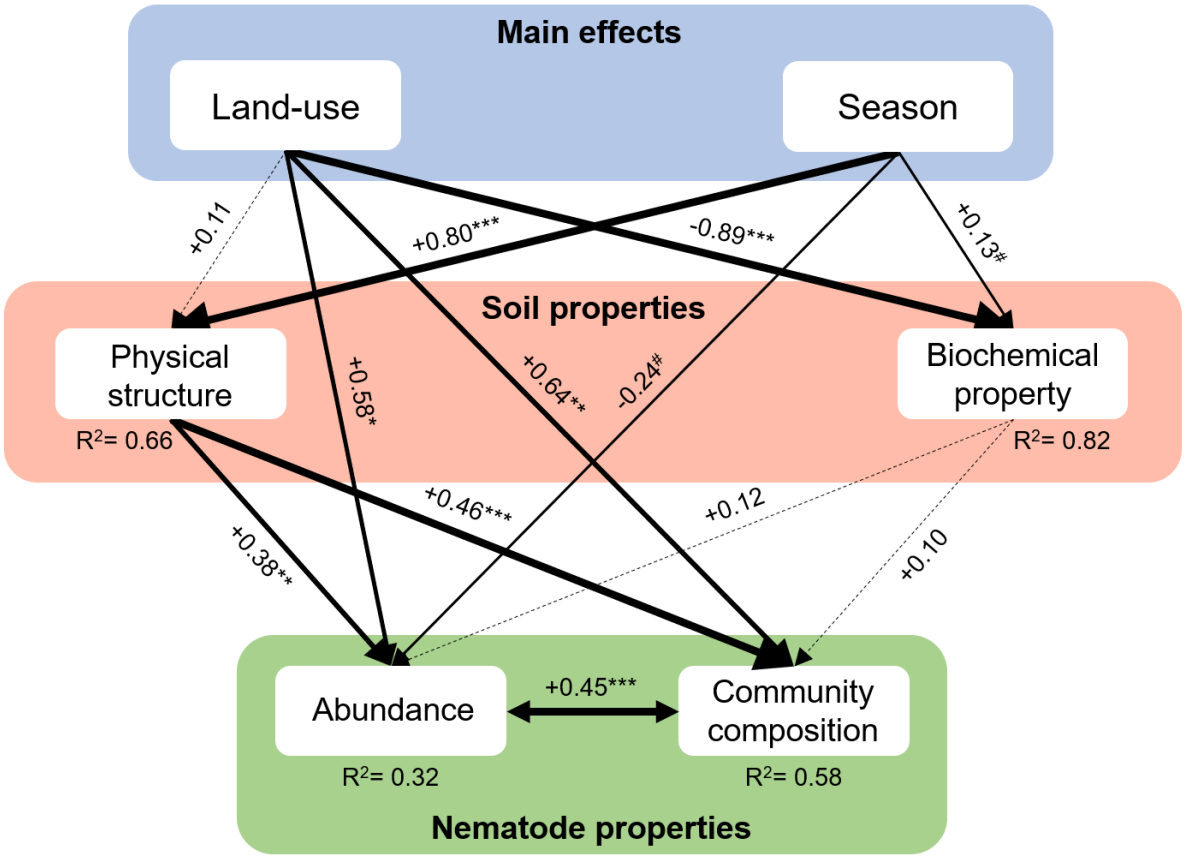

Figure 3.6 Structural equation model depicting how land use and season affect nematode abundance and community composition and how far these are mediated by soil properties. Numbers next to arrows indicate standardized path coefficients (robust standard errors of coefficients). Solid lines indicate significant relationships, and dash lines indicate non-significant pathways ($p > 0.1$). Lines with double-sided arrows indicate potential relationship between covariances. #, *, **, *** indicate significant differences at 0.1, 0.05, 0.01 and 0.001 levels, respectively. The parameters of model are $\chi^2 = 0.084$, GIF = 0.999, $p = 0.959$, RMSEA = 0.000, SRMR = 0.005 (n = 40, bootstrap = 1000).

An even clearer pattern emerged when linking nematode community properties with soil properties separately for each land use. In annual cropland, the association of nematode abundances with a range of microstructure properties was very strong for bacterivores and fungivores and total nematode abundance, but not for omnivore-predators and plant-parasites, suggesting other limitations at this higher trophic level. Moreover, community indices (EI, SI, CI, MI) showed hardly any correlation with soil properties (Figure 3.7a). In grassland, the strong

association of nematode abundances with microstructure properties vanished completely (Figure 3.7b). Only a few associations for feeding-group-specific richness and diversity with soil water content and microbial biomass remained. Interestingly, this land-use effect was reversed, when considering the complexity of the nematode co-occurrence network at the taxon level (Figure 3.7c, d). The perennial grassland showed 21.6 % and 21.9 % higher average connectivity and graph density of nematode co-occurrence network compared to the annual cropland (Table 3.1). Thus, there are more nematode species linked with each other and stronger similarity of environmental preferences and mutualistic relationships in the nematode taxa in grassland. The average path length and modularity followed the opposite trend, indicating that nematode species are more closely linked and the co-occurrence network of grassland consists of more integrated subgroups of nematode species.

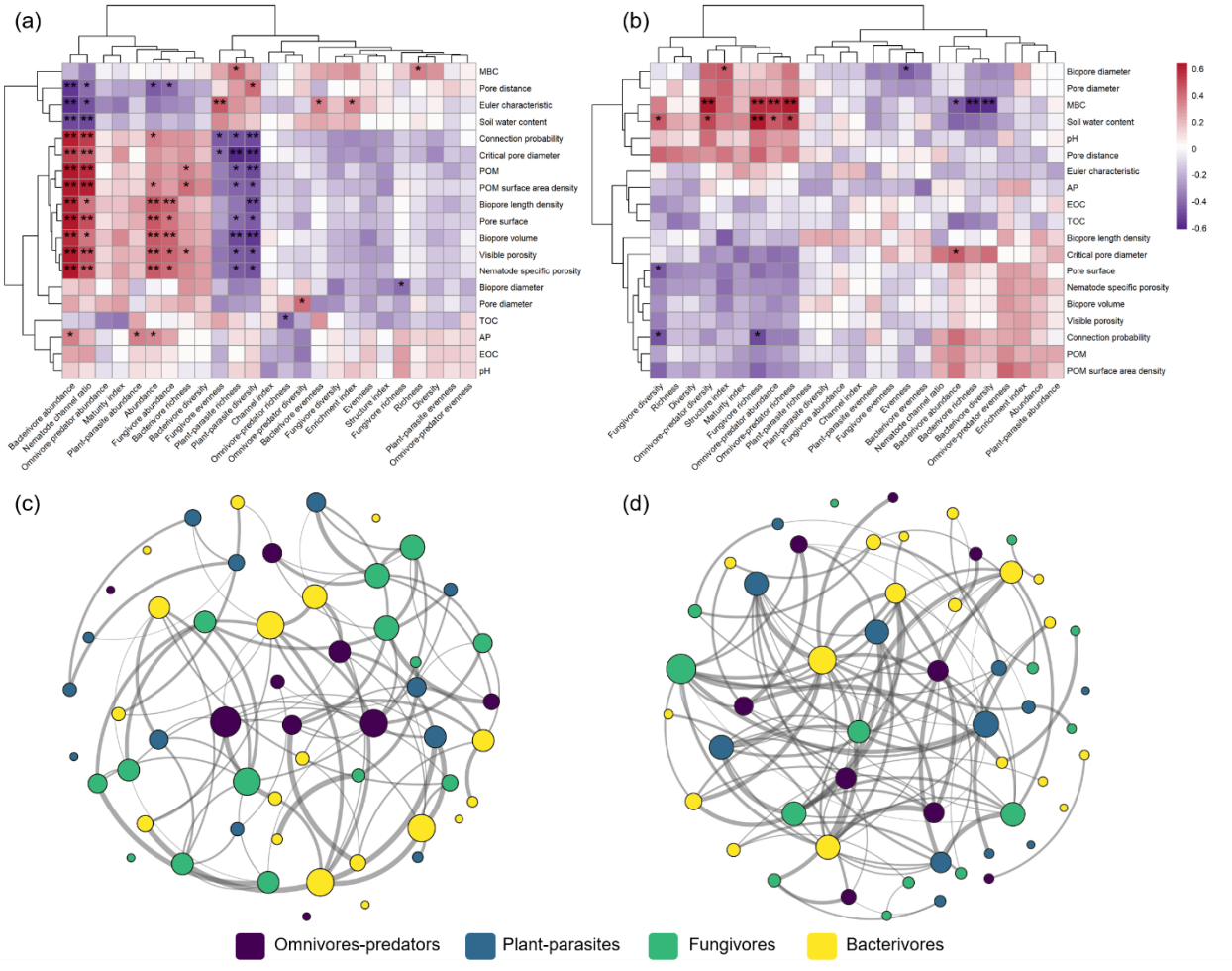

Figure 3.7 Spearman correlation analysis between nematode properties and bulk soil variables and soil

microstructure properties as influenced by land use: (a) annual cropland, (b) perennial grassland. POM, particulate organic matter; MBC, microbial biomass carbon; TOC, total organic carbon; EOC, extractable organic carbon; AP, available phosphorus. *, ** indicate significant differences at 0.05 and 0.01 levels, respectively. Interaction networks among soil nematode taxa between different land uses: (c) annual cropland, (d) perennial grassland. A connection stands for a strong (Spearman's ρ >0.5) and significant (P < 0.05) correlation for two individual nematode taxa. The taxa are colored by feeding groups. For each panel, the size of each node is proportional to the number of connections, and the thickness of each connection between two nodes is proportional to the value of Spearman's correlation coefficients.

Table 3.1 Topological properties of co-occurring nematode taxa networks obtained under two land uses.

Network metrics	annual cropland	perennial grassland
Number of nodes	53	53
Number of edges	88	107
Average connectivity	3.321	4.038
Average clustering coefficient	0.349	0.267
Average path length	3.463	3.295
Network diameter	8	9
Graph density	0.064	0.078
Modularity	0.627	0.422

3.4 Discussion

3.4.1 Land use, seasonality, and climate effects on soil physicochemical and nematode community

Bulk and microstructure properties differed significantly between land uses, thus creating distinct microhabitats for nematodes. Carbon inputs and microbial activity, reflected by TOC, POM, EOC and MBC content, were greater under the perennial grassland as compared to annual cropland (Hu et al., 2024; Johansson et al., 2023; Rui et al., 2022). Pore connectivity and average biopore diameter were significantly higher under the perennial grassland due to the higher rooting density, carbon input, biological activity (DuPont et al., 2010; Huang et al., 2023; Li et al., 2024b; Rui et al., 2022), and no structure disturbance by plowing (Schlüter et al., 2022b). Our study supports the first hypothesis that compared to annual cropland, perennial grassland had higher

nematode abundance, with NCR closer to bacterial decomposition pathways due to the higher carbon resources and lower disturbance. Furthermore, our results showed that microbial-feeding and plant-feeding nematode abundance increased in perennial grassland compared with annual cropland since these typically increase with plant species richness and functional diversity, providing a wide range of ecological niches for nematodes (Cortois et al., 2017; Eisenhauer et al., 2017; Hooper et al., 2000; Siebert et al., 2020). Additionally, the repeated disturbance by plowing in annual croplands is known to reduce nematode abundance and altered nematode community and food web structure through environmental disturbance (Landi et al., 2018; Lenz & Eisenbeis, 2000; Zhang et al., 2015).

The shift of nematode community is governed by environmental disturbance, which is also driven by climatic conditions, including the combination of seasonal dynamics and climate treatment. In our study, the seasonality effect was evident for soil water content and many individual microstructural properties related to it, demonstrating that soil structure is not static. Therefore, the habitable pore space of nematodes does not only change with water content, but also due to crack formation, root growth, faunal activity, and tillage (Bronick & Lal, 2005; Meurer et al., 2020; Pires et al., 2017). Unlike land-use and seasonality, climate change showed only subtle effects on microstructure properties (Table S3.1). This is in contrast to findings by Peng et al. (2022), who reported double soil porosity and triple pore number differences within soil aggregates under large-scale climate gradients with 0.15-fold mean annual precipitation and double annual temperature, probably because the climate modulation at the GCEF is much subtler, featuring only slightly higher average temperatures (up to 1.14 °C), as well as 10 % increased precipitation in spring and fall in combination with 20 % precipitation reduction in summer. The climate effect manifested itself in a soil water content surplus in June thereby also diluting EOC contents, especially in perennial grassland. The summer shortage and fall surplus caused no differences in soil water content between climate treatments in November, as all soils were already at field capacity. Hence, climate mainly affects microhabitat properties by modulating the water-filled pore space available to nematodes, which changes much more drastically with season.

Seasonality affected species richness and also induced a shift in community composition, interestingly without changing the total nematode abundance. A severe decline in nematode survival and reproduction was only reported for a soil water content of 5-10 % (Kardol et al., 2010), which was not yet reached in June. Consistent with our second hypothesis, the climate effect on

nematode community composition was most evident for grassland in June, for which the differences in soil water contents were also highest.

In summary, the large and expected variation of microhabitat and nematode community properties with land use intensity and climatic conditions at the GCEF, rendered this dataset as a suitable basis for testing the strength of bottom-up regulation of nematodes by the habitable pore space and resource accessibility.

3.4.2 Links between soil properties and nematode community properties

The third hypothesis was also confirmed by the data. There was no universal relationship between nematode community properties and microhabitat properties across land uses, climate treatments, and seasons. Instead, the coupling of nematode abundance with microhabitat properties was much stronger under high land-use intensity in which the nematode community is less stable against environmental perturbations. The strong association of bacterivore and fungivore abundance (but not plant-parasite and omnivore-predator abundance) with a number of macrohabitat properties across all seasons and climate treatments indicates that the effect of climatic conditions on nematodes at lower trophic levels is clearly mediated by bottom-up regulation through microhabitat properties in these disturbed systems. This bottom-up regulation is further substantiated by the strong or missing association of soil water content with bacterivores and fungivores, respectively (Finlay & Thorn, 2019; Jamieson et al., 2002; Shao et al., 2015). Pore connectivity significantly affects the spatial distribution of bacteria (Juyal et al., 2020) and rate of fungal hyphal growth (Pajor et al., 2010). Therefore, the connectivity of soil pores can modulate the establishment of bacterivore and fungivore nematode communities after disturbances. Increasing pore connectivity can also enhance interactions between nematodes and predators, thus facilitating top-down regulation (Erktan et al., 2020). However, clear causal effects are hard to derive from these associations. Just because microcracks formed more connected pore networks in June, does not mean that these microcracks would constitute a good habitat for nematodes, as they are air-filled and presumably have low resource availability. In general, the impact of the habitable pore space on nematode abundance should be large, when it limits their existence and movement in soil, e.g. in compacted or dry soil (Bouwman & Arts, 2000; de Oliveira Cardoso et al., 2012; Fujimoto et al., 2010). Moreover, the estimation of the habitable pore space and its association with nematode community properties might differ between studies with different

sampling techniques. Intact soil cores as in this study may contain a lot of inter-aggregate pores especially in plowed soil, which are probably less favorable for nematodes even though they are in the habitable pore size range (Erktan et al., 2020; Neher et al., 1999), whereas studies with individual soil aggregates (Jiang et al., 2017; Jiang et al., 2018; Schlüter et al., 2022a) deliberately do not probe these pores.

Strikingly, the combined impact of season and climate treatment on nematode community properties was not mediated by the investigated bulk soil and microhabitat properties at all in perennial grassland. Perennial grassland seemed to be regulated by other processes, e.g. top-down regulation by predators (Chen et al., 2013; Erktan et al., 2020). Furthermore, a salient feature of the nematode community in perennial grassland was the higher connectivity of its co-occurrence network at the taxa level, which was consistent with previous findings that land-use intensification resulted in lower-density networks (Creamer et al., 2016; Liu et al., 2023) and that more resilient nematode communities related to high-diversity grasslands (Cesarz et al., 2017). The complexity of plant-soil-nematode feedbacks in the field poses a challenge for determining the primary drivers for nematode abundance (van der Putten et al., 2016). More complex network structure among nematode taxa under perennial grassland may be a potential reason for higher elasticity and resilience of the nematode community and a stronger decoupling from environmental microhabitat properties (Felipe-Lucia et al., 2020). Other community traits like the maturity index, channel index, structure index, or enrichment index hardly correlated with any of the investigated soil properties (Figure S3.2). Apparently, they were much more affected by random variation or regulated by other processes, which were not correlated with the investigated treatments and soil properties. Soil temperature, sand content, micronutrient content, plant cover, and predation pressure may be the potential main drivers (da Silva et al., 2020; Li et al., 2023c; Zhou et al., 2022).

Hardly any attempts have been made so far to relate nematode community properties to image-derived properties of their habitats by X-ray CT. This study is only the second after Schlüter et al. (2022a) that we are aware of. The simple relationships between morphological microhabitat features and nematode community traits found by Schlüter et al. (2022a) in irrigated vineyard soils for one sampling date was at odds with the more complex regulation across land uses, climate treatments, and seasons at the GCEF. More microhabitat studies on intact field soils from long-term trials are necessary to substantiate, under which conditions nematode community properties

are expected to decouple from microhabitat properties. Such future studies should jointly consider bottom-up and top-down effects on soil food webs.

3.5 Conclusion

Land use and seasonality had clear and separable effects on the nematode community and soil properties, whereas climate modulations towards future climatic conditions featured complex interactions with the former. Higher land-use intensity caused decreased biopore diameter, lower pore connectivity, particulate organic matter content, microbial biomass carbon, and at the same time lower nematode abundance and weaker nematode community co-occurrence networks. Bacterivore and fungivore abundances were strongly associated with features of the habitable pore space across seasons and climate treatments in periodically disturbed annual cropland, but not in perennial grassland. The coupling of microhabitat properties with nematode community properties therefore depended on land-use intensity. Our work adds to the understanding of bottom-up regulation of nematode community traits by microhabitat properties under field conditions.

4 Linking soil structure and root growth across land use systems and climate conditions

Abstract

Root-soil structure interactions play a critical role in regulating plant productivity, water and nutrient cycling, and overall soil health. These interactions are shaped by both land-use systems and climate change, which alter root system traits and soil physical properties through changes in vegetation composition, disturbance regimes, and environmental conditions. However, the extent to which root traits influence and respond to soil microstructure under varying land-use intensities and future climate scenarios remains poorly understood. Here, we combined non-destructive X-ray CT to quantify soil structural and root-derived traits with destructive root analysis using WinRhizo to assess root traits, thereby linking soil structure and root growth in a field trial comprising five land-use types (two croplands and three grasslands) under ambient and future climate scenarios. The future climate scenario reflected regional projections of increased temperature and modified precipitation regimes. Measurements were carried out in the spring of a dry year (2022) with lower and a normal year (2023) with higher water availability. We found that grasslands consistently maintained higher root length density (RLD), bioporosity, and pore connectivity than croplands, reflecting the influence of perennial root systems and reduced disturbance. In croplands, RLD was more strongly correlated with soil moisture and bulk density than grasslands, likely reflecting that root proliferation in croplands were more sensitive to changes in the soil physical environment. Moreover, the feedback of root growth on soil structure varied with root diameter, with finer roots contributing more to biopore formation and connectivity due to their higher abundance and ability to penetrate soil, particularly under dry conditions, whereas, thicker roots were less abundant and often followed pre-existing macropores. The future climate scenario had limited effects on root or soil structural traits due to its modest shifts in temperature and precipitation regimes. These findings advance our mechanistic understanding of root-soil interactions to support ecosystem resilience under land-use intensification and climate change.

4.1 Introduction

Soil structure and root growth are fundamental components of soil health and ecosystem functioning (Fatichi et al., 2020; Gregory, 2006). Their interaction governs key soil processes such as water and nutrient cycling, biological activity, and plant productivity (Jin et al., 2017; Meurer et al., 2020). Soil structure directly influences root growth by determining the physical accessibility of pores, air, and water. Maintaining an intact and connected soil structure is essential for supporting a functional root system, whereas structural degradation, such as compaction and crusting, can severely restrict root penetration and resource acquisition (Bengough, 2003; Xiong et al., 2022b). In turn, root growth and turnover actively modify soil structure dynamics through mechanical and biochemical processes (Lucas, 2021). As roots grow, they create and expand pores, displace soil particles, and secrete exudates that stimulate aggregation and microbial activity (Giuliani et al., 2024). Root decay further contributes to biopore formation and organic matter incorporation (Wendel et al., 2022; Witzgall et al., 2024). The bidirectional relationship between root growth and soil structure is both complex and dynamic, encompassing the formation of biopores, rhizodeposition, and aggregate stabilization processes (Lucas, 2021; Mueller et al., 2024). Understanding these interactions is critical for optimizing soil health and informing sustainable land management practices.

Root-soil structure interactions are not static but are strongly modulated by land use and climate change, which shapes plant community composition, rooting patterns, and the frequency and intensity of soil disturbance (Frouz, 2024; Meurer et al., 2020; van der Putten et al., 2013). Grasslands and croplands represent two contrasting land-use systems that differ fundamentally in their vegetation characteristics, root system architecture, and management regimes (Le Provost et al., 2021; Schädler et al., 2019; Yu et al., 2025). Perennial grasslands typically support dense, fibrous root systems that persist across seasons, continuously contributing to the formation and the stabilization of biopore networks (DuPont et al., 2014; Jiang et al., 2023). These systems are generally characterized by minimal soil disturbance, which allows for the gradual development of structurally connected pore networks. In contrast, annual croplands are subject to frequent mechanical disturbances, such as tillage and harvesting, which can disrupt soil structure and existing pore channels, and weaken root-structure feedbacks (Lynch, 2019; Or et al., 2021). Moreover, fallow periods without active root growth in many cropping systems interrupt the

continuous biological processes essential for sustaining and regenerating pore connectivity and structural integrity (Han et al., 2015; Quigley & Kravchenko, 2022). In addition to land-use effects, climate change introduces further complexity into root-soil interactions, particularly through shifts in temperature and precipitation patterns that alter soil moisture availability and biological activity (George et al., 2024; Jin et al., 2017). Elevated temperatures influence root growth and soil structure by increasing root metabolic rates and elongation, while simultaneously accelerating organic matter decomposition and microbial activity, which can destabilize soil aggregates and modify pore networks (Patah & Othman, 2024; Yin et al., 2013). Changes in precipitation patterns primarily affect root and soil structure through shifts in soil moisture availability, which regulates root elongation, branching, and vertical distribution (Yaffar et al., 2024). Prolonged drying may enhance soil mechanical impedance and limit biopore formation, whereas excessive wetting can reduce aggregate stability and oxygen diffusion, both of which constrain root development and disrupt soil structural integrity (Lozano et al., 2022; Pires et al., 2020). Although land-use and climate change effects on aboveground productivity and root plasticity are well documented (Colombi et al., 2024; Hiernaux et al., 2009), the responses of root-soil structural dynamics to climatic variability remain poorly understood. In particular, the extent to which root traits, such as length, diameter, and spatial distribution, both influence and respond to soil microstructural properties across varying land-use intensities under future climate scenarios has received limited empirical investigation.

Recent advances in X-ray computed tomography (CT) have enabled non-destructive, high-resolution quantification of soil pore structure and root architecture in three dimensions (Lucas et al., 2022; Phalempin et al., 2025). This technique allows for the simultaneous measurement of key structural traits, including root diameter and integrity, bioporosity, and pore connectivity, within undisturbed soil cores (Phalempin et al., 2025; Weller et al., 2022). Despite its potential, few studies have applied X-ray CT in field-based experiments that incorporate both land-use intensity and climate treatments, especially in temperate agroecosystems. There is a clear need for integrated approaches that move beyond static characterizations of soil or root traits, toward mechanistic investigations of their coupled dynamics.

The objective of this study was to investigate how climatic variations influence the soil structure-root interactions under different land-use systems and how these patterns are affected by a future climate scenario involving modified seasonal precipitation regimes and higher temperature.

We integrated non-destructive X-ray CT with traditional destructive root coring and scanning via WinRhizo to comprehensively investigate root-soil structure interactions in cropland and grassland systems under ambient and future climate scenarios at the Global Change Experimental Facility (GCEF) in Central Germany. Soil cores were collected over two contrasting spring seasons, a dry year (2022) and a normal year (2023), to investigate how land use and climate conditions jointly influence root development and soil microstructure. Specifically, we tested the following hypotheses: (1) grasslands will show higher microstructural stability and more developed root systems than croplands due to the presence of perennial vegetation and the absence of tillage, (2) under dry conditions, root growth in croplands becomes more dependent on existing pore networks than in grasslands, due to lower structural stability and the absence of perennial root systems, (3) the feedback of root growth to soil microstructure is closely dependent on the root diameter, with finer roots more strongly contributing to the formation and stabilization of pore networks.

4.2 Material & Methods

4.2.1 Study site and experimental set-up

The study was conducted at the Global Change Experimental Facility (GCEF) in Bad Lauchstädt, Germany, which combines two climate scenarios with five representative land-use types in a large-scale split-plot design. The site features a Haplic Chernozem under a sub-continental climate, and the future climate scenario simulates projected conditions for Central Germany by 2070–2100. The five land-use systems include two croplands (conventional and organic farming) and three grasslands (intensive meadow, extensive meadow, and extensive pasture). Detailed site characteristics, climate manipulation, and land-use management practices are provided in **Chapter 1 Section 1.2**. This chapter is based on data collected between 2022 and 2023, covering two contrasting climatic conditions: a dry spring in 2022 and a relatively wet spring in 2023. The detailed information about precipitation and irrigation patterns of both climate scenarios and the management of each land-use type in the GCEF from 2022 to 2023 are provided in **Chapter 2 Subsection 2.2.1**.

4.2.2 Root sampling and analysis

Cylindrical soil cores were taken in May 2022 and 2023 using a 5-cm-diameter soil auger. Two cores were taken per subplot at 0-15 cm depth. In total, 200 soil cores were collected (2 climate scenarios × 5 land-use types × 5 treatment replicates × 2 sampling replicates per subplot × 2 sampling years). All samples were stored at 4 °C immediately to inhibit microbial activity and prevent root decay.

All soil cores were washed within a week after sampling with tap water over 0.63 mm sieves to extract the roots from the soil, with each sample requiring about 40 minutes to process. Care was taken to minimize damage to the root system during washing. The collected roots were stored in a 50 % ethanol solution (Rotisol) prior to analysis. Roots were scanned on a flatbed scanner at 400 dpi (EPSON Perfection V700). Then the obtained images were analyzed using WinRHIZO Pro™ (Version 2019a, Regent Instruments, Canada) to measure root characteristics, i.e., root length density and root length distribution in different root diameter ranges.

4.2.3 Soil structure sampling and analysis

Two or three undisturbed soil cores per subplot were taken in May 2022 and 2023 from a depth of 5-10 cm with aluminum rings (5.6 cm diameter, 4 cm height) to characterize the microstructure. Totally, 250 soil cores were sampled and stored at 4 °C in sealed plastic bags to avoid desiccation prior to X-ray CT scanning.

X-ray microtomography was employed to non-destructively analyze soil structural features at high resolution (30 µm voxel size). Following grayscale normalization and correction of imaging artifacts, image segmentation was performed using nnUNet, a self-configuring deep-learning framework optimized for biomedical image segmentation. This approach allowed for the accurate classification of eight distinct material classes, including mineral matrix, various pore types (e.g., root channels, earthworm burrows, abiotic pores), and organic components such as fresh roots, decaying roots, and non-root-derived particulate organic matter (other POM). Compared to previous machine learning methods, the deep-learning-based segmentation significantly improved accuracy and reduced false positives. Morphological analyses of the segmented volumes were conducted using the Soil Structure Library protocol, enabling quantification of key structural traits such as visible porosity, pore connectivity, pore size

distribution, and pore surface area. In addition, composite classes were used to assess biologically relevant features, including root length density, biopore volume, and the contribution of biopores to total porosity. Further technical details of the scanning procedure, segmentation workflow, and structural trait quantification are provided in **Chapter 2 Subsection 2.2.3**. Based on the findings of **Chapter 2** and the rationale outlined in the introduction, specific soil microstructural properties were selected to explore their relationships with root traits. These included total porosity, bioporosity, other POM, and connection probability, which were used to examine potential structural controls on RLD. In addition, volume fraction of root channels and the fraction of fresh roots were used as indicators to assess feedbacks of root growth on soil microstructure. These variables were chosen due to their functional relevance in root-soil interactions and their capacity to reflect biologically driven structural changes in the rhizosphere.

Volumetric soil moisture in the collected soil cores was determined by weight loss after oven drying at 105 °C for 48 hours. Bulk density was calculated with the final soil dry weight divided by the core volume (100 cm^3).

4.2.4 Statistical analysis

All statistical analyses were conducted using R 4.1.3. Linear mixed-effects models (LMMs) were fitted using the "*lmer"* function in the "*lme4"* package (Bates, 2005), incorporating random intercepts to account for the split-plot design and repeated measures. These models were applied to analyze soil microstructure properties, root length density (RLD), bulk density, and soil moisture. Land use, climate, year, and their interactions were fixed factors, while year (sampling time), and subplot nested within main plot served as random effects. Models were fitted using maximum likelihood (ML) estimation, and likelihood ratio tests (χ^2 ratio) were used to assess the significance of fixed effects through stepwise model comparison. We used the "*emmeans*" package (Lenth et al., 2018) to further analyze significant interactions, by running post-hoc pairwise comparisons of estimated marginal means between treatment levels if LMMs yielding significant effects of land-use types and interactions between land use and climate. Principal component analysis (PCA) was further performed using the "*rda*" function in "*vegan*" package (Anderson, 2001) to achieve a dimensionality reduction of soil bulk or microstructure properties driven by land use, climate, and season. Two-way permutational multivariate analysis of variance (PERMANOVA) was performed using the "*cmdscale*" function in "*vegan*" package to quantitatively evaluate the significance of

the differences in RLD and soil microstructure properties among treatments in two years. Linear regression analysis was performed to assess relationships between RLD and soil structure properties. Figures were produced with the ggplot2 package (Wickham, 2011).

4.3 Results

4.3.1 Soil moisture and bulk density

Soil moisture differed significantly among land-use types, climate scenarios, and between years. In line with the higher spring precipitation in 2023, soil moisture levels were 30.2-62.7 % greater than those observed in the dry spring of 2022 (Figure 4.1). Moreover, croplands in 2022 exhibited 19.6-39.5 % higher soil moisture than grasslands, with minimal differences between ambient and future climate scenarios. In contrast, 2023 had significant increase in soil moisture across all land-use types, especially under the future climate scenario. EM and EP showed the strongest moisture gains under the future climate scenario.

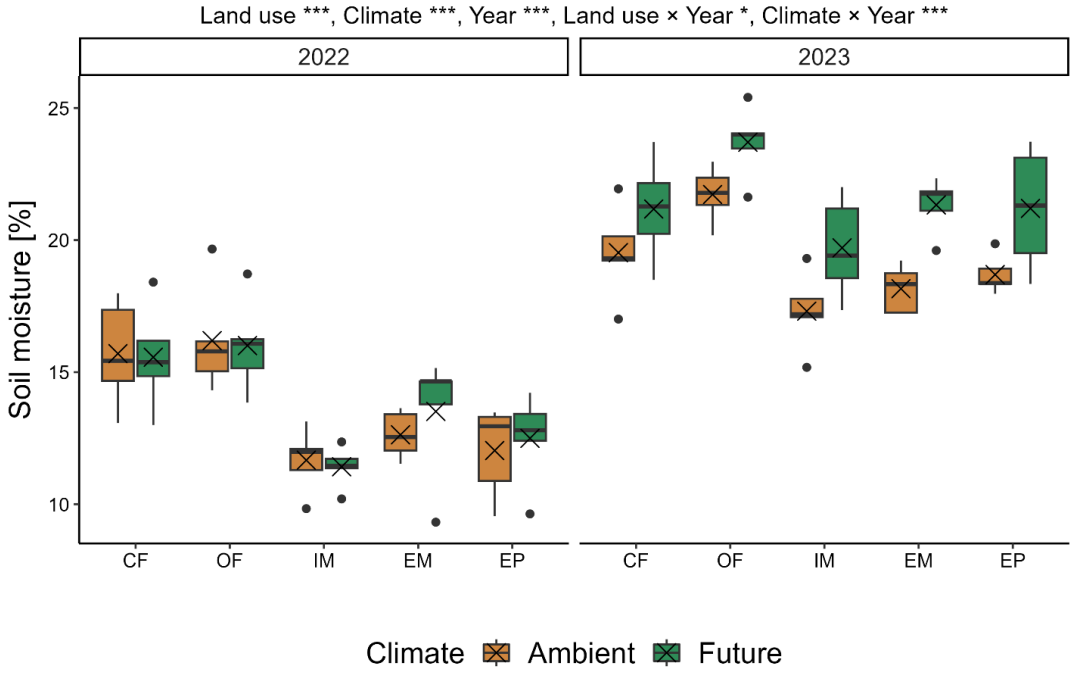

Figure 4.1 Effect of land use on volumetric soil moisture at 5-10 cm depth under ambient and future climate scenarios in 2022 and 2023. CF, OF, IM, EM and EP represent conventional farming, organic farming, intensive meadow, extensive meadow and extensive pasture, respectively. Significant differences between land use, climate, year, interaction of land use and year, interaction of land use and climate are indicated * ($p < 0.05$), ** ($p < 0.01$) and *** ($p < 0.001$). Box plots represent the 0, 25, 50, 75, and 100 percentile and

cross symbols the arithmetic mean (n = 5).

Bulk density ranged from 1.28 to 1.56 g cm^{-3} across all treatments, with greater variability observed in croplands due to mechanical disturbance through tillage (Figure 4.2). Significant effects of land use, year and their interactions were detected, with grasslands generally exhibiting slightly higher bulk density than croplands. In croplands, bulk density was slightly lower in 2023 than in 2022, indicating a modest interannual changes. The future climate scenario showed no significant effect on bulk density across the five land-use systems.

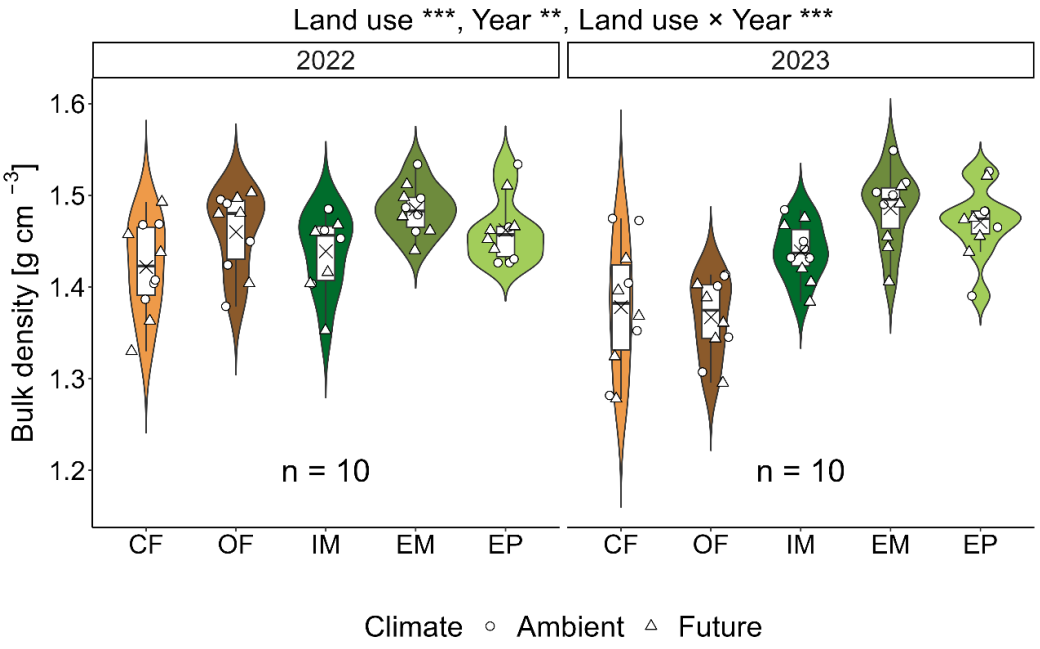

Figure 4.2 Effect of land use on bulk density at 5-10 cm soil depth under ambient and future climate scenarios in 2022 and 2023. CF, OF, IM, EM and EP represent conventional farming, organic farming, intensive meadow, extensive meadow and extensive pasture, respectively. Significant differences between land use, year, interaction of land use and year are indicated ** ($p < 0.01$) and *** ($p < 0.001$). Box plots represent the 0, 25, 50, 75, and 100 percentile and cross symbols the arithmetic mean (n = 10). Jitter points represent individual sub-plots.

4.3.2 Root length density and root length distribution

RLD in the 0-15 cm soil layer varied significantly across land-use systems ($p < 0.001$), with grasslands exhibiting 4.4-6.4 times higher RLD compared to croplands (Figure 4.3a). No significant differences were observed between CF and OF systems. Among grasslands, EM had

29.3% higher RLD than IM, while EP did not differ significantly from both EM and IM. In contrast, the future climate scenario and interannual variability (year) had no significant effect on RLD.

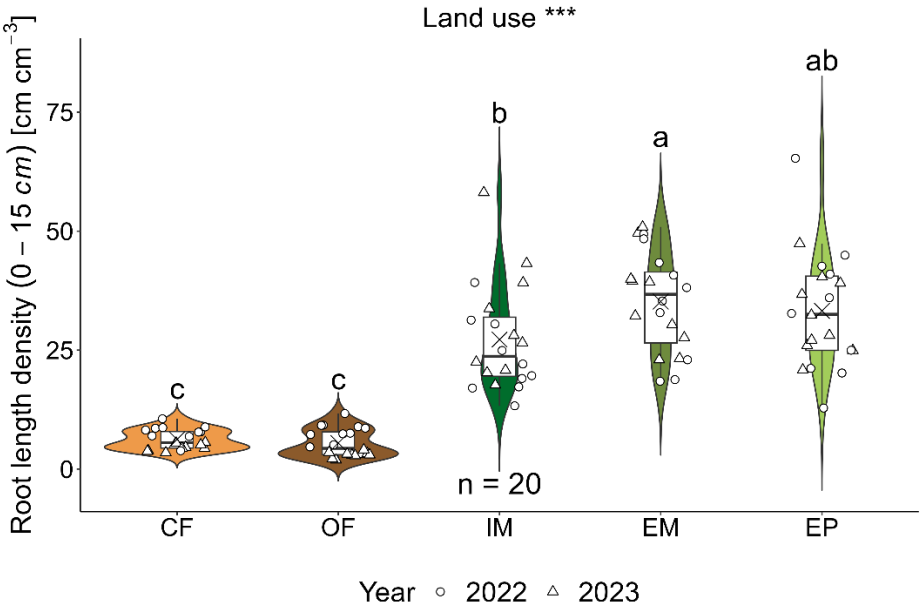

Figure 4.3 Root length density at 0-15 cm soil depth across different land-use types across ambient and future climate scenarios in 2022 and 2023. Boxes represent the 0, 25, 50, 75, and 100 percentiles, and cross symbols represent the arithmetic mean (n = 20). CF, OF, IM, EM and EP represent conventional farming, organic farming, intensive meadow, extensive meadow and extensive pasture, respectively. Different letters indicate significant differences between land-use types ($p < 0.05$). In conventional and organic farming systems, winter barley was cultivated in 2022, while triticale and white clover were grown in 2023. Root samples were collected in early May, corresponding to the period of rapid root growth in Central Germany.

Root systems across all land-use types were dominated by fine roots (< 0.2 mm in diameter), accounting for over 75 % of total root length in most treatments (Figure 4.4). The length density of roots with 0.1-0.3 mm diameter range were significantly higher in grasslands than croplands, reflecting greater fine-root investment of stable perennial systems. Specifically, ≤ 0.1 mm roots represented the largest fraction in grasslands, contributing up to about 40 %, especially in IM. Moreover, the 0.1-0.2 mm roots were more prominent in CF, particularly in 2023. In contrast, coarse roots (> 0.3 mm) consistently comprised the smallest fraction (< 15 %), with slightly higher proportions in grasslands and a slight decline in CF under the wetter conditions of 2023.

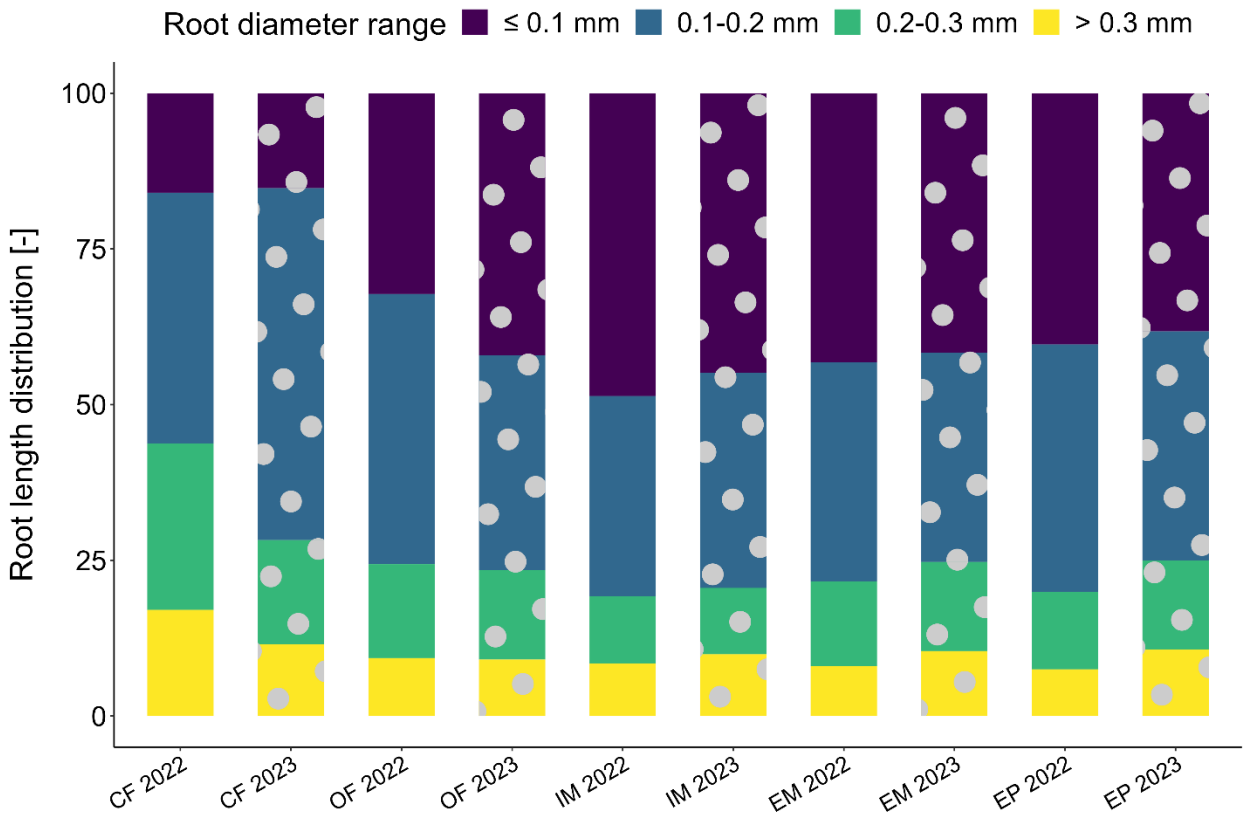

Figure 4.4 Root length distribution of root diameter ranges at 0-15 cm soil depth for each land-use type in two years. Values are arithmetic mean ± standard error (n = 5). Different shading patterns distinguish the 2022 and 2023 data. CF, OF, IM, EM and EP represent conventional farming, organic farming, intensive meadow, extensive meadow and extensive pasture, respectively.

4.3.3 Soil microstructure and root turnover properties

Total visible porosity did not show a clear pattern between croplands and grasslands due to the high variability (Figure 4.5a), whereas the visible porosity of biological origin (bioporosity) of grasslands was 15.4-100.0 % higher than that of croplands (Table 4.1-4.2). However, connection probability of pore was significantly affected by land use, with grasslands generally exhibiting 13.4-46.4 % higher connection probability than croplands (Figure 4.5b). In 2023, connection probability in croplands, especially in OF, significantly decreased compared to 2022, whereas connection probability in grasslands remained stable across years and climate treatments. No significant climate effect was observed for either porosity or connection probability.

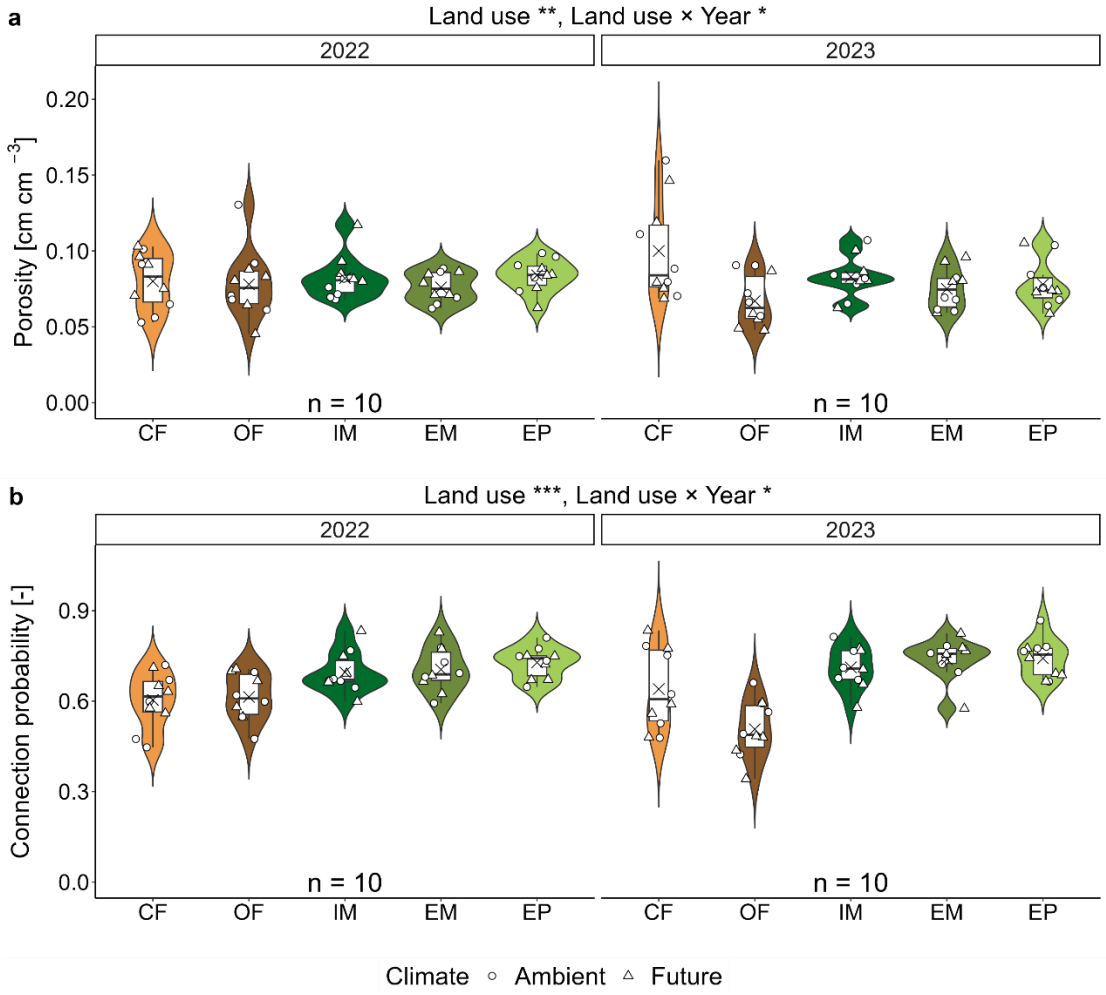

Figure 4.5 Effect of land use on visible porosity (a) and pore connection probability (b) at 5-10 cm depth under ambient and future climate scenarios in 2022 and 2023. CF, OF, IM, EM and EP represent conventional farming, organic farming, intensive meadow, extensive meadow and extensive pasture, respectively. Significant differences between land use, and interaction of land use and year are indicated * ($p < 0.05$), ** ($p < 0.01$) and *** ($p < 0.001$). Box plots represent the 0, 25, 50, 75, and 100 percentile and cross symbols the arithmetic mean (n = 10). Jitter points represent individual sub-plots.

The fraction of fresh roots (i.e. the contribution fresh roots to all roots) was always highest for croplands (0.85-0.91) and in a lower range for extensive grasslands (0.50-0.59) due to higher fraction of fresh roots and lower decaying roots in croplands (Figure 4.6a, Table 4.1). The volume fraction of root channels in grasslands was 92.0-270.3 % higher than croplands regardless of year (Figure 4.6b). In 2023, root channels in croplands decreased by 25.9-27.3 % than 2022, whereas values in grasslands remained relatively stable across years.

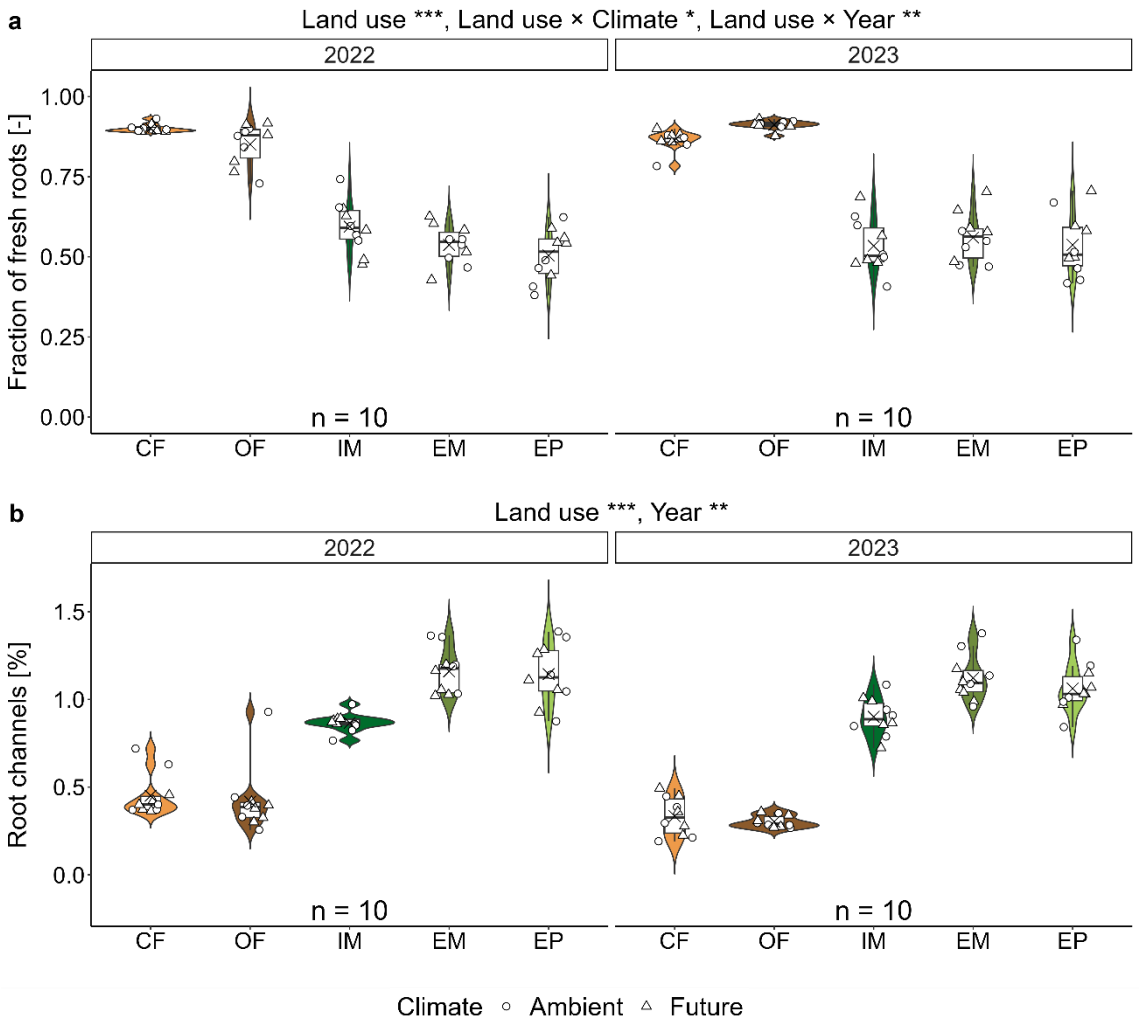

Figure 4.6 Effect of land use on fraction of fresh roots (a) and root channels (b) under ambient and future climate scenarios in 2022 and 2023. CF, OF, IM, EM and EP represent conventional farming, organic farming, intensive meadow, extensive meadow and extensive pasture, respectively. Significant differences between land use, climate, year, interaction of land use and year, interaction of land use and climate are indicated * ($p < 0.05$), ** ($p < 0.01$) and *** ($p < 0.001$). Box plots represent the 0, 25, 50, 75, and 100 percentile and cross symbols the arithmetic mean (n = 10). Jitter points represent individual sub-plots.

4.3.4 Links between root traits and soil structure properties

Principal component analysis (PCA) revealed clear separation of land use based on soil microstructure, RLD, root length distribution, and root turnover in both years, with stronger differentiation in 2022 (Figure 4.7). In 2022, the first two principal components explained 56.1 % of the total variance (PCA1: 36.3 %, PCA2: 19.8 %, Figure 4.7a). Croplands with low RLD clustered near root channels, 0.1-0.2 mm roots, 0.2-0.3 mm roots, > 0.3 mm roots, porosity and

other pores, whereas grasslands were more closely associated with greater RLD, < 0.1 mm roots, fresh roots, biopore diameter, pore diameter, bioporosity, fraction of roots, and connection probability.

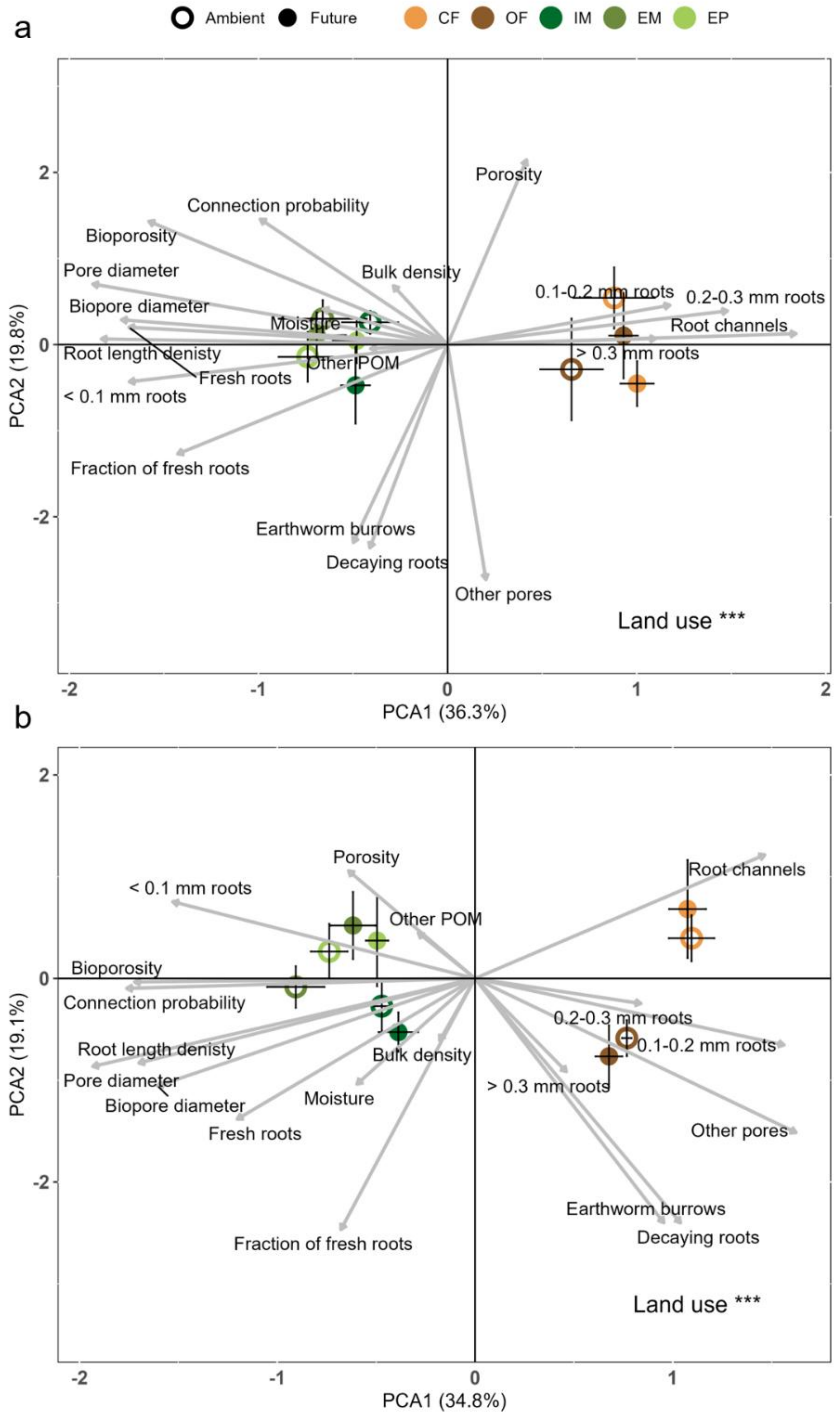

Figure 4.7 The first two principal components based on soil moisture, root traits, and microstructure

variables as influenced by land use and climate in (a) 2022 and (b) 2023. CF, OF, IM, EM and EP represent conventional farming, organic farming, intensive meadow, extensive meadow and extensive pasture, respectively. Results of two-way PERMANOVA are shown in the bottom, right corner of figure. *: $p < 0.05$, ***: $p < 0.001$. Short black lines indicate the key variables to improve interpretability in crowded regions of the PCA plot.

In 2023, PCA1 and PCA2 explained 53.9 % of the variance (PCA1: 34.8 %, PCA2: 19.1 %, Figure 4.7b). Croplands clustered in the positive PCA1 region and were characterized by higher abundances of 0.1-0.2 mm roots, 0.2-0.3 mm roots, decaying roots, and root channels. In contrast, grasslands were located along the negative PCA1 axis, associated with greater bioporosity, pore connectivity, root length density, and biopore diameter, reflecting more developed and continuous pore networks. Root structural traits such as fine root fractions and fresh root biomass aligned more closely with biopores and connectivity metrics.

A weak effect of climate scenarios was observed in both years, with only slight shifts in the distribution of ambient and future climate treatments within each land-use type.

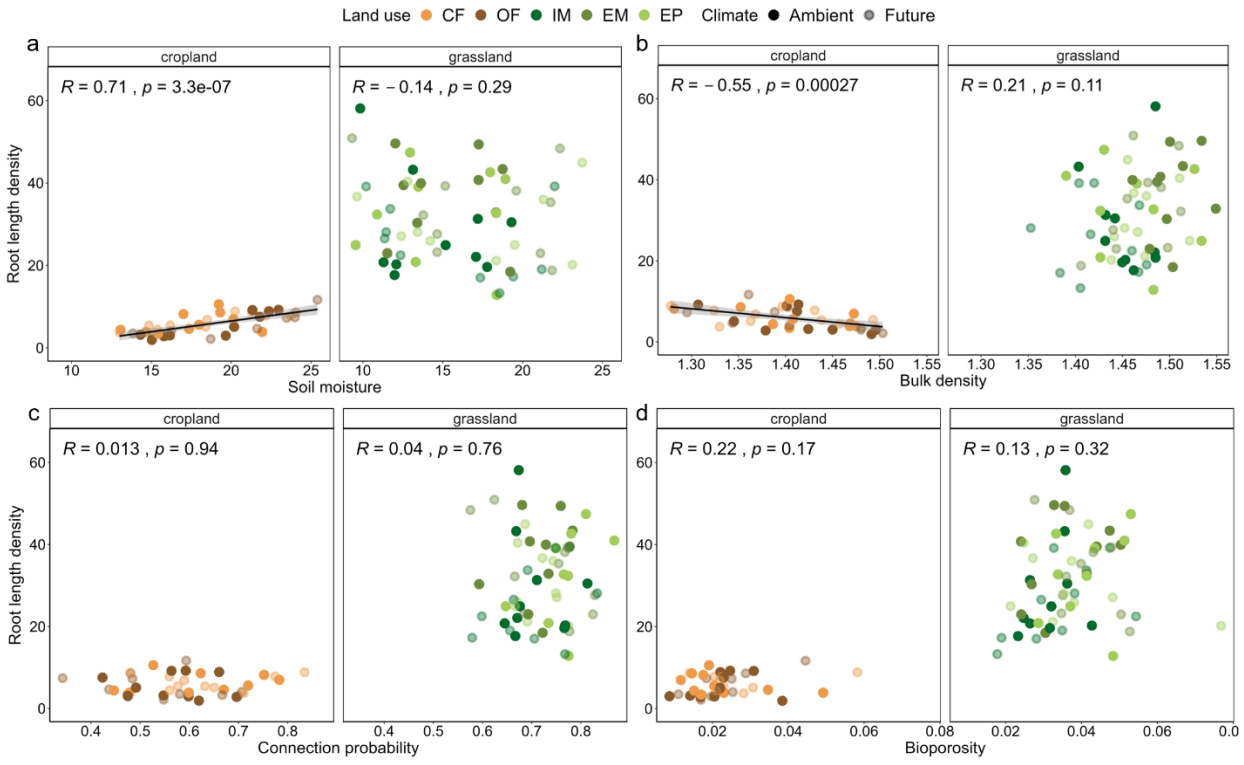

Figure 4.8 Linear relationships between root length density (RLD) and soil properties across five land-use systems under ambient and future climate scenarios in 2022 and 2023. (a) Soil moisture, (b) Bulk density, (c) Connection probability, (d) Bioporosity. Shaded areas represent the 95 % confidence intervals, displayed only for significant relationships ($p < 0.05$). CF, OF, IM, EM and EP represent conventional farming, organic farming, intensive meadow, extensive meadow and extensive pasture, respectively.

RLD showed contrasting relationships with soil structural properties across croplands and grasslands (Figure 4.8). In croplands, RLD was positively correlated with soil moisture (R = 0.71, $p < 0.001$) and negatively correlated with bulk density (R = –0.55, $p < 0.001$), indicating that higher water availability and lower compaction favored root growth. In contrast, these relationships were absent or weak in grasslands, where neither soil moisture nor bulk density significantly correlated with RLD. Additionally, no significant correlations were observed between RLD and pore network properties such as connection probability and bioporosity in either land-use system.

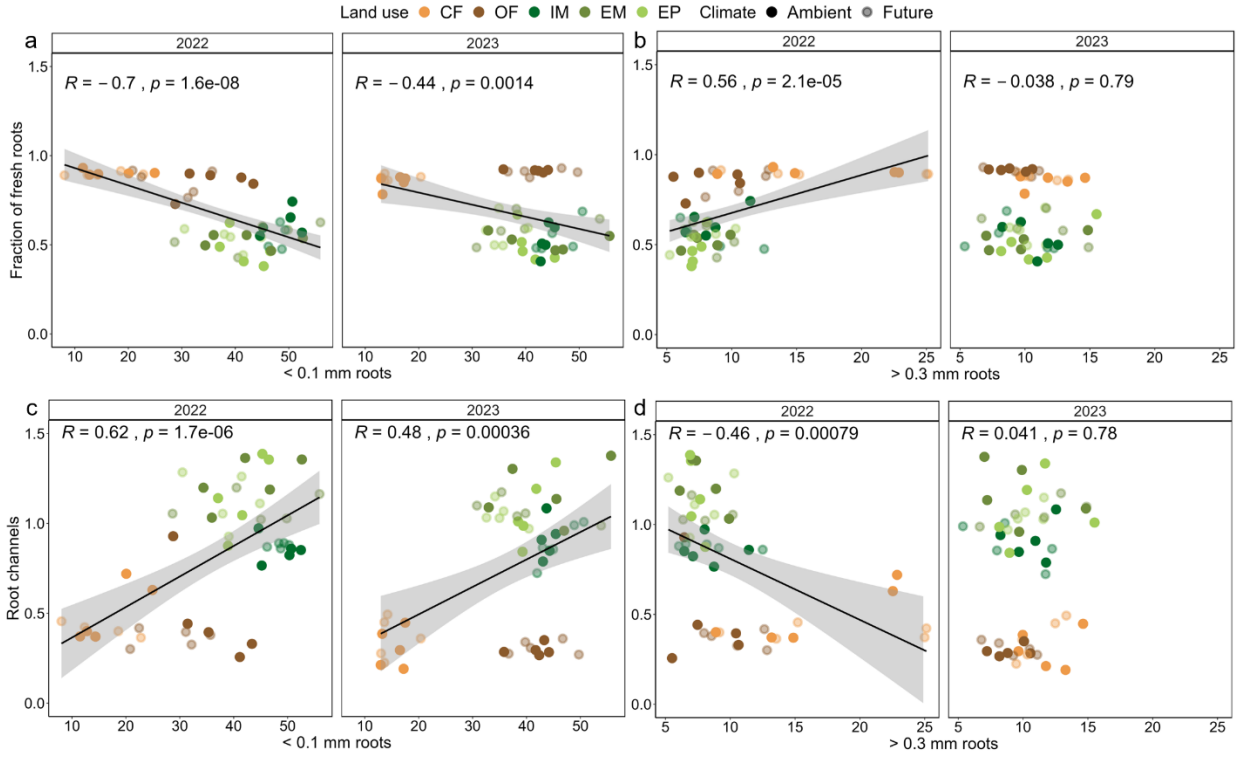

Figure 4.9 Linear relationships between root length distribution of fine roots and root turnover rates across five land-use systems under ambient and future climate scenarios in 2022 and 2023. (a) < 0.1 mm roots and fraction of fresh roots, (b) > 0.3 mm roots and fraction of fresh roots, (c) < 0.1 mm roots and root channels, (d) > 0.3 mm roots and root channels. Shaded areas represent the 95 % confidence intervals, displayed only for significant relationships ($p \leq 0.05$). CF, OF, IM, EM and EP represent conventional farming, organic farming, intensive meadow, extensive meadow and extensive pasture, respectively.

Significant correlations were observed between root diameter classes and both the fraction of fresh roots and root channels, with stronger relationships in the dry year of 2022 (Figure 4.9). The fraction of fresh roots was negatively correlated with < 0.1 mm roots in both years, but more strongly in 2022 (R = –0.7, $p < 0.001$) than in 2023 (R = –0.44, p = 0.0013) (Figure 4.9a). In

contrast, > 0.3 mm roots were positively associated with the fraction of fresh roots in 2022 (R = 0.56, $p < 0.001$), but this relationship was absent in 2023 (Figure 4.9b). Similarly, root channels were positively correlated with < 0.1 mm roots, with stronger correlation in 2022 ($R = 0.62$, $p <$ 0.001) than in 2023 ($R = 0.48$, $p < 0.001$) (Figure 4.9c), while > 0.3 mm roots were negatively related to root channels in 2023 ($R = –0.46$, $p < 0.001$), but not in 2023 (Figure 4.9d).

4.4 Discussion

4.4.1 Land-use-driven differences in soil structure-root interactions and limited climate effects

Our results support our first hypothesis that grasslands exhibited higher microstructural stability and more developed root systems than croplands, due to the presence of perennial vegetation and the absence of tillage. Across both the dry spring of 2022 and the normal spring of 2023, grasslands consistently exhibited greater bioporosity, larger biopore diameters, and higher pore connection probability, indicating more persistent and functionally connected soil pore networks (Bacq-Labreuil et al., 2018; Peth et al., 2008). Root length density (RLD) in grasslands was found to be 4.4-6.4 times higher than in croplands, reflecting the contribution of dense, fibrous root systems and minimal mechanical disturbance. These findings align with previous studies emphasizing the role of perennial vegetation and reduced management intensity in sustaining soil structural integrity (DuPont et al., 2014).

However, contrary to our second hypothesis, root growth in croplands did not show a stronger dependency on structural attributes such as bioporosity or connection probability. When croplands and grasslands were analyzed separately, no significant correlations were observed between RLD and any structural parameters, including total porosity, bioporosity, or pore connectivity. Although significant correlations emerged when both land-use systems were pooled, these likely reflect broader structural differences between systems rather than within-system structure-root interactions. These findings contrast with earlier studies that found strong links between root surface area and pore development under different grassland management intensities (Kuka et al., 2013; Kuka & Joschko, 2024). A likely explanation for this discrepancy is that under our soil conditions, pore space and aeration was not limiting for root growth (Schlüter et al., 2022b), reducing the influence of structural constraints on root proliferation. Additionally, the mismatch between depth ranges for root sampling (0-15 cm) and CT-based structural measurements (5-10

cm) may have weakened the correlations. It is also possible that our structural metrics, derived from total pore space, overlooked key macropores or localized features that are most relevant for root growth (Casero, 2018; Jin et al., 2017). Interestingly, RLD was significantly associated with soil moisture and bulk density in croplands but not in grasslands, indicating that root development in croplands was more responsive to variations in the physical soil environment. This suggests that in the absence of well-developed perennial root systems and persistent biopores, root growth in croplands may be more constrained by short-term changes in abiotic conditions rather than long-term structural features (Benjamin et al., 2007).

Root system and its integrity also reflected distinct land-use legacies and actively shape the surrounding microstructure, i.e. the formation of longer-lived macropores and stable biopore networks (Mueller et al., 2024). Our results showed the fraction of fresh roots was substantially lower in grasslands compared to croplands, likely due to continuous vegetation activity in grasslands, in contrast to the seasonal interruption of growth in croplands. In croplands, microbial decomposition of root biomass is accelerated during fallow periods, while in grasslands, a continuous supply of exudates sustains microbial communities, reducing reliance on root tissue (Huang et al., 2014; Zhalnina et al., 2018). Grasslands consistently had higher volume fraction of root channels, which remained stable across years, suggesting that the legacy effects of grassland root systems were further reflected in the stability of soil microstructure across years (Frouz, 2024). This probably because roots promote the development of rhizosheaths and root-soil contact zones that stabilize aggregates and enhance porosity (Mueller et al., 2024). Grasses like *Lolium perenne* produce more persistent rhizosheaths than cereals like barley, contributing to aggregate stability and enhanced root-soil contact (Burak et al., 2021; Haynes & Francis, 2006).

In contrast, croplands exhibited lower RLD and more variable structural properties compared to grasslands. Root systems in croplands are typically shallower and less fibrous, driven by annual crop rotations and selective breeding for aboveground productivity rather than root system development (Lynch, 2019). Moreover, regular mechanical disturbances such as tillage, along with the seasonal absence of vegetative cover, disrupt soil structure and pore continuity (Carter, 1988; Pires et al., 2017). These features reduce the formation and persistence of biopores, thereby limiting opportunities for root reuse of existing connected pore networks (Lucas et al., 2022). As a result, croplands are less able to sustain root-soil structure feedbacks. For instance, cropland in dry 2022 had significantly lower RLD than in normal 2023, probably due to both of the insufficient

water availability and limited structural connectivity for the reuse of previous root channels (Lucas et al., 2022).

The future climate scenario showed no significant effects on soil microstructure, RLD, and their interactions, this is likely due to the relatively moderate nature of the imposed changes, only slightly elevated average temperatures and a 10 % increase in spring precipitation. Such mild shifts may not have been sufficient to induce measurable alterations in soil physical structure or root development patterns, particularly over a short-term observation period. Substantial structural changes typically require more intense or prolonged climatic stressors (Leuther et al., 2023; Liu et al., 2024a; Peng et al., 2022; Xiong et al., 2019b). Similarly, root systems, with high plasticity, may not exhibit significant architectural adjustments in response to minor climatic variations over just one or two growing seasons (Hanslin et al., 2019; Kano-Nakata et al., 2019).

4.4.2 Microstructural controls on root proliferation and its feedbacks under contrasting moisture conditions

Our findings show that the influence of soil structure on root proliferation varies with water availability and is modulated by root traits. A weak but significant positive correlation between bulk density and root growth was observed in the relatively wet spring of 2023. This suggests that under higher moisture, mechanical impedance was alleviated, allowing roots to penetrate denser soil regions more readily (Vaz et al., 2011). In contrast, during the dry spring of 2022, low moisture amplified soil strength and physical constrains, restricting root proliferation and decoupling RLD from bulk density (Whitmore & Whalley, 2009). These findings underscore that the influence of bulk density on root growth is highly dependent on soil water availability and may only become apparent when moisture conditions alleviate mechanical impedance.

In both years, when pooling both croplands and grasslands, bioporosity and pore connection probability consistently exhibited stronger correlations with RLD than total visible porosity and bulk density, especially in dry 2022, suggesting that biologically derived pore networks play a more significant role in shaping root distribution, particularly under suboptimal moisture conditions. Biopores, formed by decaying roots, earthworms, and other soil fauna, are typically cylindrical, vertically oriented, and physically connected across depth layers (Stolze et al., 2022; Wendel et al., 2022). These properties establish them as effective preferential pathways for root elongation, particularly under compacted or dry soil conditions where the formation of new pores

is energetically constrained (Colombi et al., 2017; Xiong et al., 2022a). Furthermore, higher pore connectivity ensures that roots can extend into deeper soil layers without encountering physical barriers, facilitating access to subsoil water reserves and nutrients (Dal Ferro et al., 2014; Kopke et al., 2015).

Importantly, our results also support our third hypothesis which suggests that the feedback of roots on soil structure is closely linked to root diameter. The abundance of fine roots (< 0.1 mm roots) was strongly positively correlated with root channel volume in both 2022 and 2023, with stronger associations during the dry year. In contrast, thicker roots (> 0.3 mm roots) showed a negative relationship with root channels in 2022 and no significant correlation in 2023. This probably indicates that fine roots, due to their ability to exploit narrow biopores and generate persistent pore structures upon decomposition, play a dominant role in shaping soil structure under moisture-limited conditions (DuPont et al., 2014; Lucas et al., 2022). These feedbacks weakened in 2023, when favorable moisture conditions allowed root proliferation throughout the matrix, decreasing reliance on biopores. Root growth became less dependent on pre-existing pore architecture, likely due to reduced mechanical impedance, allowing roots to proliferate more freely through the soil matrix.

Additionally, our results showed that the fraction of fresh roots was negatively correlated with fine roots and positively with thicker roots, especially in 2022. This suggests that thicker roots are more likely to be long-lived or structurally integrated into the soil matrix, while fine roots may contribute more to rapid turnover during low input of fresh roots under moisture-limited conditions (Chen & Brassard, 2012). The strong correlation between root diameter distribution and root channel development emphasizes the structural legacy effects of root systems and their role in shaping pore architecture. In croplands, where fresh root biomass was higher, the greater turnover is likely driven by both soil cultivation, which physically disrupts root systems, and a lack of continuous exudate supply, leading microbes to decompose root tissues more rapidly, ultimately resulting in shorter-lived root structures that contribute less to long-term biopore stability.

Together, these findings highlight the bidirectional interactions between root systems and soil structure, particularly under drought. Systems with high fine root abundance and minimal disturbance, such as grasslands, appear more capable of reinforcing and maintaining connected pore networks that support resilient water and nutrient uptake. In contrast, annual cropping systems with frequent soil disturbance may require management interventions such as reduced tillage or

cover cropping to restore structural connectivity and enhance root functionality under climate variability.

4.5 Conclusion

Our study demonstrates that soil structure-root interactions are primarily modulated by land use and, to a lesser extent, by the future climate scenario. Perennial grasslands consistently exhibited higher root length density, bioporosity, and pore connectivity compared to croplands, emphasizing the role of continuous root presence and reduced mechanical disturbance in promoting stable and connected pore networks. In contrast, root growth in croplands was more strongly correlated with soil moisture and bulk density than grasslands, indicating that the root proliferation in croplands was more sensitive to variations in the soil physical environment, whereas the root growth in grasslands exhibited higher stability. Importantly, our findings show that the feedback of root growth to soil structure are strongly dependent on root diameter, with fine roots contributing more substantially to biopore formation and pore network stabilization, particularly under dry conditions. The future climate scenario did not show effect on soil structure, root traits, and their interactions due to the tiny climatic variations. These insights emphasize the need to preserve root-derived structural features in agroecosystems and highlight the potential of management strategies that promote fine-root development and pore connectivity to enhance soil resilience under increasing climate variability.

5 Legacy effects of climate extremes on deep soil water storage and water use efficiency across different land-use systems

Abstract

Climate extremes, including multiyear droughts and extreme rainfall events, are projected to intensify, threatening the global water cycle and reducing agricultural productivity. Deep soil water storage plays a key role in buffering extremes, yet its influence on plant productivity and water use across land-use systems remains insufficiently understood. Here, we monitored soil moisture dynamics over three years and vegetation responses in a long-term field trial comprising five land-use types (two croplands: conventional & organic farming; three grasslands: intensive meadow, extensive meadow & pasture). The monitoring period captured both prolonged droughts and an extreme rainfall. We found strong legacy effects of past droughts on deep soil water storage (30-110 cm), which decoupled plant productivity from short-term climate fluctuations. Extensive grasslands exploited the deep soil water storage more efficiently than intensive grasslands and croplands, because of longer transpiration demand and higher interception caused by the perennial vegetation cover. In turn, water use efficiency increased with land-use intensity, driven by shorter growing periods in croplands and higher mowing frequency in intensive grasslands. Our findings highlight how land-use practices shape ecosystem responses to climate extremes and underscore the need to incorporate deep soil water dynamics into sustainable land-management strategies under future climate conditions.

Mengqi Wu * [a] , Christiane Roscher [b, c], Martin Schädler [c, d], Mika Tarkka [e], Doris Vetterlein [a], Steffen Schlüter [a]

* corresponding authorship (mengqi.wu@ufz.de)

a Department of Soil System Science, Helmholtz-Centre for Environmental Research (UFZ), Halle, Germany

b Department Physiological Diversity, Helmholtz-Centre for Environmental Research (UFZ), Leipzig, Germany

c German Centre of Integrative Biodiversity Research (iDiv) Halle-Jena-Leipzig, Leipzig, Germany

d Department of Community Ecology, Helmholtz-Centre for Environmental Research (UFZ), Halle, Germany

e Department of Soil Ecology, Helmholtz-Centre for Environmental Research (UFZ), Halle, Germany

This chapter is submitted to Communications earth & environment: Mengqi Wu, Christiane Roscher, Martin Schädler, Mika Tarkka, Doris Vetterlein, Steffen Schlüter. "Legacy effects of climate extremes on deep soil water storage and water use efficiency across different land-use systems", submitted: 07.07.2025

5.1 Introduction

Extreme drought and precipitation events, projected to increase in frequency, duration and intensity with human-induced climate change, threaten the global water cycle and agricultural productivity (Chen et al., 2025; Maurel & Nacry, 2020; Wunsch et al., 2022). Soil water content, a critical mediator between meteorological conditions and biogeochemical processes (Li et al., 2024c; Sun et al., 2025; Vicente-Serrano et al., 2025), governs root and shoot growth dynamics and thus ecosystem productivity (Tissink et al., 2025; Vereecken et al., 2022; Zuo et al., 2006). Yet, the supply of precipitation and the storage of water in the topsoil often fail to meet the water demands of plants, particularly during peak growth (Ali et al., 2021; Wang et al., 2024a). Deep soil water storage, which is accessible to plant roots, may play an unaccounted role in buffering against summer droughts, sustaining aboveground growth and belowground ecosystem stability under extreme climatic conditions (Wang et al., 2024b). However, the extent to which deep soil water storage stabilizes plant productivity and ecosystem functions under climate extremes across different land-use systems remains poorly understood.

The spatiotemporal distribution of soil water is strongly influenced by land-use type and intensity through the differences in vegetation cover, root system activity, and the timing and duration of water use across the growing season (Spera et al., 2016; Wang-Erlandsson et al., 2022; Yu et al., 2025; Zhao et al., 2017b). Understanding how ecosystems respond differently to climate extremes under various land-use types and intensities is critical to predict future ecosystem services. For example, annual cropland and perennial grassland differ markedly in plant community composition, root system phenology, and seasonal water demand (Fan et al., 2015; Wang et al., 2024b; Yang et al., 2024b). Grasslands, dominated by perennial plant species, typically maintain dense and continuous vegetation cover throughout the year, while croplands undergo seasonal cycles of sowing and harvest, leading to periods of low cover or even bare ground and increased evaporative water loss from the topsoil (Bagley et al., 2017; Wang et al., 2012). Moreover, croplands are characterized by shallow, fast-developing root systems that concentrate water uptake during a short peak growth stage, whereas grasslands support deeper and more persistent root networks that sustain water uptake and continuous transpiration throughout the growing season (Holmes & Rice, 1996; Swindon et al., 2019). These contrasting root and

vegetation cover dynamics result in distinct seasonal patterns of soil water depletion and influence the ecosystem's capacity to withstand climate extremes (Maestre et al., 2016; Scherzinger et al., 2024). Additionally, land-use intensity, characterized by fertilization dose, tillage intensity in croplands, or mowing frequency, the use of a few grass cultivars or a more diverse species composition in grasslands, can further modify root development and vegetation cover, this in turn affects water uptake efficiency and soil water distribution (Rose et al., 2011; Spera et al., 2016). The interaction between land-use type and intensity and a projected future climate scenario in shaping soil water dynamics, and the potential implications of this for plant productivity under climate extremes, remains unclear.

In particular, the relationship between rooting density and water availability remains poorly understood, complicating efforts to interpret plant responses to climate extremes. This complexity arises from several reasons: (1) water uptake is not uniform across the entire root system but can be root type specific, is higher close to root tips and can be altered by the presence of root hairs (Ahmed et al., 2018; Segal et al., 2008); (2) spatial heterogeneity in soil water can decouple the water uptake patterns from root density distribution (Carminati et al., 2016); and (3) elevated root densities may reflect nutrient foraging strategies rather than water demand (Lynch, 2019). This mismatch between root distribution and water uptake poses a critical challenge for understanding the plant adjustment to extreme climate conditions. The structure and function of deep rooting systems and their contribution to deep soil water uptake remain poorly understood, particularly under field conditions (Draye et al., 2010; Pierret et al., 2016). These uncertainties hinder a comprehensive evaluation of the extent to which shifts in rooting patterns constitute an effective mechanism for coping with water stress under changing climate.

Plants rely on different strategies that enhance water uptake and improve water use efficiency (WUE) to maintain productivity under climate extremes. In agricultural systems, management strategies include selecting or breeding for cultivars with inherently higher WUE, optimizing cropping system and soil tillage regimes in croplands or adjusting mowing schedules in grasslands (Condon et al., 2004; Rose et al., 2011; Sun et al., 2018). While such strategies may delay the onset of drought stress, they often have limited effectiveness in sustaining overall productivity under prolonged water deficits (Leakey et al., 2019). Drought resistance tends to decline with increasing land-use intensity as higher productivity is mostly associated with higher water demand (Bazzichetto et al., 2024; Korell et al., 2024; Van Sundert et al., 2021), potentially exacerbating

ecosystem vulnerability under intensified management regimes. In grasslands, diverse plant communities contribute to ecosystem resistance under climate extremes by combining shallow- and deep-rooting species, which enhances partitioning of soil water resources and minimizes competition under water stress (Craine et al., 2012; Isbell et al., 2015; Weides et al., 2024). Increasing attention has been paid to the legacy effect of climate extremes: persistent alterations in soil water availability that extend beyond the period of stress itself (Bastos et al., 2020; Liu et al., 2025a; Muller & Bahn, 2022; Sun et al., 2022). This legacy of soil water storage may reshape subsequent rooting patterns, alter plant community composition, and influence WUE, with significant implications for the sustainability of plant production systems under ongoing climate change.

The extent to which deep soil water storage, driven by the legacy effect of climate extremes, can buffer productivity loss and affect WUE under future climate scenario remains poorly understood. Therefore, we made use of a unique experimental platform, Global Change Experimental Facility – GCEF (see Schädler et al. (2019)), in which a realistic future climate scenario is compared against ambient climate across five land-use types (two croplands and three grasslands), each representing a gradient of land-use intensities.

The objective of this study was to investigate how climate extremes influence spatiotemporal patterns of soil water storage under different land-use types and how these patterns are affected by a future climate scenario involving modified seasonal precipitation and higher temperature. We further aimed to investigate whether and how legacy effects of deep soil water storage influence plant productivity and WUE in response to climate extremes that we observed in a three-year monitoring campaign. We hypothesized that, (1) topsoil water content is primarily driven by atmospheric forcing, but deep soil water content is regulated by root water uptake and legacy effect of past soil moisture conditions. (2) On an annual basis, croplands maintain a higher soil water content than grasslands due to their sparser root systems and shorter growing season, whereas the impact of the future climate scenario on deep soil water storage is unclear and should be clarified by this study. Furthermore, we expected that (3) crops achieve higher yields than grasslands due to breeding for resource efficiency and rapid growth, whereas extensive grasslands, with greater plant diversity, are most resistant to climate extremes. Intensive grasslands, characterized by low diversity but permanent cover, are expected to be less resilient than extensive grasslands but more stable than croplands, due to perennial root systems and continuous cover. Finally, we

hypothesized that (4) plant adjustment to drought conditions and limitations in deep soil water supply would mainly occur through higher WUE and less through changing rooting patterns or changes in vegetation composition. These hypotheses were tested through three years of monitoring soil water content profiles, yield, and WUE across all five land-use types and two climate scenarios. Interpretation of the observed growth and water uptake patterns was supported by data on plant community composition and root length density profiles collected during peak growth. Our analysis explicitly accounted for site-specific precipitation history and interannual climatic variability, providing a robust context for evaluating land use and climate interactions on ecosystem water dynamics and productivity.

5.2 Material & Methods

5.2.1 Site description

The study was conducted at the Global Change Experimental Facility (GCEF) in Bad Lauchstädt, Germany, which combines two climate scenarios with five representative land-use types in a large-scale split-plot design. The site features a Haplic Chernozem under a sub-continental climate, and the future climate scenario simulates projected conditions for Central Germany by 2070–2100. The five land-use systems include two croplands (conventional farming (CF) and organic farming (OF)) and three grasslands (intensive meadow (IM), extensive meadow (EM), and extensive pasture(EP)). Detailed site characteristics, climate manipulation, and land-use management practices are provided in **Chapter 1 Section 1.2**. This chapter is based on data collected between 2022 and 2024. The precipitation and irrigation patterns of both climate scenarios and the management of each land-use type in the GCEF from 2022 to 2024 are summarized in Figure 5.1. The cumulative growing season rainfall (GSR), measured as total precipitation and irrigation from April to October, was almost twice as high in 2023 and 2024 as in 2022 (Figure 5.1a).

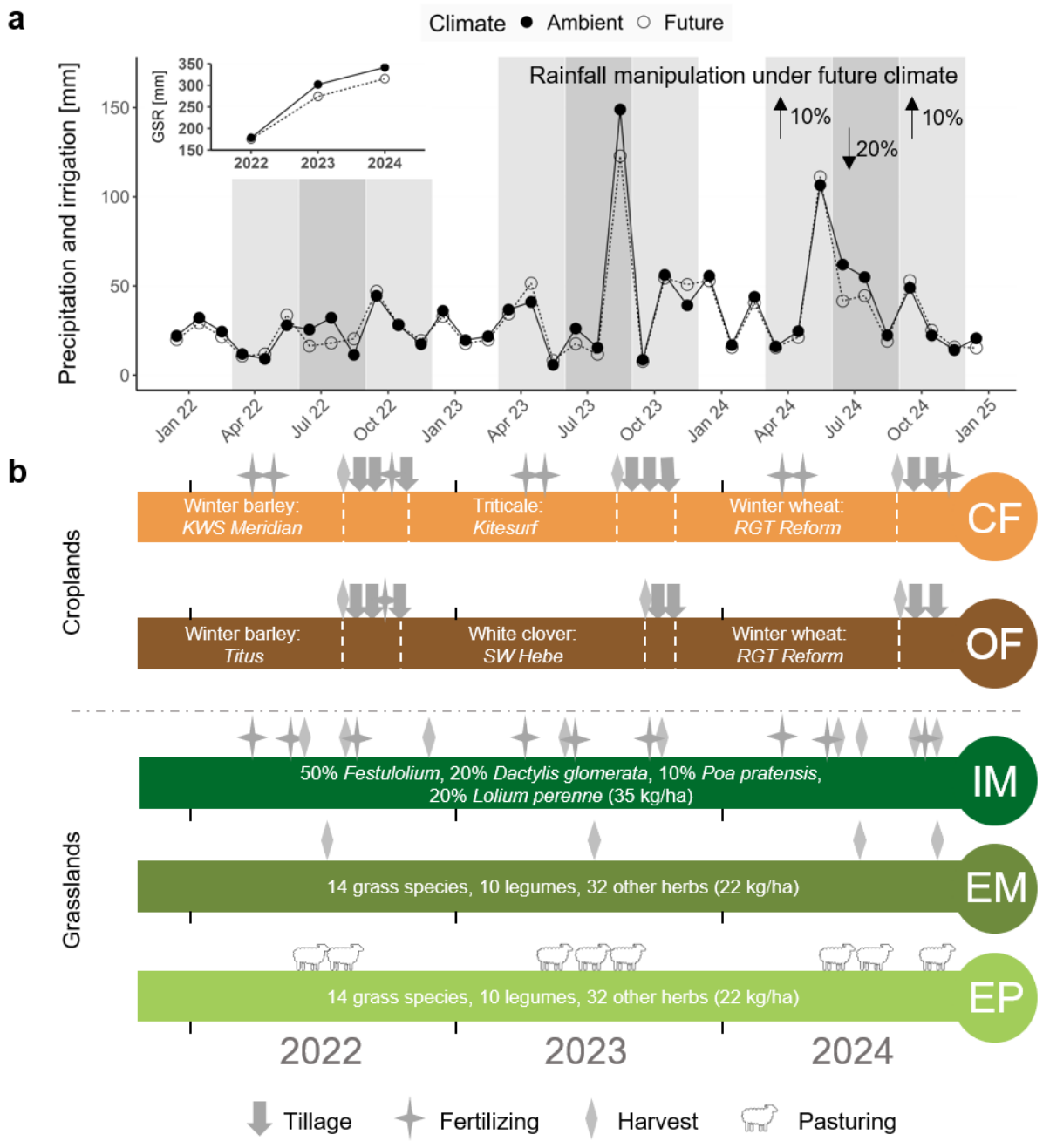

Figure 5.1 Monthly precipitation and irrigation (a) and land-use management (b) at the Global Change Experimental Facility (GCEF) from 2022 to 2024. Growing season rainfall (GSR) represents the total precipitation and irrigation from April to October for each year under two climate scenarios. CF, OF, IM, EM and EP represent conventional farming, organic farming, intensive meadow, extensive meadow and extensive pasture, respectively. The light shaded area represents the increased rainfall during spring and autumn in the future climate scenario, and the dark shaded area represents the decreased rainfall during summer in the future climate scenario. Compared to the ambient climate, the future climate rainfall manipulation increased spring and autumn rainfall by 10 % (arrow up), while decreasing summer rainfall

by 20 % (arrow down). The plant species under grasslands refer to Schädler et al. (2019).

5.2.2 Meteorological water deficit and standardized precipitation-evapotranspiration index (SPEI)

The meteorological water deficit and SPEI are widely used to identify and quantify wet and dry climate events in ecological studies. Meteorological water deficit is the difference between precipitation and potential evapotranspiration. SPEI is derived from the non-exceedance probability of the water deficit, fitted to a three-parameter log-logistic distribution to account for common negative values (Beguería et al., 2014). Values below -1.28 and above 1.28 indicate extreme dry and wet conditions, respectively (Isbell et al., 2015). Precipitation is calculated as the sum of precipitation and irrigation, whereas potential evapotranspiration is estimated using the Penman-Monteith equation, with solar radiation derived from the diurnal temperature range following the Hargreaves method (Hargreaves & Allen, 2003). As no crop-specific parameters are included, this estimate reflects atmospheric demand rather than actual plant evapotranspiration. The daily precipitation and temperature data used for water deficit and SPEI calculations were obtained from the German Meteorological Service (DWD) weather station in Bad Lauchstädt (https://opendata.dwd.de/climate_environment/CDC/observations_germany/climate/daily/kl/) and aggregated to monthly values. The water deficit was also aggregated to monthly values, whereas the SPEI of a given month represented the 3-month average of this month and the two antecedent months to account for seasonal hydrological consistency. Detailed descriptions of the water deficit and SPEI calculation can be found in Vicente-Serrano et al. (2010) and Schnabel et al. (2022). The "*SPEI*" package in R (Beguería et al., 2017) was used for analysis.

5.2.3 Soil water content and storage profiles

Soil moisture profiles were monitored at each subplot using time domain reflectometry (TDR) probe at approximately weekly to bi-weekly intervals from April 2022 to December 2024. The device was a TRIME-PICO T3/IPH44 probe (IMKO Micromodultechnik GmbH, Ettlingen, Germany), which allows non-destructive determination of soil volumetric water content in a soil profile (Kano-Nakata et al., 2019). On each subplot of five land-use types, a soil auger was used to drill down to 110-120 cm and install the plastic access tubes. The soil volumetric water content

of each layer was calculated as the average of two measurements and were made at depths of 10, 20, 30, 50, 70, 90 and 110 cm. The probe was rotated by 90° between two measurements to compensate for the elliptical sensitivity of the measuring field. Missing data on the croplands from July to October/November in three years were due to the removal of access tubes between harvest in summer and tillage in fall. Topsoil and deep soil water storage were calculated as the average soil water content during the growing season (the period from the first day when the mean daily temperature consistently exceeds 5 °C (the minimum threshold for the growth of most grassland and crop species in Central Germany) until harvest in early July) in the 0-30 cm and 30-110 cm soil layers, respectively. The change in topsoil and deep soil water storage was assessed by comparing at the beginning and end of the growing season.

To check the accuracy of the TDR, the monitoring data were calibrated by a comparison with four volumetric water content measurements ranging from saturated soil water content to the permanent wilting point using a balance and the TDR probe in an access tube at the center of a homogeneous soil column (34 cm diameter, 35 cm height). The soil column consisted of sieved topsoil material from the GCEF that was compacted to a representative bulk density for the site (1.44 g cm^{-3}). To facilitate a homogeneous moisture profile across the sensor depth, a new soil column was packed for each water content and the water was already added before packing for the lower target water contents and partly added from the top after packing for the higher target water content with sufficient time for equilibration. Volumetric water contents were derived from the known dry weight and bulk density of the soil column determined after oven-drying at 105 °C for 48 hours. This calibration resulted in the regression equation $Y = 1.63X - 1.63$, $R2 = 0.997$, $p < 0.01$, $n = 4$, where X is the soil moisture measured by TDR and Y is the calculated soil moisture. The calibration was determined once and used for the entire monitoring period.

5.2.4 Root sampling and analysis

Root samples were collected in May 2022 and 2023 from three soil depth layers (0-15, 15-30, and 30-50 cm) across two climate scenarios and five land-use types, resulting in 600 depth-specific samples. Root length density and diameter distribution were assessed using WinRHIZO Pro™ after careful extraction and preservation of roots. Detailed information on the sampling scheme, processing, and analysis procedures is provided in **Chapter 4 subsection 4.2.2**.

In addition, root length density was adjusted using correction coefficients specific to land use and year to obtain correlated root length density, as fresh roots primarily contribute to root water uptake. Fresh roots cannot be distinguished from root residues, that were dead before sampling, during root washing and sorting and also not with image analysis with WinRhizo software. These correction coefficients were estimated independently as the relative proportion of fresh roots to total roots (Figure S5.2), derived from X-ray CT images of intact soil cores (Phalempin et al., 2025b), which were taken in the same soil depths shortly after root sampling. The proportion of fresh roots was 85.1-91.2 % in croplands and 50.4-59.4 % in grasslands, detailed information is provided in **Chapter 2 subsection 2.2.3**.

5.2.5 Vegetation recording

Shortly before root sampling, an area of 30 cm in diameter, centered on the sampling points for soil coring, was marked with a metal frame in the grassland subplots. All plant species rooting within this area were recorded and species-level cover as well as total vegetation cover were estimated to the nearest percentage.

5.2.6 Evapotranspiration and water use efficiency

Evapotranspiration (ET) was estimated using the soil water balance equation (Zeleke & Wade, 2012) as follows:

$$ET = P + I + \Delta S - R - D + CR \qquad [mm]$$

where ET is the evapotranspiration (mm), P is precipitation (mm) (referring to the values measured under the automated proofs), I is irrigation application (mm), ΔS is soil water storage change (mm) (soil water content at the start minus soil water content at the end of a given period for the 0-110 cm depth), R is surface runoff (mm), D is drainage from the root zone and CR is capillary rise to the root zone. Due to the deep soil profile and the large water holding capacity, runoff is zero in the field. Due to the deep groundwater table (about 32 m below surface), capillary rise is negligible. Lysimeters with 1 m deep intact soil monoliths on-site featured no seepage at the lower boundary during three years. Therefore, R, D and CR were set to zero in this study (Sun et al., 2010). The net change in water content during peak growth used to link with root length density at 0-50 cm depth was calculated as the cumulative water input ($P + I$) and ΔS in the 0-50 cm depth over eight weeks spanning four weeks before to four weeks after root sampling.

Water use efficiency (WUE) is defined as yield divided by *ET*. The cumulative *ET* was calculated from the first day when the mean temperature consistently exceeds 5 °C until the day before harvest. Yield data was obtained from machine harvest records on all subplots, where the sum of grain and straw was taken for the croplands. Harvest dates for croplands and grasslands were synchronized through linear interpolation of the biomass production between two cuts in the meadows to ensure comparability between land-use types. Extensive pastures were excluded from WUE estimation because biomass removal by sheep grazing could not be accurately determined.

5.2.7 Statistical analysis

All statistical analyses were conducted using R 4.1.3. Linear mixed-effects models (LMMs) were fitted using the "*lmer*" function in the "*lme4*" package (Bates, 2005), incorporating random intercepts to account for the split-plot design and repeated measures. These models were applied to analyze soil water content and storage at different depths, root length density at different depths, total vegetation cover, and water use efficiency. To account for the compositional nature of functional group data, we calculated log-ratios using grass as the reference group. Specifically, we computed the log-ratio of forb to grass (log(forb/grass)) and legume to grass (log(legume/grass)). These log-ratios were then analyzed jointly in a linear mixed-effects model to capture functional group dependence. Land use, climate, year, and their interactions were fixed factors, while year (sampling time), and subplot nested within main plot served as random effects. For models involving root length density, sampling depth, as well as its interaction with land use and year, were additionally tested. Models were fitted using maximum likelihood (ML) estimation, and likelihood ratio tests (χ^2 ratio) were used to assess the significance of fixed effects through stepwise model comparison. We used the "*emmeans*" package (Lenth et al., 2018) to further analyze significant interactions, by running post-hoc pairwise comparisons of estimated marginal means between treatment levels if LMMs yielding significant effects of land-use types and interactions between land use and climate. Linear regression analysis was performed to assess relationships between net change in water content and correlated root length density. We used the "*lme*" function in the "*piecewiseSEM*" package (Lefcheck et al., 2015) to develop structure equation modeling (SEM) to further uncover the direct and indirect contributions of land use, climate scenario, and climate extremes (SPEI) to yield and water use efficiency (Figure S5.3). Prior to scaling, the categorical levels of land use were ordered as CF, IM, OF, and EM to reflect the gradient of land-

use intensity. SPEI, topsoil water storage, deep soil water storage, yield, and water use efficiency were the measured values during the growing seasons until crop harvest. The dataset under extensive pasture was excluded because the yield and water use efficiency were missing. If the initial model was identified as saturated based on Shipley's test of d-separation, indicating by a non-significant *Fisher's C* statistic (*Chi-square* distributed), non-significant paths were subsequently removed to gain a reduced/best-fitted model (Shipley, 2009). Figures were produced with the ggplot2 package (Wickham et al., 2016).

5.3 Results

5.3.1 SPEI and soil water content spatiotemporal dynamics for three years

The SPEI values indicate mild- to extreme drought conditions (-2.39 < SPEI < -0.09) throughout 2022, followed by wetter conditions in mid- and late- 2023 and moderate drought to extreme wet conditions (-1.20 < SPEI < 2.08) in 2024 (Figure 5.2a). Notably, a heavy rainfall event in August 2023 resulted in a water surplus of 142 mm, causing the SPEI to shift abruptly from -2.17 in July to 0.77 in August. The consequences of interannual changes in atmospheric forcing on soil water profiles are demonstrated exemplarily for extensive meadows under ambient climate scenario (Figure 5.2b). The soil moisture at 0-20 cm depth was closely related with the SPEI (looking three months backward in time, $R^2 = 0.57$, $p < 0.001$) and to a lesser degree also with monthly water deficit ($R^2 = 0.23$, $p = 0.005$) (Figure 5.2, S5.4). Summer drought conditions persisted in deeper soil layers, with water content approaching the permanent wilting point, which for our site is at 14.9 % volumetric water content. However, precipitation alleviated these conditions in topsoil, resulting in drier deep soil than topsoil throughout most of the monitoring period. The legacy effect of summer drought was manifested by the long duration for infiltration fronts to reach the depth of 100 cm (five months in 2022, two months in 2023). In 2024, increased precipitation led to higher soil water content well above the permanent wilting point throughout the profile and the entire time, making it the wettest year in the monitoring period (Figure 5.2b). The heavy rain event in August 2023 (on average 5.8 mm per day, with a maximum daily rainfall of 59.3 mm and a cumulative total of 180.4 mm) caused short-term water ponding, but eventually the entire volume of precipitation was taken up by the soil profile without raising the water content to field capacity (at 40.7 % soil water content) due to the enormous soil water deficit at the time

(305 mm available capacity) (Figure 5.1a, 5.2b).

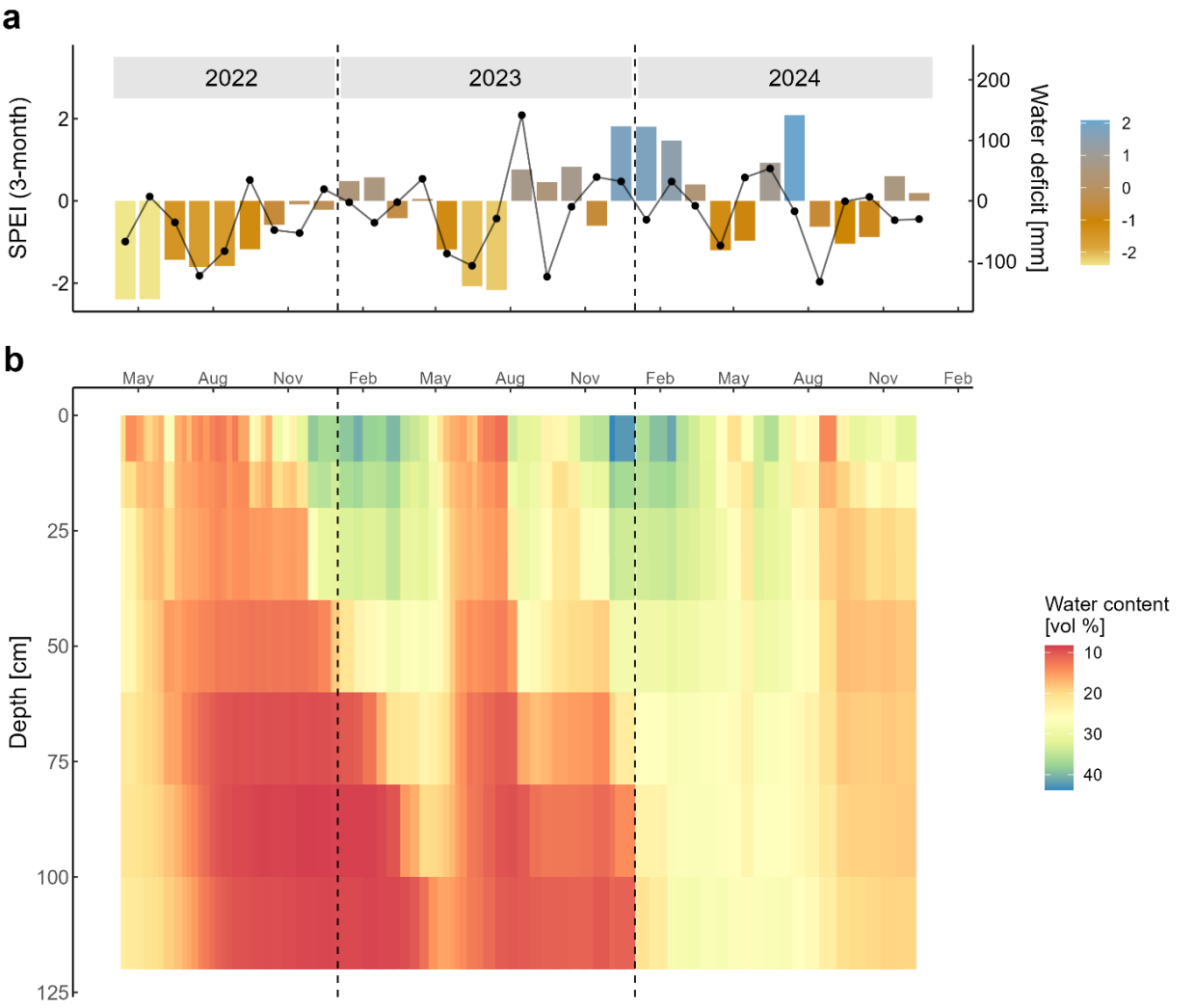

Figure 5.2 Time-series dynamics of meteorological aridity index, water deficit and soil water content from 2022 to 2024. (a) Monthly standardized precipitation-evapotranspiration index (SPEI) with a 3-month timescale and meteorological water deficit, where positive values indicate wetter conditions and negative values indicate drier conditions. (b) Temporal variation in soil water content across different soil depths (0-110 cm), shown exemplarily for extensive meadows under ambient climate. The dashed vertical lines separate the three years of observation. The color scale is bounded by water content at the permanent wilting point and at field capacity.

5.3.1.1 Comparison of soil water content between cropland and grassland

Cropland exhibited consistently higher soil water content than grassland across the entire soil profile, except for 0-10 cm depth in which cropland was drier (Figure 5.3a). The discrepancy in

average soil water content between cropland and grassland increased with depth. Specifically, when averaged across the period for which data is available in both croplands and grasslands, soil water content in cropland was 7.6-7.8 % lower than in grassland at 0-10 cm depth, but 4.0-15.8 % greater at 20-50 cm depth, and 17.8-31.9 % higher at 50-110 cm depth ($p < 0.05$, Figure 5.3a, Table S5.1). The future climate scenario did not affect average soil water content compared to ambient climate irrespective of soil depth (Table S5.1).

In the topsoil (0-30 cm), soil moisture exhibited strong seasonal fluctuations, characterized by pronounced increases during winter and declines in summer (Figure 5.3b). In contrast, the deep soil layer (30-110 cm) displayed a more gradual, delayed response, with cropland maintaining higher soil moisture than grassland during winter 2022, most of 2023, and spring 2024. Differences between climate scenarios were evident, but they were episodic and depended on land-use types. From January to June 2023, the water content of deep cropland soil under the future climate scenario was higher than under the ambient climate, reflecting the percolation of added irrigation in autumn of 2022 and spring of 2023. In contrast, the water content of deep grassland soil remained consistently lower after the heavy rainfall event in August 2023, as 20% of this event was shielded in the future climate scenario.

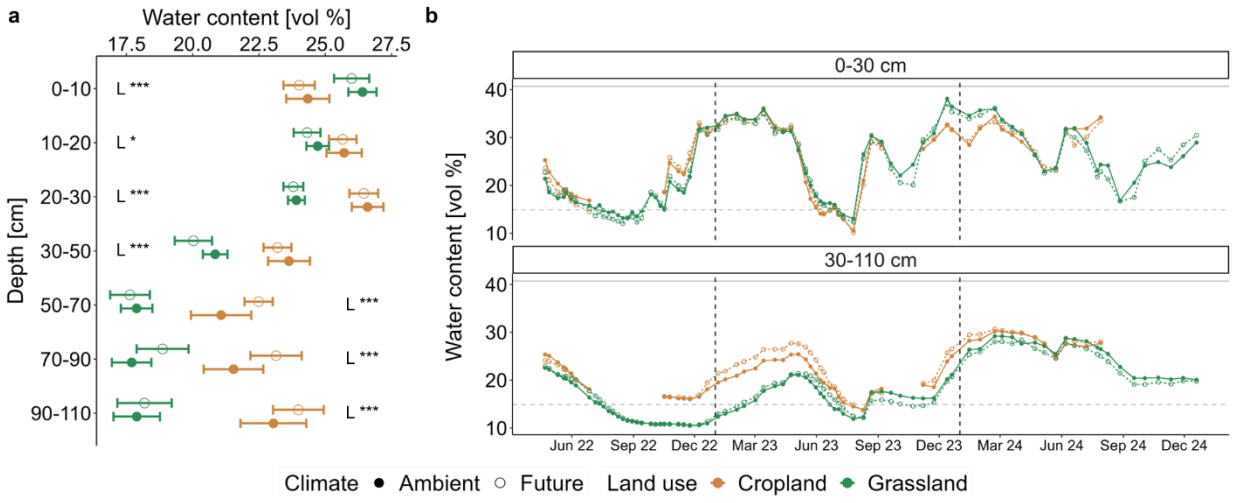

Figure 5.3 Effects of land use and the future climate scenario on soil moisture at different depths. (a) Soil water content at different depths (0-110 cm) under two land-use types (cropland and grassland) and two climate scenarios (ambient and future). Values represent arithmetic mean ± standard error (n = 5). Significant differences between cropland and grassland (L) at different depths are indicated * ($p < 0.05$), and *** ($p < 0.001$). (b) Temporal dynamics of soil water content in the shallow (0-30 cm) and deeper (30-110 cm) soil layers from April 2022 to December 2024, comparing cropland and grassland under ambient and future climate scenarios. The two vertical black dashed lines are used to separate the three years. The

solid gray line represents field capacity, and the dashed line represents the wilting point.

5.3.1.2 Comparison of soil water content between conventional and organic farming

No significant differences were observed in 0-20 cm depth, but organic farming consistently exhibited higher soil water content than conventional farming in deeper soil layers ($p < 0.05$, Figure 5.4a, Table S5.1). The differences between the two farming systems were more pronounced under the ambient climate scenario, with organic farming maintaining 6.4-17.9 % higher water content levels ($p < 0.05$, Figure 5.4a, Table S5.1). Higher soil moisture in the deeper soil under organic farming was most evident during the dry years of 2022 and 2023, but disappeared during the wetter year of 2024 (Figure 5.4b). Under the future climate scenario, soil water content in conventional farming was significantly higher from January to June 2023 in the deep soil layers as a delayed response to irrigation, but declined below ambient climate levels after August 2023 because of precipitation shielding.

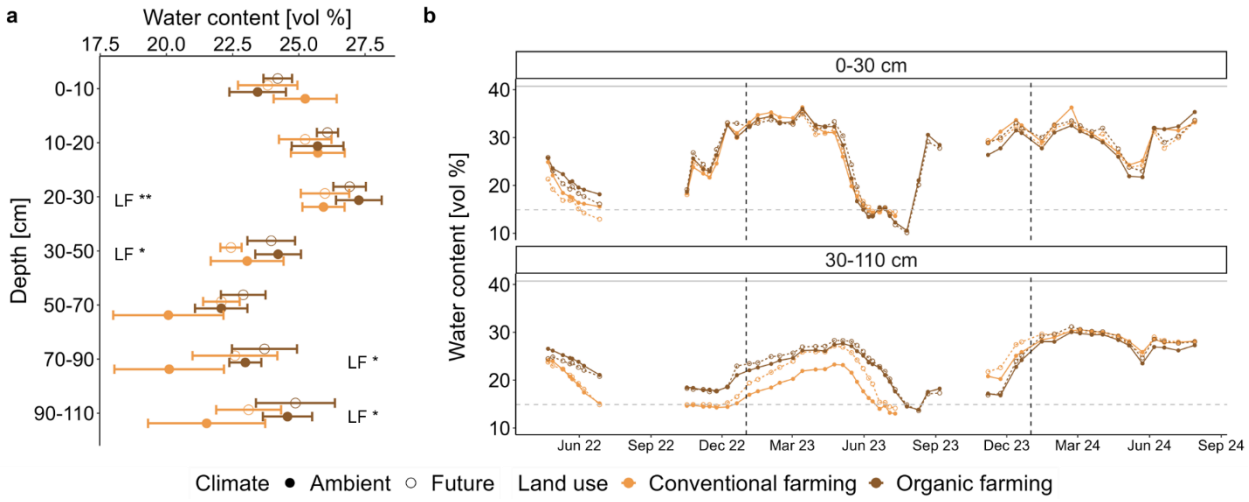

Figure 5.4 Effects of land use and the future climate scenario on soil moisture at different depths. (a) Soil water content at different depths (0-110 cm) under two croplands (conventional farming and organic farming) and two climate scenarios (ambient and future). Values represent arithmetic mean ± standard error (n = 5). Significant differences between conventional farming and organic farming (LF) at different depths are indicated * ($p < 0.05$) and ** ($p < 0.01$). (b) Temporal dynamics of soil water content in the shallow (0-30 cm) and deeper (30-110 cm) soil layers from April 2022 to July 2024, comparing conventional farming and organic farming under ambient and future climate scenarios. The two vertical black dashed lines are used to separate the three years. The solid gray line represents field capacity, and the dashed line represents the wilting point.

5.3.1.3 Comparison of soil water content between intensive and extensive grasslands

Compared to extensive meadows and pastures, intensive meadows had drier topsoil but moister deeper soil layers (Figure 5.5a, Table S5.1). On average, soil water content in intensive meadows across the entire profile was 21.9-41.8 % and 13.1-18.6 % higher under ambient and future climate scenarios, respectively (Figure 5.5a). The gap between deep soil water contents of intensive and extensive grasslands opened when the storage was declining in late summer and became smaller, when the storage was refilled in spring (Figure 5.5b). Under the future climate scenario, deep soil water content significantly declined after September 2023 compared to ambient climate, when the 20 % deficit of the August rain event started to reach the subsoil. This discrepancy was strongest in intensive meadows, as the antecedent soil moisture was the same and persisted until the end of the monitoring period in December 2024 ($p < 0.05$). However, in extensive pastures, soil water content under the future climate scenario was initially higher, a result of the additional irrigation in autumn and spring, but dropped below ambient climate levels after September 2023 (Figure 5.5b).

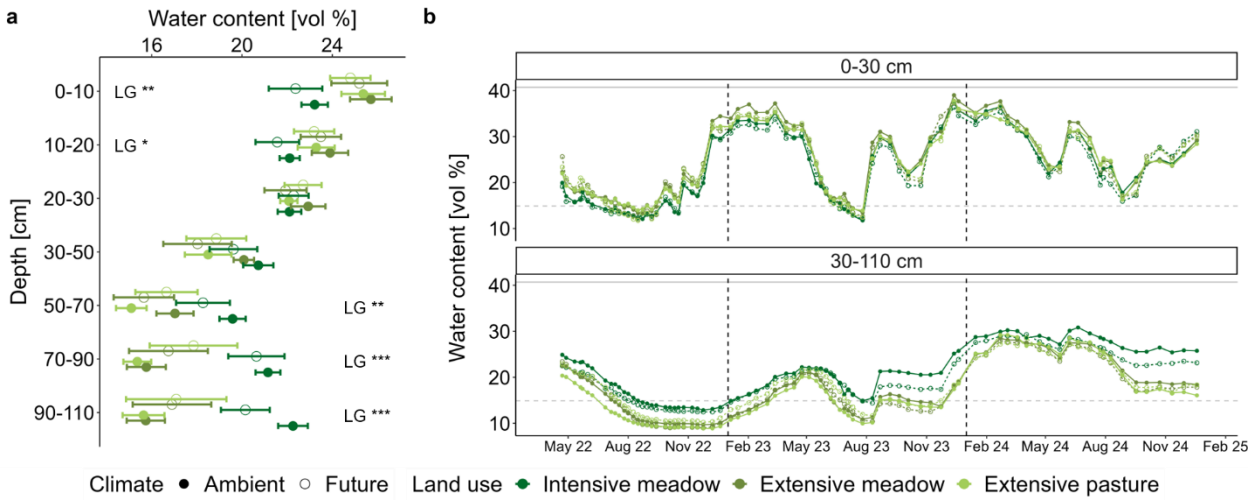

Figure 5.5 Effects of land use and the future climate scenario on soil moisture at different depths. (a) Soil water content at different depths (0-110 cm) under three grasslands (intensive meadow, extensive meadow and extensive pasture) and two climate scenarios (ambient and future). Values represent arithmetic mean ± standard error (n = 5). Significant differences between three grassland types (LG) at different depths are indicated * ($p < 0.05$), ** ($p < 0.01$), and *** ($p < 0.001$). (b) Temporal dynamics of soil water content in the shallow (0-30 cm) and deeper (30-110 cm) soil layers from April 2022 to December 2024, comparing intensive meadow, extensive meadow and extensive pasture under ambient and future climate scenarios. The two vertical black dashed lines are used to separate the three years. The solid gray line represents field capacity, and the dashed line represents the wilting point.

5.3.2 Root length density (RLD), root length distribution, and vegetation cover

RLD in grasslands was 3.6-5.5 times higher than in croplands, with the highest values observed in extensive meadows and lowest values in organic farming (Figure 5.6a). From 0-15 cm to 15-30cm and 30-50 cm soil depth, RLD in grasslands were 3.0-12.0 times, 2.7-7.4 times and 1.6-3.4 times as high as in croplands (Figure 5.6b, Table S5.2-5.3). Across all land-use types, RLD decreased with increasing soil depth at similar proportions.

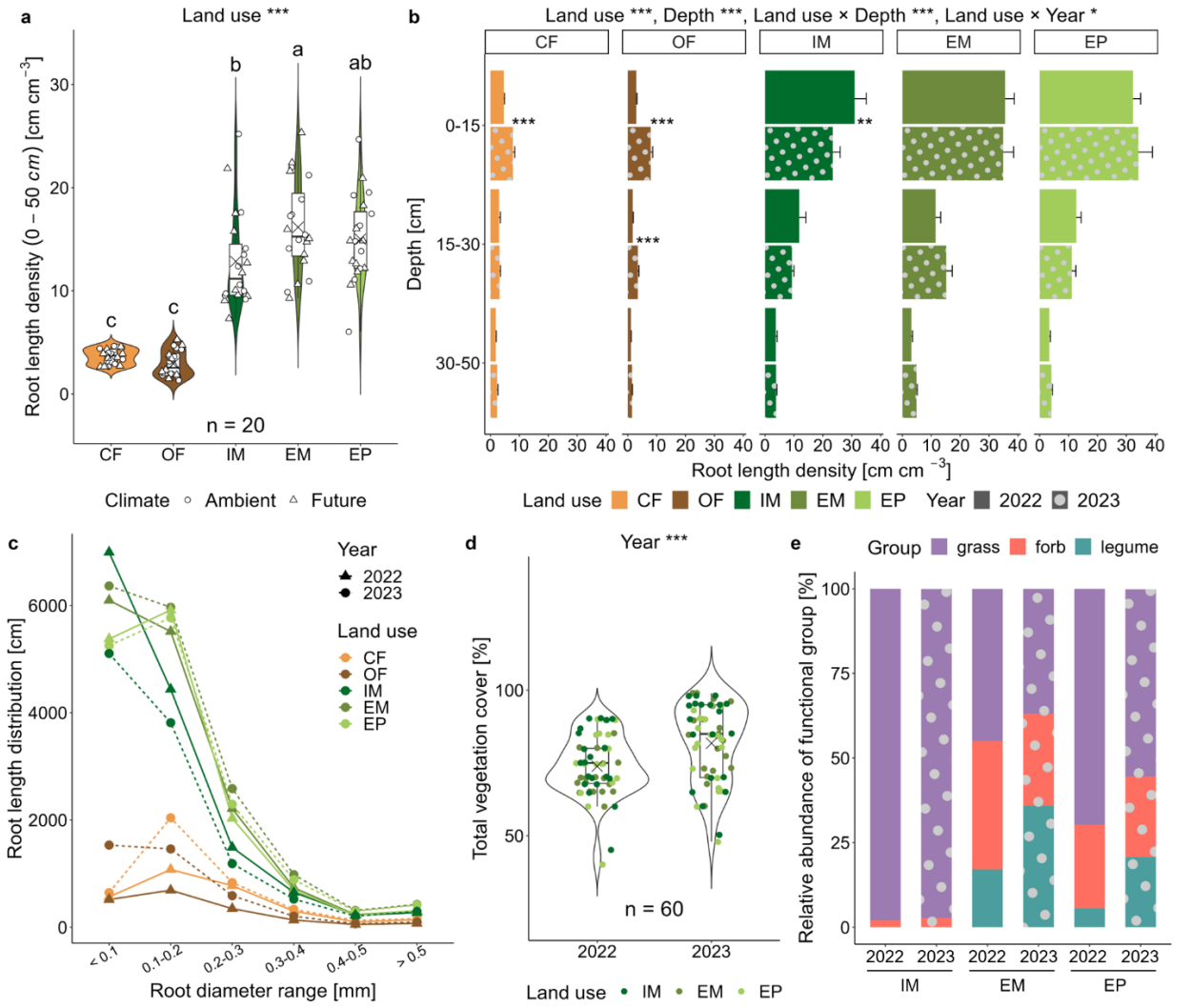

Figure 5.6 Root length density across different land-use types and soil depths across ambient and future climate scenarios. (a) Violin plots showing root length density (0-50 cm soil depth) across five land-use types. Boxes represent the 0, 25, 50, 75, and 100 percentiles, and cross symbols represent the arithmetic mean (n = 20). Different letters indicate significant differences between land-use types ($p < 0.05$). (b) Distribution of root length density across three soil depths (0-15 cm, 15-30 cm, and 30-50 cm) for each

land-use type. Values are arithmetic mean ± standard error (n = 5). Different shading patterns distinguish the 2022 and 2023 data. In conventional and organic farming systems, winter barley was cultivated in 2022, while triticale and white clover were grown in 2023. Root samples were collected in early May, corresponding to the period of rapid root growth in Central Germany. Significant differences between 2022 and 2023 are indicated by asterisks between two bars (** $p < 0.01$, *** $p < 0.001$). (c) Root length distribution across five land-use types, categorized by root diameter classes. Distinct point shapes and line types represent the years 2022 and 2023. (d) Violin plots showing fractional vegetation coverage between 2022 and 2023 for three grassland types. Box plots represent the 0, 25, 50, 75, and 100 percentiles, and cross symbols represent the arithmetic mean (n = 60). Different letters indicate significant differences between two years ($p < 0.05$). (e) Relative abundance of plant functional groups (grass, forb, and legume) for each grassland type in two years. CF, OF, IM, EM and EP represent conventional farming, organic farming, intensive meadow, extensive meadow and extensive pasture, respectively. Significant differences between land use, depth, year, interaction of land use and depth, land use and year are indicated * ($p < 0.05$), ** ($p < 0.01$), and *** ($p < 0.001$).

A significant interaction of land use and year suggested interannual variability in RLD, particularly in croplands at 0-30 cm depths (Figure 5.6b). Compared to 2022, the RLD in 2023 increased by 69.9 % in conventional farming at 0-15 cm depth, 102.9 % and 166.2 % in organic farming at 0-15 cm and 15-30 cm depth, but decreased by 32.3 % in intensive meadow at 0-15 cm depth ($p < 0.01$, Figure 5.6b, Table S5.2-5.3).

RLD was greater in grasslands than in croplands for all root diameter classes, but especially for fine roots (< 0.2 mm) (Figure 5.6c, S5.5). Fine roots (< 0.1 mm) were the most abundant diameter class in intensive meadows, whereas other land-use types had as many or more roots in the 0.1-0.2 mm diameter range. Notably, the length density of roots with 0.1-0.3 mm diameter range were significantly higher in extensive meadows and pastures than in intensive meadows (Figure 5.6c).

Across all three grassland types, the total vegetation cover of the soil surface was higher in 2023 than in 2022 (Figure 5.6d, Table S5.2-5.3). The relative abundance of plant functional groups (grass, forb, legume) and functional group dependence varied both across land-use types and between years (Figure 5.6e, Table S5.2-5.3). The higher total vegetation cover for extensive meadows and pastures in 2023 as compared to 2022, was mainly caused by a higher relative abundance (Figure 5.6e) and summed cover per functional group (Figure S5.6) of legumes.

Furthermore, the future climate scenario had no significant effect on overall RLD (0-50 cm), RLD at individual depth intervals, root length distribution, total vegetation cover, and plant functional group dependence (Table S5.2).

5.3.3 Soil water depletion and root water uptake patterns

Changes in both topsoil and deep soil water storage during the growing season significantly varied across land-use types and years (Figure S5.7, Table S5.2, S5.4). In both the topsoil (0-30 cm) and deep soil layer (30-110 cm), croplands generally experienced greater water depletion than grasslands, particularly in the drought years of 2022 and 2023. The highest topsoil water depletion occurred in 2023, while deep soil water storage depletion peaked in 2022, suggesting pronounced deep water uptake during the extreme drought in 2022. In contrast, soil water storage in 2024 showed minimal change or slight increases across all land-use types.

The relationship between corrected RLD and net change in water content ($P + \Delta S$) in the same depth profiles (0-50 cm) during the period of peak growth (eight weeks centered around root sampling in May) differed between croplands and grasslands in both years (Figure 5.7). In croplands, a strong negative correlation ($R^2 = 0.53$, $p < 0.001$) emerged in 2022 (dry period), but disappeared in 2023 (wet period), indicating that the annual crops relied on the limited shallow soil water storage in 2022, but decoupled the water uptake from the actual RLD under sufficient water supply in 2023. In contrast, perennial grasslands with an extensive root system showed no correlation between shallow RLD and net change in water content at 0-50 cm depth in the dry period of 2022, perhaps because of a shift toward deep root water uptake. A negative correlation ($R^2 = 0.33$, $p < 0.001$) for grasslands emerged in 2023, when the initial soil water contents in the topsoil were higher (close to field capacity, Figure 5.5b) and shallow soil water storage change was greater (Figure 5.7).

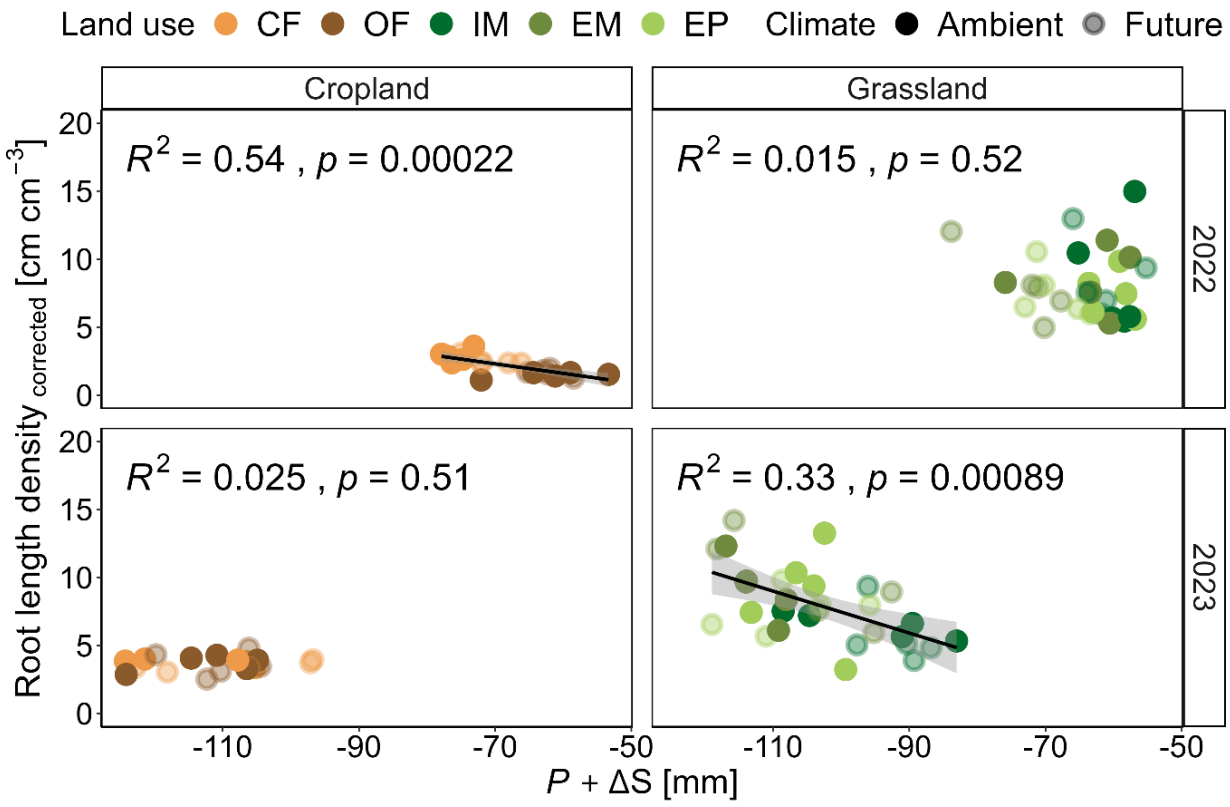

Figure 5.7 Linear regression between net change in water content and corrected root length density across different land-use types, ambient and future climate scenarios, and years. The net change was calculated as the sum of precipitation and the change between soil water content (0-50 cm depth) between four weeks before and four weeks after root sampling, reflecting the amount of available water depleted during this peak growth period. Shaded areas represent the 95 % confidence intervals, displayed only for significant relationships ($p < 0.05$). CF, OF, IM, EM and EP represent conventional farming, organic farming, intensive meadow, extensive meadow and extensive pasture, respectively.

5.3.4 Yield, evapotranspiration and water use efficiency

Annual yield across all land-use types increased consistently with water supply from 2022 to 2024 (Figure S5.8). Using the normal precipitation regime in 2024 as a reference point, the yield drop in the severe drought year of 2022 was found to be 27.8 %, 30.0 %, 32.6 % and 34.5 % for conventional farming, organic farming, intensive meadow and extensive meadow, respectively. Despite interannual variability, the yield differences among land-use types remained stable: conventional farming > intensive meadow > organic farming > extensive meadow. Conventional farming produced 55.40-136.50 % higher yields than organic farming, while intensive meadow yielded 61.69-100.61 % more plant biomass than extensive meadow.

Yield increased with increasing evapotranspiration (ET) during the growing season across all land-use types and both climate scenarios (Figure 5.8a), reflecting interannual changes in drought intensity (Figure 5.2a). Interannual variability in ET was evident. In the absence of drought in 2024, ET was highest on average, regardless of land use. It was 9.5 % lower under the future climate scenario than under the ambient climate and this gap was consistent across land-use types, indicating that it is mainly caused by the precipitation shielding in summer, when ET demand is highest. During the drought years of 2022 and 2023 (yield in dry periods of 2023 before heavy rainfall in August), ET was lower on average. It was higher under conventional (and organic) farming compared to grasslands. Consistent trends imposed by the future climate scenario vanished.

Water use efficiency (WUE) varied significantly across land-use types and years, with 17.6-54.7% higher WUEs in croplands than in grasslands (Figure 5.8b, Table S5.2, S5.4). Conventional farming consistently exhibited the highest WUE (4.48-6.60 kg m^{-3}), whereas extensive meadows had the lowest (1.89-2.78 kg m^{-3}), suggesting that agricultural intensification increases WUE. WUE in intensive meadows was 65.3-87.4 % higher than in extensive meadows ($p < 0.05$, Table S5.2, S5.4). The drought years of 2022 and 2023 caused an increased water use efficiency compared to the normal year of 2024 in all land uses except for the white clover in the organic farming crop rotation of 2023. The future climate scenario only affected WUE under conventional farming, increasing it by 23.6 % in 2023 and decreasing it by 19.6 % in 2024 compared to ambient climate ($p < 0.05$, Table S5.2, S5.4).

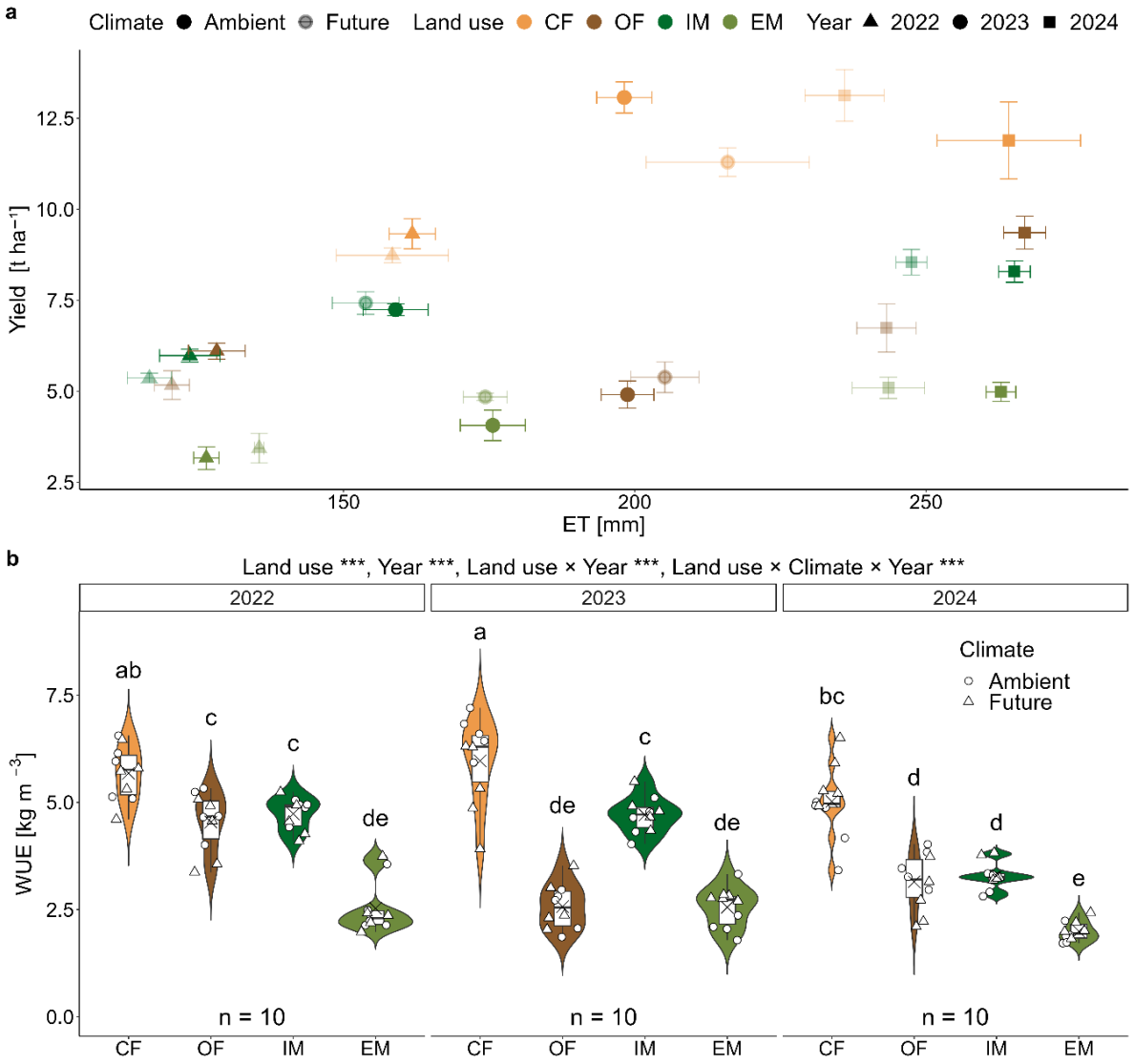

Figure 5.8 Relationship between evapotranspiration (ET) and yield during growing season across different land-use types, ambient and future climate scenarios, and years (a). Values represent arithmetic mean ± standard error (n = 5). (b) Violin plots of water use efficiency across land-use types and years under ambient and future climate scenarios. Boxes represent the 0, 25, 50, 75, and 100 percentile and cross symbols the arithmetic mean (n = 10). Different letters indicate significant differences among land-use types and three years ($p < 0.05$). Significant differences between land use, climate, year, interaction of land use and year, land use, climate and year are indicated *** ($p < 0.001$). The growing season of evapotranspiration, yield and water use efficiency refers to the period from when daily mean temperatures consistently exceed 5 °C until crop harvest. CF, OF, IM and EM represent conventional farming, organic farming, intensive meadow, and extensive meadow, respectively.

5.3.5 Relationship between soil water storage and plant productivity

The SEM revealed that SPEI during the growing season significantly influenced both topsoil and deep soil water storage, although its effect was comparatively weaker on deep soil water storage because of legacy effects (Figure 5.9). In contrast, land use and the future climate scenario exhibited smaller our even negligible effects on water storage terms, respectively (paths removed in the final model). WUE was directly and strongly affected by land use and SPEI, with small indirect effects through water storage terms. Yield was closely associated with WUE, directly and strongly affected by land use, but the strong SPEI effect on yield was clearly mediated by both water storage terms. These combined observations indicated that yield was mainly driven by water availability and the trade-off between growth and maintenance. The model explained a substantial proportion of the variance in WUE (R^2 = 0.76), yield (R^2 = 0.81) and topsoil water storage during the growing season (R^2 = 0.81), all of which exceeded the explained variance in deep soil water storage (R^2 = 0.45) suggesting again the impact of legacy effects on deep water cycling.

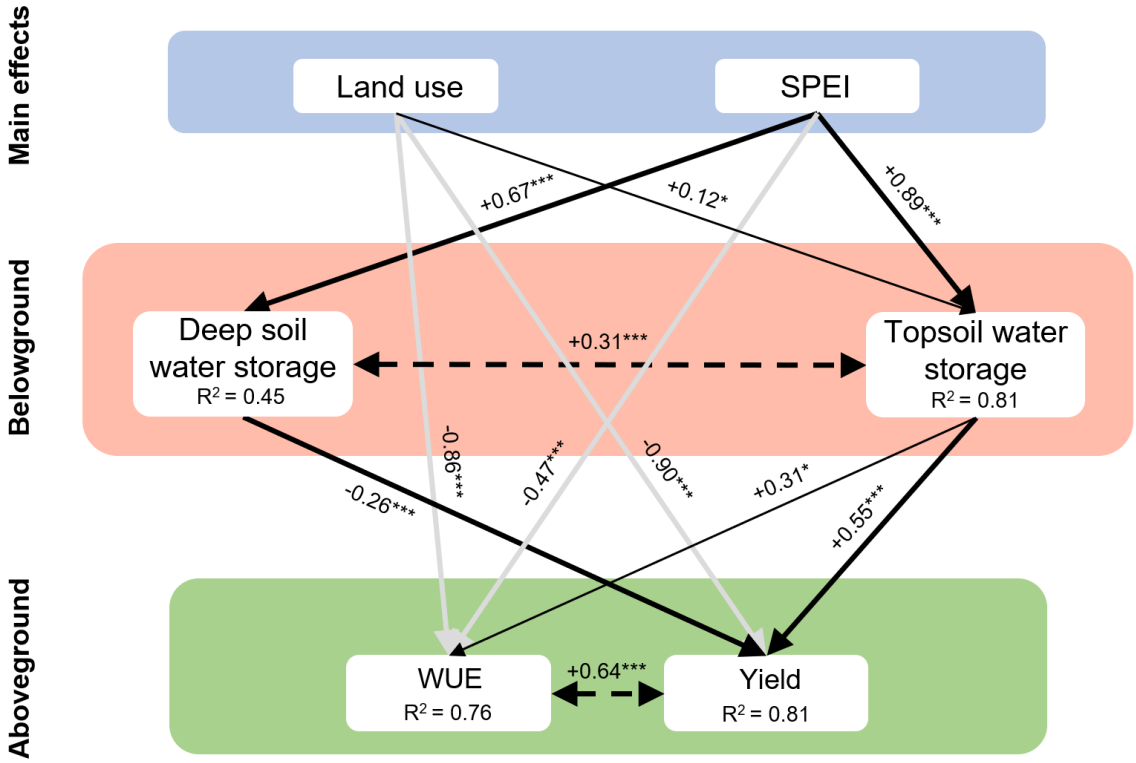

Figure 5.9 Structural equation model depicting how land use and climate extremes affect water use

efficiency and yield and how far these are mediated by soil water storage. Numbers next to arrows indicate standardized path coefficients (robust standard errors of coefficients). Solid lines indicate significant relationships ($p < 0.05$), and gray lines represent the direct pathways. Lines with double-sided arrows indicate potential relationship between covariances. *, **, *** indicate significant differences at 0.05, 0.01 and 0.001 levels, respectively. Prior to scaling, the categorical levels of land use were ordered as CF, IM, OF, and EM to reflect the gradient of land-use intensity. All variables included in the model are continuous measures. The parameters of model are *Fisher's C* = 3.119, $p = 0.21$, $df = 2$.

5.4 Discussion

5.4.1 Effect of climate extremes on topsoil and deep soil water storage

Our results supported the first hypothesis that topsoil water dynamics were primarily controlled by atmospheric forcing in terms of radiation, temperature, and precipitation, and were closely coupled to short-term climatic variability. Shallow soil water content at 0-20 cm depth was tightly linked to the SPEI throughout a three-year monitoring period with two extended droughts (2022, 2023), a heavy summer rain event (2023) and a normal year (2024), indicating that the shallow soil water storage closely tracked precipitation inputs and evapotranspiration (ET) losses, with a rapid turnover and limited buffering capacity under changing climatic conditions (Good et al., 2015; Warter et al., 2021).

In contrast, deep soil water exhibited a stronger "memory" effect on climate variation, particularly during extreme drought events. This finding further supported our hypothesis that deep soil water storage is governed by the legacy effect of past soil moisture conditions. Prolonged periods of negative SPEI led to persistent depletion of deep soil water storage, resulting in an inversion of the soil moisture profiles with depth (soil water content under equilibrium would normally increase with depth due to gravity) that reflected the legacy effects of droughts, while the shallow soil water fluctuated around higher levels following moderate rain events that failed to induce deep infiltration. Notably, infiltration fronts required approximately five months in 2022 and two months in 2023 to reach 100 cm depth after drought, illustrating the delayed replenishment of deep soil moisture. This delay is not only governed by the low unsaturated hydraulic conductivity of dry soils but is further exacerbated by concurrent plant water uptake during infiltration, which reduces the amount of water available for percolation (Bens et al., 2006; Rickard et al., 2025). The persistence of drought in deep soil layers restricts plant water access, delaying phenological development, and influencing ecosystem productivity (Bastos et al., 2020; Sun et al.,

2022; Wu et al., 2018). Furthermore, extreme droughts pushed deep soil water content toward the plant wilting point for extended periods, while topsoil water storage recovered more quickly following precipitation. These patterns aligned with a global modeling study demonstrating increased drying of deep soil layers (> 20 cm) during the growing season under a future climate scenario, although not specific to our study site (Schlaepfer et al., 2017).

As drought extremes intensify, understanding how rooting strategies influence soil water use becomes increasingly critical. Deep rooting can confer drought resistance by accessing subsoil water (Fan et al., 2017; Lynch, 2013), but its effectiveness remains debated due to high metabolic costs and limited deep soil water storage (Figueroa-Bustos et al., 2020; Palta & Turner, 2018; Rasmussen et al., 2019). The effectiveness of the rooting strategy is highly context-dependent, influenced by field conditions and land-use systems (Li et al., 2022a; Lynch, 2019; van der Bom et al., 2020). If the unsaturated hydraulic conductivity of the bulk soil is high, like for the silt loam at this site, then water flow towards the roots sustains efficient root water uptake, reducing the need for extensive root systems (Jorda et al., 2022; Schlüter et al., 2013). Additionally, a heavy rain event in August 2023 substantially replenished deep soil water, offering a long-lasting storage for subsequent dry spells (Feldman et al., 2024). However, this recharge occurred post-harvest for the croplands (outside the main growing season), limiting its immediate benefit for crop productivity. In grasslands, although harvest timing is more flexible and depends on the biomass accumulation (typically one or two cuts in extensive meadow, and up to three in intensive meadow), late-summer rainfall was also unlikely to substantially improve productivity. This is probably because the peak growth of grasses generally occurs in late spring during flowering, and later in the season, declining photoperiod and photosynthesis limit further growth (Brookshire & Weaver, 2015). Thus, deep water storage remains a vital buffer in upland soils without groundwater access, mitigating mismatches between water supply and plant demand.

5.4.2 Effect of land use and future climate scenario on deep water storage

Croplands significantly reduced both the extent and duration of water shortage in deep soil compared to grasslands, primarily due to the 3-4 months bare soil phase after harvest in croplands, reducing water loss by transpiration, as compared to a longer period of ET losses in grasslands through the continuous transpiration of perennial plant species (Spera et al., 2016; Wu et al., 2021). Our results showed that croplands had 4.0-31.9 % higher average soil water content than

grasslands across a 10-110 cm depth profile. This finding primarily supported the second hypothesis that croplands maintain a higher soil water content than grasslands on an annual basis. These results are in accordance with previous studies showing that the conversion of cropland to grassland primarily lead to reduced soil moisture (Gao et al., 2011; Wang et al., 2024b). Another reason for higher soil water content in croplands may be reduced rainfall interception due to sparser and seasonal variable canopies, which allow for more efficient precipitation infiltration into the topsoil, especially during early growth stages (Lian et al., 2022; Lin et al., 2020). The third reason may be the lower root water uptake on the annual basis in croplands than grasslands due to the lower root length density (Bayala & Prieto, 2019), which might be more critical in coarse textured soil with less efficient water flow through soil due to low unsaturated hydraulic conductivity. Notably, the differences in soil water content among different land-use types became increasingly pronounced with depth and were especially evident during dry years, further supporting the legacy effects of deep soil water storage discussed earlier and suggesting that soil water "legacy effects" following droughts are influenced by both vegetation phenology and water use patterns (Zeng et al., 2021).

Furthermore, land-use intensity significantly influences the deep soil water storage, particularly during the climate extremes. The organic farming without mineral fertilization consistently exhibited higher soil water content in deep soil layer compared to conventional farming (highest land-use intensity), particularly during the dry years of 2022 and 2023, likely because nutrient limitations constrained plant growth and thus reduced transpiration and overall ET demand (Barton et al., 2009). In grassland systems, intensive meadow with fertilization, only four forage grass species, and frequent mowing showed lower soil water levels in the topsoil but significantly and consistently higher soil water content in the deeper layers than unfertilized extensive meadows and pastures (lowest land-use intensity). This contrast may be explained by a combination of factors: reduced rooting depth due to early stage of root system development, rapid shoot re-growth after frequent mowing events, and regular fertilization that promote aboveground biomass production and increase water uptake from shallow layers at initially low transpiration rates (Fan et al., 2017; Prechsl et al., 2015; Rose et al., 2011). Additionally, limited canopy cover after mowing reduces interception surface shading, while low plant diversity constrains vertical ET buffering (He & Richards, 2015). This pattern likely also reflects the relatively recent establishment of the intensive meadow, which was ploughed and re-sown in 2020, and may not

yet have developed fully functional and deeper rooting networks characteristic of older, undisturbed grassland (Korell et al., 2024). Notably, the differences in the deep soil water storage between intensive meadow and extensive grasslands were amplified following the heavy rainfall event in August 2023, with the discrepancy becoming even stronger under the wettest conditions in 2024. The capacity of land-use systems to retain or deplete deep soil water following recharge events depend on vegetation community composition and root distribution, which in turn affect infiltration pathways and soil hydraulic properties (Cui et al., 2019; Fischer et al., 2014; Fischer et al., 2014b; Shi et al., 2021). Thus, our findings suggest that both land-use types and intensities modulated the capacity to access and retain deep water, with croplands and intensive grasslands retaining more water than extensive grasslands due to lower transpiration and shallower rooting.

Our results indicate that the future climate scenario further modulated deep soil water storage through interactions with land-use types, especially during the extreme events, by the altered precipitation regimes and increased temperature. Under conventional farming, the future climate scenario exhibited higher deep soil water content than ambient climate when the legacy effect of drought was most dominant (January to June 2023), likely due to the added irrigation during fall and spring, which allowed deeper infiltration and water retention when atmospheric demand was low (Peterson & Westfall, 2005). In contrast, intensive meadow under the future scenario exhibited lower deep soil water content following heavy rain events (August 2023 and June 2024), as 20 % of summer rain events were shielded and large events cause large absolute differences. The future climate scenario effect might be greater in intensive meadow than in extensive meadow, probably due to the dominance of shallow-rooted grass species in these systems, which more rapidly depleted surface moisture but were less effective at utilizing or retaining water at depth. Additionally, lower plant diversity and frequent mowing could have influenced water use patterns, leading to less effective recharge in deeper layer under high-intensity rainfall (Rodriguez‐Iturbe et al., 2001). These patterns highlight the importance of both seasonal deep soil water dynamics and system-specific water use strategies in mediating land-use responses to altered precipitation regimes. Deep soil water storage acts as a critical buffer during climatic extremes, but its effectiveness depends heavily on land-use practices, rooting depth distributions and vegetation composition.

5.4.3 Responses of plant productivity on climate extreme and land-use-based adjustment strategies

Our results supported the third hypothesis: croplands generally produced 47.0-63.5 % higher yields than grasslands, reflecting crop breeding for high resource use efficiency and rapid aboveground biomass production within a short growth period (Leakey et al., 2019). In contrast, grasslands comprising perennial and diverse species, exhibited extended growth periods and lower yield optimization. Productivity was further influenced by land-use intensity, with the lowest yields observed in extensive meadows across years, likely due to lower initial water content and the absence of fertilization. Furthermore, yield was modulated by interannual climate variability and its interaction with land-use systems. Highest yields occurred in the normal year 2024, while significant declines were observed in the drought year 2022 and to a lesser extent in 2023. Notably, the decrease of yields in 2022 relative to 2024 was similar (~ 30 %) across croplands and grasslands, indicating that the extensive grasslands did not exhibit higher resistance to climate extremes. This contradicts our hypothesis and previous findings from the same field site (Isbell et al., 2015; Korell et al., 2024). That is probably due to the differences in the study period (2015-2022), the intensive meadow system being established in 2020, and the fact that the yield analyzed in the current study was based on machine harvesting, as is usual in agriculture. In contrast, Korell et al. (2024) analyzed manually harvested biomass cut close to the ground level, which also included the pastures.

Deep soil water storage partially buffered yield losses against drought extremes. In 2022, the pronounced decline in deep soil water storage indicated its use to maintain productivity during extreme drought. In 2023, despite a summer drought, yields were higher, likely due to uptake of topsoil water and sustained by the infiltration of winter and spring precipitation, with the wetting front reaching the deep soil by March, and supplemented by late-season rainfall recharge. In contrast, the normal conditions in 2024 eliminated the need to access deeper water reservoirs. Our SEM revealed that extreme climates exerted indirect effect on yield through changes in both topsoil and deep soil water storage during the growing season. These findings suggested that deep soil water provides critical buffering, but is insufficient to fully compensate for severe topsoil moisture deficits, particularly under prolonged drought.

Additional coping mechanisms, such as shifts in root patterns, plant community composition,

and improved WUE are essential under extreme drought (Qi et al., 2018; Zwicke et al., 2015). We observed positive correlation between RLD and net change in water content during peak growth, emerging under grasslands in 2023 and croplands in 2022, indicating that root water uptake shifted between topsoil and deep layer depending on drought severity (Bristiel et al., 2018; Zwicke et al., 2015). In grasslands, deep-rooted perennial species, especially the forbs, likely facilitate deep soil water uptake during extreme drought through their dense and persistent root system networks (Barkaoui et al., 2016; Hanslin et al., 2019; Künzi et al., 2025). However, deeper rooting may not be the dominant adjustment mechanism, as efficient water uptake can occur with sparse roots, and high RLD is often more critical for nutrient acquisition (Jorda et al., 2022). In croplands, RLD varied more across years, with higher values in the topsoil in 2023 linked to better moisture availability. Yet, yield variation likely reflects both climate-driven root responses and crop-specific traits, such as finer roots under organic management (Wong et al., 2023). We observed that the total vegetation cover and relative abundance of legumes slightly increased in 2023, suggesting the ability of grasslands with high species richness to undergo year-to-year changes in species composition depending on environmental conditions and species interactions. However, this interpretation is limited by several factors. RLD data only extend to a depth of 50 cm and may be influenced by the effects of crop rotation. Furthermore, vegetation community data are only available for grasslands and do not include observations from 2024. This restricts our ability to fully assess root and community-level responses.

Croplands exhibited significantly higher ET than grasslands in 2022 and 2023, likely due to higher transpiration from fast-growing annual crops with greater leaf area (Li et al., 2015; Rajan et al., 2014). In 2024, ET rates became comparable across all land-use types, suggesting that increased transpiration potential in grasslands (Spera et al., 2016). Croplands consistently had a higher WUE than grasslands, and the WUE showed higher correlation coefficient with yield than RLD, supporting our fourth hypothesis that adaptations to drought and deep soil water limitations would rely more on WUE than on shifts in rooting patterns or plant community. This likely reflects breeding strategies that enhance biomass production, drought tolerance, and stomatal regulation (Haworth et al., 2021; Sun et al., 2019; Turner, 2004; Zhang et al., 2023). In contrast, deep-rooted and drought-resilient grassland perennials often show higher ET losses and lower yield responsiveness, as well as the water loss during maintenance without growth, may contribute to lower WUE (Ponton et al., 2006; Poppe Terán et al., 2023). Furthermore, extensive grasslands

include a high proportion of perennial species capable of clonal regeneration through rhizomes or other belowground tissues, which can sustain transpiration without proportional aboveground biomass gain (Volaire, 2018). Notably, WUE was 65.3-87.4 % higher in intensive meadow than extensive meadow, probably due to the high frequency of mowing, and the application of fertilizer promoting aboveground growth during the peak productivity (Rose et al., 2011).

The future climate scenario showed limited effect on yield but altered water cycling. In 2024, yields were unaffected by the reduced in precipitation, likely due to other limiting factors such as nutrients regulating plant growth during this normal year (Basso & Ritchie, 2018; Fu et al., 2022). During the drought years, legacy effects of additional irrigation in autumn and spring became more relevant, causing greater deep soil water storage, which elevated the ET in the growing season to levels comparable to ambient climate, rendering its effect on yield again negligible. However, root biomass and plant community composition remained unchanged, possibly due to shallow sampling, moderate climatic changes, and ecosystem buffering capacity (Kühn et al., 2022).

Overall, while deep soil water storage provided partial drought buffering, WUE optimization emerges as the dominant adjustment strategy under climate extremes. High-intensity systems, such as conventional farming, maintain productivity through efficient water use and flexible responses to future scenarios. These findings highlight the need for adaptive management to sustain productivity under intensifying climate variability.

5.5 Conclusion

Our study highlights the role of deep soil water storage in buffering plant productivity against climate extremes. Unlike shallow soil moisture, the storage of water in deeper soil responds more slowly to climatic fluctuations. This can help to sustain the supply of water to plants and their productivity during prolonged droughts. However, this buffering capacity is not unlimited. Extreme droughts can thoroughly exploit deep storage, particularly when topsoil moisture is severely depleted. This drives deep soil water content toward the plant wilting point, resulting in a situation that persists until the subsequent year. Conventional farming can enhance deep soil water uptake during drought extremes by proper root systems and increased fertilization, whereas intensive meadow management was beneficial to deep soil water retention through higher mowing frequency. These practices enhance water uptake efficiency and help maintain productivity under extreme conditions. The future climate scenarios had weaker impact on the water cycle than

climate extremes. Management strategies such as optimizing water use efficiency and promoting species or cultivars with appropriate growth spans and rooting systems that align with seasonal water availability can help stabilize productivity. These findings underscore the importance of deep soil water storage and context-specific management practices for maintaining ecosystem resistance and sustainability in an increasingly variable climate.

6 Synthesis and Conclusion

6.1 Summary and discussions

This thesis aimed to contribute to a better understanding of how soil structure and moisture regulate key soil biotic functions under global change. Specifically, it investigated the impact of two important global change factors (climate change and land use) on soil structure and moisture, and examined how these physical changes influence key soil biological processes at the micro-scale, including carbon cycling (**Chapter 2**), nematode community (**Chapter 3**), and root growth (**Chapter 4**). By progressively integrating these findings, the study further assessed how plant-soil interactions shape ecosystem productivity across different land-use systems under climate extremes (**Chapter 5**). Through a multi-scale approach and multiyear field data from the Global Change Experimental Facility (GCEF), this thesis addressed a series of overarching research questions, outlined in detail in **Chapter 1.3**. These questions were explored across the subsequent chapters, each corresponding to a peer-reviewed publication or manuscript. Collectively, these studies establish clear links between soil physical properties, biological processes, and ecosystem functioning (Figure 6.1). The findings indicate that land use exerts a dominant and consistent influence on soil microstructural development, biotic interactions, and ecosystem buffering capacity, whereas the future climate scenario plays a subtler role by modifying water availability and shaping biological responses. Enhancing biologically derived pore networks, promoting fine-root development, and increasing deep soil water retention capacity will be critical strategies for strengthening ecosystems resilience and sustainability under increasing climate variability.

6.1.1 Land use as a primary driver of soil structure and associated functions

The findings of this thesis consistently demonstrated that land-use type exerts a predominant influence on soil structural dynamics and associated biological functions across all chapters (Figure 6.1). By employing advanced deep-learning-based X-ray CT image segmentation (Arzt et al., 2022; Isensee et al., 2021; Phalempin et al., 2025), this study was able to extract unprecedented detail from intact soil cores, including multiple pore classes and particulate organic matter (POM). Complementing this, continuous monitoring of soil moisture profiles down to 110 cm over a three-

year period captured a wide range of climatic conditions, including prolonged droughts and an extreme rainfall event, thereby enabling the assessment of both immediate and legacy effects of climate variability. These innovative methodological approaches revealed that soil microstructure, moisture dynamics, and various biotic functions respond strongly and predictably to land-use types.

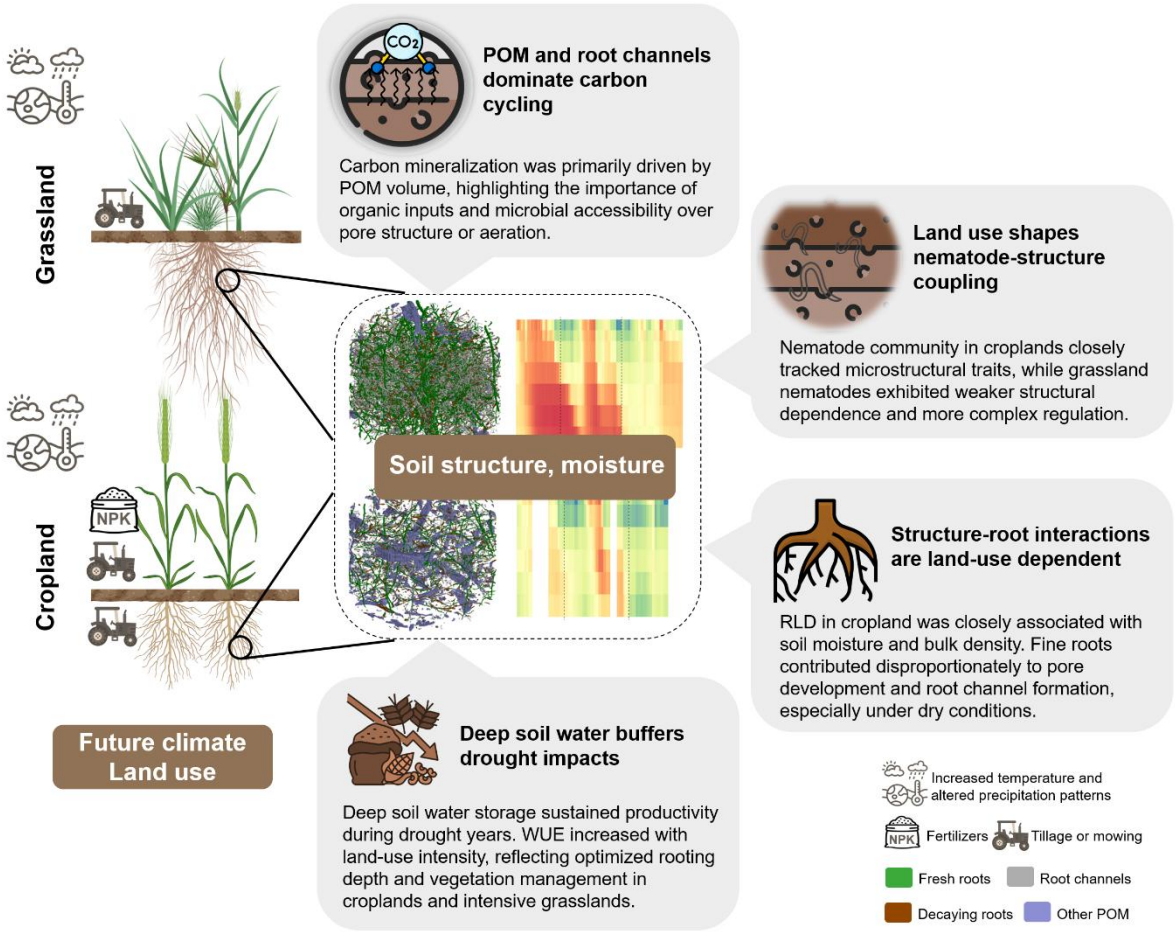

Figure 6.1 Conceptual summary of land-use and climate change impacts on soil structure, moisture, and biotic functions across croplands and grasslands at the Global Change Experimental Facility (GCEF). POM: particulate organic matter, RLD: root length density, WUE: water use efficiency.

Land use exerted a strong influence on both soil microstructure and moisture. Perennial grasslands promoted the development of a biologically driven, well-connected pore network characterized by higher bioporosity, root channel density, and pore connectivity, attributes that remained stable over time due to continuous root input and the absence of tillage (Leuther et al., 2023; Lucas et al., 2019). However, despite this stable pore structure, grasslands exhibited lower volumetric soil moisture than croplands, particularly at the deep soil layers and under drought

conditions, likely due to continuous transpiration and rainfall interception, deeper rooting systems, and higher root water uptake (Bayala & Prieto, 2019; Lian et al., 2022; Wu et al., 2021). In contrast, croplands exhibited lower pore connectivity and root channel density, likely due to periodic tillage and short-lived root systems (Kaur et al., 2024; Peng et al., 2023; Ren et al., 2024b), yet they retained higher topsoil and deep soil moisture, partly owing to reduced transpiration and rainfall interception during fallow periods. These soil physical structural differences reflect contrasting disturbance regimes, rooting strategies and vegetation cover between perennial and annual systems (Jiang et al., 2023; Kuka & Joschko, 2024).

Heterotrophic respiration and organic carbon fractions were strongly influenced by land use, with grasslands exhibiting higher levels of extractable organic carbon (EOC), microbial biomass carbon (MBC) and soil organic carbon (SOC) than croplands. These organic carbon fraction differences reflected underlying structural contrasts. Perennial grasslands accumulated more soil organic carbon than croplands, driven by continuous plant inputs, microbial biomass, and stabilization of POM (Bai & Cotrufo, 2022). Root channels were particularly important, showing strong associations with SOC, labile carbon pools, and heterotrophic respiration, highlighting their role as microbial hotspots (Kravchenko & Guber, 2017; Kravchenko et al., 2019). Soil moisture further emerged as a critical driver of heterotrophic respiration by regulating microbial activity. In contrast, bulk structural metrics like total porosity and bulk density showed limited predictive power, underscoring that carbon cycling is more tightly linked to specific pore types than to bulk soil structure. These findings may reflect differences in soil moisture, texture, or non-limiting aeration in microbial hotspots under our conditions (Schlüter et al., 2022b) and C cycling may be driven more by specific pore types and microscale environments than by bulk structural metrics (Patel et al., 2021). Additionally, unmeasured factors such as enzyme activity, carbon use efficiency, and microbial colonization likely play important roles in regulating carbon dynamics. These results highlight the importance of focusing on biologically driven pore networks when assessing land-use impacts on soil carbon processes.

Nematode abundance and community composition were significantly shaped by land use, with grasslands supporting higher nematode abundance, particularly of bacterivores and plant-parasites, than croplands. This reflected more favorable microhabitat conditions in grasslands, including higher microbial activity, POM content, along with greater biopore diameter and pore connectivity (DuPont et al., 2010; Hu et al., 2024; Johansson et al., 2023; Rui et al., 2022). In

contrast, frequent tillage and lower plant diversity in croplands led to degraded pore structure and simplified nematode food webs characteristic of disturbed systems (Landi et al., 2018; Lenz & Eisenbeis, 2000). Microstructural properties offer valuable insights into the physical context of soil biota, but their predictive power depends on environmental context and trophic interactions. Bacterivore and fungivore abundances in croplands were closely linked to pore connectivity and carbon availability, suggesting bottom-up regulation under disturbed conditions (Jamieson et al., 2002; Shao et al., 2015). In grasslands, however, these relationships were weaker, possibly due to top-down controls like predation and internal trophic dynamics (Cesarz et al., 2017; Felipe-Lucia et al., 2020). The greater co-occurrence network complexity in grasslands supports this interpretation. Importantly, biologically relevant pore metrics, such as biopore diameter and connectivity, proved more informative than bulk indicators like total porosity or bulk density (Erktan et al., 2020; Jiang et al., 2018; Schlüter et al., 2022a). Still, the explanatory power of these properties remained limited, especially in grasslands, highlighting the complexity of interactions within soil food webs (de Vries et al., 2012; Long et al., 2024). Additionally, unmeasured factors such as temperature, plant cover, and soil texture likely also contributed to nematode community variation (Li et al., 2023c; Zhou et al., 2022). These results emphasize the relevance of biologically mediated pore networks and resource accessibility as key determinants of nematode community responses to land-use change.

Land use was also the dominant driver of soil structure-root interactions. Perennial grasslands consistently exhibited higher root length density (RLD), bioporosity, and pore connectivity compared to croplands, supporting more stable and biologically active soil pore networks that reduced mechanical resistance and improved resource accessibility (Jarvis, 2007; Kautz, 2014). In contrast, croplands, subject to periodic tillage and short-term root proliferation, showed disrupted structure and lower RLD, with reduced capacity for roots to reuse existing pore systems, particularly under dry conditions (Liu et al., 2024; Lynch, 2019; White & Kirkegaard, 2010). The relationship between roots and soil structure is both land-use dependent and bidirectional. In croplands, RLD was closely linked to soil moisture and bulk density, while in grasslands, stable pore networks likely minimized structural constraints. Moreover, RLD showed no significant correlation with bioporosity or pore connectivity further supported that pore space and aeration was non-limiting under our soil conditions. The root growth and its integrity, in turn, reshape the soil structure. For example, fine roots in particular contributed to the development and stabilization

of biopores, especially under drought, suggesting a feedback loop whereby root growth reinforces structural connectivity (DuPont et al., 2014; Lucas et al., 2022). Grasslands maintained both lower fraction of fresh roots and higher volumes of root channels across years, highlighting the legacy effects of continuous root turnover in undisturbed systems (Gill & Jackson, 2000; Wang et al., 2019e). In croplands, however, higher fresh root biomass but lower root channel stability implied faster root turnover and limited structural persistence, increasing vulnerability to moisture stress (Hales & Miniat, 2016). These findings underscore the need to consider root-driven feedbacks in soil structural development, particularly the role of fine roots in sustaining biopore networks that enhance soil resilience to moisture variability or climatic stress.

Yield production and water use efficiency (WUE) were significantly influenced by land use. Croplands consistently exhibited higher productivity and WUE than grasslands, reflecting targeted breeding and management for short-term efficiency (Leakey et al., 2019). Their ability to access deep soil water, enhanced by reduced transpiration during fallow periods and more efficient infiltration, contributed to yield stability under moderate drought. However, this advantage depends on high external inputs and may decline if deep water reserves are depleted during prolonged droughts. Grasslands, especially extensive meadows, offered greater ecological buffering through perennial cover and species diversity but did not consistently outperform croplands during dry years. Limited WUE, constrained rooting plasticity, and drought legacies may have reduced their resilience (Bazzichetto et al., 2024; Jackson et al., 2024). Intensive meadows reached higher WUE due to frequent mowing and fertilization but may compromise long-term root development and subsoil water retention (Barkaoui et al., 2016; Künzi et al., 2025). These results highlight a trade-off between ecosystem productivity and resistance.

6.1.2 Limited and context-dependent effects of future climate scenarios

Soil structure and various biotic functions were less sensitive to the moderate shifts induced by the future climate scenario. The future climate scenario had limited effects on topsoil microstructure, carbon cycling, nematode community, root proliferation and yield production and their relationships, likely due to the moderate climatic changes applied, i.e. 0.55 °C higher temperatures, ~10 % more spring/autumn precipitation, and 20 % less in summer. In dry years, however, the overall lack of rainfall meant there was little water to redistribute, limiting the impact of the future climate treatment. Probably because substantial alterations in soil microstructure, C

stabilization, nematode community, root growth, and yield production generally require extreme climatic drivers such as wetting-drying/freezing-thaw cycles, longer timescales, or broader climatic gradients (Leuther et al., 2023; Liu et al., 2024a; Peng et al., 2022; Sierra et al., 2024). In contrast, seasonality, representing stronger climatic variability, played a substantial role in shaping soil physical conditions and nematode community dynamics. Variations in soil moisture across spring and autumn influenced both bulk and microstructural properties, leading to fluctuations in habitable pore space and resource accessibility (Meurer et al., 2020; Pires et al., 2017).

Subtle but notable effects of the future climate scenario were observed in the subsoil. In croplands, a slight increase in biopore formation below the plow layer was detected, likely driven by deeper root growth under dry conditions and the higher adaptive capacity of subsoil microbial communities to climatic changes (Fan et al., 2017; Peng et al., 2025; van Veelen et al., 2020). In contrast, such plasticity was not evident in grasslands, where diverse and undisturbed perennial root systems contributed to more buffered and stable structural responses (Korell et al., 2024; Maurel & Nacry, 2020). Moreover, the future climate scenario increased the heterotrophic respiration in the wet spring of 2023, but not in the dry spring of 2022, probably because the increased precipitation and irrigation promoted the release of protected organic matter (Huang & Hall, 2017). Additionally, seasonal changes in temperature and precipitation under the future climate scenario modified deep soil water dynamics. Croplands benefited from additional irrigation, enhancing deep soil water storage, while intensive meadows exhibited reduced deep moisture due to rapid surface water loss and limited infiltration capacity (Peterson & Westfall, 2005; Rodriguez-Iturbe et al., 2001; Shi et al., 2021).

6.1.3 Trade-offs and synergies in soil and agricultural management under climate change

This synthesis underscores that POM and biologically derived pore structures, such as biopores and root channels, play a pivotal role in supporting essential ecosystem functions, including carbon stabilization, microbial activity, nematode community, and root proliferation. Practices that promote continuous root input and minimize physical disturbance, such as perennial vegetation and reduced tillage, consistently enhance soil structure and functional resilience.

In croplands, our findings point to a trade-off between agronomic productivity and long-term resource sustainability. Conventional farming achieved higher yields and WUE, especially under drought conditions, due to optimized root development and nutrient management. However, these

benefits were accompanied by lower biopore stability and diminished root integrity, indicating reduced structural resilience. In contrast, organic farming maintained higher deep soil water storage but exhibited lower yields due to lack of fertilizers. This underscores a fundamental trade-off in agricultural sustainability between maximizing short-term productivity and maintaining long-term ecosystem stability and soil water retention capacity.

Grasslands showed a similar pattern. Intensive meadows, enhanced by fertilization and frequent mowing, supported higher yields, WUE, and deep soil water content. Yet, these benefits came at the cost of lower resilience to climate extremes, likely due to reduced plant diversity. In contrast, extensively managed grasslands, with perennial species and minimal disturbance, fostered greater biopore connectivity, lower fresh root turnover, and more persistent root-soil feedbacks. While contributing less to food production, these systems provide essential co-benefits such as biodiversity conservation, carbon sequestration, and hydrological regulation.

These findings mirror broader societal challenges. Productivity-focused systems like conventional farming and intensive meadow dominate due to market demands and food security objectives. Yet their long-term environmental costs, including soil degradation and carbon losses, raise concerns under future climate scenarios. In contrast, conservation-oriented practices offer co-benefits in terms of soil health, water storage, and structural resilience, despite lower yield potential. Future solutions may lie in hybrid systems that integrate high-efficiency cropping with sustainable practices, such as cover cropping, reduced tillage, and crop diversification, to jointly support yield and ecosystem stability.

Finally, deep soil water storage emerged as a critical buffer against climate extremes. Management strategies that enhance infiltration (e.g., reduced tillage, diverse meadow, fine-root species) and limit evapotranspiration (e.g., optimized mowing or fallow periods) can increase the availability of subsoil water during droughts, supporting system resilience in the face of intensifying weather variability.

Overall, this thesis contributes to the GLIMPSE program by providing mechanistic insights into how land use and climate change jointly shape soil structure, root development, and belowground biotic interactions, and how these processes regulate water and carbon cycling in agricultural ecosystems. Through integrative analysis of soil microstructure, root traits, nematode communities, and deep soil water storage under ambient and future climate scenarios, the work advances understanding of soil-plant-microbe feedbacks critical for ecosystem resilience. The

findings offer valuable implications for managing soil physical and biological functions to enhance sustainability and adaptive capacity in agroecosystems under global change.

6.2 Limitations

Despite the comprehensive analysis of soil structure and moisture effects on biotic functions under different land-use and climate scenarios, this thesis has several limitations, both in methodology and scope, that warrant consideration.

Methodological limitations: (1) Although high-resolution X-ray CT provided detailed insights into pore-scale structural features, limitations in sample size, spatial resolution, and image segmentation may have constrained the ability to fully quantify functional pore networks relevant for microbial and faunal movement (Helliwell et al., 2013; Lucas et al., 2020). Additionally, CT-derived structural traits were limited to relatively small soil cores on 5-10 cm depth, which may not capture the full spatial heterogeneity of root systems or biopore networks at the field scale. (2) Timing and depth of sampling (5-10 cm vs. 0-15 cm, a few weeks apart) and mismatches between sample types (undisturbed cores vs. bulk soil), may have constrained the detection of stronger structure-function relationships. (3) While the study captured seasonal and interannual variability, the relatively short observation period, particularly under future climate treatments, limits the ability to detect long-term structural changes or delayed biotic responses. Many soil processes, especially those related to structure formation and biological adaptation, occur over decadal timescales (Meurer et al., 2020; Totsche et al., 2024). (4) The experimental manipulation of future climate at the GCEF, involving only moderate increases in temperature and adjustments in precipitation patterns, may not have been sufficient to trigger pronounced changes in soil structure or biotic responses. Moreover, the large interannual variability in precipitation likely overshadowed the comparatively subtle effects of the future climate scenario. This suggests that the ecological consequences of more extreme or prolonged climatic stressors remain underrepresented within the current experimental timeframe.

Scope limitations: (1) Although this study integrated both microhabitat (pore-scale) and macrohabitat (bulk) soil properties, the interpretation of their respective influence on soil fauna, particularly nematodes, was limited by the absence of direct measurements of microbial communities, carbon use efficiency, enzymatic activity, and trophic interactions (Pereira et al., 2024). Without these data, it remains challenging to disentangle the relative contributions of

bottom-up (e.g., substrate availability, microbial biomass) versus top-down (e.g., predation) controls on soil biotic responses across land-use and climate treatments (van Bommel et al., 2024). Moreover, while soil carbon fractions were assessed, carbon fluxes such as soil respiration or net ecosystem exchange were not measured, limiting the ability to mechanistically attribute observed changes in soil C to microbial or root-derived processes (Xu & Shang, 2016). (2) Root-soil interactions were assessed only during spring sampling campaigns, which may have overlooked important seasonal dynamics such as root turnover, phenological shifts, and late-season water uptake. Additionally, root trait analyses focused primarily on morphological parameters, root length density and diameter, without incorporating physiological or biochemical traits (e.g., exudation rates, root respiration, or mycorrhizal associations) that play key roles in soil structure formation and biological activity (Mueller et al., 2024). (3) Finally, while associations between soil structure, root traits, and biotic communities were established, the specific mechanisms linking pore architecture to biological processes (e.g., microbial colonization, nematode mobility, carbon stabilization pathways) were inferred rather than directly tested.

6.3 Future work

This thesis provides novel insights into the interactions between soil structure, water dynamics, plant productivity, and biotic functions under climate variability and land-use change. However, based on my results, several aspects warrant further research to deepen and broaden the current findings:

Integration of microbial and multi-trophic interactions: The development and preservation of biologically generated pore structures, such as root channels, are central to enhancing soil C cycling and resilience, particularly under perennial vegetation and low-disturbance regimes. Future research should aim to increase the temporal resolution of sampling to capture seasonal dynamics, include direct measurements of microbial functional traits (e.g. enzyme activity, carbon use efficiency), and evaluate structural effects under more extreme climate conditions. Moreover, integrating high-resolution pore data with isotopic or molecular markers of carbon fate could help clarify how specific microstructural features contribute to long-term C stabilization (Coppola et al., 2024; Quigley et al., 2018). While nematode communities were analyzed as key bioindicators, future studies should include microbial communities, microbial functional traits (e.g., extracellular enzyme activity, biomass turnover), and trophic linkages to

disentangle bottom-up and top-down controls on soil food webs under changing environmental conditions (van Bommel et al., 2024).

Coupling hydrological modeling with structural data: Future studies should integrate pore-scale structural features into hydrological models to improve simulations of water infiltration, retention, and root uptake under varying land-use and climate conditions. Our findings highlight the importance of biopores, especially root channels, as preferential water and carbon flow pathways. However, most models rely on simplified parameters (e.g., bulk porosity), overlooking pore connectivity and spatial heterogeneity. Coupling X-ray CT-derived metrics with models like HYDRUS-1D or OpenSimRoot would allow for more realistic predictions of water dynamics, evapotranspiration, and water use efficiency (Postma et al., 2017; Singh & Verdi, 2024). This approach could also test how structural degradation or recovery affects infiltration during extreme rain or root access to deep water after drought, improving scenario-based planning for sustainable land management under climate change.

Evaluating management interventions for structural restoration: Future research should explore how targeted land management strategies, such as reduced tillage, cover cropping, organic amendments, or pasture diversification, can restore or enhance soil structure and associated functions in degraded systems. This is particularly relevant given our findings that perennial grasslands promoted more stable biopore networks, higher pore connectivity, and greater root-soil interactions compared to annually tilled croplands. Additionally, intensive land-use practices were associated with reduced root channel formation and lower structural continuity, limiting resilience to climate extremes. Testing restoration-oriented practices could help determine whether biologically formed soil structures, such as biopores and connected pore networks, can be rebuilt over time, and whether these improvements lead to better water retention, carbon storage, and root growth, especially in systems affected by repeated drought. Such practices may be essential for improving long-term resilience and reversing structural degradation in intensively managed agricultural systems under future climate change.

Appendices

Appendices for chapter 2

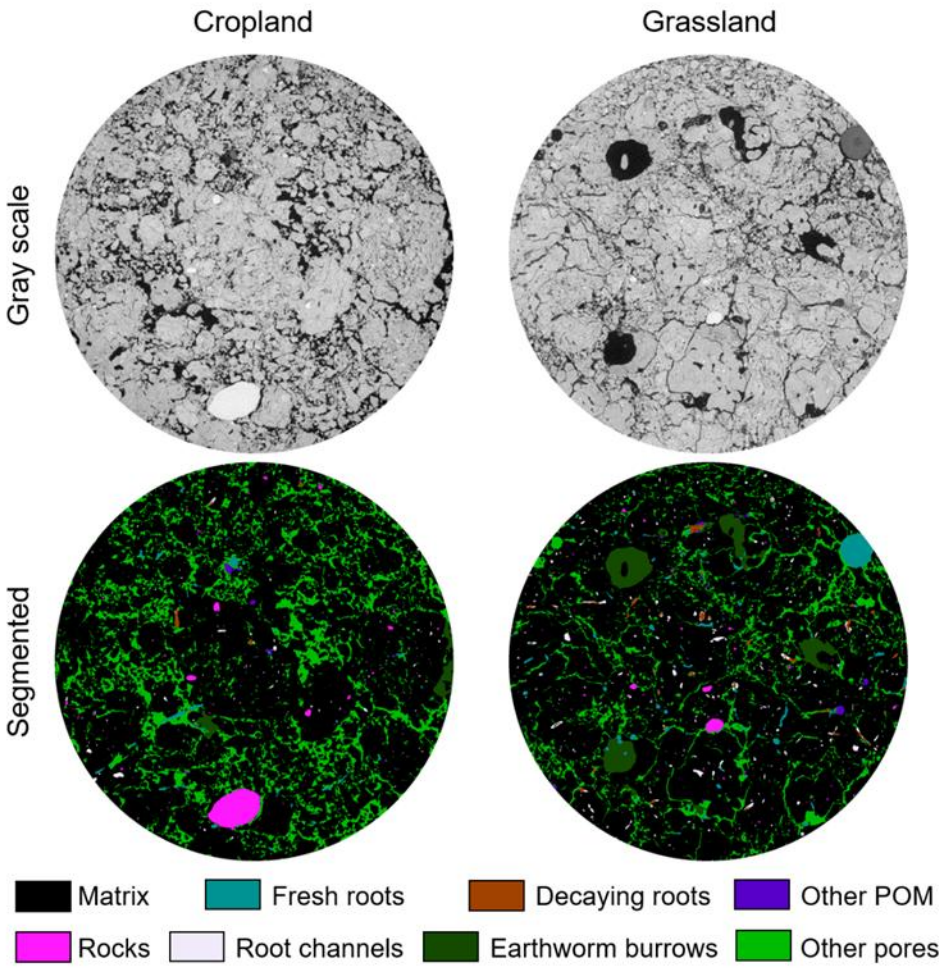

Figure S2.1 Representative X-ray CT cross-sections of soil cores from cropland (left) and grassland (right) systems, shown in gray scale (top row) and segmented format (bottom row).

Figure S2.2 Correlation matrix of soil parameters. Matrix shows Spearman rank correlations between all 49 soil variables. MAT: mean annual soil temperature, POM: particulate organic matter, AP: available phosphorus, C/N: carbon nitrogen ratio, TN: total nitrogen, EN: extractable nitrogen, MBN: microbial biomass nitrogen, SOC: soil organic carbon, EOC: extractable organic carbon, MBC: microbial biomass carbon.

Table S2.1a Pairwise correlations of soil parameters and carbon cycling.

Properties with heterotrophic respiration	r	p	Properties with EOC	r	p
POM	0.409	0.000	MBC	0.648	0.000
Fraction of bioporosity	0.405	0.000	Fraction of fresh roots	-0.581	0.000
Bioporosity	0.341	0.000	Decaying root length density	0.539	0.000
Biopore	0.341	0.000	Decaying roots	0.531	0.000
Pore diameter	0.338	0.000	Root length density	0.521	0.000
Fresh root length density	0.329	0.000	Root volume	0.503	0.000
Biopore surface area density	0.314	0.000	Root channels	0.484	0.000
Root length density	0.307	0.000	pH	0.466	0.000
Biopore diameter	0.306	0.000	Biopore surface area density	0.462	0.000
MBC	0.301	0.000	Biopore length density	0.445	0.000
Other POM	0.291	0.001	Connection probability	0.443	0.000
Earthworm burrows	0.289	0.001	Connection probability of biopore	0.428	0.000
Decaying root length density	0.280	0.001	Fresh root length density	0.419	0.000
Connection probability of biopore	0.277	0.001	Other POM	0.413	0.000
Soil moisture	0.265	0.002	MBN	0.404	0.000
Root volume	0.263	0.002	Mean biopore breath	0.393	0.000
Other pores	-0.249	0.004	SOC	0.386	0.000
Biopore length density	0.221	0.012	Fresh roots	-0.385	0.000
Mean biopore breadth	0.219	0.013	AP	0.365	0.000
Biopore distance	-0.210	0.017	Biopore distance	-0.354	0.000
Decaying roots	0.209	0.018	Biopore	0.327	0.000
pH	0.195	0.028	Bioporosity	0.327	0.000
AP	0.179	0.046	Critical biopore diameter	0.302	0.000
Bulk density	-0.171	0.056	Critical pore diameter	0.293	0.001
Critical pore diameter	0.163	0.070	TN	0.288	0.001
Pore surface area density	-0.158	0.081	DN	0.270	0.002
DN	-0.152	0.094	Rocks volume	0.232	0.008
Critical biopore diameter	0.149	0.100	Earthworm burrows	0.230	0.009
Pore distance	0.142	0.121	Mean pore breadth	-0.213	0.016
MBN	0.137	0.135	Decaying root diameter	0.207	0.019
Root channels	0.130	0.157	Fraction of bioporosity	0.190	0.032
Rocks volume	0.125	0.173	Soil moisture	-0.188	0.035
Fresh roots	0.123	0.178	Root diameter	0.166	0.066
Pores	-0.116	0.204	Bulk density	0.158	0.081
Decaying root diameter	-0.115	0.207	Fresh root diameter	0.158	0.081
SOC	0.110	0.231	Matrix volume	-0.136	0.136
TN	0.109	0.238	Pores	0.135	0.139
EOC	0.103	0.266	Porosity	0.131	0.152
Porosity	-0.069	0.459	Pore distance	-0.120	0.189
Mean pore breadth	-0.061	0.522	Heterotrophic respiration	0.103	0.266
Mean annual soil temperature	-0.060	0.523	POM	0.097	0.295
Matrix volume	0.050	0.599	Pore surface area density	0.086	0.358
Fresh root diameter	0.047	0.618	Mean annual soil temperature	0.082	0.382
Fraction of fresh roots	-0.038	0.692	Biopore diameter	-0.066	0.480
Root diameter	0.023	0.817	Pore diameter	0.054	0.567
Soil temperature	0.011	0.913	Soil temperature	0.052	0.585
C/N	-0.005	0.960	C/N	0.016	0.876
Connection probability	-0.001	0.992	Other pores	0.001	0.991

Notes: Spearman rank correlations coefficients and associated p-values in increasing order. POM: particulate organic matter, AP: available phosphorus, C/N: carbon nitrogen ratio, TN: total nitrogen, EN: extractable nitrogen, MBN: microbial biomass nitrogen, SOC: soil organic carbon, EOC: extractable organic carbon, MBC: microbial biomass carbon.

Table S2.1b Pairwise correlations of soil parameters and carbon cycling.

Properties with MBC	r	p	Properties with SOC	r	p
Root length density	0.712	0.000	TN	0.756	0.000
Decaying root length density	0.679	0.000	Biopore distance	-0.612	0.000
Root volume	0.656	0.000	Mean biopore breath	0.598	0.000
MBN	0.647	0.000	Biopore length density	0.550	0.000
EOC	0.647	0.000	Fraction of bioporosity	0.538	0.000
Fresh root length density	0.627	0.000	Biopore surface area density	0.514	0.000
Biopore surface area density	0.617	0.000	Root channels	0.500	0.000
Decaying roots	0.615	0.000	Fresh root length density	0.494	0.000
Other POM	0.614	0.000	Root length density	0.484	0.000
Fraction of fresh roots	0.604	0.000	Biopore	0.476	0.000
Root channels	0.581	0.000	Bioporosity	0.475	0.000
Biopore length density	0.557	0.000	Mean pore breath	-0.468	0.000
Mean biopore breath	0.500	0.000	Earthworm burrows	0.454	0.000
Connection probability	0.494	0.000	MBC	0.433	0.000
Connection probability of biopore	0.476	0.000	Other POM	0.432	0.000
Biopore distance	0.473	0.000	Decaying root length density	0.423	0.000
Biopore	0.433	0.000	Pore diameter	0.418	0.000
Bioporosity	0.420	0.000	Fraction of fresh root	-0.411	0.000
SOC	0.420	0.000	Root volume	0.411	0.000
Critical pore diameter	0.389	0.000	Connection probability of biopore	0.387	0.000
Critical biopore diameter	0.341	0.000	EOC	0.386	0.000
TN	0.340	0.000	Bulk density	0.375	0.000
Fresh roots	0.328	0.000	Other pores	-0.373	0.000
Fraction of bioporosity	0.301	0.000	Decaying roots	0.364	0.000
Earthworm burrows	0.292	0.001	Fresh roots	-0.356	0.000
AP	0.283	0.001	Mean annual soil temperature	0.350	0.000
Heterotrophic respiration	0.280	0.001	Pore surface area density	-0.313	0.000
pH	0.209	0.017	Biopore diameter	0.243	0.005
Rocks volume	0.199	0.023	Critical biopore diameter	0.241	0.006
POM	0.182	0.039	Critical pore diameter	0.236	0.007
Mean pore breadth	0.135	0.132	Connection probability	0.222	0.012
Root diameter	0.108	0.235	Soil temperature	-0.201	0.023
Pore diameter	0.102	0.264	Pore distance	0.178	0.047
Fresh root diameter	0.072	0.440	DN	0.127	0.166
Soil moisture	0.055	0.559	C/N	0.118	0.196
Matrix volume	0.041	0.666	Soil moisture	-0.111	0.229
Porosity	-0.018	0.855	Heterotrophic respiration	0.110	0.231
Pore distance	-0.075	0.416	AP	0.110	0.231
Mean annual soil temperature	-0.093	0.308	Decaying root diameter	-0.108	0.242
Pore	-0.120	0.182	Fresh root diameter	0.100	0.278
Decaying root diameter	-0.123	0.173	root diameter	0.097	0.296
C/N	-0.133	0.141	MBN	0.093	0.316
Other pores	-0.149	0.095	Rocks volume	-0.076	0.415
Bulk density	-0.171	0.053	Pore	-0.073	0.432
Biopore diameter	-0.211	0.015	Matrix volume	0.071	0.447
Pore surface area density	-0.370	0.000	Porosity	-0.059	0.532
Soil temperature	-0.494	0.000	POM	0.013	0.904
DN	-0.607	0.000	pH	-0.008	0.937

Notes: Spearman rank correlations coefficients and associated p-values in increasing order. POM: particulate organic matter, AP: available phosphorus, C/N: carbon nitrogen ratio, TN: total nitrogen, EN: extractable nitrogen, MBN: microbial biomass nitrogen, SOC: soil organic carbon, EOC: extractable organic carbon, MBC: microbial biomass carbon.

Table S2.2 Topological properties of co-occurring nematode taxa networks obtained under two land uses.

Selected parameters	Co-correlated parameters and their respective correlation coefficients
Rocks volume	
Other POM	biopore surface area density (0.84), connection probability of biopore (0.80), biopore surface area density (0.84), root length density (0.88), root volume (0.93), biopore length density (0.82), fresh root length density (0.90)
Decaying roots	fraction of fresh roots (-0.81), biopore surface area density (0.80), root length density (0.87), root volume (0.89), decaying root length density (0.96)
Fresh roots	
Root channels	fraction of fresh roots (-0.81), biopore surface area density (0.90), biopore breath (0.93), biopore distance (-0.90), root length density (0.84), root volume (0.80), biopore length density (0.95), biopore (0.83)
Earthworm burrows	biopore (0.94), pore diameter (0.88), biopore diameter (0.88), bioporosity (0.93)
Other pores	matrix volume (-0.82), pores (0.85), porosity (0.82), pore surface area density (0.94)
POM	
Mean pore breadth	
Connection probability	
Pore distance	pore surface area density (-0.88)
Critical pore diameter	critical biopore diameter (0.96)
Biopore diameter	pore diameter (0.91)
Fraction of bioporosity	pore diameter (0.82)
Fresh root diameter	root diameter (0.97)
Decaying root diameter	
Bulk density	
Soil moisture	
Mean annual soil temperature	
Soil temperature	
Heterotrophic respiration	
pH	
AP	
SOC	
TN	
C/N	
EOC	
EN	
MBC	
MBN	

Notes: The 30 parameters on the left were kept for further model selection, whereas parameters on the right were filtered out since they were strongly co-correlated ($r > 0.8$ or $r < -0.8$). POM: particulate organic matter, AP: available phosphorus, C/N: carbon nitrogen ratio, TN: total nitrogen, EN: extractable nitrogen, MBN: microbial biomass nitrogen, SOC: soil organic carbon, EOC: extractable organic carbon, MBC: microbial biomass carbon.

Table S2.3 Linear mixed-effects models (LMMs) on the effects of land use, year and their interactions on soil microstructure, bulk and carbon cycling properties.

Properties	Landuse		Year		Land use × Year	
	Chisq	*p*	Chisq	*p*	Chisq	*p*
Matrix volume	3.55	0.47	50.18	**<0.001**	7.71	0.103
Rocks volune	2.84	0.584	2.22	0.136	9.62	**0.047**
Particulate organic matter	30.84	**<0.001**	0.35	0.553	19.56	**<0.001**
Pores	2.01	0.733	56.96	**<0.001**	6.54	0.163
Biopore	225.97	**<0.001**	0.45	0.505	22.12	**<0.001**
Fraction of fresh roots	792.98	**<0.001**	35.62	**<0.001**	13.46	**0.009**
Other POM	238.45	**<0.001**	0.40	0.527	17.42	**0.002**
Decaying roots	312.21	**<0.001**	14.28	**<0.001**	23.84	**<0.001**
Fresh roots	80.47	**<0.001**	9.02	0.003	8.26	0.082
Root channels	768.48	**<0.001**	2.29	0.130	22.30	**<0.001**
Earthworm burrows	102.85	**<0.001**	0.82	0.364	11.57	**0.021**
Other pores	11.89	**0.018**	46.50	**<0.001**	4.51	0.342
Porosity	4.12	0.390	45.75	**<0.001**	9.45	**0.051**
Pore surface area density	8.77	0.067	40.11	**<0.001**	9.08	0.059
Mean pore breadth	53.41	**<0.001**	7.80	**0.005**	4.60	0.331
Pore diameter	64.58	**<0.001**	13.45	**<0.001**	5.12	0.275
Connection probability	74.17	**<0.001**	37.82	**<0.001**	4.80	0.308
Pore distance	14.16	**0.007**	34.29	**<0.001**	4.24	0.375
Critical pore diameter	62.57	**<0.001**	0.00	0.995	1.43	0.838
Bioporosity	231.54	**<0.001**	0.51	0.474	21.86	**<0.001**
Biopore surface area density	595.31	**<0.001**	1.79	0.182	18.19	**0.001**
Mean biopore breadth	685.65	**<0.001**	10.36	**0.001**	17.11	**0.002**
Biopore diameter	27.10	**<0.001**	7.05	**0.008**	7.82	0.098
Connection probability of biopore	201.32	**<0.001**	2.89	**0.089**	13.71	**0.008**
Biopore distance	486.20	**<0.001**	10.27	**0.001**	13.91	**0.008**
Critical biopore diameter	61.96	**<0.001**	0.09	0.761	1.75	0.781
Fraction of bioporosity	165.37	**<0.001**	40.64	**<0.001**	5.35	0.254
Fresh root diameter	60.69	**<0.001**	0.76	0.382	14.33	**0.006**
Fresh root length density	396.06	**<0.001**	7.28	**0.007**	4.92	0.296
Decaying root diameter	61.82	**<0.001**	46.13	**<0.001**	21.07	**<0.001**
Decaying root length density	644.75	**<0.001**	0.51	0.474	4.77	0.311
Root diameter	62.26	**<0.001**	1.46	0.227	13.79	**0.008**
Root length density	622.03	**<0.001**	0.12	0.727	9.45	**0.051**
Root volume	360.53	**<0.001**	7.40	**0.007**	20.52	**<0.001**
Biopore length density	764.18	**<0.001**	0.76	0.385	17.37	**0.002**
Soil moisture	81.19	**<0.001**	1.13	0.287	20.55	**<0.001**
Bulk density	25.32	**<0.001**	1.84	0.175	20.61	**<0.001**
Heterotrophic respiration	26.84	**<0.001**	16.70	**<0.001**	10.05	**0.040**
pH	33.26	**<0.001**	4.93	**0.026**	0.76	0.944
Available phosphorus	32.40	**<0.001**	0.05	0.816	2.06	0.724
Soil organic carbon	110.92	**<0.001**	1.44	0.230	48.48	**<0.001**
Total nitrogen	44.38	**<0.001**	10.87	**<0.001**	23.37	**<0.001**
Carbon nitrogen ratio	1.12	0.890	4.33	**0.037**	1.26	0.868
Soil temperature	57.20	**<0.001**	2.01	0.157	6.20	0.185
Mean annual soil temperature	4.23	0.376	0.19	0.665	14.21	**0.007**
Extractable orgaic carbon	102.88	**<0.001**	8.06	**0.005**	7.19	0.126
Microbial biomass carbon	253.71	**<0.001**	0.83	0.363	4.57	0.334
Extractable nitrogen	57.63	**<0.001**	2.79	0.095	8.84	0.065
Microbial biomass nitrogen	80.56	**<0.001**	1.93	0.165	4.16	0.385

Notes: Significant p values ($p < 0.05$) are in bold.

Table S2.4 Linear mixed-effects models (LMMs) on the effects of climate, year and their interactions on soil microstructure, bulk and carbon cycling properties.

Properties	Land use		Climate		Year		Land use × Climate		Land use × Year		Climate × Year		Land use × Climate × Year	
	Chisq	*p*	Chisq	*p*	Chisq	*p*	Chisq	*p*	Chisq	*p*	Chisq	*p*	Chisq	*p*
Matrix volume	27.49	**<0.001**	0.72	0.396	4.66	**0.031**	5.26	0.262	2.59	0.629	0.35	0.553	5.89	0.207
Rocks volume	2.57	0.631	0.33	0.565	9.84	**<0.001**	7.39	0.117	7.13	0.129	0.08	0.778	4.25	0.374
Decaying roots	182.82	**<0.001**	0.44	0.506	46.61	**<0.001**	1	0.91	14.68	**0.005**	0	0.982	2.97	0.562
Fresh roots	129.83	**<0.001**	0.59	0.442	7.07	**0.008**	0.48	0.976	40.67	**<0.001**	0.26	0.608	1.44	0.837
Other POM	131.58	**<0.001**	0.98	0.322	0	0.96	6.75	0.15	5.21	0.266	0.01	0.907	5.95	0.203
Root channels	1160.52	**<0.001**	0.85	0.357	11.14	**0.001**	1.5	0.827	17.33	**0.002**	1.48	0.225	8.38	0.079
Earthworm burrows	14.92	**0.005**	0.49	0.483	4.03	**0.045**	1.63	0.803	4.76	0.312	2.44	0.118	5.85	0.21
Other pores	60.15	**<0.001**	3.28	0.07	2.29	0.131	5.33	0.255	18.12	**0.001**	0.12	0.732	3.23	0.52
Particulate organic matter	10	**0.04**	0.81	0.367	9.85	**0.002**	1.36	0.852	27.84	**<0.001**	0.18	0.674	1.01	0.909
Pores	24.77	**<0.001**	1.51	0.22	6.56	**0.01**	4.59	0.332	8.36	0.079	0.31	0.575	6.19	0.186
Biopore	33.84	**<0.001**	0.46	0.498	0.81	0.368	1.48	0.83	14.15	**0.007**	2.67	0.103	4.53	0.339
Fraction of fresh roots	912.49	**<0.001**	1.61	0.204	0.39	0.531	9.56	**0.049**	13.74	**0.008**	1	0.317	3.4	0.493
Porosity	27.16	**<0.001**	1.22	0.269	3.73	0.054	4.98	0.289	3.29	0.511	0.24	0.628	5.39	0.249
Pore surface area density	35.59	**<0.001**	0.7	0.404	1.47	0.225	5.78	0.217	16.12	**0.003**	0.36	0.549	1.9	0.753
Mean pore breadth	33.61	**<0.001**	2.75	0.097	18.01	**<0.001**	7.72	0.102	26.97	**<0.001**	0.91	0.34	2.17	0.704
Pore diameter	11.02	**0.026**	0.42	0.516	1.28	0.258	3.13	0.536	10.24	**0.037**	2.39	0.122	2.31	0.679
Connection probability	75.42	**<0.001**	2.56	0.11	4.53	**0.033**	1.14	0.888	16.37	**0.003**	0.2	0.652	8.33	0.08
Pore distance	8.96	0.062	0.06	0.812	4.52	**0.034**	5.26	0.262	11.34	**0.023**	0	0.968	0.2	0.995
Critical pore diameter	15.5	**0.004**	0.59	0.443	0.26	0.607	4.6	0.331	7.92	0.095	0.83	0.361	5.45	0.244
Bioporosity	36.38	**<0.001**	0.37	0.542	1.02	0.312	1.37	0.849	13.97	**0.007**	2.44	0.119	4.26	0.372
Biopore surface area density	430.94	**<0.001**	0.47	0.493	0.93	0.336	0.89	0.927	22.14	**<0.001**	3.31	0.069	5.28	0.259
Mean biopore breadth	866.34	**<0.001**	6.31	**0.012**	0.53	0.468	3.7	0.448	14.2	**0.007**	3.25	0.072	8.91	0.064
Biopore diameter	1.72	0.787	0.33	0.565	2.37	0.123	3.94	0.414	6.39	0.172	1.29	0.257	4.8	0.309
Connection probability of biopore	71.84	**<0.001**	1.5	0.22	0.04	0.847	4.74	0.315	25.01	**<0.001**	0.83	0.362	6.46	0.167
Biopore distance	490.07	**<0.001**	3.96	**0.047**	18.74	**<0.001**	2.36	0.67	31.66	**<0.001**	3.08	0.079	5.29	0.259
Critical biopore diameter	23.84	**<0.001**	0.57	0.452	1.01	0.315	3.57	0.468	8.48	0.075	0.55	0.459	8.9	0.064
Fraction of bioporosity	83.07	**<0.001**	1.34	0.247	2.93	0.087	3.32	0.507	27.94	**<0.001**	3.34	0.068	2.9	0.574
Fresh root diameter	10.2	**<0.001**	0.02	0.898	0.85	0.356	2.94	0.568	4.29	0.368	0	0.954	2.68	0.613
Fresh root length density	284.57	**<0.001**	0.82	0.366	5.49	**0.019**	2.35	0.671	8.33	0.08	0.07	0.799	6.12	0.19
Decaying root diameter	14.9	**0.005**	0.62	0.432	18.38	**<0.001**	4.15	0.386	9.01	0.061	0.28	0.595	6.15	0.188
Decaying root length density	473.05	**<0.001**	1.17	0.279	67.89	**<0.001**	4.5	0.342	21.77	**<0.001**	0.01	0.912	5.17	0.271
Root diameter	9.48	**<0.001**	0.09	0.769	0.04	0.838	2.86	0.581	3.31	0.507	0	0.975	1.93	0.749
Root length density	519.54	**<0.001**	0.03	0.869	13.49	**<0.001**	0.88	0.928	16.46	**0.002**	0.01	0.915	6.49	0.166
Root volume	220.98	**<0.001**	0.26	0.613	7.79	**0.005**	4.66	0.324	12.36	**0.015**	0	0.971	5.19	0.268
Biopore length density	892.19	**<0.001**	1.24	0.266	9.62	**0.002**	2.83	0.586	30.37	**<0.001**	2.55	0.11	6.66	0.155
Soil moisture	116.32	**<0.001**	19.12	**<0.001**	523.92	**<0.001**	2.6	0.627	11.87	**0.018**	14.68	**<0.001**	0.25	0.993
Bulk density	71.56	**<0.001**	2.83	0.093	8.18	**0.004**	4.79	0.309	26.83	**<0.001**	1.12	0.289	2.32	0.677
Heterotrophic respiration	9.57	**0.048**	2.93	0.087	38.98	**<0.001**	7.05	0.133	7.85	0.097	5.61	**0.018**	4.94	0.294
pH	24.79	**<0.001**	7.08	**0.008**	0.68	0.409	9.52	**0.049**	2.46	0.651	0.05	0.827	0.6	0.963
Available phosphorus	13.28	**0.01**	7.69	**0.006**	0.11	0.735	4.42	0.352	1.03	0.906	0.36	0.547	1.46	0.834
Soil organic carbon	195.65	**<0.001**	1.32	0.251	0.1	0.75	3.89	0.421	1.01	0.908	0.03	0.872	1.26	0.868
Total nitrogen	66.84	**<0.001**	0	0.947	5.15	**0.023**	5.2	0.267	0.91	0.923	0.03	0.865	3.12	0.539
Carbon nitrogen ratio	2.68	0.613	0.73	0.393	17.3	**<0.001**	5.16	0.272	0.97	0.915	0.14	0.709	4.97	0.291
Soil temperature	89.62	**<0.001**	2.8	0.094	106.09	**<0.001**	2.52	0.641	42.1	**<0.001**	1.63	0.202	2.34	0.674
Mean annual soil temperature	30.21	**<0.001**	6.66	**0.01**	0.2	0.652	3.22	0.522	17.6	**0.001**	0.51	0.473	1.56	0.815
Extractable organic carbon	130.39	**<0.001**	0.27	0.601	19.42	**<0.001**	28.84	**<0.001**	10.98	**0.027**	0.62	0.43	5.96	0.202
Microbial biomass carbon	193.98	**<0.001**	0.54	0.461	23.41	**<0.001**	8.6	0.072	13.75	**0.008**	0.1	0.749	4.97	0.291
Extractable nitrogen	109.24	**<0.001**	0.33	0.567	0.28	0.599	1.61	0.808	18.88	**0.001**	0.4	0.529	12.87	**0.012**
Microbial biomass nitrogen	73.39	**<0.001**	0.77	0.38	27.38	**<0.001**	6.76	0.149	9.19	0.056	0.03	0.856	21.24	**<0.001**

Notes: Significant *p* values ($p < 0.05$) are in bold.

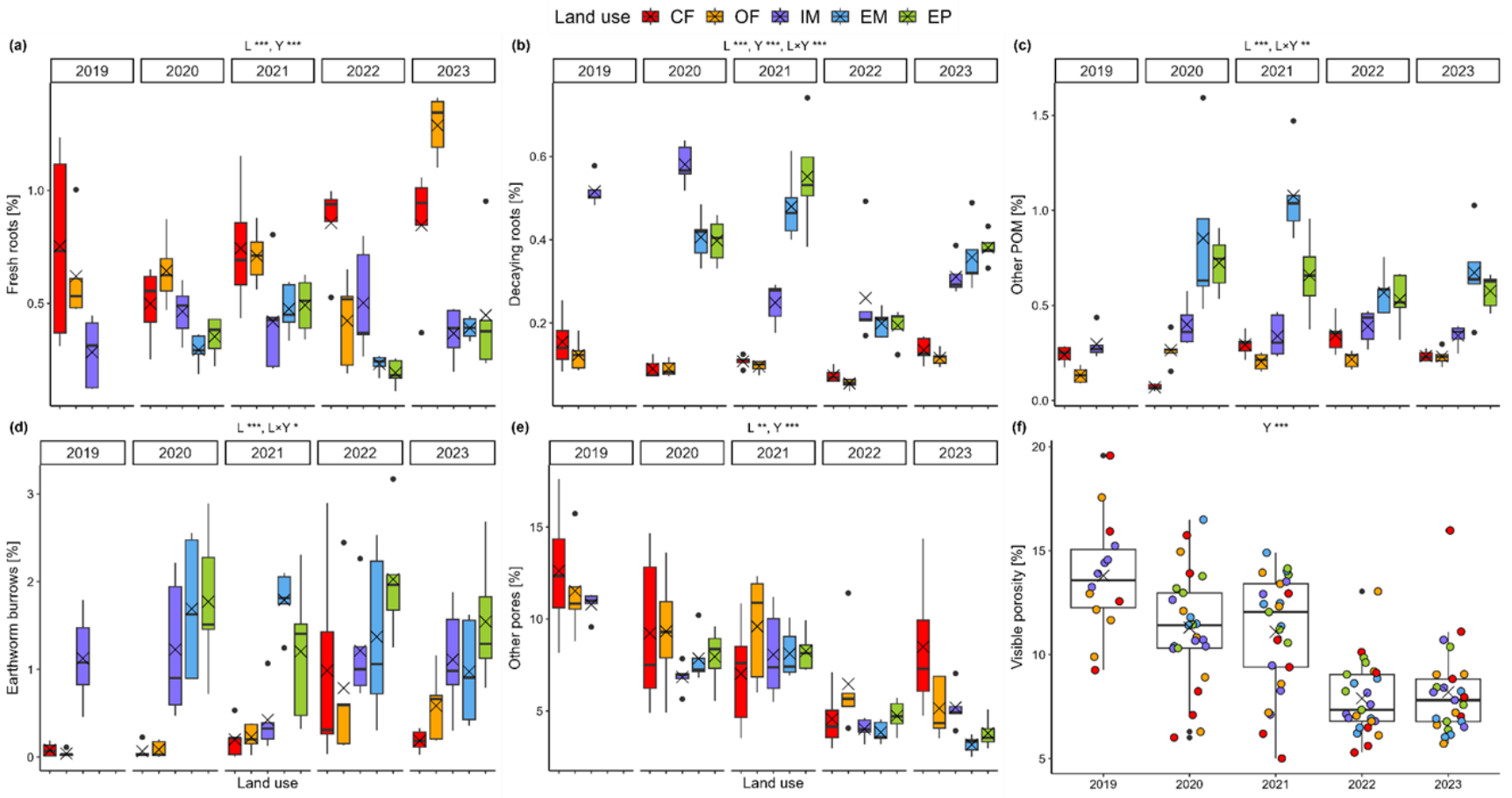

Figure S2.3 Effect of land use on soil microstructure characteristic over five years. (a) Fresh roots, (b) Decaying roots, (c) Other POM, (d) Earthworm burrows, (e) Other pores, (f) Visible porosity. CF, OF, IM, EM and EP represent conventional farming, organic farming, intensive meadow, extensive meadow and extensive pasture, respectively. Significant differences between land use (L), year (Y), interaction of land use and year (L×Y) are indicated * ($p < 0.05$), ** ($p < 0.01$), and *** ($p < 0.001$). Box plots represent the 0, 25, 50, 75, and 100 percentile and cross symbols the arithmetic mean (n = 5).

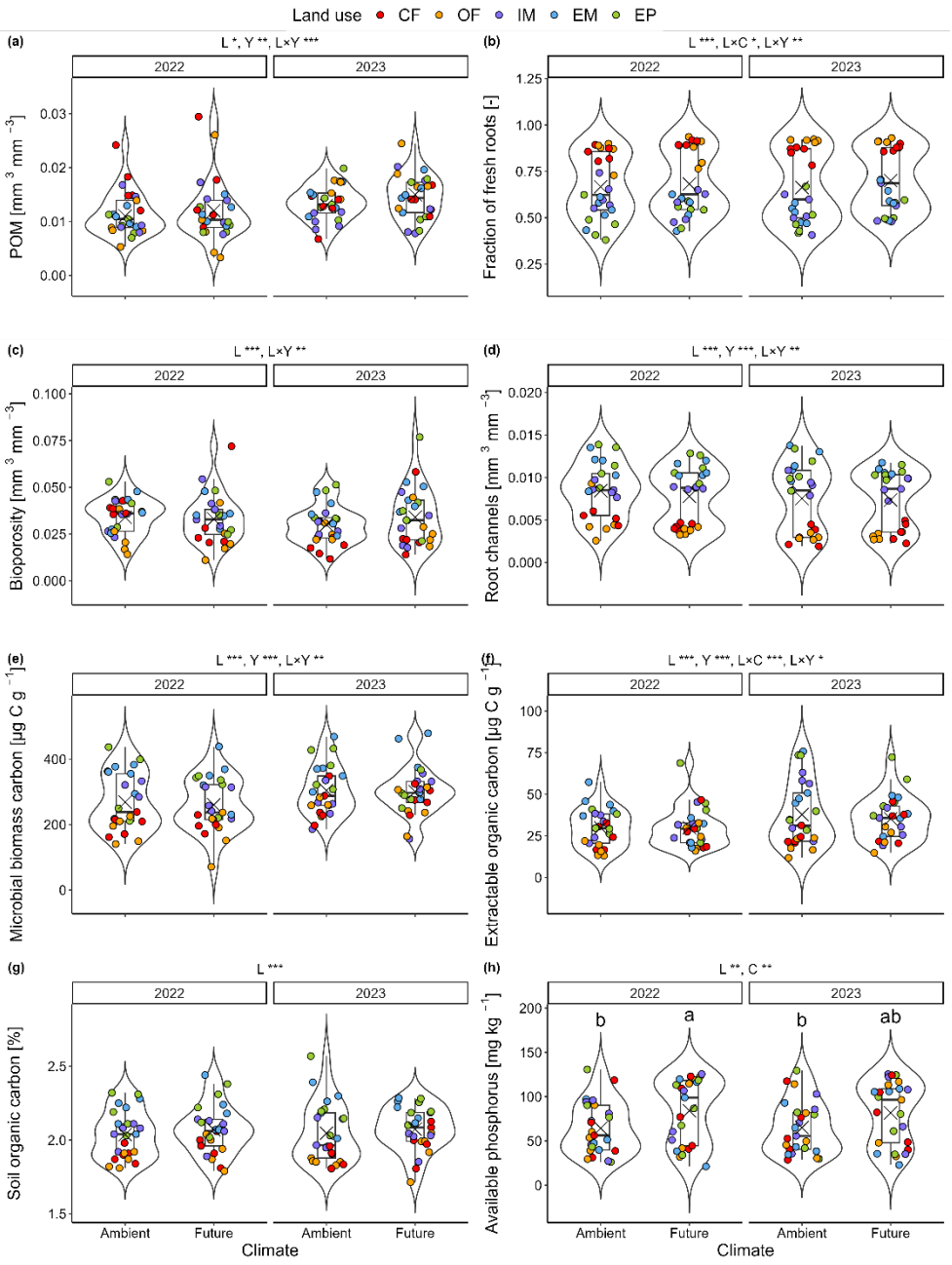

Figure S2.4 Effect of land use and climate change on available phosphorus, soil microstructure, and carbon contents properties in year of 2022 and 2023. (a) POM, (b) Fraction of fresh roots, (c) Bioporosity, (d) Root channels, (e) Microbial biomass carbon, (f) Extractable organic carbon, (g) Soil organic carbon, (h) Available phosphorus. Significant differences between land use (L), climate (C), year (Y), interaction of land use and climate (L×C), land use and year (L×Y), and climate and year (C×Y) are indicated * ($p < 0.05$), ** ($p < 0.01$), and *** ($p < 0.001$). Box plots represent the 0, 25, 50, 75, and 100 percentile and cross symbols the arithmetic mean (n = 25). Different letters indicate significant differences ($p < 0.05$) among treatments.

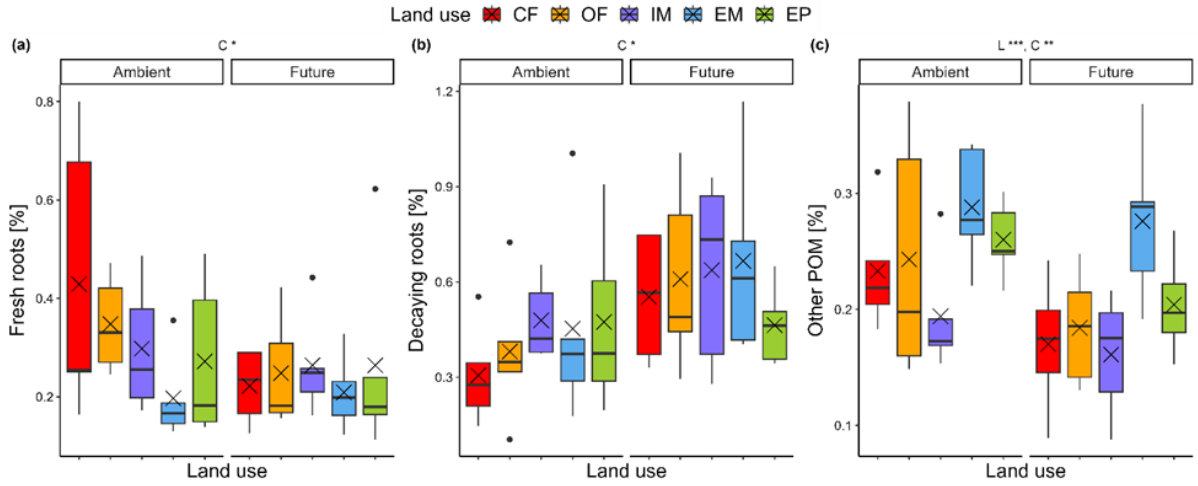

Figure S2.5 Effect of land use and climate change on three particulate organic matter fractions on deep soil layers (35-40 cm) in 2023. (a) Fresh roots, (b) Decaying roots, (c) Other POM. CF, OF, IM, EM and EP represent conventional farming, organic farming, intensive meadow, extensive meadow and extensive pasture, respectively. Significant differences between land use (L) and climate (C) are indicated * ($p < 0.05$), ** ($p < 0.01$), and *** ($p < 0.001$). Box plots represent the 0, 25, 50, 75, and 100 percentile and cross symbols the arithmetic mean (n = 5).

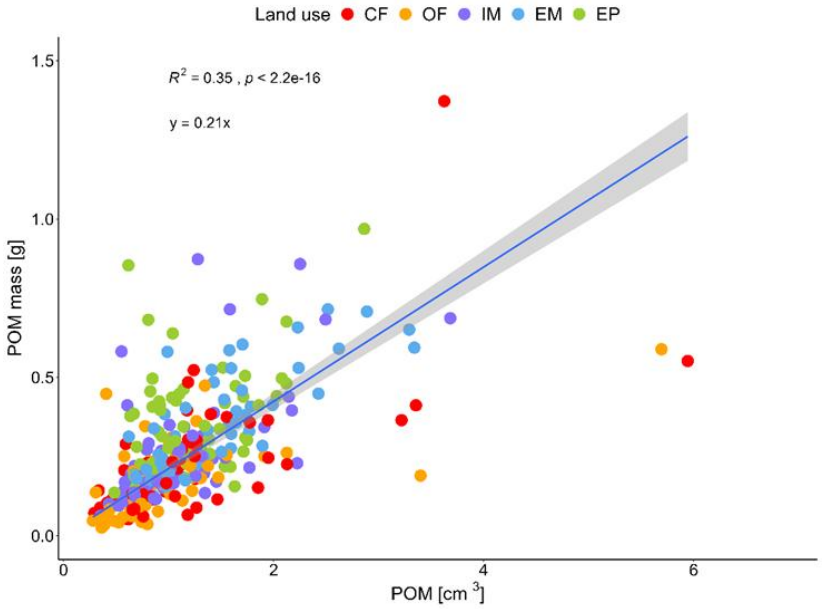

Text S2.1 Particulate organic carbon (POC) was quantified based on the volume fraction of particulate organic matter (POM) derived from X-ray CT data for each soil core. The total POM volume per unit soil volume was obtained by dividing the number of POM-classified voxels by the total number of soil voxels ($mm^3\ mm^{-3}$) and converted to $cm^3\ cm^{-3}$. The POM density (0.21 g cm^{-3}) was estimated from a regression analysis between measured POM mass and POM volume as follows. Subsequently, POM mass per gram of soil was then derived by multiplying the POM volume by the estimated POM density and the bulk density of each individual soil core. Finally, POC was calculated by multiplying the estimated POM mass by a carbon content factor of 17 %, a representative value for particulate organic matter. The final results were expressed as grams of POC per gram of soil.

Table S2.5a Overview of soil microstructure properties on deep layer (35-40 cm) in 2023.

Properties	Units	Ambient					Future				
		CF	OF	IM	EM	EP	CF	OF	IM	EM	EP
Matrix volume	$mm^3\ mm^{-3}$	0.94±0.01	0.92±0.026	0.92±0.006	0.93±0.005	0.92±0.013	0.93±0.019	0.94±0.008	0.91±0.004	0.91±0.01	0.93±0.011
Rocks volune	$mm^3\ mm^{-3}$	0.004±0.001	0.002±0.001	0.003±0.001	0.002±0.001	0.002±0	0.002±0.001	0.002±0	0.002±0.001	0.001±0	0.002±0
Particulate organic matter	%	0.01±0.001	0.01±0.001	0.01±0.001	0.009±0.002	0.01±0.002	0.009±0.001	0.01±0.002	0.011±0.002	0.012±0.002	0.009±0.001
Pores	%	0.04±0.009	0.06±0.025	0.07±0.005	0.06±0.004	0.07±0.011	0.06±0.019	0.05±0.006	0.08±0.003	0.07±0.009	0.06±0.01
Biopore	%	0.02±0.004	0.03±0.004	0.04±0.004	0.04±0.004	0.04±0.003	0.04±0.01	0.04±0.007	0.04±0.004	0.05±0.005	0.04±0.006
Fraction of fresh roots	%	0.5±0.095	0.51±0.058	0.38±0.047	0.33±0.035	0.37±0.063	0.3±0.067	0.29±0.041	0.32±0.049	0.27±0.034	0.34±0.061
Other POM	%	0.23±0.023	0.24±0.047	0.19±0.023	0.29±0.023	0.26±0.015	0.17±0.032	0.18±0.022	0.16±0.023	0.28±0.031	0.2±0.02
Decaying roots	%	0.31±0.07	0.38±0.1	0.48±0.056	0.45±0.144	0.47±0.128	0.55±0.113	0.61±0.13	0.64±0.132	0.67±0.139	0.46±0.056
Fresh roots	$mm^3\ mm^{-3}$	0.43±0.129	0.35±0.043	0.3±0.059	0.2±0.041	0.27±0.072	0.22±0.041	0.25±0.052	0.26±0.048	0.21±0.035	0.26±0.092
Root channels	$mm^3\ mm^{-3}$	1.18±0.321	1.17±0.239	1.62±0.079	1.83±0.301	1.82±0.31	1.9±0.472	1.95±0.28	1.89±0.338	2.29±0.226	1.94±0.172
Earthworm burrows	$mm^3\ mm^{-3}$	0.28±0.092	0.76±0.191	1.68±0.35	0.83±0.141	1.28±0.332	0.9±0.517	0.77±0.318	0.91±0.119	1.11±0.407	1.48±0.416
Other pores	-	2.77±0.74	4.5±2.343	3.45±0.388	3.25±0.289	3.8±0.972	3.41±1.04	2.37±0.197	4.68±0.21	3.87±0.485	2.89±0.477
Porosity	$mm^3\ mm^{-3}$	0.05±0.009	0.07±0.025	0.08±0.006	0.07±0.005	0.08±0.012	0.07±0.019	0.06±0.008	0.09±0.004	0.08±0.01	0.07±0.011
Pore surface area density	$mm^2\ mm^{-3}$	0.89±0.168	1.06±0.306	1.05±0.06	1.08±0.075	1.14±0.184	1.05±0.254	0.9±0.058	1.33±0.034	1.22±0.104	1.02±0.102
Mean pore breadth	mm	0.89±0.19	0.72±0.054	0.84±0.051	0.95±0.058	0.93±0.119	0.83±0.178	0.79±0.029	1.05±0.041	1±0.05	0.91±0.054
Pore diameter	mm	0.32±0.009	0.37±0.039	0.57±0.099	0.44±0.05	0.49±0.068	0.37±0.049	0.42±0.093	0.37±0.023	0.47±0.089	0.64±0.097
Connection probability	-	0.56±0.045	0.61±0.158	0.77±0.018	0.65±0.025	0.65±0.088	0.72±0.038	0.62±0.066	0.75±0.014	0.71±0.039	0.66±0.05
Pore distance	mm	0.31±0.041	0.3±0.027	0.26±0.01	0.25±0.013	0.26±0.022	0.29±0.053	0.27±0.013	0.23±0.01	0.23±0.012	0.25±0.014
Critical pore diameter	mm	0.56±0.097	0.56±0.067	0.58±0.087	0.63±0.134	0.62±0.074	0.63±0.126	0.55±0.033	0.64±0.085	0.7±0.111	0.55±0.108
Bioporosity	$mm^3\ mm^{-3}$	0.02±0.004	0.03±0.004	0.04±0.004	0.04±0.004	0.04±0.003	0.04±0.01	0.04±0.006	0.04±0.004	0.05±0.005	0.04±0.006
Biopore surface area density	$mm^2\ mm^{-3}$	0.29±0.051	0.32±0.039	0.42±0.014	0.44±0.047	0.45±0.048	0.41±0.088	0.43±0.046	0.45±0.057	0.52±0.038	0.45±0.033
Mean biopore breadth	mm	0.23±0.036	0.26±0.025	0.32±0.005	0.35±0.022	0.33±0.027	0.29±0.048	0.32±0.019	0.34±0.03	0.37±0.012	0.33±0.012
Biopore diameter	mm	0.47±0.039	0.59±0.09	0.84±0.161	0.66±0.112	0.72±0.146	0.5±0.081	0.55±0.131	0.58±0.055	0.68±0.149	0.9±0.155
Connection probability of biopore	-	0.21±0.04	0.43±0.158	0.29±0.06	0.15±0.019	0.16±0.032	0.22±0.05	0.24±0.058	0.12±0.036	0.28±0.015	0.29±0.036
Biopore distance	mm	0.51±0.039	0.48±0.028	0.41±0.003	0.4±0.013	0.41±0.015	0.44±0.042	0.41±0.017	0.41±0.022	0.38±0.008	0.4±0.009
Critical biopore diameter	mm	0.53±0.108	0.48±0.114	0.5±0.058	0.62±0.139	0.53±0.096	0.54±0.151	0.49±0.044	0.58±0.094	0.64±0.103	0.5±0.116
Fraction of bioporosity	-	0.52±0.07	0.49±0.083	0.56±0.025	0.52±0.022	0.55±0.053	0.53±0.061	0.61±0.038	0.45±0.038	0.54±0.011	0.59±0.01
Fresh root diameter	mm	0.29±0.013	0.28±0.03	0.52±0.279	0.28±0.018	0.29±0.011	0.23±0.014	0.25±0.037	0.26±0.024	0.26±0.015	0.23±0.011
Fresh root length density	$mm\ mm^{-3}$	0.14±0.01	0.16±0.012	0.18±0.019	0.23±0.042	0.19±0.004	0.16±0.016	0.17±0.016	0.17±0.02	0.24±0.032	0.2±0.014
Decaying root diameter	mm	0.22±0.009	0.22±0.017	0.23±0.007	0.21±0.011	0.22±0.011	0.24±0.007	0.25±0.011	0.24±0.005	0.22±0.016	0.22±0.006
Decaying root length density	$mm\ mm^{-3}$	0.34±0.063	0.37±0.06	0.55±0.071	0.51±0.103	0.5±0.095	0.55±0.103	0.55±0.077	0.62±0.13	0.71±0.073	0.53±0.071
Root diameter	mm	0.27±0.01	0.27±0.015	0.37±0.105	0.26±0.008	0.27±0.009	0.25±0.012	0.28±0.008	0.26±0.004	0.26±0.006	0.24±0.004
Root length density	$mm\ mm^{-3}$	0.39±0.057	0.44±0.042	0.5±0.043	0.62±0.102	0.58±0.091	0.58±0.104	0.57±0.073	0.63±0.104	0.72±0.071	0.55±0.04
Root volume	$mm^3\ mm^{-3}$	0.44±0.054	0.5±0.056	0.55±0.041	0.6±0.108	0.6±0.109	0.59±0.096	0.65±0.095	0.65±0.107	0.77±0.099	0.54±0.045
Biopore length density	$mm^3\ mm^{-3}$	0.86±0.166	1.02±0.119	1.34±0.033	1.43±0.116	1.41±0.131	1.23±0.266	1.3±0.11	1.47±0.142	1.58±0.082	1.39±0.087
Bulk density	$g\ cm^{-3}$	1.61±0.082	1.62±0.108	1.66±0.071	1.65±0.081	1.56±0.049	1.6±0.08	1.76±0.044	1.59±0.086	1.65±0.084	1.67±0.085
Soil moisture	%	18.15±0.636	19.49±0.572	18.8±0.308	19.79±0.415	19.83±0.53	18.7±0.819	19.67±0.55	19.41±0.574	20.34±0.395	19.99±0.527

Notes: Values are arithmetic mean ± standard error (n = 5). CF, OF, IM, EM and EP represent conventional farming, organic farming, intensive meadow, extensive meadow and extensive pasture.

Table S2.5b Linear mixed-effects models (LMMs) about the effect of land use, climate change and interaction on soil microstructure properties on deep layer (35-40 cm) in 2023.

Properties	Landuse		Climate		Land use × Climate	
	Chisq	*P*	Chisq	*P*	Chisq	*P*
Matrix volume	4.358	0.36	0.249	0.618	3.02	0.555
Rocks volune	12.335	**0.015**	3.646	0.056	5.092	0.278
Particulate organic matter	0.91	0.923	0.351	0.553	2.204	0.698
Pores	4.857	0.302	0.27	0.604	3.574	0.467
Biopore	9.728	**0.045**	3.734	0.053	4.043	0.4
Fraction of fresh roots	7.494	0.112	8.346	**0.004**	7.379	0.117
Other POM	21.461	**<0.001**	8.295	**0.004**	1.616	0.806
Decaying roots	3.205	0.524	4.415	**0.036**	2.423	0.659
Fresh roots	6.921	0.14	4.747	**0.029**	7.31	0.12
Root channels	6.232	0.182	8.494	**0.004**	2.437	0.656
Earthworm burrows	12.651	**0.013**	0.1	0.752	6.989	0.136
Other pores	2.021	0.732	0.038	0.845	6.8	0.147
Porosity	4.52	0.34	0.428	0.513	3.416	0.491
Pore surface area density	4.503	0.342	0.372	0.542	3.932	0.415
Mean pore breadth	8.428	0.077	1.103	0.294	3.062	0.547
Pore diameter	14.143	**0.007**	0.193	0.661	9.392	0.052
Connection probability	7.84	0.098	0.995	0.319	2.54	0.637
Pore distance	11.84	**0.019**	2.091	0.148	0.603	0.963
Critical pore diameter	1.922	0.75	0.126	0.723	1.035	0.904
Bioporosity	9.836	**0.043**	3.811	0.051	4.512	0.341
Biopore surface area density	12.045	**0.017**	6.214	**0.013**	2.908	0.573
Mean biopore breadth	25.47	**<0.001**	5.8	**0.016**	2.68	0.613
Biopore diameter	13.9	**0.008**	0.03	0.854	5.48	0.241
Connection probability of biopore	8.38	0.079	0.16	0.69	16.32	**0.003**
Biopore distance	24.08	**<0.001**	6.03	**0.014**	5.96	0.202
Critical biopore diameter	2.71	0.607	0.14	0.713	0.36	0.986
Fraction of bioporosity	4.7	0.32	0.13	0.716	12.9	0.012
Fresh root diameter	3.84	0.427	2.73	0.099	3.07	0.547
Fresh root length density	23.78	**<0.001**	0.17	0.683	0.83	0.935
Decaying root diameter	7.67	0.105	1.88	0.171	1.58	0.812
Decaying root length density	7.74	0.102	6.57	**0.01**	2.28	0.684
Root diameter	5.05	0.283	1.92	0.166	4.19	0.381
Root length density	9.43	0.051	5.43	**0.02**	2.94	0.567
Root volume	6.7	0.153	2.47	0.116	3.82	0.431
Biopore length density	22.15	**<0.001**	5.86	**0.015**	3.13	0.536
Bulk density	5.49	0.241	0.13	0.715	8.92	0.063
Soil moisture	16.5	**0.002**	1.97	0.16	0.47	0.976

Notes: Significant p values ($p < 0.05$) are in bold.

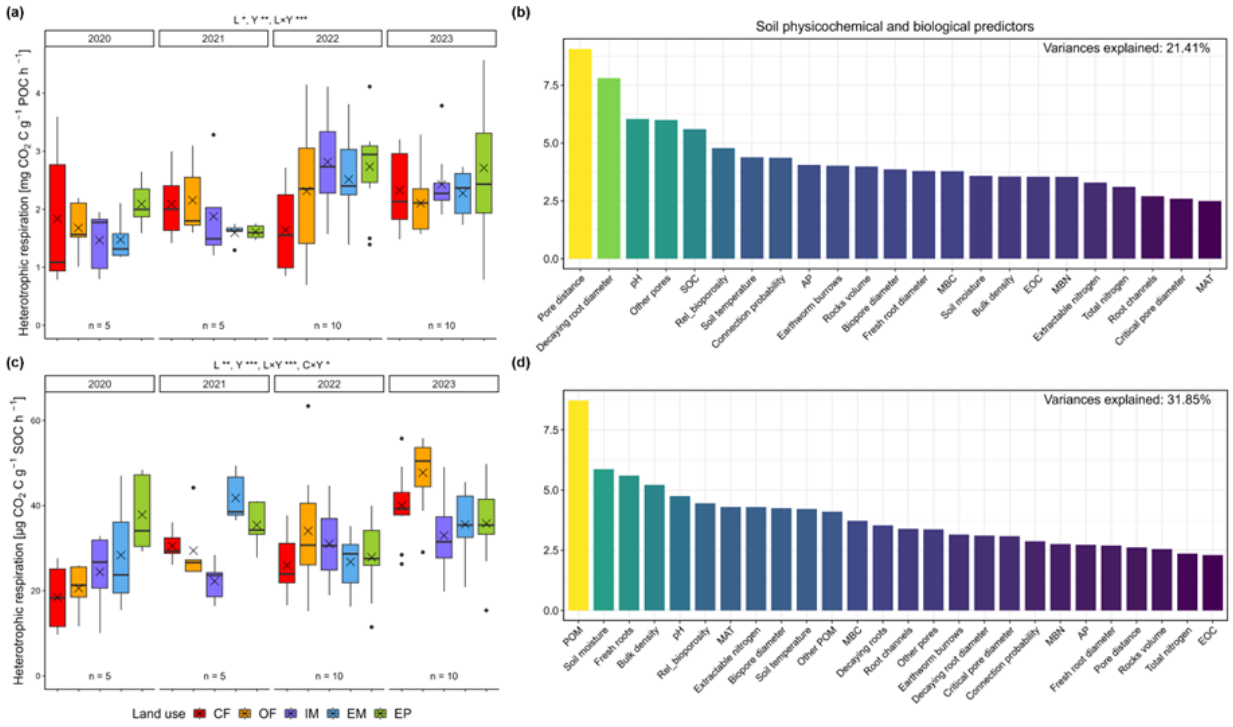

Figure S2.6 Response of adjusted heterotrophic respiration to variations in land use and climate change, and their relative importance of the most importance soil physicochemical and biological predictors. (a) Heterotrophic respiration parameterized by POC, (b) relative important of predictors for POC-parameterized heterotrophic respiration (excluding fresh roots, decaying roots, other POM and total POM), (c) Heterotrophic respiration parameterized by SOC, (d) relative important of predictors for SOC-parameterized heterotrophic respiration (excluding SOC). The heterotrophic respiration data are presented as grouped box plots (the thick solid line represents the median, the lower and upper hinges correspond to the first and third quartiles), with cross symbol demotes mean value. Predictors are displayed on the x-axis. Total variances explained of random forest model are shown in the top, right corner of figure. POM: particulate organic matter, MBC: microbial biomass carbon, EOC: extractable organic carbon, SOC: soil organic carbon, MBN: microbial biomass nitrogen, AP: available phosphorus, Rel_bioporosity: Fraction of bioporosity, MAT: mean annual soil temperature.

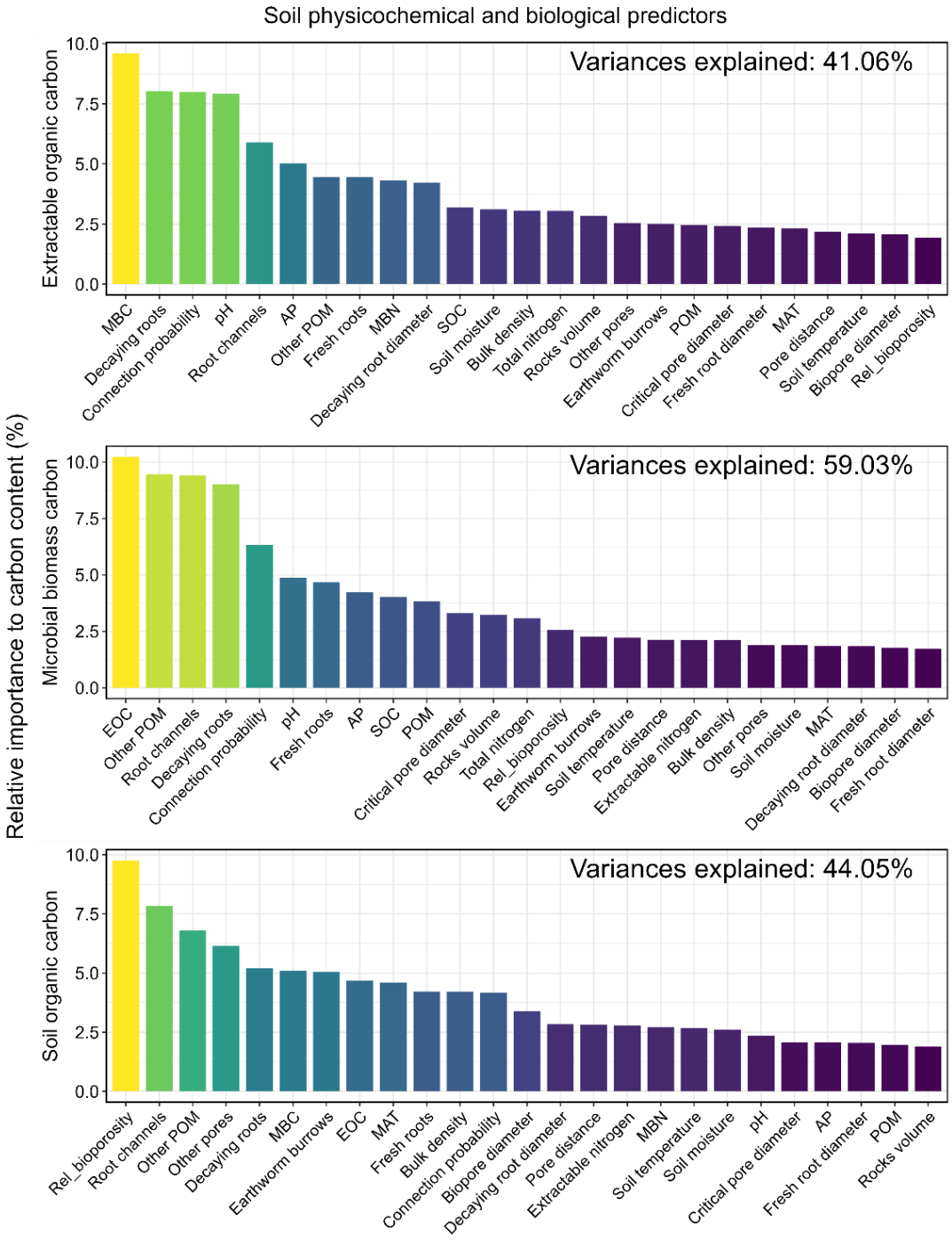

Figure S2.7 Relative importance of the most importance soil physicochemical and biological predictors of soil carbon contents. Predictors are displayed on the x-axis. POM: particulate organic matter, MBC: microbial biomass carbon, EOC: extractable organic carbon, SOC: soil organic carbon, MBN: microbial biomass nitrogen, AP: available phosphorus, Rel_bioporosity: fraction of bioporosity, MAT: mean annual soil temperature. Total variances explained of random forest model are shown in the top, right corner of figure.

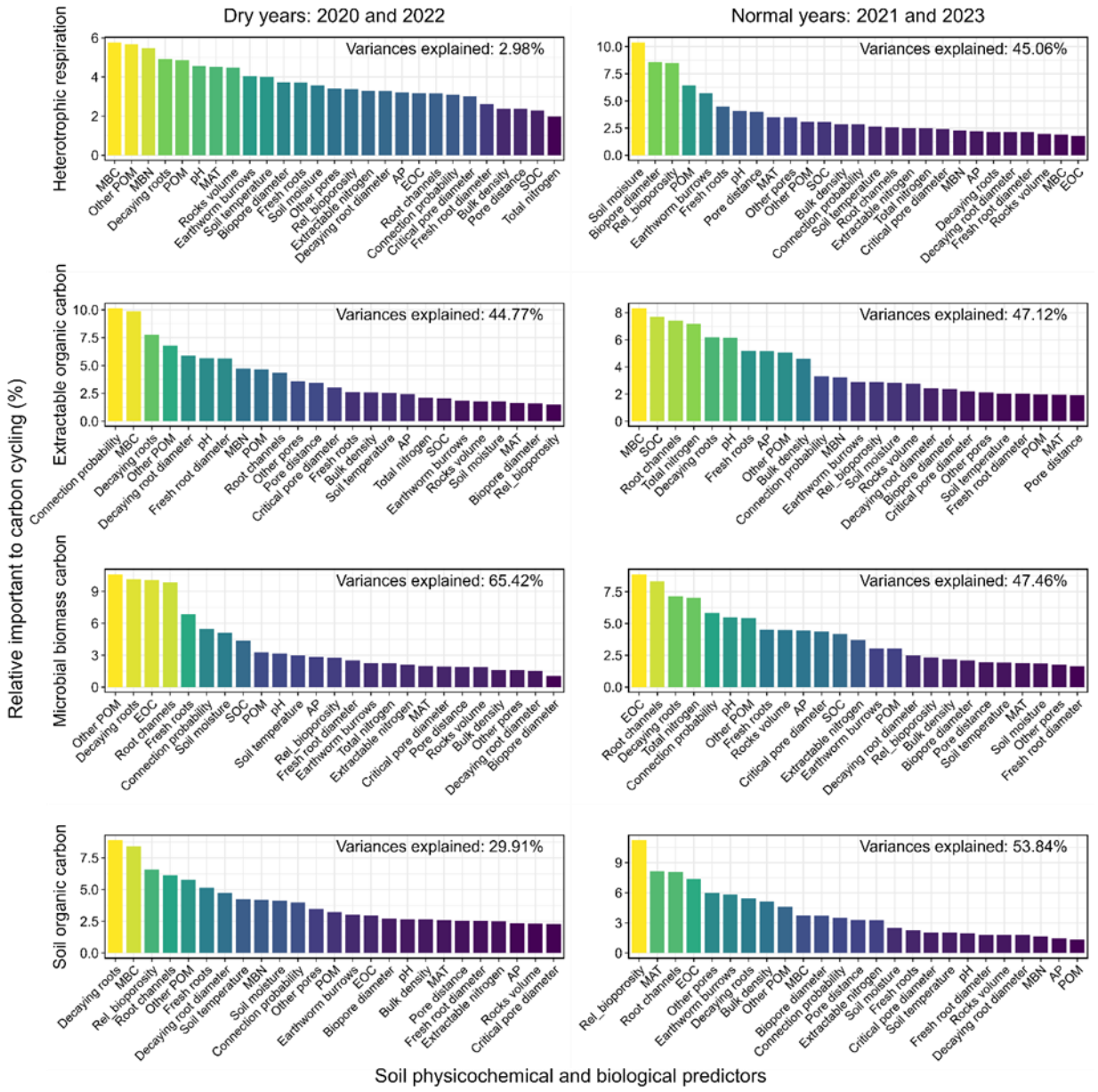

Figure S2.8 Relative importance of the most importance soil physicochemical and biological predictors of soil carbon cycling during dry and wet years. Predictors are displayed on the x-axis. POM: particulate organic matter, MBC: microbial biomass carbon, DOC: dissolved organic carbon, SOC: soil organic carbon, MBC: microbial biomass nitrogen, AP: available phosphorus, Rel_bioporosity: fraction of bioporosity, MAT: mean annual soil temperature. Total variances explained of random forest model are shown in the top, right corner of figure.

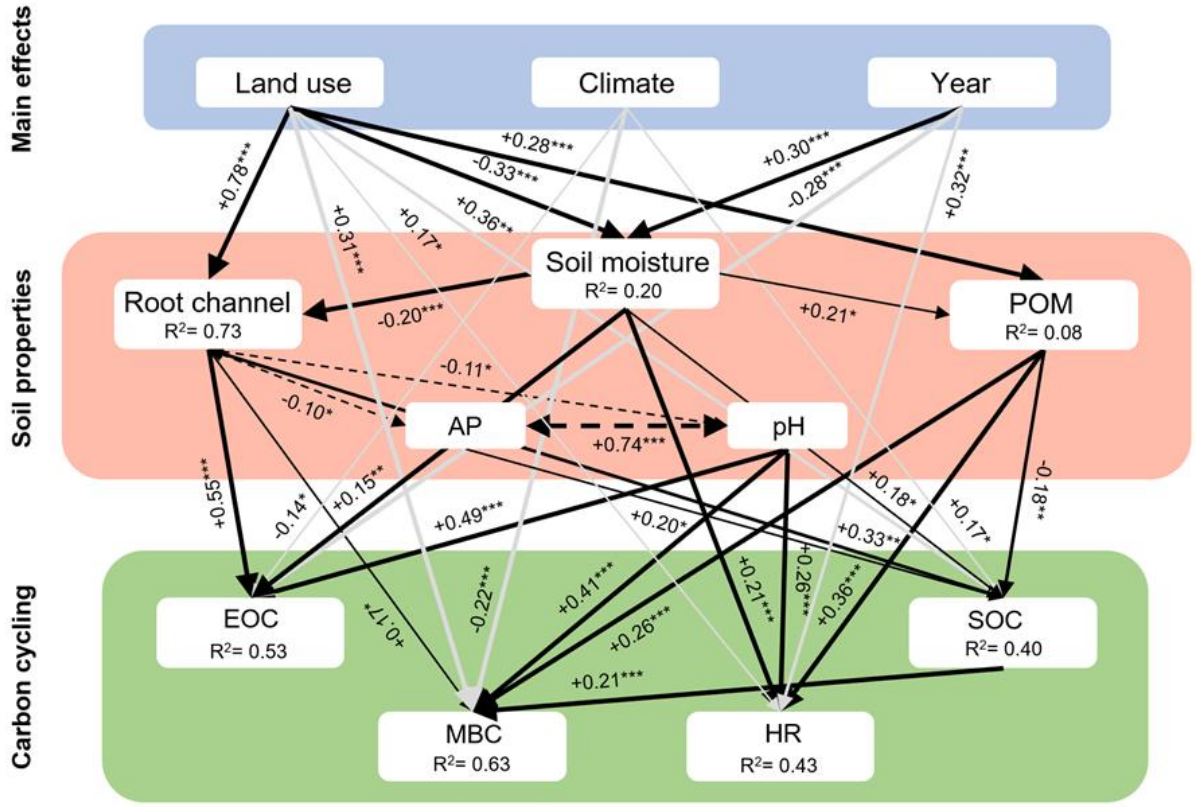

Figure S2.9 Structural equation modeling depicting how land use, climate and year effect carbon cycling and how far these are mediated by soil properties. Numbers next to arrows indicate standardized path coefficients (robust standard errors of coefficients). Black solid arrows indicate significant relationship, dashed double-sided arrows denote potential covariances. Gray solid lines indicate the direct effect of main effects on carbon cycling. Line width reflects the level of statistical significance. *, **, *** indicate significant differences at 0.05, 0.01 and 0.001 levels, respectively. POM: particulate organic matter, MBC: microbial biomass carbon, EOC: extractable organic carbon, SOC: soil organic carbon, HR: heterotrophic respiration, AP: available phosphorus. The parameters of model are χ^2 /df = 1.323, GIF = 0.963, p = 0.118, RMSEA = 0.046, SRMR = 0.052 (n = 150, bootstrap = 1000).

Appendices for chapter 3

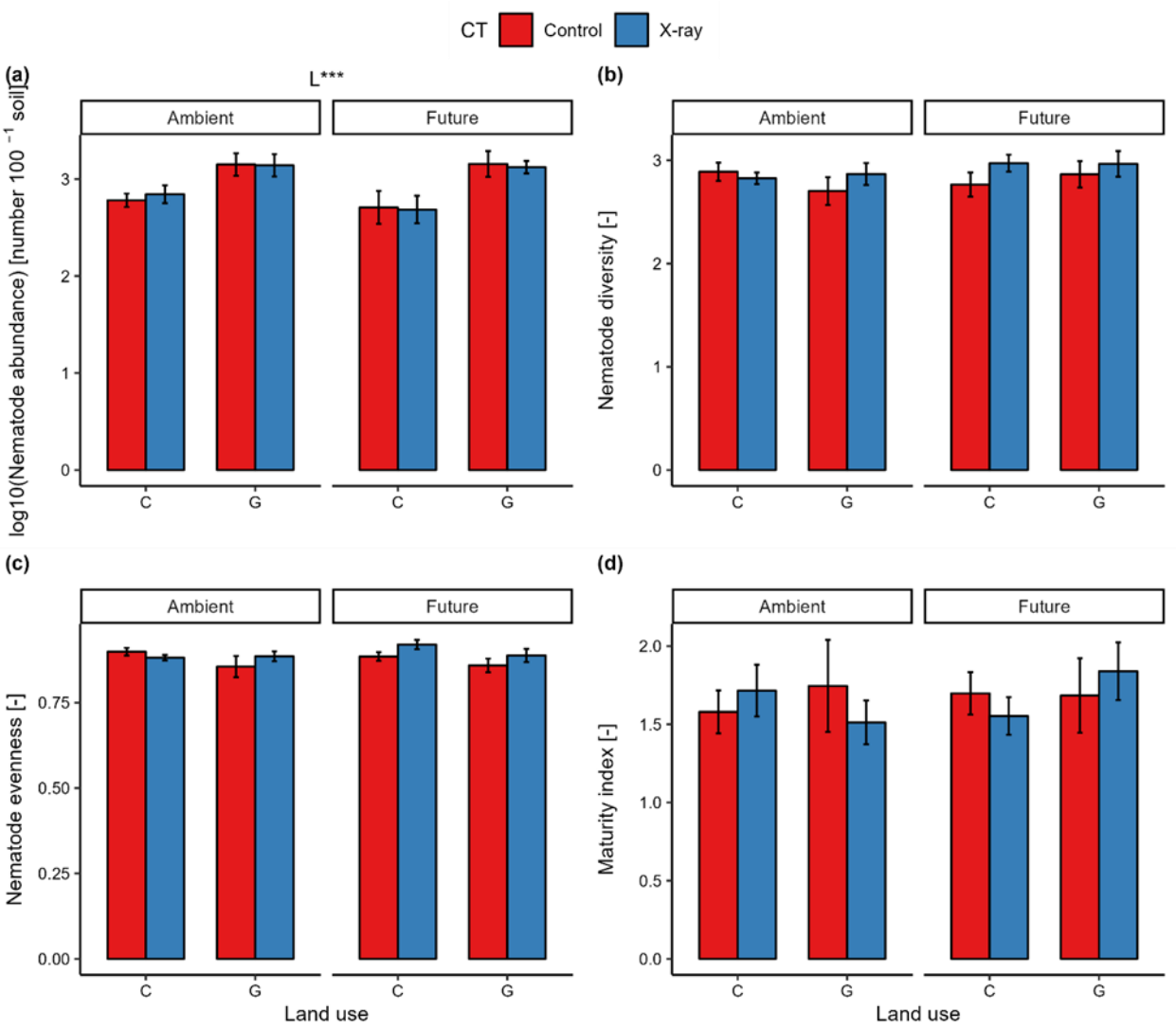

Figure S3.1 Effect of X-ray radiation on the nematode community properties (a) $\log_{10}$(nematode abundance), (b) nematode diversity, (c) nematode evenness, and (d) Maturity Index. Values are arithmetic mean ± standard error (n = 5). C, G represent annual cropland and perennial grassland, respectively. Control and X-ray represent without radiation and with radiation, respectively. Significant differences ($p < 0.001$) between land uses (L) are shown.

Table S3.1 Overview of soil microstructure and bulk properties.

Properties	Unit	Ambient				Future			
		November 2021		June 2022		November 2021		June 2022	
		annual cropland	perennial grassland	annual cropland	perennial grassland	annual cropland	perennial grassland	annual cropland	perennial grassland
Particulate organic matter	$mm^3\ mm^{-3}$	0.011±0.002	0.017±0.001	0.018±0.002	0.022±0.001	0.011±0.001	0.015±0.001	0.018±0.002	0.022±0.003
Biopore diameter	mm	1.433±0.087	1.847±0.243	1.551±0.079	1.996±0.131	1.283±0.077	1.902±0.132	1.392±0.026	1.873±0.186
Biopore length density	$mm\ mm^{-3}$	0.077±0.013	0.058±0.004	0.103±0.014	0.081±0.008	0.093±0.018	0.067±0.004	0.130±0.020	0.091±0.024
Biopore volume	$mm^3\ mm^{-3}$	0.032±0.007	0.035±0.004	0.049±0.007	0.051±0.006	0.036±0.009	0.037±0.003	0.060±0.010	0.051±0.010
Visible porosity	$mm^3\ mm^{-3}$	0.050±0.010	0.049±0.007	0.094±0.013	0.096±0.011	0.059±0.012	0.058±0.004	0.11±0.022	0.088±0.019
Pore surface area density	$mm^2\ mm^{-3}$	1.947±0.309	1.485±0.106	3.343±0.394	3.001±0.244	2.670±0.480	1.875±0.173	3.792±0.492	2.778±0.618
Euler characteristic	mm^{-3}	42.50±2.745	22.99±2.162	18.94±3.542	5.904±5.810	51.89±4.386	29.63±6.696	18.16±9.531	15.14±8.449
Pore diameter	mm	0.175±0.035	0.223±0.046	0.169±0.016	0.231±0.021	0.119±0.019	0.230±0.031	0.149±0.012	0.231±0.036
Connection probability	−	0.146±0.105	0.472±0.068	0.771±0.046	0.836±0.025	0.265±0.108	0.508±0.041	0.782±0.069	0.764±0.066
Pore distance	mm	0.119±0.008	0.147±0.005	0.103±0.006	0.108±0.004	0.102±0.008	0.131±0.008	0.097±0.005	0.12±0.012
Critical pore diameter	mm	0.068±0.016	0.220±0.014	0.200±0.044	0.363±0.053	0.062±0.019	0.162±0.013	0.177±0.012	0.218±0.020
Nematode specific porosity	$mm^3\ mm^{-3}$	0.032±0.007	0.029±0.002	0.057±0.009	0.054±0.006	0.038±0.008	0.034±0.003	0.070±0.014	0.052±0.013
Soil water content	−	0.241±0.009	0.242±0.005	0.107±0.004	0.118±0.009	0.235±0.004	0.233±0.007	0.131±0.016	0.151±0.018
pH	−	6.61±0.256	6.42±0.237	6.50±0.244	6.35±0.224	6.76±0.253	6.56±0.254	6.63±0.260	6.45±0.243
Available phosphorous	$mg\ P\ (100g)^{-1}$ soil	5.862±1.497	5.372±1.131	6.318±1.550	6.172±1.041	7.255±1.410	7.010±1.762	7.893±1.655	7.892±2.054
Total organic carbon	%	1.932±0.044	2.171±0.057	1.901±0.022	2.156±0.037	1.991±0.039	2.218±0.036	1.947±0.043	2.140±0.053
Extractable organic carbon	$\mu g\ C\ g^{-1}$ soil	22.06±3.330	26.00±3.330	24.19±3.370	44.78±3.490	26.29±4.860	27.92±6.260	28.00±5.190	25.41±3.670
Microbial biomass carbon	$\mu g\ C\ g^{-1}$ soil	392.3±20.68	532.3±26.22	199.4±14.40	354.3±15.80	420.2±19.19	525.0±34.04	202.6±9.721	341.9±22.88

Notes: Values are arithmetic mean ± standard error (n = 5).

Table S3.2 Linear mixed-effects models (LMMs) on the effects of climate, land use, season and their interactions on soil microstructure and bulk properties.

Properties	Climate		Land use		Season		Climate*Land use		Climate*Season		Land use*Season		Climate*Land use*Season	
	F value	***P* value**	**F value**	***P* value**	**F value**	***P* value**	**F value**	***P* value**	**F value**	***P* value**	**F value**	***P* value**	**F value**	***P* value**
Particulate organic matter	0.338	0.572	12.66	**0.003**	24.18	**<0.001**	0.233	0.636	0.043	0.839	0.225	0.641	0.098	0.759
Biopore diameter	0.595	0.463	32.34	**<0.001**	1.018	0.323	0.489	0.491	0.291	0.594	0.098	0.757	0.242	0.628
Biopore length density	2.028	0.180	7.318	**0.015**	6.127	**0.029**	0.365	0.554	0.068	0.799	0.174	0.682	0.053	0.822
Biopore volume	0.503	0.492	0.023	0.882	9.842	**0.009**	0.409	0.531	0.073	0.791	0.339	0.568	0.220	0.645
Visible porosity	0.488	0.498	0.436	0.519	21.18	**<0.001**	0.576	0.459	0.076	0.788	0.307	0.587	0.543	0.472
Pore surface area density	1.719	0.200	6.535	**0.016**	23.33	**<0.001**	0.963	0.335	0.753	0.393	0.010	0.923	0.110	0.743
Euler characteristic	2.015	0.181	12.55	**0.003**	26.56	**<0.001**	0.198	0.662	0.193	0.668	2.482	0.135	0.612	0.446
Pore diameter	0.396	0.547	24.71	**<0.001**	0.129	0.728	1.894	0.188	0.113	0.745	0.059	0.812	0.496	0.491
Connection probability	0.256	0.617	10.92	**0.003**	88.88	**<0.001**	0.790	0.382	1.352	0.255	7.807	**0.009**	0.000	0.999
Pore distance	1.796	0.205	17.69	**<0.001**	11.41	**0.005**	0.923	0.351	3.719	0.078	1.910	0.186	0.644	0.434
Critical pore diameter	6.882	**0.022**	50.34	**<0.001**	25.27	**<0.001**	7.408	**0.015**	1.364	0.266	0.589	0.454	1.195	0.290
Nematode specific porosity	0.823	0.382	1.858	0.192	16.28	**0.002**	0.561	0.465	0.003	0.960	0.480	0.498	0.430	0.521
Soil water content	2.430	0.130	1.255	0.272	253.8	**<0.001**	0.068	0.796	6.656	**0.015**	1.263	0.271	0.169	0.684
pH	2.342	0.201	18.97	**<0.001**	6.264	**0.020**	0.070	0.793	0.188	0.669	0.148	0.704	0.037	0.849
Available phosphorous	2.383	0.198	0.578	0.455	5.717	**0.025**	0.112	0.740	0.052	0.821	0.256	0.617	0.008	0.932
Total organic carbon	1.241	0.274	57.39	**<0.001**	1.968	0.170	0.390	0.537	0.397	0.533	0.022	0.882	0.164	0.688
Extractable organic carbon	0.355	0.583	13.88	**0.002**	7.740	**0.024**	16.24	**<0.001**	9.028	**0.017**	3.858	0.067	10.89	**0.005**
Microbial biomass carbon	0.043	0.837	95.81	**<0.001**	196.4	**<0.001**	0.853	0.364	0.294	0.592	0.806	0.377	0.124	0.728

Notes: Significant p values ($p < 0.05$) are in bold.

Table S3.3 Overview of nematode community properties.

Properties	Unit	Ambient				Future			
		November 2021		June 2022		November 2021		June 2022	
		annual cropland	perennial grassland	annual cropland	perennial grassland	annual cropland	perennial grassland	annual cropland	perennial grassland
Abundance	nr 100^{-1} g soil	766.3±177.3	1641±561.4	730.5±157.5	1802±285.6	577.6±141.8	1386±216.6	1134±259.7	1252±193.5
Richness	–	24.80±1.280	25.80±2.350	24.80±1.880	24.60±0.810	25.60±1.910	28.40±2.140	20.60±1.080	25.20±1.240
Diversity	–	2.830±0.060	2.868±0.110	2.874±0.110	2.861±0.050	2.973±0.080	2.966±0.120	2.636±0.050	2.863±0.040
Evenness	–	0.882±0.010	0.886±0.010	0.898±0.010	0.894±0.010	0.920±0.010	0.888±0.020	0.873±0.010	0.889±0.010
Nematode channel ratio	–	0.170±0.050	0.500±0.070	0.420±0.010	0.430±0.030	0.310±0.030	0.270±0.040	0.330±0.050	0.540±0.060
Channel index	–	70.40±8.310	35.80±16.60	60.80±10.70	59.00±12.70	43.00±5.400	60.50±11.70	61.10±10.30	28.40±9.700
Maturity index	–	1.720±0.170	1.510±0.140	1.860±0.170	1.220±0.110	1.550±0.120	1.840±0.180	1.670±0.120	1.720±0.160
Enrichment index	–	54.49±3.000	61.53±7.200	49.00±5.500	51.12±4.900	64.73±3.200	53.05±3.400	50.44±1.500	67.85±6.200
Structure index	–	72.80±8.300	79.60±4.800	70.00±2.900	69.60±3.300	77.00±2.500	80.80±4.500	75.50±3.100	72.60±2.400
Bacterivore abundance	nr 100^{-1} g soil	69.70±21.00	390.0±169.8	213.1±62.30	322.5±52.80	99.1±28.30	175.9±18.90	198.9±45.30	458.2±88.10
Fungivore abundance	nr 100^{-1} g soil	309.8±44.20	377.7±121.8	289.5±75.60	438.5±87.00	208.5±55.50	517.9±99.20	413.5±96.20	394.5±74.90
Plant-parasite abundance	nr 100^{-1} g soil	328.1±128.3	717.1±213.7	189.5±41.80	978.5±162.3	232.2±60.60	547.9±127.9	474.8±148.4	353.9±53.70
Omnivores-predator abundance	nr 100^{-1} g soil	58.60±20.80	156.6±80.60	81.90±37.30	158.3±81.10	37.70±14.10	144.5±27.20	47.00±11.50	45.90±14.90
Bacterivore richness	–	4.600±1.290	6.600±1.470	8.600±0.750	7.600±0.680	6.800±1.430	5.400±0.510	5.400±0.810	9.600±0.810
Fungivore richness	–	6.800±0.580	6.400±0.250	6.200±0.580	5.400±0.400	6.600±0.510	7.200±0.200	6.400±0.510	5.200±0.580
Plant-parasite richness	–	9.000±0.450	8.200±0.580	7.800±0.970	9.200±0.490	9.400±0.680	10.40±1.360	6.200±0.580	8.400±0.510
Omnivores-predator richness	–	4.400±1.210	4.600±1.170	3.600±0.930	2.800±0.370	2.800±0.580	5.400±0.930	2.600±0.510	2.000±0.450
Bacterivore diversity	–	1.570±0.240	1.540±0.240	1.890±0.090	1.790±0.100	1.650±0.210	1.430±0.110	1.360±0.110	1.870±0.110
Fungivore diversity	–	1.660±0.070	1.560±0.140	1.570±0.110	1.550±0.060	1.760±0.100	1.700±0.080	1.540±0.090	1.420±0.080
Plant-parasite diversity	–	1.920±0.060	1.790±0.090	1.810±0.130	1.920±0.070	1.970±0.100	1.960±0.210	1.530±0.080	1.910±0.070
Omnivores-predator diversity	–	1.460±0.200	1.310±0.220	1.060±0.270	0.860±0.140	0.840±0.180	1.420±0.150	1.020±0.110	0.980±0.130
Bacterivore evenness	–	0.880±0.030	0.850±0.050	0.890±0.020	0.890±0.020	0.910±0.010	0.860±0.030	0.840±0.030	0.830±0.030
Fungivore evenness	–	0.880±0.010	0.840±0.070	0.870±0.020	0.930±0.030	0.930±0.020	0.860±0.050	0.840±0.040	0.880±0.030
Plant-parasite evenness	–	0.870±0.020	0.860±0.020	0.900±0.020	0.870±0.020	0.880±0.030	0.850±0.040	0.850±0.020	0.900±0.020
Omnivores-predator evenness	–	0.950±0.030	0.920±0.020	0.800±0.070	0.910±0.030	0.860±0.070	0.880±0.020	0.910±0.040	0.870±0.070

Notes: Values are arithmetic mean ± standard error (n = 5).

Table S3.4 Linear mixed-effects models (LMMs) on the effects of climate, land use, season and their interactions on nematode community properties.

Properties	Climate		Land use		Season		Climate*Land use		Climate*Season		Land use*Season		Climate*Land use*Season	
	F value	***p* value**	**F value**	***p* value**	**F value**	***p* value**	**F value**	***p* value**	**F value**	***p* value**	**F value**	***p* value**	**F value**	***p* value**
Abundance	0.369	0.576	25.13	**<0.001**	0.690	0.430	3.166	0.094	0.203	0.665	0.739	0.403	2.397	0.141
Richness	0.002	0.969	3.144	0.089	4.132	0.053	2.037	0.166	2.291	0.143	0.017	0.898	0.421	0.523
Diversity	0.001	0.973	1.279	0.269	3.322	0.081	0.768	0.390	4.829	**0.038**	0.670	0.421	1.712	0.203
Evenness	0.102	0.752	0.223	0.641	0.461	0.503	0.238	0.629	4.409	**0.045**	1.367	0.252	2.724	0.110
Nematode channel ratio	0.146	0.722	16.08	**<0.001**	13.24	**0.001**	1.578	0.221	0.789	0.383	0.301	0.588	19.21	**<0.001**
Channel index	0.637	0.448	3.609	0.070	0.000	0.990	0.611	0.442	1.031	0.320	0.412	0.527	9.368	**0.005**
Maturity index	1.299	0.263	1.462	0.236	0.159	0.692	7.942	**0.008**	0.121	0.730	2.575	0.118	0.228	0.636
Enrichment index	1.378	0.274	1.586	0.220	1.692	0.206	0.084	0.774	1.925	0.178	4.174	0.052	8.259	**0.008**
Structure index	1.130	0.304	0.410	0.531	2.901	0.108	0.229	0.639	0.061	0.808	1.472	0.243	0.002	0.965
Bacterivore abundance	0.108	0.744	15.92	**<0.001**	5.694	**0.024**	0.238	0.630	2.545	0.122	0.022	0.883	4.203	**0.050**
Fungivore abundance	0.187	0.688	6.467	**0.018**	0.375	0.546	0.136	0.715	0.043	0.838	1.537	0.227	4.217	0.051
Plant-parasite abundance	1.375	0.306	29.79	**<0.001**	0.236	0.640	15.28	**0.001**	0.044	0.839	0.021	0.886	11.06	**0.004**
Omnivores-predator abundance	0.378	0.556	7.865	**0.013**	3.978	0.081	0.185	0.673	0.000	0.995	3.228	0.091	0.395	0.539
Bacterivore richness	0.005	0.946	1.707	0.201	7.192	**0.011**	0.383	0.540	0.572	0.455	0.799	0.378	8.742	**0.006**
Fungivore richness	0.218	0.644	1.962	0.172	8.744	**0.006**	0.218	0.644	0.218	0.644	2.931	0.098	1.187	0.285
Plant-parasite richness	0.009	0.927	3.112	0.087	6.285	**0.017**	1.457	0.236	5.388	**0.027**	2.491	0.124	0.216	0.646
Omnivores-predator richness	0.288	0.595	1.152	0.291	11.55	**0.002**	0.512	0.479	0.032	0.859	2.048	0.162	2.048	0.162
Bacterivore diversity	1.307	0.263	0.141	0.711	3.011	0.094	1.024	0.320	1.041	0.316	2.592	0.119	3.546	0.070
Fungivore diversity	0.107	0.746	1.565	0.221	5.969	**0.021**	0.027	0.870	2.816	0.104	0.007	0.932	0.372	0.547
Plant-parasite diversity	0.044	0.835	1.239	0.274	2.107	0.156	1.429	0.241	2.476	0.125	3.679	0.064	0.233	0.633
Omnivores-predator diversity	0.872	0.357	2.196	0.148	10.64	**0.003**	0.528	0.473	1.015	0.321	0.859	0.361	5.003	**0.032**
Bacterivore evenness	0.704	0.449	1.464	0.238	0.448	0.510	0.121	0.731	4.098	0.054	1.224	0.280	0.001	0.981
Fungivore evenness	0.000	0.985	0.001	0.974	0.007	0.936	0.210	0.650	2.955	0.097	4.615	**0.041**	0.036	0.850
Plant-parasite evenness	0.050	0.825	0.259	0.615	0.698	0.410	0.915	0.346	0.019	0.890	1.413	0.243	2.288	0.140
Omnivores-predator evenness	0.520	0.491	0.230	0.636	0.289	0.596	0.535	0.471	1.101	0.304	0.222	0.642	1.624	0.215

Notes: Significant p values ($p < 0.05$) are in bold.

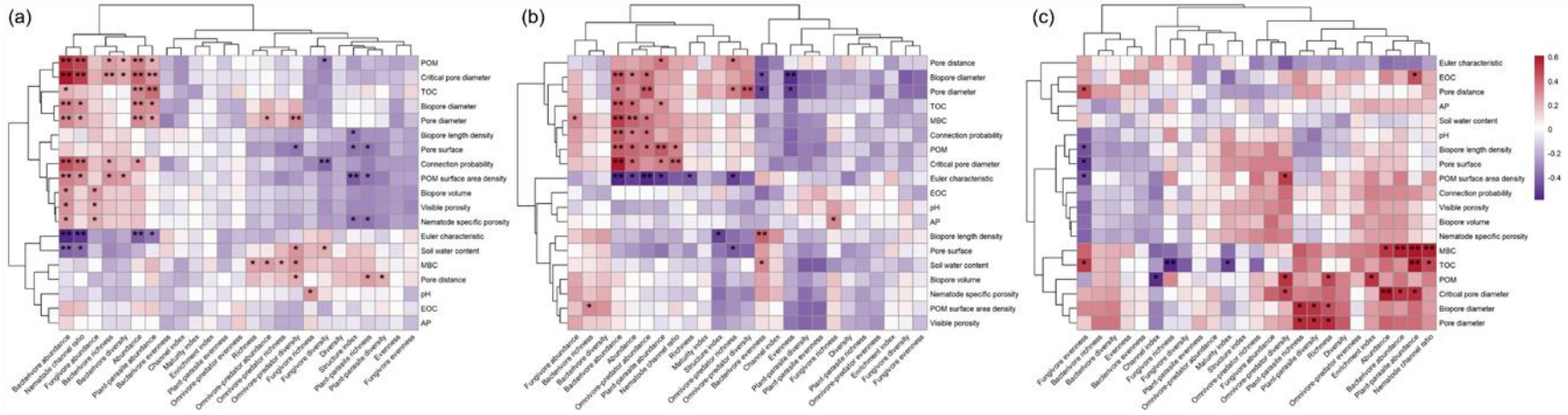

Figure S3.2 Spearman correlation analysis between nematode properties and bulk soil variables and soil microstructure properties as influenced by season. (a) all dataset, (b) November 2021, (c) June 2022. POM, particulate organic matter; MBC, microbial biomass carbon; TOC, total organic carbon; EOC, extractable organic carbon. *, ** indicate significant differences at 0.05 and 0.01 levels, respectively.

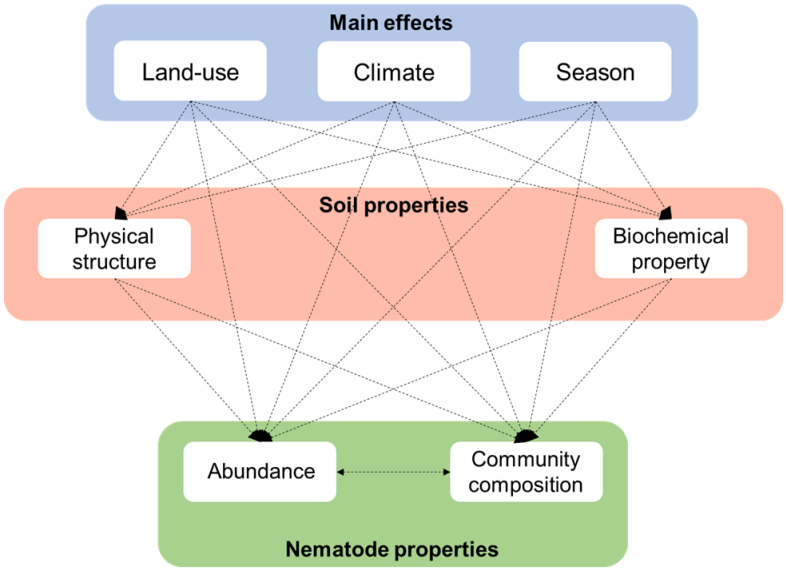

Figure S3.3 Initial structural equation modeling depicting how soil properties affect total nematode abundance and community composition driven by land use, climate and season factors. Lines indicate potential pathways. Lines with double sided arrow indicate potential relationship between covariances. The parameters of model are χ^2 = 0.010, GIF = 1.000, p = 0.921, RMSEA = 0.000, SRMR = 0.001, n = 40, bootstrap = 1000.

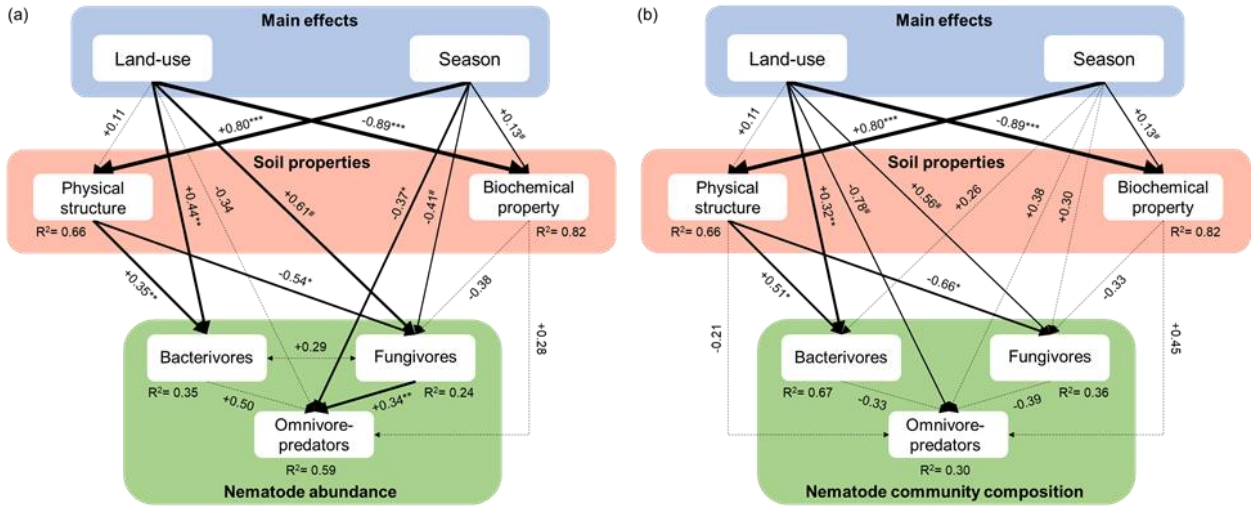

Figure S3.4 Structural equation modeling depicting how soil properties affect free-living (a) nematode abundance and (b) community composition based on feeding group driven by land use and season factors. Numbers next to arrows indicate standardized path coefficients (robust standard errors of coefficients). Solid lines indicate significant relationships and dash lines indicate non-significant pathways (p > 0.1). Lines with double sided arrow indicate potential relationship between covariances. $^{\#}$, *, **, *** indicate significant differences at 0.1, 0.05, 0.01 and 0.001 levels, respectively. The parameters of models are (a) χ^2 = 2.325, GIF = 0.984, p = 0.676, RMSEA = 0.000, SRMR = 0.016, n = 40, bootstrap = 1000, (b) χ^2 = 1.386, GIF = 0.990, p = 0.709, RMSEA = 0.000, SRMR = 0.018, n = 38, bootstrap = 1000.

Appendices for chapter 4

Table S4.1a Overview of root, soil physical properties in 2022.

Properties	Units	2022									
		Ambient					Future				
		CF	OF	IM	EM	EP	CF	OF	IM	EM	EP
Other POM	%	0.345±0.04	0.217±0.02	0.391±0.04	0.569±0.05	0.530±0.06	0.294±0.02	0.234±0.05	0.4±0.03	0.717±0.11	0.444±0.02
Decaying roots	%	0.074±0.01	0.055±0.01	0.260±0.06	0.199±0.02	0.194±0.02	0.079±0.01	0.057±0.01	0.249±0.04	0.192±0.03	0.227±0.04
Fresh roots	%	0.857±0.09	0.423±0.09	0.502±0.11	0.232±0.02	0.193±0.03	0.825±0.16	0.441±0.12	0.607±0.17	0.255±0.04	0.289±0.06
Root channels	%	0.498±0.07	0.470±0.12	0.855±0.03	1.228±0.06	1.161±0.10	0.403±0.02	0.364±0.02	0.878±0.01	1.093±0.04	1.128±0.07
Earthworm burrows	%	0.987±0.54	0.787±0.43	1.213±0.28	1.372±0.43	2.029±0.32	0.885±0.25	0.725±0.23	1.762±0.35	1.410±0.29	1.400±0.44
Other pores	%	4.573±0.72	6.472±1.28	4.035±0.26	3.845±0.26	4.736±0.39	6.237±0.44	5.380±0.75	5.138±0.84	4.195±0.37	4.395±0.37
Fraction of fresh roots	-	0.905±0.01	0.848±0.03	0.623±0.04	0.522±0.02	0.473±0.04	0.897±0.00	0.854±0.03	0.566±0.04	0.551±0.04	0.536±0.03
Porosity	$mm^3\ mm^{-3}$	0.073±0.01	0.084±0.01	0.073±0.00	0.074±0.01	0.088±0.01	0.087±0.01	0.072±0.01	0.091±0.01	0.078±0.00	0.079±0.01
Pore diameter	mm	0.445±0.06	0.344±0.06	0.475±0.05	0.476±0.06	0.527±0.06	0.409±0.02	0.398±0.05	0.463±0.07	0.483±0.06	0.445±0.05
Connection probability	-	0.582±0.05	0.587±0.04	0.684±0.02	0.695±0.03	0.743±0.03	0.626±0.03	0.64±0.03	0.707±0.04	0.715±0.04	0.713±0.02
Bioporosity	$mm^3\ mm^{-3}$	0.03±0.005	0.03±0.002	0.04±0.003	0.02±0.002	0.03±0.004	0.03±0.002	0.04±0.004	0.03±0.005	0.04±0.006	0.05±0.002
Biopore diameter	mm	0.771±0.07	0.666±0.06	0.754±0.06	0.750±0.08	0.861±0.08	0.805±0.07	0.797±0.11	0.770±0.11	0.778±0.08	0.729±0.06
Bulk density	$g\ cm^{-3}$	1.427±0.02	1.448±0.02	1.458±0.02	1.491±0.01	1.457±0.02	1.416±0.03	1.473±0.02	1.420±0.02	1.478±0.01	1.466±0.01
Soil moisture	%	15.70±0.90	16.19±0.92	11.67±0.55	12.63±0.40	12.03±0.78	15.57±0.88	16.01±0.8	11.42±0.35	13.51±1.07	12.50±0.78
Root length density	$cm\ cm^{-3}$	4.38±0.37	2.78±0.22	32.01±8.00	36.47±4.55	32.92±4.78	4.83±0.37	3.20±0.31	30.00±2.91	34.65±4.86	31.66±2.89
< 0.1 mm roots	%	16.73±2.52	36.01±2.78	48.65±1.58	42.36±3.39	41.89±1.80	15.20±2.54	28.45±2.90	48.58±0.68	43.99±4.61	38.77±2.38
0.1-0.2 mm roots	%	40.78±4.08	41.93±2.38	32.16±1.48	36.09±2.22	38.94±1.16	39.78±2.59	44.88±1.60	32.19±1.53	34.36±2.20	40.48±1.44
0.2-0.3 mm roots	%	26.02±1.31	13.96±1.50	10.83±0.54	13.68±0.83	11.85±0.50	27.41±1.75	16.17±1.02	10.75±0.60	13.55±1.98	13.06±0.72
> 0.3 mm roots	%	16.47±2.73	8.10±1.04	8.36±0.86	7.87±0.68	7.32±0.23	17.61±3.20	10.50±1.00	8.48±1.15	8.10±0.68	7.69±0.86

Notes: Values are arithmetic mean ± standard error (n = 5).

Table S4.1b Overview of root, soil physical properties in 2023.

Properties	Units	2023									
		Ambient					Future				
		CF	OF	IM	EM	EP	CF	OF	IM	EM	EP
Other POM	%	0.234±0.01	0.231±0.02	0.341±0.03	0.673±0.11	0.576±0.04	0.273±0.02	0.320±0.10	0.455±0.09	0.658±0.01	0.502±0.04
Decaying roots	%	0.135±0.01	0.116±0.01	0.311±0.02	0.358±0.04	0.381±0.02	0.127±0.01	0.125±0.01	0.339±0.04	0.338±0.07	0.331±0.06
Fresh roots	%	0.846±0.12	1.288±0.06	0.367±0.05	0.391±0.02	0.448±0.13	0.961±0.09	1.329±0.14	0.525±0.18	0.539±0.09	0.461±0.10
Root channels	%	0.306±0.05	0.296±0.01	0.914±0.05	1.173±0.08	1.074±0.09	0.361±0.05	0.311±0.02	0.889±0.05	1.071±0.03	1.050±0.03
Earthworm burrows	%	0.187±0.06	0.584±0.18	1.112±0.28	0.976±0.27	1.545±0.33	1.060±0.76	0.753±0.28	0.752±0.27	2.006±0.27	1.932±1.05
Other pores	%	8.486±1.70	5.146±0.73	5.197±0.51	3.179±0.21	3.798±0.37	7.197±1.05	3.254±0.30	5.209±0.45	3.643±0.38	3.405±0.21
Fraction of fresh roots	-	0.851±0.02	0.916±0.00	0.528±0.04	0.521±0.02	0.499±0.05	0.876±0.01	0.908±0.01	0.541±0.04	0.600±0.04	0.576±0.04
Porosity	$mm^3\ mm^{-3}$	0.102±0.02	0.075±0.01	0.083±0.01	0.068±0.00	0.079±0.01	0.098±0.02	0.059±0.01	0.082±0.01	0.082±0.01	0.077±0.01
Pore diameter	mm	0.252±0.01	0.386±0.04	0.390±0.05	0.454±0.09	0.504±0.07	0.393±0.11	0.490±0.07	0.335±0.06	0.559±0.04	0.545±0.16
Connection probability	-	0.633±0.06	0.546±0.04	0.727±0.03	0.739±0.02	0.771±0.03	0.648±0.07	0.467±0.04	0.697±0.04	0.740±0.04	0.713±0.02
Bioporosity	$mm^3\ mm^{-3}$	0.04±0.005	0.04±0.004	0.04±0.003	0.05±0.003	0.04±0.005	0.04±0.005	0.04±0.004	0.04±0.004	0.04±0.004	0.04±0.009
Biopore diameter	mm	0.478±0.04	0.776±0.08	0.751±0.12	0.675±0.13	0.763±0.12	0.757±0.19	0.865±0.12	0.607±0.09	0.840±0.07	0.771±0.21
Bulk density	$g\ cm^{-3}$	1.397±0.04	1.376±0.02	1.448±0.01	1.511±0.01	1.470±0.02	1.360±0.03	1.358±0.02	1.430±0.02	1.461±0.02	1.473±0.01
Soil moisture	%	19.53±0.80	21.73±0.47	17.31±0.66	18.16±0.4	18.69±0.33	21.18±0.88	23.71±0.61	19.71±0.85	21.33±0.47	21.20±1.03
Root length density	$cm\ cm^{-3}$	7.64±1.11	7.99±0.79	25.69±2.29	36.97±5.33	38.89±8.47	8.00±0.36	7.92±1.14	21.17±4.61	32.72±5.34	29.45±4.78
< 0.1 mm roots	%	15.49±0.99	41.47±1.47	43.85±0.47	43.72±3.95	40.87±1.27	14.98±1.37	42.73±2.38	45.87±1.67	39.62±3.87	35.58±1.32
0.1-0.2 mm roots	%	56.28±2.12	34.70±1.67	34.71±0.65	33.38±2.03	34.99±2.03	56.76±1.78	34.28±1.08	34.45±1.09	33.81±1.39	38.69±1.11
0.2-0.3 mm roots	%	16.38±0.65	14.87±0.21	10.8±0.20	13.16±1.36	13.21±0.66	17.15±1.34	13.84±1.23	10.5±0.84	15.47±1.38	15.38±0.51
> 0.3 mm roots	%	11.86±0.95	8.97±0.61	10.64±0.76	9.74±1.41	10.93±1.30	11.11±0.76	9.15±0.78	9.18±1.27	11.10±1.43	10.35±0.55

Notes: Values are arithmetic mean ± standard error (n = 5).

Table S4.2 Linear mixed-effects models (LMMs) on the effects of climate, land use, season and their interactions on nematode community properties.

Properties	Land use		Climate		Year		Land use*Climate		Land use*Year		Climate*Year		Land use*Climate*Year	
	F value	*p* value	F value	*p* value	F value	*p* value	F value	*p* value	F value	*p* value	F value	*p* value	F value	*p* value
Decaying roots	182.82	**<0.001**	0.44	0.506	46.61	**<0.001**	1.00	0.910	14.68	**0.005**	0.00	0.982	2.97	0.562
Fresh roots	129.83	**<0.001**	0.59	0.442	7.07	**0.008**	0.48	0.976	40.67	**<0.001**	0.26	0.608	1.44	0.837
Other POM	131.58	**<0.001**	0.98	0.322	0.00	0.960	6.75	0.150	5.21	0.266	0.01	0.907	5.95	0.203
Root channels	1160.52	**<0.001**	0.85	0.357	11.14	**0.001**	1.50	0.827	17.33	**0.002**	1.48	0.225	8.38	0.079
Earthworm burrows	14.92	**0.005**	0.49	0.483	4.03	**0.045**	1.63	0.803	4.76	0.312	2.44	0.118	5.85	0.210
Other pores	60.15	**<0.001**	3.28	0.070	2.29	0.131	5.33	0.255	18.12	**0.001**	0.12	0.732	3.23	0.520
Fraction of fresh root	912.49	**<0.001**	1.61	0.204	0.39	0.531	9.56	**0.049**	13.74	**0.008**	1.00	0.317	3.4	0.493
Porosity	27.16	**<0.001**	1.22	0.269	3.73	0.054	4.98	0.289	3.29	0.511	0.24	0.628	5.39	0.249
Pore diameter	11.02	**0.026**	0.42	0.516	1.28	0.258	3.13	0.536	10.24	**0.037**	2.39	0.122	2.31	0.679
Connection probability	75.42	**<0.001**	2.56	0.110	4.53	**0.033**	1.14	0.888	16.37	**0.003**	0.20	0.652	8.33	0.080
Bioporosity	36.38	**<0.001**	0.37	0.542	1.02	0.312	1.37	0.849	13.97	**0.007**	2.44	0.119	4.26	0.372
Biopore diameter	1.72	0.787	0.33	0.565	2.37	0.123	3.94	0.414	6.39	0.172	1.29	0.257	4.80	0.309
Soil moisture	116.32	**<0.001**	19.12	**<0.001**	523.92	**<0.001**	2.60	0.627	11.87	**0.018**	14.68	**<0.001**	0.25	0.993
Bulk density	71.56	**<0.001**	2.83	0.093	8.18	**0.004**	4.79	0.309	26.83	**<0.001**	1.12	0.289	2.32	0.677
Root length density	293.56	**<0.001**	1.09	0.296	0.05	0.816	2.09	0.719	8.29	0.082	0.81	0.367	0.90	0.924
< 0.1 mm roots	500.81	**<0.001**	3.19	0.074	0.13	0.715	3.48	0.482	25.28	**<0.001**	0.17	0.676	6.30	0.178
0.1-0.2 mm roots	190.75	**<0.001**	0.55	0.457	1.85	0.174	2.49	0.646	119.80	**<0.001**	0.07	0.782	1.87	0.760
0.2-0.3 mm roots	326.01	**<0.001**	3.44	0.064	12.92	**<0.001**	2.36	0.670	108.41	**<0.001**	0.02	0.884	5.34	0.254
> 0.3 mm roots	62.13	**<0.001**	0.33	0.568	0.23	0.632	1.74	0.783	36.16	**<0.001**	1.08	0.230	1.32	0.858

Notes: Significant p values ($p < 0.05$) are in bold.

Appendices for chapter 5

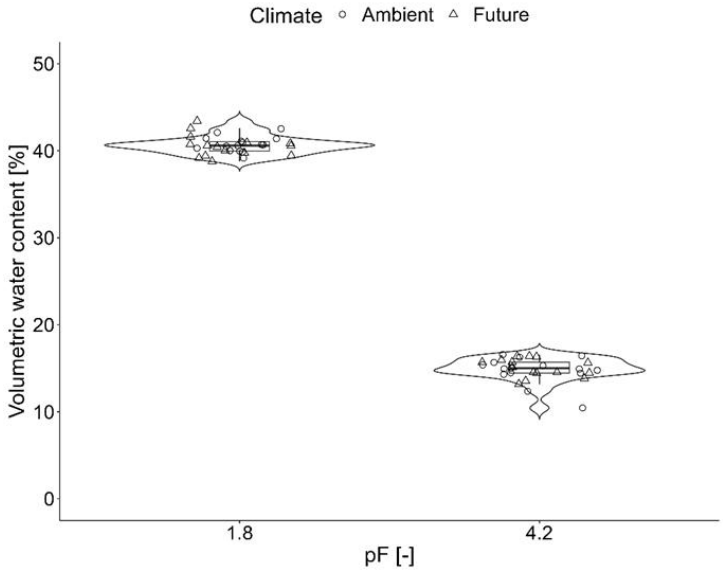

Figure S5.1 Water retention characteristics were measured with the evaporation method (Hyprop, METER Group) and the dew point hygrometer method (WP4C, METER Group). The volumetric water content at pF1.8 and pF4.2 represent the field capacity and permanent wilting point.

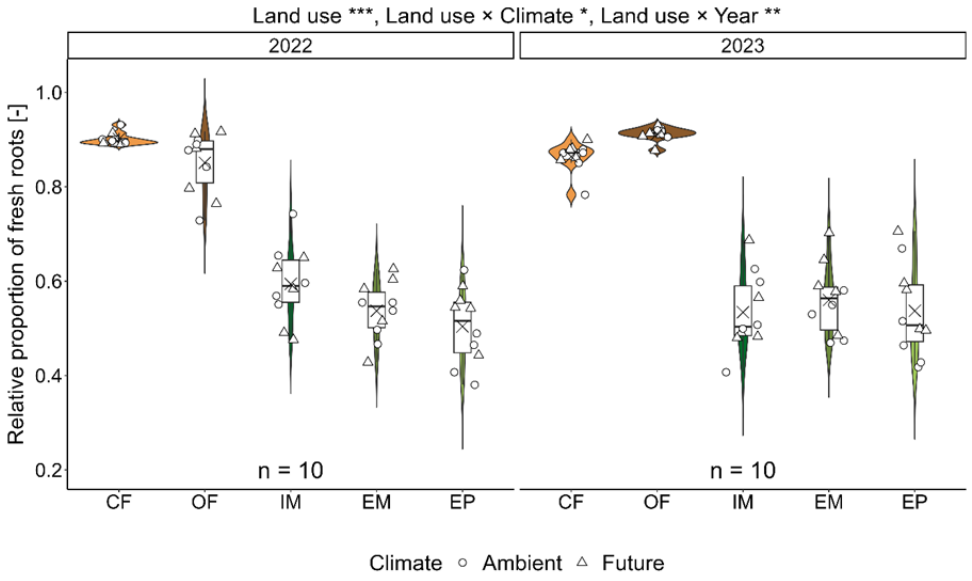

Figure S5.2 Violin plots showing relative proportion of fresh roots across five land use types and two years. Box plots represent the 0, 25, 50, 75, and 100 percentile and cross symbols the arithmetic mean (n = 10). CF, OF, IM, EM and EP represent conventional farming, organic farming, intensive meadow, extensive meadow and extensive pasture, respectively. Significant differences between land use, climate, year, interaction of land use and climate, land use and year are indicated * ($p < 0.05$), ** ($p < 0.01$), and *** ($p < 0.001$).

Table S5.1 Overview of soil water content on different soil layers and their results of linear mixed-effects models (LMMs).

	Land use	Climate	0-10 cm	10-20 cm	20-30 cm	30-50 cm	50-70 cm	70-90 cm	90-110 cm
Treatment	Cropland	Ambient	24.34±0.81	25.71±0.66	26.6±0.6	23.63±0.79	21.07±1.14	21.54±1.12	23.05±1.24
		Future	24.01±0.59	25.66±0.52	26.45±0.54	23.2±0.53	22.49±0.53	23.15±0.97	23.99±0.96
	Grassland	Ambient	26.4±0.53	24.72±0.43	23.91±0.32	20.85±0.47	17.89±0.59	17.7±0.74	17.89±0.88
		Future	25.99±0.66	24.32±0.5	23.79±0.38	20.03±0.7	17.64±0.75	18.87±0.98	18.18±1.03
LMMs	Land use	χ^2	11.306	6.303	40.302	23.996	29.058	19.180	29.860
		p value	**<0.000**	**0.012**	**<0.001**	**<0.001**	**<0.001**	**<0.001**	**<0.001**
	Climate	χ^2	0.411	0.327	0.097	1.113	0.325	2.179	0.315
		p value	0.522	0.567	0.756	0.292	0.569	0.140	0.575
	Land use * Climate	χ^2	0.005	0.140	0.001	0.101	1.246	0.055	0.106
		p value	0.945	0.709	0.974	0.751	0.264	0.814	0.745
Treatment	Conventional farming	Ambient	25.24±1.19	25.72±1.01	25.93±0.79	23.05±1.37	20.07±2.08	20.11±2.07	21.52±2.21
		Future	23.82±1.12	25.24±0.99	25.99±0.91	22.44±0.4	22.07±0.69	22.59±1.6	23.1±1.23
	Organic farming	Ambient	23.49±1.11	25.99±1	27.59±0.88	24.58±0.89	22.78±1.03	23.7±0.6	25.09±0.94
		Future	24.32±0.57	26.42±0.39	27.38±0.62	24.55±0.85	23.66±0.81	24.37±1.24	25.4±1.49
LMMs	Land use	χ^2	1.046	1.696	7.225	4.673	3.638	4.400	4.647
		p value	0.306	0.193	**0.007**	**0.031**	0.056	**0.036**	**0.031**
	Climate	χ^2	0.101	0.001	0.019	0.145	1.639	1.515	0.483
		p value	0.750	0.974	0.890	0.703	0.200	0.218	0.487
	Land use * Climate	χ^2	3.338	0.649	0.056	0.118	0.248	0.501	0.221
		p value	0.068	0.420	0.813	0.731	0.618	0.479	0.639
Treatment	Intensive meadow	Ambient	23.22±0.59	22.11±0.45	22.10±0.52	20.73±0.67	19.59±0.58	21.15±0.55	22.26±0.65
		Future	22.37±1.19	21.56±0.97	22.29±0.66	19.62±1.06	18.27±1.19	20.64±1.25	20.15±1.08
	Extensive meadow	Ambient	25.71±0.92	23.90±0.81	22.93±0.76	20.08±0.46	17.03±0.82	15.77±0.86	15.74±0.85
		Future	25.19±1.24	23.49±0.90	21.93±0.93	18.03±1.52	15.65±1.34	16.75±1.75	16.90±1.74
	Extensive pasture	Ambient	25.37±0.96	23.29±0.82	22.08±0.38	18.50±1.03	15.10±0.68	15.37±0.62	15.64±0.93
		Future	24.80±0.89	23.19±0.89	22.71±0.82	18.86±1.32	16.66±1.38	17.85±1.94	17.09±2.22
LMMs	Land use	χ^2	10.619	6.945	0.159	4.728	12.388	20.448	23.817
		p value	**0.005**	**0.031**	0.924	0.094	**0.002**	**<0.001**	**<0.001**
	Climate	χ^2	0.796	0.340	0.015	1.141	0.246	1.116	0.022
		p value	0.372	0.560	0.904	0.285	0.620	0.291	0.881
	Land use * Climate	χ^2	0.041	0.101	1.792	2.913	3.222	1.721	2.942
		p value	0.980	0.951	0.408	0.233	0.200	0.423	0.230

Notes: Values are arithmetic mean ± standard error (n = 5). Significant *p* values ($p < 0.05$) are in bold.

Table S5.2 Linear mixed-effects models (LMMs) on the effects of climate, land use, year and their interactions on root, vegetation cover and functional group dependence, yield and water related properties.

Properties	Land use		Climate		Year		Land use * Climate		Land use * Year		Climate * Year		Land use * Climate * Year	
	$\chi 2$	*p* value	$\chi 2$	*p* value	$\chi 2$	*p* value	$\chi 2$	*p* value	$\chi 2$	*p* value	$\chi 2$	*p* value	$\chi 2$	*p* value
Evapotranspiration	94.81	**<0.001**	13.89	**<0.001**	2604.84	**<0.001**	1.66	0.797	103.42	**<0.001**	33.97	**<0.001**	8.69	**<0.001**
Yield	1096.62	**<0.001**	2.54	0.111	190.69	**<0.001**	11.27	**0.010**	58.49	**<0.001**	1.05	0.590	34.85	**<0.001**
Water use efficiency	695.76	**<0.001**	0.13	0.723	86.71	**<0.001**	6.27	0.099	86.88	**<0.001**	4.37	0.112	32.23	**<0.001**
Topsoil water storage	22.43	**0.004**	1.59	0.902	215.45	**<0.001**	1.45	0.835	10.01	**0.040**	0.01	0.979	4.00	0.407
Deep soil water storage	41.40	**<0.001**	3.55	0.616	43.26	**<0.001**	3.33	0.504	5.42	0.247	0.08	0.782	3.18	0.528
Change of topsoil water storage	36.82	**<0.001**	5.10	0.403	6.86	**0.008**	5.01	0.286	29.22	**<0.001**	0.02	0.881	7.43	0.115
Change of deep soil water storage	159.84	**<0.001**	16.55	**0.005**	188.52	**<0.001**	1.43	0.839	34.38	**<0.001**	0.86	0.353	0.35	0.986
Root length density (0-15 cm)	293.56	**<0.001**	1.09	0.296	0.05	0.816	2.09	0.719	8.29	0.082	0.81	0.367	0.90	0.924
Root length density (15-30 cm)	149.11	**<0.001**	0.71	0.399	0.16	0.690	2.51	0.643	8.97	0.062	0.85	0.356	5.09	0.279
Root length density (30-50 cm)	172.66	**<0.001**	0.09	0.761	16.81	**<0.001**	4.56	0.336	11.07	**0.026**	0.03	0.854	4.18	0.383
Root length density (0-50 cm)	100.04	**<0.001**	0.13	0.718	0.13	0.721	0.14	0.998	2.59	0.629	0.04	0.848	0.40	0.982
Corrected root length density	223.42	**<0.001**	0.39	0.533	2.13	0.144	0.45	0.979	20.64	**<0.001**	0.13	0.724	1.33	0.857
Root length in < 0.1 mm diameter	267.87	**<0.001**	0.61	0.434	0.18	0.672	1.14	0.889	9.90	**0.042**	0.38	0.537	0.52	0.972
Root length in 0.1-0.2 mm diameter	311.08	**<0.001**	0.15	0.701	1.53	0.216	0.27	0.992	6.61	0.158	0.03	0.870	2.11	0.716
Root length in 0.2-0.3 mm diameter	485.12	**<0.001**	0.00	0.976	3.48	0.062	1.25	0.869	12.14	**0.016**	0.26	0.613	5.34	0.254
Root length in 0.3-0.4 mm diameter	366.45	**<0.001**	0.12	0.735	9.19	**0.002**	1.50	0.827	22.21	**<0.001**	0.00	0.984	3.25	0.517
Root length in 0.4-0.5 mm diameter	280.98	**<0.001**	0.76	0.382	12.25	**<0.001**	4.29	0.368	13.57	**0.009**	0.32	0.573	2.68	0.614
Root length in > 0.5 mm diameter	198.36	**<0.001**	4.93	**0.026**	12.89	**<0.001**	3.51	0.476	7.72	0.102	0.98	0.322	1.79	0.773
Net change in water content	65.20	**<0.001**	0.00	0.997	1106.39	**<0.001**	7.63	0.105	19.60	**<0.001**	5.89	**0.015**	5.82	0.213
Total vegetation cover	1.78	0.411	0.07	0.792	12.85	**<0.001**	3.62	0.164	1.92	0.382	2.30	0.129	2.06	0.357
Functional group dependence	618.05	**<0.001**	1.17	0.279	22.22	**<0.001**	7.84	**0.020**	3.99	0.136	0.24	0.625	0.11	0.947

Notes: Significant *p* values ($p < 0.05$) are in bold.

Table S5.3 Overview of root, yield and water related properties.

Year	Climate	Land-use	Total vegetation cover [%]	RA of grass [%]	RA of forb [%]	RA of legume [%]	RLD $_{0\text{-}15\ cm}$ [cm cm^{-3}]	RLD $_{15\text{-}30\ cm}$ [cm cm^{-3}]	RLD $_{30\text{-}50\ cm}$ [cm cm^{-3}]	RLD $_{0\text{-}50\ cm}$ [cm cm^{-3}]	RLD $_{corrected}$ [cm cm^{-3}]	$P + \Delta S$ [mm]
2022	Ambient	CF	-	-	-	-	4.38±0.37	3.60±0.77	2.05±0.33	3.22±0.23	2.90±0.21	-75.81±0.83
		OF	-	-	-	-	2.78±0.22	1.78±0.42	0.93±0.19	1.74±0.12	1.48±0.10	-61.98±3.09
		IM	68.6±3.71	96.7±2.0	3.3±2.0	-	32.01±7.99	10.63±2.37	3.66±0.53	14.25±3.16	8.47±1.88	-59.67±1.49
		EM	71.1±2.16	45.0±6.5	35.7±6.1	19.3±5.5	36.47±4.55	11.97±2.24	3.42±0.63	15.90±1.96	8.54±1.05	-63.68±3.19
		EP	76.0±4.52	63.3±6.3	31.1±6	5.6±1.4	32.92±4.78	12.13±0.74	3.16±0.47	14.78±1.51	7.45±0.76	-60.16±1.35
	Future	CF	-	-	-	-	4.83±0.33	2.42±0.18	1.60±0.27	2.81±0.16	2.54±0.14	-70.64±1.57
		OF	-	-	-	-	3.20±0.31	1.66±0.13	1.25±0.08	1.96±0.14	1.67±0.12	-62.19±1.09
		IM	81.9±2.35	99.2±0.6	0.8±0.6	-	30.00±2.92	12.99±4.23	3.81±0.82	14.42±2.08	8.57±1.23	-61.60±1.80
		EM	71.3±2.27	44.9±4.2	40.3±3.6	14.8±3.7	34.65±4.86	11.07±2.93	2.91±0.27	14.88±2.15	7.99±1.15	-72.97±2.81
		EP	74.3±3.06	76.2±4.3	18.1±3.7	5.7±2.2	31.66±2.89	13.14±3.53	3.55±0.56	14.86±1.68	7.49±0.85	-68.63±1.84
2023	Ambient	CF	-	-	-	-	7.64±1.11	3.31±0.48	2.77±0.37	4.39±0.13	3.80±0.11	-113.06±4.05
		OF	-	-	-	-	7.99±0.79	3.13±0.29	1.78±0.06	4.05±0.29	3.69±0.26	-112.20±3.44
		IM	84.8±4.53	97.2±0.6	2.7±0.6	-	25.69±2.29	9.64±0.81	3.79±0.39	12.11±0.8	6.47±0.43	-95.36±4.81
		EM	83.8±3.20	39.0±5.2	25.2±3.5	35.8±5.1	36.97±5.33	11.95±1.59	4.56±0.23	16.50±1.80	9.24±1.01	-112.42±1.65
		EP	83.4±5.19	49.0±6.4	30.3±7.1	20.6±4.5	38.89±8.47	10.14±2.33	3.87±0.66	16.26±3.10	8.73±1.67	-105.13±2.34
	Future	CF	-	-	-	-	8.00±0.36	2.98±0.48	1.89±0.30	4.05±0.18	3.50±0.16	-108.19±5.34
		OF	-	-	-	-	7.92±1.14	3.84±0.64	1.17±0.23	4.00±0.45	3.64±0.41	-110.62±2.69
		IM	80.9±4.63	97.1±0.8	2.8±0.7	-	21.17±4.61	8.97±1.21	3.85±0.40	10.58±1.78	5.65±0.95	-92.05±2.07
		EM	80.1±4.65	34.9±5.3	29.1±5.4	35.9±3.9	32.72±5.34	18.41±3.41	5.18±0.53	17.41±2.68	9.75±1.50	-105.03±5.21
		EP	77.7±3.91	61.5±7.0	17.4±4.8	20.9±5.8	29.45±4.78	12.00±1.89	4.28±0.42	14.15±1.31	7.60±0.71	-107.50±3.89

Notes: Values are arithmetic mean ± standard error (n = 5). CF, OF, IM, EM and EP represent conventional farming, organic farming, intensive meadow, extensive meadow and extensive pasture, respectively. RA of grass: relative abundance of grass, RA of forb: relative abundance of forb, RA of grass: relative abundance of forb, RLD $_{0\text{-}15\ cm}$: root length density on 0-15 cm depth, RLD $_{15\text{-}30\ cm}$: root length density on 15-30 cm depth, RLD $_{30\text{-}50\ cm}$: root length density on 30-50 cm depth, RLD $_{0\text{-}50\ cm}$: root length density on 0-50 cm depth, RLD $_{corrected}$: corrected root length density, $P + \Delta S$: net change in water content during peak growth.

Table S5.4 Overview of yield and water related properties.

Climate	Land use	Year	ET [mm]	Yield [kg ha^{-1}]	WUE [kg m^{-1}]	Topsoil storage [mm/mm]	Deep soil storage [mm/mm]	Δ water $_{0\text{-}30\ cm}$ [mm]	Δ water $_{30\text{-}110\ cm}$ [mm]
Ambient	CF	2022	161.82±3.96	9.33±0.42	5.78±0.29	0.184±0.002	0.200±0.010	-8.71±0.19	-13.41±0.89
		2023	198.22±4.74	13.07±0.43	6.60±0.21	0.201±0.013	0.182±0.026	-16.28±0.62	-12.06±0.74
		2024	264.21±12.33	11.89±1.06	4.48±0.30	0.293±0.014	0.287±0.009	2.47±0.69	-2.89±2.17
	OF	2022	128.26±4.86	6.10±0.22	4.78±0.24	0.212±0.008	0.243±0.014	-6.59±0.98	-7.12±0.69
		2023	198.77±4.53	4.91±0.37	2.48±0.22	0.202±0.009	0.241±0.008	-18.88±0.89	-4.72±0.71
		2024	266.94±3.60	9.36±0.45	3.51±0.19	0.285±0.015	0.275±0.007	2.97±0.68	-5.19±1.22
	IM	2022	123.63±5.19	5.98±0.18	4.85±0.11	0.168±0.007	0.227±0.012	-4.70±0.53	-5.87±0.60
		2023	158.97±5.58	7.24±0.17	4.58±0.19	0.200±0.004	0.200±0.009	-13.62±0.97	-0.24±0.68
		2024	265.18±2.72	8.29±0.30	3.13±0.11	0.285±0.005	0.292±0.005	0.86±0.45	0.64±0.80
	EM	2022	126.46±2.17	3.17±0.31	2.51±0.27	0.187±0.009	0.199±0.012	-5.39±0.62	-7.57±0.47
		2023	175.64±5.58	4.07±0.42	2.33±0.27	0.220±0.006	0.167±0.007	-15.48±0.43	-6.86±1.56
		2024	262.88±2.55	4.98±0.26	1.89±0.09	0.299±0.008	0.271±0.005	1.66±0.62	0.06±1.35
	EP	2022	134.22±4.65	-	-	0.185±0.009	0.174±0.015	-4.78±0.41	-8.55±0.93
		2023	172.88±8.55	-	-	0.216±0.006	0.160±0.011	-14.56±0.51	-4.49±0.85
		2024	265.26±3.40	-	-	0.289±0.006	0.275±0.004	0.27±0.66	0.40±0.59
Future	CF	2022	158.39±9.62	8.73±0.20	5.58±0.31	0.165±0.017	0.200±0.012	-7.08±0.40	-11.37±0.56
		2023	215.96±14.00	11.30±0.39	5.34±0.45	0.205±0.011	0.215±0.015	-15.41±0.71	-10.94±2.46
		2024	236.02±6.79	13.13±0.71	5.57±0.29	0.284±0.011	0.285±0.005	0.45±1.07	-1.31±1.33
	OF	2022	120.56±3.00	5.17±0.39	4.30±0.35	0.198±0.007	0.231±0.017	-8.15±0.60	-4.82±0.57
		2023	205.17±5.84	5.39±0.42	2.65±0.27	0.210±0.004	0.249±0.010	-18.44±0.78	-4.98±0.86
		2024	243.22±5.08	6.74±0.66	2.79±0.30	0.290±0.005	0.285±0.005	0.01±0.65	-3.13±1.34
	IM	2022	116.69±3.79	5.36±0.13	4.62±0.21	0.162±0.013	0.207±0.019	-4.51±0.42	-4.49±0.35
		2023	153.82±5.72	7.43±0.3.1	4.84±0.19	0.204±0.008	0.200±0.013	-13.48±0.25	1.53±0.89
		2024	247.51±2.65	8.55±0.35	3.45±0.14	0.277±0.005	0.280±0.007	-0.12±0.30	0.72±0.39
	EM	2022	135.53±0.81	3.44±0.41	2.54±0.31	0.197±0.011	0.206±0.023	-7.79±0.50	-7.48±0.36
		2023	174.34±3.75	4.85±0.10	2.78±0.03	0.216±0.007	0.174±0.018	-15.35±1.16	-2.78±0.88
		2024	243.56±6.21	5.10±0.29	2.09±0.10	0.285±0.011	0.264±0.014	0.28±1.21	-0.68±1.06
	EP	2022	126.26±6.33	-	-	0.195±0.014	0.207±0.027	-5.74±0.71	-5.47±0.58
		2023	176.62±4.46	-	-	0.214±0.005	0.187±0.018	-16.36±0.71	-1.60±0.82
		2024	241.43±4.73	-	-	0.292±0.007	0.264±0.014	0.36±0.87	1.52±0.34

Notes: Values are arithmetic mean ± standard error (n = 5). CF, OF, IM, EM and EP represent conventional farming, organic farming, intensive meadow, extensive meadow and extensive pasture, respectively. ET: evapotranspiration, WUE: water use efficiency, Δ water $_{0\text{-}30\ cm}$: change of topsoil water storage, Δ water $_{30\text{-}110\ cm}$: change of deep soil water storage.

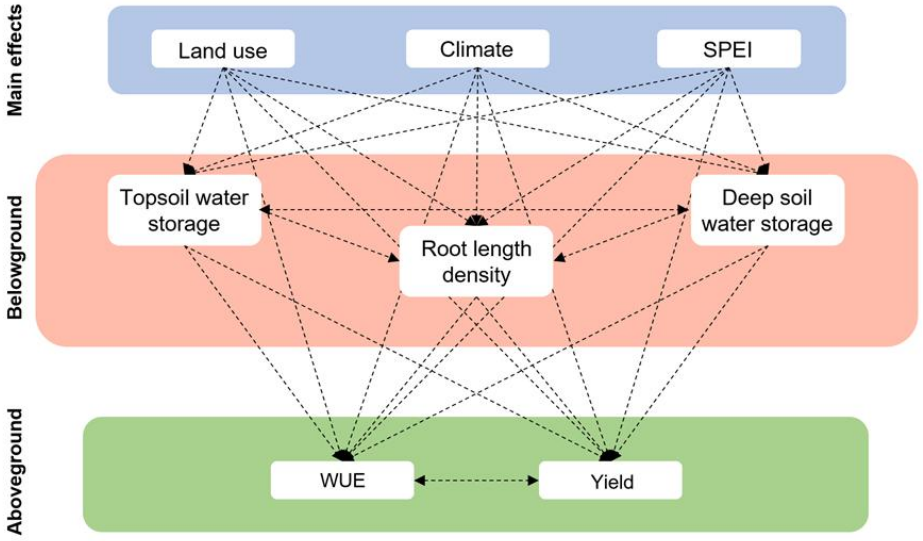

Figure S5.3 Initial structural equation model depicting how soil water storage and root length density affect water use efficiency and yield driven by land use, climate and climate extremes. Numbers next to arrows indicate standardized path coefficients (robust standard errors of coefficients). Lines indicate potential pathways. Lines with double sided arrow indicate potential relationship between covariances. Prior to scaling, the categorical levels of land use were ordered as CF, IM, OF, and EM to reflect the gradient of land-use intensity. All variables included in the model are continuous measures. The parameters of model are *Fisher's C* = 20.145, $p = 0.000$, $df = 4$.

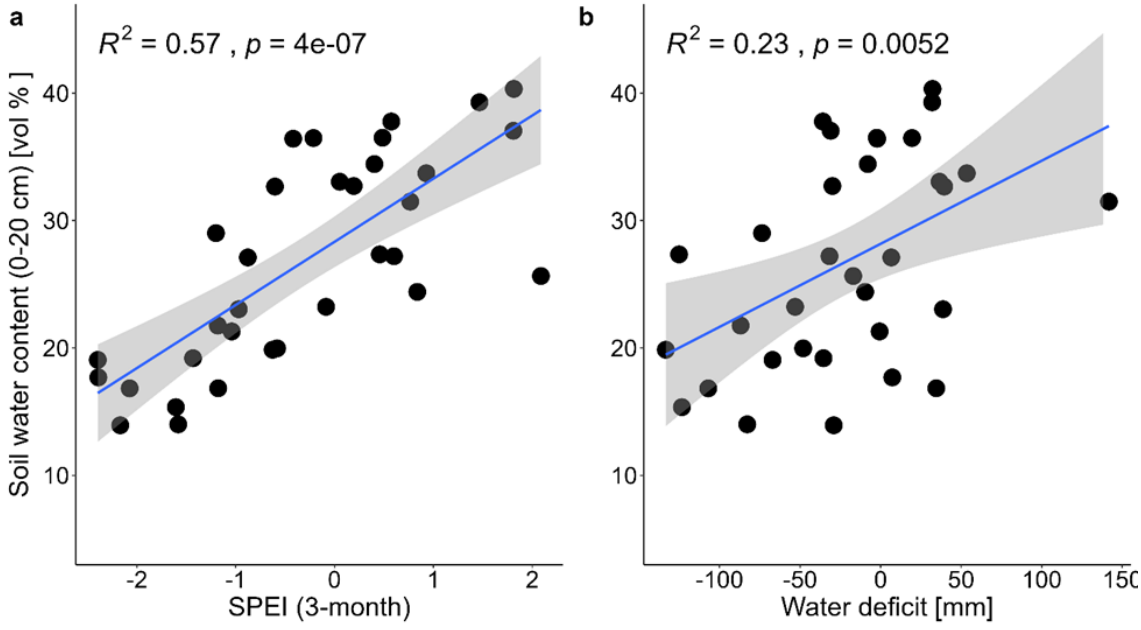

Figure S5.4 Linear regression between shallow soil water content (0-20 cm) and meteorological aridity index or water deficit. (a) Standardized precipitation-evapotranspiration index (SPEI) with a 3-month timescale. (b) meteorological water deficit.

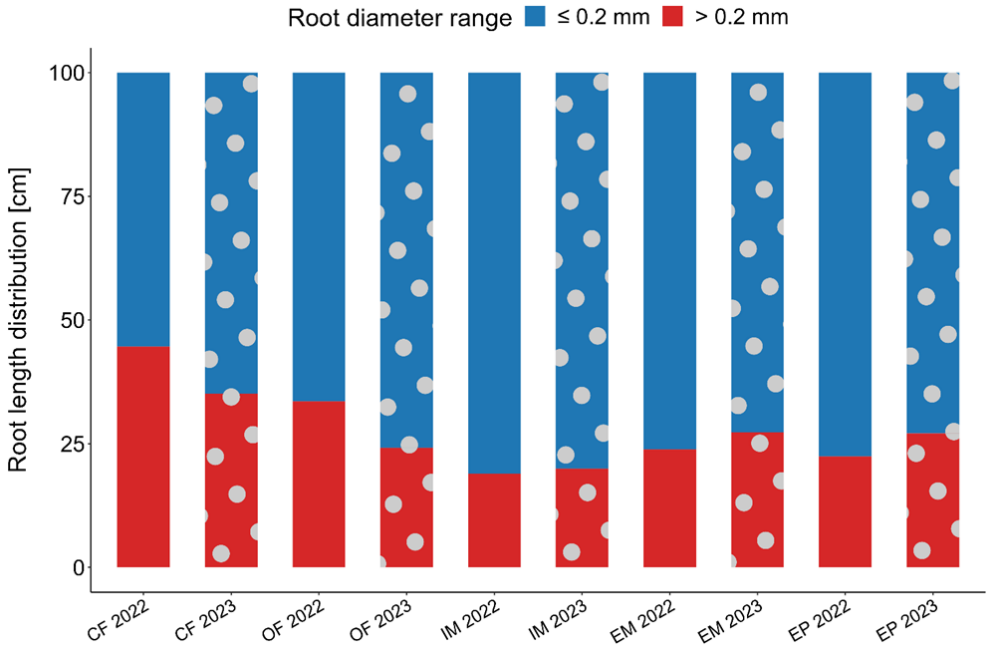

Figure S5.5 Relative proportion of root length ranges (≤ 0.2 mm and > 0.2 mm) across five land-use types and two years. CF, OF, IM, EM and EP represent conventional farming, organic farming, intensive meadow, extensive meadow and extensive pasture, respectively.

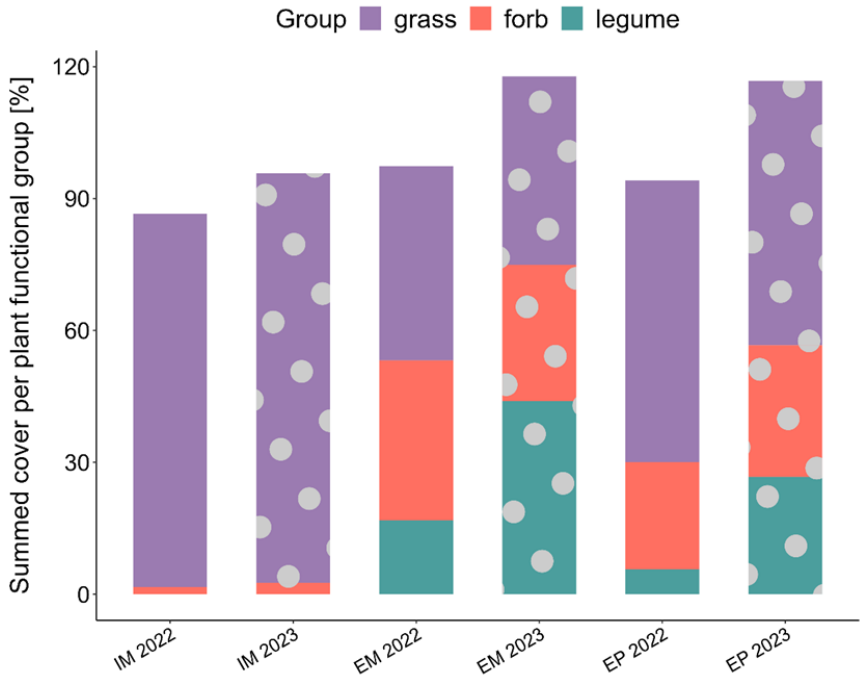

Figure S5.6 Summed cover per plant functional groups (grass, forb, and legume) across three grassland types and two years. IM, EM and EP represent intensive meadow, extensive meadow and extensive pasture, respectively.

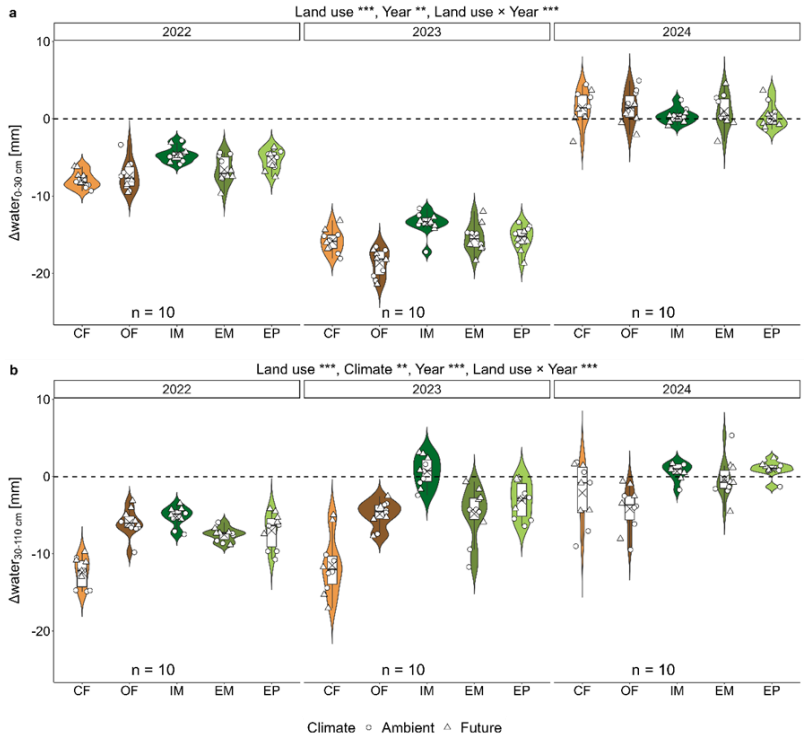

Figure S5.7 Changes in soil water storage during growing season under different land-use types and future climate scenario across three years. (a) change of topsoil (0-30 cm) water storage, (b) change of deep soil (30-110 cm) water storage. Box plots represent the 0, 25, 50, 75, and 100 percentiles, and cross symbols represent the arithmetic mean (n = 10). Growing season refers to the period from when daily mean temperatures consistently exceed 5 °C until crop harvest. Box plots represent the 0, 25, 50, 75, and 100 percentile and cross symbols the arithmetic mean (n = 10). Significant differences between land use, climate, year, interaction of land use and year, land use, climate and year are indicated ** ($p < 0.01$) and *** ($p < 0.001$). CF, OF, IM and EM represent conventional farming, organic farming, intensive meadow, and extensive meadow, respectively.

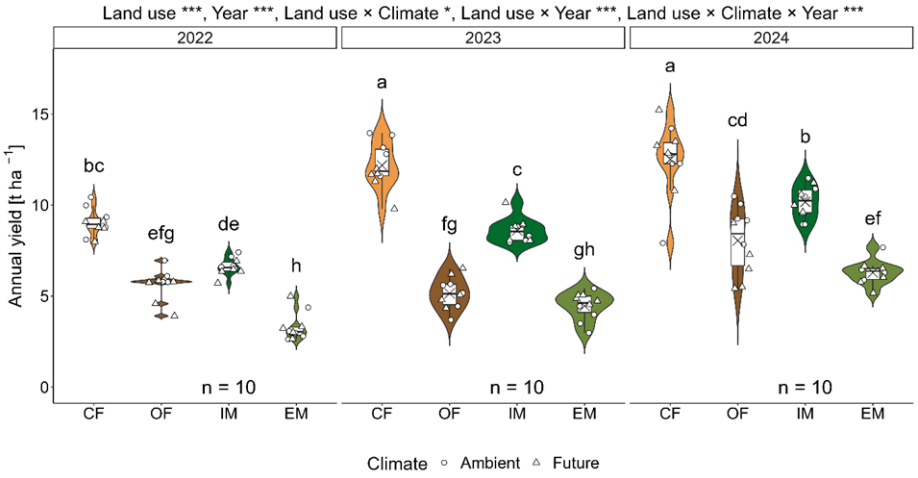

Figure S5.8 Effect of land use, future climate scenario on annual yield across three years. CF, OF, IM and EM represent conventional farming, organic farming, intensive meadow, and extensive meadow respectively.

Bibliography

Acharya, B. S., Rasmussen, J., & Eriksen, J. (2012). Grassland carbon sequestration and emissions following cultivation in a mixed crop rotation. *Agriculture, Ecosystems & Environment*, *153*, 33-39. https://doi.org/10.1016/j.agee.2012.03.001

Adhikari, K., Anderson, K. R., Smith, D. R., Owens, P. R., Moore, P. A., & Libohova, Z. (2023). Identifying key factors controlling potential soil respiration in agricultural fields. *Agricultural & Environmental Letters*, *8*, e20117. https://doi.org/10.1002/ael2.20117

Ahmed, M. A., Zarebanadkouki, M., Meunier, F., Javaux, M., Kaestner, A., & Carminati, A. (2018). Root type matters: measurement of water uptake by seminal, crown, and lateral roots in maize. *Journal of Experimental Botany*, *69*, 1199-1206. https://doi.org/10.1093/jxb/erx439

Ajayi, A. E., Faloye, O. T., Reinsch, T., & Horn, R. (2021). Changes in soil structure and pore functions under long term/continuous grassland management. *Agriculture, Ecosystems & Environment*, *314*, 107407. https://doi.org/10.1016/j.agee.2021.107407

Ali, G., Wang, Z., Li, X., Jin, N., Chu, H., & Jing, L. (2021). Deep soil water deficit and recovery in alfalfa fields of the Loess Plateau of China. *Field Crops Research*, *260*, 107990. https://doi.org/10.1016/j.fcr.2020.107990

Altermann, M., Rinklebe, J., Merbach, I., Körschens, M., Langer, U., & Hofmann, B. (2005). Chernozem—Soil of the Year 2005. *Journal of Plant Nutrition and Soil Science*, *168*, 725-740. https://doi.org/10.1002/jpln.200521814

Anderson, M. J. (2001). A new method for non-parametric multivariate analysis of variance. *Austral Ecology*, *26*(1), 32-46. https://doi.org/10.1046/j.1442-9993.2001.01070.x

Angst, G., Potapov, A., Joly, F. X., Angst, S., Frouz, J., Ganault, P., & Eisenhauer, N. (2024). Conceptualizing soil fauna effects on labile and stabilized soil organic matter. *Nature Communications*, *15*, 5005. https://doi.org/10.1038/s41467-024-49240-x

Aochi, Y. O., & Farmer, W. J. (2005). Impact of soil microstructure on the molecular transport dynamics of 1,2-dichloroethane. *Geoderma*, *127*, 137-153. https://doi.org/10.1016/j.geoderma.2004.11.024

Arzt, M., Deschamps, J., Schmied, C., Pietzsch, T., Schmidt, D., Tomancak, P., Haase, R., & Jug, F. (2022). LABKIT: Labeling and Segmentation Toolkit for Big Image Data. *Frontiers in Computer Science*, *4*, 777728. https://doi.org/10.3389/fcomp.2022.777728

Asbjornsen, H., Shepherd, G., Helmers, M., & Mora, G. (2008). Seasonal patterns in depth of water uptake under contrasting annual and perennial systems in the Corn Belt Region of the Midwestern U.S. *Plant and Soil*, *308*, 69-92. https://doi.org/10.1007/s11104-008-9607-3

Awang, Z., Wan Afthanorhan, W. M. A., & Asri, M. A. M. (2015). Parametric and Non Parametric Approach in Structural Equation Modeling (SEM): The Application of Bootstrapping. *Modern Applied Science*, *9*, 58-67. https://doi.org/10.5539/mas.v9n9p58

Bacq-Labreuil, A., Crawford, J., Mooney, S. J., Neal, A. L., Akkari, E., McAuliffe, C., Zhang, X., Redmile-Gordon, M., & Ritz, K. (2018). Effects of cropping systems upon the three-dimensional architecture of soil systems are modulated by texture. *Geoderma*, *332*, 73-83. https://doi.org/10.1016/j.geoderma.2018.07.002

Bacq-Labreuil, A., Neal, A. L., Crawford, J., Mooney, S. J., Akkari, E., Zhang, X., Clark, I., & Ritz, K. (2020). Significant structural evolution of a long-term fallow soil in response to agricultural management practices requires at least 10 years after conversion. *European Journal of Soil Science*, *72*, 829-841. https://doi.org/10.1111/ejss.13037

Bagley, J. E., Kueppers, L. M., Billesbach, D. P., Williams, I. N., Biraud, S. C., & Torn, M. S. (2017). The influence of land cover on surface energy partitioning and evaporative fraction regimes in the U.S. Southern Great Plains. *Journal of Geophysical Research: Atmospheres*, *122*, 5793-5807.

https://doi.org/10.1002/2017jd026740

Bai, Y., & Cotrufo, M. F. (2022). Grassland soil carbon sequestration: Current understanding, challenges, and solutions. *Science*, *377*, 603-608. https://doi.org/10.1126/science.abo2380

Bakonyi, G., & Nagy, P. (2001). Temperature- and moisture-induced changes in the structure of the nematode fauna of a semiarid grassland –- patterns and mechanisms. *Global Change Biology*, *6*, 697-707. https://doi.org/10.1046/j.1365-2486.2000.00354.x

Balogh, J., Pintér, K., Fóti, S., Cserhalmi, D., Papp, M., & Nagy, Z. (2011). Dependence of soil respiration on soil moisture, clay content, soil organic matter, and CO_2 uptake in dry grasslands. *Soil Biology and Biochemistry*, *43*, 1006-1013. https://doi.org/10.1016/j.soilbio.2011.01.017

Banfield, C. C., Dippold, M. A., Pausch, J., Hoang, D. T. T., & Kuzyakov, Y. (2017). Biopore history determines the microbial community composition in subsoil hotspots. *Biology and Fertility of Soils*, *53*, 573-588. https://doi.org/10.1007/s00374-017-1201-5

Banfield, C. C., Pausch, J., Kuzyakov, Y., & Dippold, M. A. (2018). Microbial processing of plant residues in the subsoil - The role of biopores. *Soil Biology & Biochemistry*, *125*, 309-318. https://doi.org/10.1016/j.soilbio.2018.08.004

Banwart, S. A., Nikolaidis, N. P., Zhu, Y.-G., Peacock, C. L., & Sparks, D. L. (2019). Soil Functions: Connecting Earth's Critical Zone. *Annual Review of Earth and Planetary Sciences*, *47*, 333-359. https://doi.org/10.1146/annurev-earth-063016-020544

Barkaoui, K., Roumet, C., & Volaire, F. (2016). Mean root trait more than root trait diversity determines drought resilience in native and cultivated Mediterranean grass mixtures. *Agriculture, Ecosystems & Environment*, *231*, 122-132. https://doi.org/10.1016/j.agee.2016.06.035

Barrios, E. (2007). Soil biota, ecosystem services and land productivity. *Ecological Economics*, *64*, 269-285. https://doi.org/10.1016/j.ecolecon.2007.03.004

Barton, L., Wan, G. G. Y., Buck, R. P., & Colmer, T. D. (2009). Nitrogen Increases Evapotranspiration and Growth of a Warm-Season Turfgrass. *Agronomy Journal*, *101*, 17-24. https://doi.org/10.2134/agronj2008.0078

Basset, C., Abou Najm, M., Ghezzehei, T., Hao, X., & Daccache, A. (2023). How does soil structure affect water infiltration? A meta-data systematic review. *Soil and Tillage Research*, *226*, 105577. https://doi.org/10.1016/j.still.2022.105577

Basso, B., & Ritchie, J. T. (2018). Evapotranspiration in High-Yielding Maize and under Increased Vapor Pressure Deficit in the US Midwest. *Agricultural & Environmental Letters*, *3*, 170039. https://doi.org/10.2134/ael2017.11.0039

Bastian, M., Heymann, S., & Jacomy, M. (2009). Gephi: An Open Source Software for Exploring and Manipulating Networks. *Proceedings of the International AAAI Conference on Web and Social Media*, *3*, 2. https://doi.org/10.1609/icwsm.v3i1.13937

Bastos, A., Ciais, P., Friedlingstein, P., Sitch, S., Pongratz, J., Fan, L., Wigneron, J. P., Weber, U., Reichstein, M., Fu, Z., Anthoni, P., Arneth, A., Haverd, V., Jain, A. K., Joetzjer, E., Knauer, J., Lienert, S., Loughran, T., McGuire, P. C., . . . Zaehle, S. (2020). Direct and seasonal legacy effects of the 2018 heat wave and drought on European ecosystem productivity. *Science Advances*, *6*, eaba2724. https://doi.org/10.1126/sciadv.aba2724

Bates, D. (2005). Fitting linear mixed models in R. *R News* 5, 27-30.

Bauke, S. L., Amelung, W., Bol, R., Brandt, L., Brüggemann, N., Kandeler, E., Meyer, N., Or, D., Schnepf, A., Schloter, M., Schulz, S., Siebers, N., von Sperber, C., & Vereecken, H. (2022). Soil water status shapes nutrient cycling in agroecosystems from micrometer to landscape scales. *Journal of Plant Nutrition and Soil Science*, *185*, 773-792. https://doi.org/10.1002/jpln.202200357

Baumann, K., Dignac, M.-F., Rumpel, C., Bardoux, G., Sarr, A., Steffens, M., & Maron, P.-A. (2012). Soil microbial diversity affects soil organic matter decomposition in a silty grassland soil. *Biogeochemistry*, *114*, 201-212. https://doi.org/10.1007/s10533-012-9800-6

Bayala, J., & Prieto, I. (2019). Water acquisition, sharing and redistribution by roots: applications to agroforestry systems. *Plant and Soil*, *453*, 17-28. https://doi.org/10.1007/s11104-019-04173-z

Bazzichetto, M., Sperandii, M. G., Penone, C., Keil, P., Allan, E., Lepš, J., Prati, D., Fischer, M., Bolliger,

R., Gossner, M. M., & de Bello, F. (2024). Biodiversity promotes resistance but dominant species shape recovery of grasslands under extreme drought. *Journal of Ecology*, *112*, 1087-1100. https://doi.org/10.1111/1365-2745.14288

Beguería, S., Vicente-Serrano, S. M., & Maintainer Santiago, B. (2017). Package 'spei'. *Calculation of the Standardized Precipitation-Evapotranspiration Index, CRAN.*

Beguería, S., Vicente-Serrano, S. M., Reig, F., & Latorre, B. (2014). Standardized precipitation evapotranspiration index (SPEI) revisited: parameter fitting, evapotranspiration models, tools, datasets and drought monitoring. *International Journal of Climatology*, *34*, 3001-3023. https://doi.org/10.1002/joc.3887

Bei, Q., Reitz, T., Schnabel, B., Eisenhauer, N., Schadler, M., Buscot, F., & Heintz-Buschart, A. (2023). Extreme summers impact cropland and grassland soil microbiomes. *The ISME Journal*, *17*, 1589-1600. https://doi.org/10.1038/s41396-023-01470-5

Beillouin, D., Cardinael, R., Berre, D., Boyer, A., Corbeels, M., Fallot, A., Feder, F., & Demenois, J. (2022). A global overview of studies about land management, land-use change, and climate change effects on soil organic carbon. *Global Change Biology*, *28*, 1690-1702. https://doi.org/10.1111/gcb.15998

Bengough, A. G. (2003). Root Growth and Function in Relation to Soil Structure, Composition, and Strength. In H. de Kroon & E. J. W. Visser (Eds.), *Ecological Studies* (Vol. 168). Springer-Verlag.

Bengough, A. G., McKenzie, B. M., Hallett, P. D., & Valentine, T. A. (2011). Root elongation, water stress, and mechanical impedance: a review of limiting stresses and beneficial root tip traits. *Journal of Experimental Botany*, *62*, 59-68. https://doi.org/10.1093/jxb/erq350

Benjamin, J. G., Mikha, M., Nielsen, D. C., Vigil, M. F., Calderón, F., & Henry, W. B. (2007). Cropping Intensity Effects on Physical Properties of a No-till Silt Loam. *Soil Science Society of America Journal*, *71*, 1160-1165. https://doi.org/10.2136/sssaj2006.0363

Benjamini, Y., & Hochberg, Y. (1995). Controlling the False Discovery Rate - a Practical and Powerful Approach to Multiple Testing. *Journal of the Royal Statistical Society Series B-Statistical Methodology*, *57*, 289-300. https://doi.org/10.1111/j.2517-6161.1995.tb02031.x

Bens, O., Wahl, N. A., Fischer, H., & Hüttl, R. F. (2006). Water infiltration and hydraulic conductivity in sandy cambisols: impacts of forest transformation on soil hydrological properties. *European Journal of Forest Research*, *126*, 101-109. https://doi.org/10.1007/s10342-006-0133-7

Bhattacharyya, R., Rabbi, S. M. F., Zhang, Y., Young, I. M., Jones, A. R., Dennis, P. G., Menzies, N. W., Kopittke, P. M., & Dalal, R. C. (2021). Soil organic carbon is significantly associated with the pore geometry, microbial diversity and enzyme activity of the macro-aggregates under different land uses. *Science of Total Environment*, *778*, 146286. https://doi.org/10.1016/j.scitotenv.2021.146286

Biswal, D. (2022). Nematodes as Ghosts of Land Use Past: Elucidating the Roles of Soil Nematode Community Studies as Indicators of Soil Health and Land Management Practices. *Applied Biochemistry and Biotechnology*, *194*, 2357-2417. https://doi.org/10.1007/s12010-022-03808-9

Blankinship, J. C., Niklaus, P. A., & Hungate, B. A. (2011). A meta-analysis of responses of soil biota to global change. *Oecologia*, *165*, 553-565. https://doi.org/10.1007/s00442-011-1909-0

Bolker, D., Bates, M. B., & Walker, S. (2015). Fitting Linear Mixed-Effects Models Using lme4. *Journal of Statistical Software*, *67*, 1-48.

Bond-Lamberty, B., & Thomson, A. (2010). Temperature-associated increases in the global soil respiration record. *Nature*, *464*, 579-582. https://doi.org/10.1038/nature08930

Bongers, T. (1990). The maturity index: an ecological measure of environmental disturbance based on nematode species composition. *Oecologia*, *83*, 14-19. https://doi.org/10.1007/BF00324627

Bongers, T., & Bongers, M. (1998). Functional diversity of nematodes. *Applied Soil Ecology*, *10*, 239-251. https://doi.org/10.1016/S0929-1393(98)00123-1

Bongers, T., & Ferris, H. (1999). Nematode community structure as a bioindicator in environmental monitoring. *Trends in Ecology & Evolution*, *14*, 224-228. https://doi.org/10.1016/S0169-5347(98)01583-3

Bouwman, L. A., & Arts, W. B. M. (2000). Effects of soil compaction on the relationships between nematodes, grass production and soil physical properties. *Applied Soil Ecology*, *14*, 213-222.

https://doi.org/10.1016/S0929-1393(00)00055-X

Bristiel, P., Roumet, C., Violle, C., & Volaire, F. (2018). Coping with drought: root trait variability within the perennial grass Dactylis glomerata captures a trade-off between dehydration avoidance and dehydration tolerance. *Plant and Soil*, *434*, 327-342. https://doi.org/10.1007/s11104-018-3854-8

Bronick, C. J., & Lal, R. (2005). Soil structure and management: a review. *Geoderma*, *124*, 3-22. https://doi.org/10.1016/j.geoderma.2004.03.005

Brookes, P. C., Landman, A., Pruden, G., & Jenkinson, D. S. (1985). Chloroform Fumigation and the Release of Soil-Nitrogen - a Rapid Direct Extraction Method to Measure Microbial Biomass Nitrogen in Soil. *Soil Biology & Biochemistry*, *17*(6), 837-842. https://doi.org/10.1016/0038-0717(85)90144-0

Brookshire, E. N., & Weaver, T. (2015). Long-term decline in grassland productivity driven by increasing dryness. *Nature Communications*, *6*, 7148. https://doi.org/10.1038/ncomms8148

Brussaard, L. (1998). Soil fauna, guilds, functional groups and ecosyste. *Applied Soil Ecology*, *9*, 123-135. https://doi.org/10.1016/S0929-1393(98)00066-3

Budhathoki, S., Lamba, J., Srivastava, P., Williams, C., Arriaga, F., & Karthikeyan, K. G. (2022). Impact of land use and tillage practice on soil macropore characteristics inferred from X-ray computed tomography. *Catena*, *210*, 105886. https://doi.org/10.1016/j.catena.2021.105886

Bundt, M., Widmer, F., Pesaro, M., Zeyer, J., & Blaser, P. (2001). Preferential flow paths: biological 'hot spots' in soils. *Soil Biology & Biochemistry*, *33*, 729-738. https://doi.org/10.1016/S0038-0717(00)00218-2

Burak, E., Quinton, J. N., & Dodd, I. C. (2021). Root hairs are the most important root trait for rhizosheath formation of barley (Hordeum vulgare), maize (Zea mays) and Lotus japonicus (Gifu). *Ann Bot*, *128*, 45-57. https://doi.org/10.1093/aob/mcab029

Burr-Hersey, J. E., Ritz, K., Bengough, G. A., & Mooney, S. J. (2020). Reorganisation of rhizosphere soil pore structure by wild plant species in compacted soils. *Journal of Experimental Botany*, *71*, 6107-6115. https://doi.org/10.1093/jxb/eraa323

Carminati, A., Zarebanadkouki, M., Kroener, E., Ahmed, M. A., & Holz, M. (2016). Biophysical rhizosphere processes affecting root water uptake. *Annals of Botany*, *118*, 561-571. https://doi.org/10.1093/aob/mcw113

Carter, M. R. (1988). Temporal Variability of Soil Macroporosity in a Fine Sandy Loam under Moldboard Plowing and Direct Drilling. *Soil & Tillage Research*, *12*, 37-51. https://doi.org/10.1016/0167-1987(88)90054-2

Casali, E., Larsbo, M., Koestel, J., & Jarvis, N. (2024). Macropore flow in relation to the geometry and topology of soil macropore networks: Re-visiting the kinematic wave equation. *Journal of Hydrology*, *630*, 130732. https://doi.org/10.1016/j.jhydrol.2024.130732

Casero, R. A., Jr. (2018). Targeting the aryl hydrocarbon receptor/polyamine biosynthesis axis of evil for cancer therapy. *The Journal of Clinical Investigation*, *128*, 4254-4256. https://doi.org/10.1172/JCI123266

Cesarz, S., Ciobanu, M., Wright, A. J., Ebeling, A., Vogel, A., Weisser, W. W., & Eisenhauer, N. (2017). Plant species richness sustains higher trophic levels of soil nematode communities after consecutive environmental perturbations. *Oecologia*, *184*, 715-728. https://doi.org/10.1007/s00442-017-3893-5

Cesarz, S., Eva Schulz, A., Beugnon, R., & Eisenhauer, N. (2019). Testing soil nematode extraction efficiency using different variations of the Baermann-funnel method. *Soil Organisms*, *91*, 61-72. https://doi.org/10.25674/so91201

Chapman, N., Miller, A. J., Lindsey, K., & Whalley, W. R. (2012). Roots, water, and nutrient acquisition: let's get physical. *Trends in Plant Science*, *17*, 701-710. https://doi.org/10.1016/j.tplants.2012.08.001

Chen, D., Zheng, S., Shan, Y., Taube, F., Bai, Y., & Briones, M. J. (2013). Vertebrate herbivore-induced changes in plants and soils: linkages to ecosystem functioning in a semi-arid steppe. *Functional Ecology*, *27*, 273-281. https://doi.org/10.1111/1365-2435.12027

Chen, H. Y. H., & Brassard, B. W. (2012). Intrinsic and Extrinsic Controls of Fine Root Life Span. *Critical Reviews in Plant Sciences*, *32*, 151-161. https://doi.org/10.1080/07352689.2012.734742

Chen, L., Brun, P., Buri, P., Fatichi, S., Gessler, A., McCarthy, M. J., Pellicciotti, F., Stocker, B., & Karger, D. N. (2025). Global increase in the occurrence and impact of multiyear droughts. *Science*, *387*, 278-284. https://doi.org/10.1126/science.ado4245

Chen, X., Xue, W., Xue, J., Griffiths, B. S., & Liu, M. (2020). Contribution of bacterivorous nematodes to soil resistance and resilience under copper or heat stress. *Soil Ecology Letters*, *2*, 220-229. https://doi.org/10.1007/s42832-020-0045-3

Chen, Z., Wang, H., Liu, X., Zhao, X., Lu, D., Zhou, J., & Li, C. (2017). Changes in soil microbial community and organic carbon fractions under short-term straw return in a rice–wheat cropping system. *Soil and Tillage Research*, *165*, 121-127. https://doi.org/10.1016/j.still.2016.07.018

Colombi, T., Braun, S., Keller, T., & Walter, A. (2017). Artificial macropores attract crop roots and enhance plant productivity on compacted soils. *Science of the Total Environment*, *574*, 1283-1293. https://doi.org/10.1016/j.scitotenv.2016.07.194

Colombi, T., Pandey, B. K., Chawade, A., Bennett, M. J., Mooney, S. J., & Keller, T. (2024). Root plasticity versus elasticity - when are responses acclimative? *Trends in Plant Science*, *29*, 856-864. https://doi.org/10.1016/j.tplants.2024.01.003

Condon, A. G., Richards, R. A., Rebetzke, G. J., & Farquhar, G. D. (2004). Breeding for high water-use efficiency. *Journal of Experimental Botany*, *55*, 2447-2460. https://doi.org/10.1093/jxb/erh277

Cooper, H. V., Sjögersten, S., Lark, R. M., Girkin, N. T., Vane, C. H., Calonego, J. C., Rosolem, C., & Mooney, S. J. (2021). Long-term zero-tillage enhances the protection of soil carbon in tropical agriculture. *European Journal of Soil Science*, *72*, 2477-2492. https://doi.org/10.1111/ejss.13111

Coppola, A. I., Druffel, E. R. M., Broek, T. A., Haghipour, N., Eglinton, T. I., McCarthy, M., & Walker, B. D. (2024). Variable aging and storage of dissolved black carbon in the ocean. *Proceedings of the National Academy of Sciences*, *121*, e2305030121. https://doi.org/10.1073/pnas.2305030121

Cortois, R., Veen, G. F., Duyts, H., Abbas, M., Strecker, T., Kostenko, O., Eisenhauer, N., Scheu, S., Gleixner, G., De Deyn, G. B., & van der Putten, W. H. (2017). Possible mechanisms underlying abundance and diversity responses of nematode communities to plant diversity. *Ecosphere*, *8*. https://doi.org/10.1002/ecs2.1719

Cosentino, D., Chenu, C., & Le Bissonnais, Y. (2006). Aggregate stability and microbial community dynamics under drying–wetting cycles in a silt loam soil. *Soil Biology and Biochemistry*, *38*, 2053-2062. https://doi.org/10.1016/j.soilbio.2005.12.022

Cotrufo, M. F., Haddix, M. L., Kroeger, M. E., & Stewart, C. E. (2022). The role of plant input physical-chemical properties, and microbial and soil chemical diversity on the formation of particulate and mineral-associated organic matter. *Soil Biology & Biochemistry*, *168*, 108648. https://doi.org/10.1016/j.soilbio.2022.108648

Cotrufo, M. F., Wallenstein, M. D., Boot, C. M., Denef, K., & Paul, E. (2013). The Microbial Efficiency-Matrix Stabilization (MEMS) framework integrates plant litter decomposition with soil organic matter stabilization: do labile plant inputs form stable soil organic matter? *Global Change Biology*, *19*, 988-995. https://doi.org/10.1111/gcb.12113

Coucheney, E., Casali, E., Jarvis, N., & Koestel, J. (2025). Air-filled porosity, its connectivity and relation to particulate organic matter in intact soil cores controls carbon emissions near saturation. *Soil and Tillage Research*, *248*, 106468. https://doi.org/10.1016/j.still.2025.106468

Craine, J. M., Ocheltree, T. W., Nippert, J. B., Towne, E. G., Skibbe, A. M., Kembel, S. W., & Fargione, J. E. (2012). Global diversity of drought tolerance and grassland climate-change resilience. *Nature Climate Change*, *3*, 63-67. https://doi.org/10.1038/nclimate1634

Creamer, R. E., Hannula, S. E., Leeuwen, J. P. V., Stone, D., Rutgers, M., Schmelz, R. M., Ruiter, P. C. d., Hendriksen, N. B., Bolger, T., Bouffaud, M. L., Buee, M., Carvalho, F., Costa, D., Dirilgen, T., Francisco, R., Griffiths, B. S., Griffiths, R., Martin, F., Silva, P. M. d., . . . Lemanceau, P. (2016). Ecological network analysis reveals the inter-connection between soil biodiversity and ecosystem function as affected by land use across Europe. *Applied Soil Ecology*, *97*, 112-124.

https://doi.org/10.1016/j.apsoil.2015.08.006

Crowther, T. W., Todd-Brown, K. E., Rowe, C. W., Wieder, W. R., Carey, J. C., Machmuller, M. B., Snoek, B. L., Fang, S., Zhou, G., Allison, S. D., Blair, J. M., Bridgham, S. D., Burton, A. J., Carrillo, Y., Reich, P. B., Clark, J. S., Classen, A. T., Dijkstra, F. A., Elberling, B., . . . Bradford, M. A. (2016). Quantifying global soil carbon losses in response to warming. *Nature*, *540*, 104-108. https://doi.org/10.1038/nature20150

Cui, Z., Wu, G.-L., Huang, Z., & Liu, Y. (2019). Fine roots determine soil infiltration potential than soil water content in semi-arid grassland soils. *Journal of Hydrology*, *578*, 124023. https://doi.org/10.1016/j.jhydrol.2019.124023

Curiel Yuste, J., Baldocchi, D. D., Gershenson, A., Goldstein, A., Misson, L., & Wong, S. (2007). Microbial soil respiration and its dependency on carbon inputs, soil temperature and moisture. *Global Change Biology*, *13*, 2018-2035. https://doi.org/10.1111/j.1365-2486.2007.01415.x

da Silva, J. V. C. d. L., Hirschfeld, M. N. C., Cares, J. E., & Esteves, A. M. (2020). Land use, soil properties and climate variables influence the nematode communities in the Caatinga dry forest. *Applied Soil Ecology*, *150*, 103474. https://doi.org/10.1016/j.apsoil.2019.103474

Dal Ferro, N., Sartori, L., Simonetti, G., Berti, A., & Morari, F. (2014). Soil macro- and microstructure as affected by different tillage systems and their effects on maize root growth. *Soil and Tillage Research*, *140*, 55-65. https://doi.org/10.1016/j.still.2014.02.003

de Oliveira Cardoso, M., Pedrosa, E. M., Rolim, M. M., Silva, E. F., & de Barros, P. A. (2012). Effects of soil mechanical resistance on nematode community structure under conventional sugarcane and remaining of Atlantic Forest. *Environmental Monitoring & Assessment*, *184*, 3529-3544. https://doi.org/10.1007/s10661-011-2206-4

de Vries, F. T., Liiri, M. E., Bjørnlund, L., Bowker, M. A., Christensen, S., Setälä, H. M., & Bardgett, R. D. (2012). Land use alters the resistance and resilience of soil food webs to drought. *Nature Climate Change*, *2*, 276-280. https://doi.org/10.1038/nclimate1368

Desrochers, J., Brye, K. R., Gbur, E., Pollock, E. D., & Savin, M. C. (2019). Long-term residue and water management practice effects on particulate organic matter in a loessial soil in eastern Arkansas, USA. *Geoderma*, *337*, 792-804. https://doi.org/10.1016/j.geoderma.2018.10.027

Dexter, A. R., Czyż, E. A., Richard, G., & Reszkowska, A. (2008). A user-friendly water retention function that takes account of the textural and structural pore spaces in soil. *Geoderma*, *143*, 243-253. https://doi.org/10.1016/j.geoderma.2007.11.010

Ding, T., Guo, Z., Qian, Y., Wang, Y., Jiang, F., Zhang, Z., & Peng, X. (2025). Interaction between POM and pore structure during straw decomposition in two soils with contrasting texture. *Soil and Tillage Research*, *245*, 106288. https://doi.org/10.1016/j.still.2024.106288

Domeignoz-Horta, L. A., Pold, G., Liu, X. A., Frey, S. D., Melillo, J. M., & DeAngelis, K. M. (2020). Microbial diversity drives carbon use efficiency in a model soil. *Nature Communications*, *11*, 3684. https://doi.org/10.1038/s41467-020-17502-z

Don, A., Schumacher, J., & Freibauer, A. (2011). Impact of tropical land-use change on soil organic carbon stocks - a meta-analysis. *Global Change Biology*, *17*, 1658-1670. https://doi.org/10.1111/j.1365-2486.2010.02336.x

Dong, Z., Hou, R., Chen, Q., Ouyang, Z., & Ge, F. (2013). Response of soil nematodes to elevated temperature in conventional and no-tillage cropland systems. *Plant and Soil*, *373*, 907-918. https://doi.org/10.1007/s11104-013-1846-2

Döscher, R. W. N., U.; Jones, C.; Rutgersson, A.; Meier, H. E. M.; Hansson, U. (2002). The Development of The Coupled Ocean-atmosphere Model Rcao For The Northern European Area. *In EGS General Assembly Conference Abstracts* (p. 1569).

Draye, X., Kim, Y., Lobet, G., & Javaux, M. (2010). Model-assisted integration of physiological and environmental constraints affecting the dynamic and spatial patterns of root water uptake from soils. *Journal of Experimental Botany*, *61*, 2145-2155. https://doi.org/10.1093/jxb/erq077

Du Preez, G., Daneel, M., De Goede, R., Du Toit, M. J., Ferris, H., Fourie, H., Geisen, S., Kakouli-Duarte, T., Korthals, G., Sánchez-Moreno, S., & Schmidt, J. H. (2022). Nematode-based indices in soil

ecology: Application, utility, and future directions. *Soil Biology and Biochemistry*, *169*, 108640. https://doi.org/10.1016/j.soilbio.2022.108640

Dungait, J. A. J., Hopkins, D. W., Gregory, A. S., & Whitmore, A. P. (2012). Soil organic matter turnover is governed by accessibility not recalcitrance. *Global Change Biology*, *18*, 1781-1796. https://doi.org/10.1111/j.1365-2486.2012.02665.x

DuPont, S. T., Beniston, J., Glover, J. D., Hodson, A., Culman, S. W., Lal, R., & Ferris, H. (2014). Root traits and soil properties in harvested perennial grassland, annual wheat, and never-tilled annual wheat. *Plant and Soil*, *381*, 405-420. https://doi.org/10.1007/s11104-014-2145-2

DuPont, S. T., Culman, S. W., Ferris, H., Buckley, D. H., & Glover, J. D. (2010). No-tillage conversion of harvested perennial grassland to annual cropland reduces root biomass, decreases active carbon stocks, and impacts soil biota. *Agriculture, Ecosystems & Environment*, *137*, 25-32. https://doi.org/10.1016/j.agee.2009.12.021

Eisenhauer, N., Lanoue, A., Strecker, T., Scheu, S., Steinauer, K., Thakur, M. P., & Mommer, L. (2017). Root biomass and exudates link plant diversity with soil bacterial and fungal biomass. *Scientific Reports*, *7*, 44641. https://doi.org/10.1038/srep44641

Erktan, A., Or, D., & Scheu, S. (2020). The physical structure of soil: Determinant and consequence of trophic interactions. *Soil Biology and Biochemistry*, *148*, 107876. https://doi.org/10.1016/j.soilbio.2020.107876

Fan, J., McConkey, B., Wang, H., & Janzen, H. (2016). Root distribution by depth for temperate agricultural crops. *Field Crops Research*, *189*, 68-74. https://doi.org/10.1016/j.fcr.2016.02.013

Fan, J., Wang, Q., Jones, S. B., & Shao, M. (2015). Soil water depletion and recharge under different land cover in China's Loess Plateau. *Ecohydrology*, *9*, 396-406. https://doi.org/10.1002/eco.1642

Fan, Y., Miguez-Macho, G., Jobbagy, E. G., Jackson, R. B., & Otero-Casal, C. (2017). Hydrologic regulation of plant rooting depth. *Proceedings of the National Academy of Sciences*, *114*, 10572-10577. https://doi.org/10.1073/pnas.1712381114

Fatichi, S., Or, D., Walko, R., Vereecken, H., Young, M. H., Ghezzehei, T. A., Hengl, T., Kollet, S., Agam, N., & Avissar, R. (2020). Soil structure is an important omission in Earth System Models. *Nature Communications*, *11*, 522. https://doi.org/10.1038/s41467-020-14411-z

Feldman, A. F., Feng, X., Felton, A. J., Konings, A. G., Knapp, A. K., Biederman, J. A., & Poulter, B. (2024). Plant responses to changing rainfall frequency and intensity. *Nature Reviews Earth & Environment*, *5*, 276-294. https://doi.org/10.1038/s43017-024-00534-0

Felipe-Lucia, M. R., Soliveres, S., Penone, C., Fischer, M., Ammer, C., Boch, S., Boeddinghaus, R. S., Bonkowski, M., Buscot, F., Fiore-Donno, A. M., Frank, K., Goldmann, K., Gossner, M. M., Holzel, N., Jochum, M., Kandeler, E., Klaus, V. H., Kleinebecker, T., Leimer, S., . . . Allan, E. (2020). Land-use intensity alters networks between biodiversity, ecosystem functions, and services. *Proceedings of the National Academy of Sciences*, *117*, 28140-28149. https://doi.org/10.1073/pnas.2016210117

Feng, R., Liu, G., Chen, Y., Wang, C., Zhang, Q., & Wang, J. (2024). Impacts of rainfall-induced physical crust on near-surface soil pore structure after drying. *Catena*, *238*, 107880. https://doi.org/10.1016/j.catena.2024.107880

Feng, R., Zhang, Y., Wang, J., Wang, Y., Zhang, N., & She, D. (2025). Effects of rainfall-induced physical crusts on soil carbon distribution and mineralization through surface pore structure. *Soil and Tillage Research*, *247*, 106373. https://doi.org/10.1016/j.still.2024.106373

Ferris, H., Bongers, T., & de Goede, R. G. M. (2001). A framework for soil food web diagnostics: extension of the nematode faunal analysis concept. *Applied Soil Ecology*, *18*, 13-29. https://doi.org/10.1016/S0929-1393(01)00152-4

Figueroa-Bustos, V., Palta, J. A., Chen, Y., Stefanova, K., & Siddique, K. H. M. (2020). Wheat Cultivars With Contrasting Root System Size Responded Differently to Terminal Drought. *Frontiers in Plant Science*, *11*, 1285. https://doi.org/10.3389/fpls.2020.01285

Finlay, R. D., & Thorn, R. G. (2019). The fungi in soil. *Modern Soil Microbiology* (3rd Edition ed.), 65-90.

Fischer, C., Roscher, C., Jensen, B., Eisenhauer, N., Baade, J., Attinger, S., Scheu, S., Weisser, W. W., Schumacher, J., & Hildebrandt, A. (2014). How do earthworms, soil texture and plant composition

affect infiltration along an experimental plant diversity gradient in grassland? *PLoS One*, *9*, e98987. https://doi.org/10.1371/journal.pone.0098987

Fischer, C., Tischer, J., Roscher, C., Eisenhauer, N., Ravenek, J., Gleixner, G., Attinger, S., Jensen, B., de Kroon, H., Mommer, L., Scheu, S., & Hildebrandt, A. (2014b). Plant species diversity affects infiltration capacity in an experimental grassland through changes in soil properties. *Plant and Soil*, *397*, 1-16. https://doi.org/10.1007/s11104-014-2373-5

Franco, A. L. C., Guan, P., Cui, S., de Tomasel, C. M., Gherardi, L. A., Sala, O. E., & Wall, D. H. (2022). Precipitation effects on nematode diversity and carbon footprint across grasslands. *Global Change Biology*, *28*, 2124-2132. https://doi.org/10.1111/gcb.16055

Freschet, G. T., Roumet, C., Comas, L. H., Weemstra, M., Bengough, A. G., Rewald, B., Bardgett, R. D., De Deyn, G. B., Johnson, D., Klimesova, J., Lukac, M., McCormack, M. L., Meier, I. C., Pages, L., Poorter, H., Prieto, I., Wurzburger, N., Zadworny, M., Bagniewska-Zadworna, A., . . . Stokes, A. (2021). Root traits as drivers of plant and ecosystem functioning: current understanding, pitfalls and future research needs. *New Phytologist*, *232*, 1123-1158. https://doi.org/10.1111/nph.17072

Freschet, G. T., Violle, C., Bourget, M. Y., Scherer-Lorenzen, M., & Fort, F. (2018). Allocation, morphology, physiology, architecture: the multiple facets of plant above- and below-ground responses to resource stress. *New Phytologist*, *219*, 1338-1352. https://doi.org/10.1111/nph.15225

Frouz, J. (2024). Plant-soil feedback across spatiotemporal scales from immediate effects to legacy. *Soil Biology and Biochemistry*, *189*, 109289. https://doi.org/10.1016/j.soilbio.2023.109289

Fu, Z., Ciais, P., Feldman, A. F., Gentine, P., Makowski, D., Prentice, I. C., Stoy, P. C., Bastos, A., & Wigneron, J. P. (2022). Critical soil moisture thresholds of plant water stress in terrestrial ecosystems. *Science Advances*, *8*, eabq7827. https://doi.org/10.1126/sciadv.abq7827

Fujimoto, T., Hasegawa, S., Otobe, K., & Mizukubo, T. (2010). The effect of soil water flow and soil properties on the motility of second-stage juveniles of the root-knot nematode (Meloidogyne incognita). *Soil Biology and Biochemistry*, *47*, 1065-1072. https://doi.org/10.1016/j.soilbio.2010.03.003

Ganault, P., Nahmani, J., Capowiez, Y., Fromin, N., Shihan, A., Bertrand, I., Buatois, B., & Milcu, A. (2024). Earthworms and plants can decrease soil greenhouse gas emissions by modulating soil moisture fluctuations and soil macroporosity in a mesocosm experiment. *PLoS One*, *19*, e0289859. https://doi.org/10.1371/journal.pone.0289859

Gao, X., Wu, P., Zhao, X., Wang, J., & Shi, Y. (2011). Effects of Land Use on Soil Moisture Variations in a Semi-Arid Catchment: Implications for Land and Agricultural Water Management. *Land Degradation & Development*, *25*, 163-172. https://doi.org/10.1002/ldr.1156

George, T. S., Chen, Y., & Oliveira, M. T. (2024). Editorial: Belowground adaptation of plants to climate change. *Plant and Soil*, *500*(, 1-10. https://doi.org/10.1007/s11104-024-06560-7

Gill, R. A., & Jackson, R. B. (2000). Global patterns of root turnover for terrestrial ecosystems. *New Phytologist*, *147*, 13-31. https://doi.org/10.1046/j.1469-8137.2000.00681.x

Giuliani, L. M., Hallett, P. D., & Loades, K. W. (2024). Effects of soil structure complexity to root growth of plants with contrasting root architecture. *Soil and Tillage Research*, *238*, 106023. https://doi.org/10.1016/j.still.2024.106023

Good, S. P., Noone, D., & Bowen, G. (2015). WATER RESOURCES. Hydrologic connectivity constrains partitioning of global terrestrial water fluxes. *Science*, *349*, 175-177. https://doi.org/10.1126/science.aaa5931

Gosling, P., Parsons, N., & Bending, G. D. (2013). What are the primary factors controlling the light fraction and particulate soil organic matter content of agricultural soils? *Biology and Fertility of Soils*, *49*, 1001-1014. https://doi.org/10.1007/s00374-013-0791-9

Gould, I. J., Quinton, J. N., Weigelt, A., De Deyn, G. B., & Bardgett, R. D. (2016). Plant diversity and root traits benefit physical properties key to soil function in grasslands. *Ecology Letters*, *19*, 1140-1149. https://doi.org/10.1111/ele.12652

Gregory, A. S., Ritz, K., McGrath, S. P., Quinton, J. N., Goulding, K. W., Jones, R. J., Harris, J. A., Bol, R., Wallace, P., Pilgrim, E. S., & Whitmore, A. P. (2015). A review of the impacts of degradation threats

on soil properties in the UK. *Soil Use and Management*, *31*, 1-15. https://doi.org/10.1111/sum.12212

Gregory, P. J. (2006). Roots, rhizosphere and soil: the route to a better understanding of soil science? *European Journal of Soil Science*, *57*, 2-12. https://doi.org/10.1111/j.1365-2389.2005.00778.x

Griffiths, B. S., & Caul, S. (1993). Migration of bacterial-feeding nematodes, but not protozoa, to decomposing grass residues. *Biology and Fertility of Soils*, *15*, 6. https://doi.org/10.1007/BF00361612

Guan, S., An, N., Zong, N., He, Y., Shi, P., Zhang, J., & He, N. (2018). Climate warming impacts on soil organic carbon fractions and aggregate stability in a Tibetan alpine meadow. *Soil Biology and Biochemistry*, *116*, 224-236. https://doi.org/10.1016/j.soilbio.2017.10.011

Guo, X., Gao, Q., Yuan, M., Wang, G., Zhou, X., Feng, J., Shi, Z., Hale, L., Wu, L., Zhou, A., Tian, R., Liu, F., Wu, B., Chen, L., Jung, C. G., Niu, S., Li, D., Xu, X., Jiang, L., . . . Zhou, J. (2020b). Gene-informed decomposition model predicts lower soil carbon loss due to persistent microbial adaptation to warming. *Nature Communications*, *11*, 4897. https://doi.org/10.1038/s41467-020-18706-z

Guo, Y., Fan, R., Zhang, X., Zhang, Y., Wu, D., McLaughlin, N., Zhang, S., Chen, X., Jia, S., & Liang, A. (2020a). Tillage-induced effects on SOC through changes in aggregate stability and soil pore structure. *Science of the Total Environment*, *703*, 134617. https://doi.org/10.1016/j.scitotenv.2019.134617

Haas, C., & Horn, R. (2018). Impact of Small-Scaled Differences in Micro-Aggregation on Physico-Chemical Parameters of Macroscopic Biopore Walls. *Frontiers in Environmental Science*, *6*, 90. https://doi.org/10.3389/fenvs.2018.00090

Hales, T. C., & Miniat, C. F. (2016). Soil moisture causes dynamic adjustments to root reinforcement that reduce slope stability. *Earth Surface Processes and Landforms*, *42*, 803-813. https://doi.org/10.1002/esp.4039

Han, E., Kautz, T., & Köpke, U. (2015). Precrop root system determines root diameter of subsequent crop. *Biology and Fertility of Soils*, *52*, 113-118. https://doi.org/10.1007/s00374-015-1049-5

Hanslin, H. M., Bischoff, A., & Hovstad, K. A. (2019). Root growth plasticity to drought in seedlings of perennial grasses. *Plant and Soil*, *440*, 551-568. https://doi.org/10.1007/s11104-019-04117-7

Hao, Y., Mao, J., Bachmann, C. M., Hoffman, F. M., Koren, G., Chen, H., Tian, H., Liu, J., Tao, J., Tang, J., Li, L., Liu, L., Apple, M., Shi, M., Jin, M., Zhu, Q., Kannenberg, S., Shi, X., Zhang, X., . . . Dai, Y. (2025). Soil moisture controls over carbon sequestration and greenhouse gas emissions: a review. *npj Climate and Atmospheric Science*, *8*, 16. https://doi.org/10.1038/s41612-024-00888-8

Hargreaves, G. H., & Allen, R. G. (2003). History and evaluation of Hargreaves evapotranspiration equation. *Journal of Irrigation and Drainage Engineering*, *129*, 53-63. https://doi.org/10.1061/(Asce)0733-9437(2003)129:1(53)

Hartmann, M., & Six, J. (2022). Soil structure and microbiome functions in agroecosystems. *Nature Reviews Earth & Environment*, *4*, 4-18. https://doi.org/10.1038/s43017-022-00366-w

Hassink, J., Bouwman, L. A., Zwart, K. B., & Brussaard, L. (1993). Relationships between Habitable Pore-Space, Soil Biota and Mineralization Rates in Grassland Soils. *Soil Biology & Biochemistry*, *25*, 47-55. https://doi.org/Doi 10.1016/0038-0717(93)90240-C

Haworth, M., Marino, G., Loreto, F., & Centritto, M. (2021). Integrating stomatal physiology and morphology: evolution of stomatal control and development of future crops. *Oecologia*, *197*, 867-883. https://doi.org/10.1007/s00442-021-04857-3

Haynes, R. J., & Francis, G. S. (2006). Changes in microbial biomass C, soil carbohydrate composition and aggregate stability induced by growth of selected crop and forage species under field conditions. *Journal of Soil Science*, *44*, 665-675. https://doi.org/10.1111/j.1365-2389.1993.tb02331.x

He, S., & Richards, K. (2015). Impact of Meadow Degradation on Soil Water Status and Pasture Management—A Case Study in Tibet. *Land Degradation & Development*, *26*, 468-479. https://doi.org/10.1002/ldr.2358

Helliwell, J. R., Sturrock, C. J., Grayling, K. M., Tracy, S. R., Flavel, R. J., Young, I. M., Whalley, W. R.,

& Mooney, S. J. (2013). Applications of X-ray computed tomography for examining biophysical interactions and structural development in soil systems: a review. *European Journal of Soil Science*, *64*, 279-297. https://doi.org/10.1111/ejss.12028

Hiernaux, P., Ayantunde, A., Kalilou, A., Mougin, E., Gérard, B., Baup, F., Grippa, M., & Djaby, B. (2009). Trends in productivity of crops, fallow and rangelands in Southwest Niger: Impact of land use, management and variable rainfall. *Journal of Hydrology*, *375*, 65-77. https://doi.org/10.1016/j.jhydrol.2009.01.032

Hirmas, D. R., Gimenez, D., Nemes, A., Kerry, R., Brunsell, N. A., & Wilson, C. J. (2018). Climate-induced changes in continental-scale soil macroporosity may intensify water cycle. *Nature*, *561*, 100-103. https://doi.org/10.1038/s41586-018-0463-x

Holmes, T. H., & Rice, K. J. (1996). Patterns of growth and soil-water utilization in some exotic annuals and native perennial bunchgrasses of California. *Annals of Botany*, *78*, 233-243. https://doi.org/10.1006/anbo.1996.0117

Hooper, D. U., Bignell, D. E., Brown, V. K., Brussaard, L., Dangerfield, J. M., Wall, D. H., Wardle, D. A., Coleman, D. C., Giller, K. E., Lavelle, P., Van der Putten, W. H., De Ruiter, P. C., Rusek, J., Silver, W. L., Tiedje, J. M., & Wolters, V. (2000). Interactions between aboveground and belowground biodiversity in terrestrial ecosystems: Patterns, mechanisms, and feedbacks. *Bioscience*, *50*, 1049-1061. https://doi.org/10.1641/0006-3568(2000)050[1049:Ibaabb]2.0.Co;2

Hoover, D. L., Knapp, A. K., & Smith, M. D. (2014). Resistance and resilience of a grassland ecosystem to climate extremes. *Ecology*, *95*, 2646-2656. https://doi.org/10.1890/13-2186.1

Hopkins, F., Gonzalez-Meler, M. A., Flower, C. E., Lynch, D. J., Czimczik, C., Tang, J., & Subke, J. A. (2013). Ecosystem-level controls on root-rhizosphere respiration. *New Phytologist*, *199*, 339-351. https://doi.org/10.1111/nph.12271

Hu, T., Malone, S. L., Rumpel, C., & Chabbi, A. (2024). Maximizing soil organic carbon stocks through optimal ploughing and renewal strategies in (Ley) grassland. *Communications Earth & Environment*, *5*, 38. https://doi.org/10.1038/s43247-024-01202-3

Huang, W., & Hall, S. J. (2017). Elevated moisture stimulates carbon loss from mineral soils by releasing protected organic matter. *Nature Communications*, *8*, 1774. https://doi.org/10.1038/s41467-017-01998-z

Huang, X. F., Chaparro, J. M., Reardon, K. F., Zhang, R. F., Shen, Q. R., & Vivanco, J. M. (2014). Rhizosphere interactions: root exudates, microbes, and microbial communities. *Botany*, *92*, 267-275. https://doi.org/10.1139/cjb-2013-0225

Huang, Y., Stein, G., Kolle, O., Kübler, K., Schulze, E.-D., Dong, H., Eichenberg, D., Gleixner, G., Hildebrandt, A., Lange, M., Roscher, C., Schielzeth, H., Schmid, B., Weigelt, A., Weisser, W. W., Shadaydeh, M., Denzler, J., Ebeling, A., & Eisenhauer, N. (2023). Enhanced stability of grassland soil temperature by plant diversity. *Nature Geoscience*, *17*, 44-50. https://doi.org/10.1038/s41561-023-01338-5

Hyväluoma, J., Niemi, P., Kinnunen, S., Brobbey, K., Miettinen, A., Keskinen, R., & Soinne, H. (2024). Comparing structural soil properties of boreal clay fields under contrasting soil management. *Soil Use and Management*, *40*, e13040. https://doi.org/10.1111/sum.13040

Isbell, F., Craven, D., Connolly, J., Loreau, M., Schmid, B., Beierkuhnlein, C., Bezemer, T. M., Bonin, C., Bruelheide, H., de Luca, E., Ebeling, A., Griffin, J. N., Guo, Q., Hautier, Y., Hector, A., Jentsch, A., Kreyling, J., Lanta, V., Manning, P., . . . Eisenhauer, N. (2015). Biodiversity increases the resistance of ecosystem productivity to climate extremes. *Nature*, *526*, 574-577. https://doi.org/10.1038/nature15374

Isensee, F., Jaeger, P. F., Kohl, S. A. A., Petersen, J., & Maier-Hein, K. H. (2021). nnU-Net: a self-configuring method for deep learning-based biomedical image segmentation. *Nature Methods*, *18*, 203-211. https://doi.org/10.1038/s41592-020-01008-z

Jackson, J., Middleton, S. L., Lawson, C. S., Jardine, E., Hawes, N., Maseyk, K., Salguero-Gómez, R., & Hector, A. (2024). Experimental drought reduces the productivity and stability of a calcareous grassland. *Journal of Ecology*, *112*, 917-931. https://doi.org/10.1111/1365-2745.14282

Jackson, R. B., Lajtha, K., Crow, S. E., Hugelius, G., Kramer, M. G., & Piñeiro, G. (2017). The Ecology of Soil Carbon: Pools, Vulnerabilities, and Biotic and Abiotic Controls. *Annual Review of Ecology, Evolution, and Systematics*, *48*, 419-445. https://doi.org/10.1146/annurev-ecolsys-112414-054234

Jacob, D., & Podzun, R. (1997). Sensitivity studies with the regional climate model REMO. *Meteorology and Atmospheric Physics*, *63*, 119-129. https://doi.org/10.1007/Bf01025368

Jamieson, R. C., Gordon, R. J., Sharples, K. E., Stratton, G. W., & Madani, A. (2002). Movement and persistence of fecal bacteria in agricultural soils and subsurface drainage water: A review. *Canadian biosystems engineering , 44*, 1-9.

Jarvis, N., Forkman, J., Koestel, J., Kätterer, T., Larsbo, M., & Taylor, A. (2017). Long-term effects of grass-clover leys on the structure of a silt loam soil in a cold climate. *Agriculture, Ecosystems & Environment*, *247*, 319-328. https://doi.org/10.1016/j.agee.2017.06.042

Jarvis, N. J. (2007). A review of non-equilibrium water flow and solute transport in soil macropores: principles, controlling factors and consequences for water quality. *European Journal of Soil Science*, *58*, 523-546. https://doi.org/10.1111/j.1365-2389.2007.00915.x

Jia, N., Li, L., Guo, H., & Xie, M. (2024). Important role of Fe oxides in global soil carbon stabilization and stocks. *Nature Communications*, *15*, 10318. https://doi.org/10.1038/s41467-024-54832-8

Jiang, X., Zhong, X., Yu, G., Zhang, X., & Liu, J. (2023). Different effects of taproot and fibrous root crops on pore structure and microbial network in reclaimed soil. *Science of the Total Environment*, *901*, 165996. https://doi.org/10.1016/j.scitotenv.2023.165996

Jiang, Y., Liu, M., Zhang, J., Chen, Y., Chen, X., Chen, L., Li, H., Zhang, X. X., & Sun, B. (2017). Nematode grazing promotes bacterial community dynamics in soil at the aggregate level. *The ISME Journal*, *11*, 2705-2717. https://doi.org/10.1038/ismej.2017.120

Jiang, Y., Zhou, H., Chen, L., Yuan, Y., Fang, H., Luan, L., Chen, Y., Wang, X., Liu, M., Li, H., Peng, X., & Sun, B. (2018). Nematodes and Microorganisms Interactively Stimulate Soil Organic Carbon Turnover in the Macroaggregates. *Frontiers in Microbiology*, *9*, 2803. https://doi.org/10.3389/fmicb.2018.02803

Jin, K., Shen, J., Ashton, R. W., Dodd, I. C., Parry, M. A., & Whalley, W. R. (2013). How do roots elongate in a structured soil? *Journal of Experimental Botany*, *64*, 4761-4777. https://doi.org/10.1093/jxb/ert286

Jin, K., White, P. J., Whalley, W. R., Shen, J., & Shi, L. (2017). Shaping an Optimal Soil by Root-Soil Interaction. *Trends in Plant Science*, *22*, 823-829. https://doi.org/10.1016/j.tplants.2017.07.008

Johansson, A., Livsey, J., Guasconi, D., Hugelius, G., Lindborg, R., & Manzoni, S. (2023). Long-term soil organic carbon changes after cropland conversion to grazed grassland in Southern Sweden. *Soil Use and Management*, *40*, e13004. https://doi.org/10.1111/sum.13004

Jones, C., Lowe, J., Liddicoat, S., & Betts, R. (2009). Committed terrestrial ecosystem changes due to climate change. *Nature Geoscience*, *2*, 484-487. https://doi.org/10.1038/ngeo555

Jones, F. G. W., Larbey, D. W., & Parrott, D. M. (1969). The influence of soil structure and moisture on nematodes, especially xiphinema, longidorus, trichodorus and heterodera spp. *Soil Biology and Biochemistry*, *1*, 153-165. https://doi.org/10.1016/0038-0717(69)90006-6

Jorda, H., Ahmed, M. A., Javaux, M., Carminati, A., Duddek, P., Vetterlein, D., & Vanderborght, J. (2022). Field scale plant water relation of maize (Zea mays) under drought – impact of root hairs and soil texture. *Plant and Soil*, *478*, 59-84. https://doi.org/10.1007/s11104-022-05685-x

Józefowska, A., Sokołowska, J., Woźnica, K., Woś, B., & Pietrzykowski, M. (2019). Tree species and soil substrate affect buffer capacity of anthroposols in afforested postmine sites in Poland. *Journal of Soil and Water Conservation*, *74*, 372-379. https://doi.org/10.2489/jswc.74.4.372

Juyal, A., Otten, W., Baveye, P. C., & Eickhorst, T. (2020). Influence of soil structure on the spread of Pseudomonas fluorescens in soil at microscale. *European Journal of Soil Science*, *72*, 141-153. https://doi.org/10.1111/ejss.12975

Kannenberg, S. A., Anderegg, W. R. L., Barnes, M. L., Dannenberg, M. P., & Knapp, A. K. (2024). Dominant role of soil moisture in mediating carbon and water fluxes in dryland ecosystems. *Nature Geoscience*, *17*, 38-43. https://doi.org/10.1038/s41561-023-01351-8

Kano-Nakata, M., Nakamura, T., Mitsuya, S., & Yamauchi, A. (2019). Plasticity in root system architecture of rice genotypes exhibited under different soil water distributions in soil profile. *Plant Production Science*, *22*, 501-509. https://doi.org/10.1080/1343943x.2019.1608836

Kardol, P., Cregger, M. A., Campany, C. E., & Classen, A. T. (2010). Soil ecosystem functioning under climate change: plant species and community effects. *Ecology*, *91*, 767-781. https://doi.org/10.1890/09-0135.1

Kaur, P., Lamba, J., Way, T. R., Balkcom, K. S., Sanz-Saez, A., & Watts, D. B. (2024). Characterization of soil pores in strip-tilled and conventionally-tilled soil using X-ray computed tomography. *Soil and Tillage Research*, *239*, 106035. https://doi.org/10.1016/j.still.2024.106035

Kautz, T. (2014). Research on subsoil biopores and their functions in organically managed soils: A review. *Renewable Agriculture and Food Systems*, *30*, 318-327. https://doi.org/10.1017/s1742170513000549

Kim, K., Guber, A., Rivers, M., & Kravchenko, A. (2020). Contribution of decomposing plant roots to N2O emissions by water absorption. *Geoderma*, *375*, 114506. https://doi.org/10.1016/j.geoderma.2020.114506

Kim, K., Juyal, A., & Kravchenko, A. (2024). Soil pore characteristics and the fate of new switchgrass-derived carbon in switchgrass and prairie bioenergy cropping systems. *Scientific Reports*, *14*, 7824. https://doi.org/10.1038/s41598-024-58444-6

Kitazume, H., Dayi, M., Tanaka, R., & Kikuchi, T. (2018). Assessment of the behaviour and survival of nematodes under low oxygen concentrations. *PLoS One*, *13*, e0197122. https://doi.org/10.1371/journal.pone.0197122

Kodešová, R., Jirků, V., Kodeš, V., Mühlhanselová, M., Nikodem, A., & Žigová, A. (2011). Soil structure and soil hydraulic properties of Haplic Luvisol used as arable land and grassland. *Soil and Tillage Research*, *111*, 154-161. https://doi.org/10.1016/j.still.2010.09.007

Kopke, U., Athmann, M., Han, E., & Kautz, T. (2015). Optimising Cropping Techniques for Nutrient and Environmental Management in Organic Agriculture. *Sustainable Agriculture Research*, *4*, 230376. https://doi.org/10.5539/sar.v4n3p15

Korell, L., Andrzejak, M., Berger, S., Durka, W., Haider, S., Hensen, I., Herion, Y., Hofner, J., Kindermann, L., Klotz, S., Knight, T. M., Linstadter, A., Madaj, A. M., Merbach, I., Michalski, S., Plos, C., Roscher, C., Schadler, M., Welk, E., & Auge, H. (2024). Land use modulates resistance of grasslands against future climate and inter-annual climate variability in a large field experiment. *Global Change Biology*, *30*, e17418. https://doi.org/10.1111/gcb.17418

Kravchenko, A. N., & Guber, A. K. (2017). Soil pores and their contributions to soil carbon processes. *Geoderma*, *287*, 31-39. https://doi.org/10.1016/j.geoderma.2016.06.027

Kravchenko, A. N., Guber, A. K., Razavi, B. S., Koestel, J., Quigley, M. Y., Robertson, G. P., & Kuzyakov, Y. (2019). Microbial spatial footprint as a driver of soil carbon stabilization. *Nature Communications*, *10*, 3121. https://doi.org/10.1038/s41467-019-11057-4

Kravchenko, A. N., Negassa, W. C., Guber, A. K., & Rivers, M. L. (2015). Protection of soil carbon within macro-aggregates depends on intra-aggregate pore characteristics. *Scientific Reports*, *5*, 16261. https://doi.org/10.1038/srep16261

Kühn, N., Spiegel, M. P., Tovar, C., Willis, K. J., & Macias-Fauria, M. (2022). Seeing roots from space: aboveground fingerprints of root depth in vegetation sensitivity to climate in dry biomes. *Environmental Research Letters*, *17*, 114062. https://doi.org/10.1088/1748-9326/ac9d4f

Kuka, K., Illerhaus, B., Fox, C. A., & Joschko, M. (2013). X-ray Computed Microtomography for the Study of the Soil–Root Relationship in Grassland Soils. *Vadose Zone Journal*, *12*, 1-10. https://doi.org/10.2136/vzj2013.01.0014

Kuka, K., & Joschko, M. (2024). Grassland management intensity determines root development, soil structure, and their interrelationship: Results of a regional study of Leptosols in the Swabian Alps. *Grassland Research*, *3*, 171-186. https://doi.org/10.1002/glr2.12077

Künzi, Y., Zeiter, M., Fischer, M., & Stampfli, A. (2025). Rooting depth and specific leaf area modify the impact of experimental drought duration on temperate grassland species. *Journal of Ecology*, *113*,

445-458. https://doi.org/10.1111/1365-2745.14468
Kutílek, M. (2004). Soil hydraulic properties as related to soil structure. *Soil and Tillage Research*, *79*, 175-184. https://doi.org/10.1016/j.still.2004.07.006
Kuzyakov, Y. (2006). Sources of CO2 efflux from soil and review of partitioning methods. *Soil Biology and Biochemistry*, *38*, 425-448. https://doi.org/10.1016/j.soilbio.2005.08.020
Kuzyakov, Y. (2010). Priming effects: Interactions between living and dead organic matter. *Soil Biology and Biochemistry*, *42*, 1363-1371. https://doi.org/10.1016/j.soilbio.2010.04.003
Lal, R. (2004). Soil carbon sequestration impacts on global climate change and food security. *Science*, *304*, 1623-1627. https://doi.org/10.1126/science.1097396
Landi, S., Papini, R., d'Errico, G., Brandi, G., Rocchini, A., Roversi, P. F., Bazzoffi, P., & Mocali, S. (2018). Effect of different set-aside management systems on soil nematode community and soil fertility in North, Central and South Italy. *Agriculture, Ecosystems & Environment*, *261*, 251-260. https://doi.org/10.1016/j.agee.2018.01.003
Lavallee, J. M., Soong, J. L., & Cotrufo, M. F. (2020). Conceptualizing soil organic matter into particulate and mineral-associated forms to address global change in the 21st century. *Global Change Biology*, *26*, 261-273. https://doi.org/10.1111/gcb.14859
Le Provost, G., Thiele, J., Westphal, C., Penone, C., Allan, E., Neyret, M., van der Plas, F., Ayasse, M., Bardgett, R. D., Birkhofer, K., Boch, S., Bonkowski, M., Buscot, F., Feldhaar, H., Gaulton, R., Goldmann, K., Gossner, M. M., Klaus, V. H., Kleinebecker, T., . . . Manning, P. (2021). Contrasting responses of above- and belowground diversity to multiple components of land-use intensity. *Nature Communications*, *12*, 3918. https://doi.org/10.1038/s41467-021-23931-1
Leakey, A. D. B., Ferguson, J. N., Pignon, C. P., Wu, A., Jin, Z., Hammer, G. L., & Lobell, D. B. (2019). Water Use Efficiency as a Constraint and Target for Improving the Resilience and Productivity of C(3) and C(4) Crops. *Annual Review of Plant Biology*, *70*, 781-808. https://doi.org/10.1146/annurev-arplant-042817-040305
Lefcheck, J., Byrnes, J., & Grace, J. (2015). Package "piecewiseSEM". *R package version* (2.3.0.1). https://doi.org/10.32614/CRAN.package.piecewiseSEM
Legland, D., Arganda-Carreras, I., & Andrey, P. (2016). MorphoLibJ: integrated library and plugins for mathematical morphology with ImageJ. *Bioinformatics*, *32*, 3532-3534. https://doi.org/10.1093/bioinformatics/btw413
Lehmann, J., & Kleber, M. (2015). The contentious nature of soil organic matter. *Nature*, *528*, 60-68. https://doi.org/10.1038/nature16069
Lei, J., Guo, X., Zeng, Y., Zhou, J., Gao, Q., & Yang, Y. (2021). Temporal changes in global soil respiration since 1987. *Nature Communications*, *12*, 403. https://doi.org/10.1038/s41467-020-20616-z
Lenth, R., Henrik, S., Jonathon, L., Paul, B., & Maxime, H. (2018). Emmeans: Estimated marginal means. *AKA least-squares means*, *1*.
Lenz, R., & Eisenbeis, G. (2000). Short-term effects of different tillage in a sustainable farming system on nematode community structure. *Biology and Fertility of Soils*, *31*, 237-244. https://doi.org/10.1007/s003740050651
Leuther, F., Fischer, D., Nunan, N., Meurer, K. H. E., & Herrmann, A. M. (2025). Soil structural indicators as predictors of biological activity under various soil management practices. *Geoderma*, *457*, 117290. https://doi.org/10.1016/j.geoderma.2025.117290
Leuther, F., Mikutta, R., Wolff, M., Kaiser, K., & Schlüter, S. (2023). Structure turnover times of grassland soils under different moisture regimes. *Geoderma*, *433*, 116464. https://doi.org/10.1016/j.geoderma.2023.116464
Lhotka, O., Kyselý, J., & Farda, A. (2017). Climate change scenarios of heat waves in Central Europe and their uncertainties. *Theoretical and Applied Climatology*, *131*, 1043-1054. https://doi.org/10.1007/s00704-016-2031-3
Li, B., Zhang, X., Morita, S., Sekiya, N., Araki, H., Gu, H., Han, J., Lu, Y., & Liu, X. (2022a). Are crop deep roots always beneficial for combating drought: A review of root structure and function, regulation and phenotyping. *Agricultural Water Management*, *271*, 107781.

https://doi.org/10.1016/j.agwat.2022.107781
Li, D., Wu, S., Liu, L., Zhang, Y., & Li, S. (2018). Vulnerability of the global terrestrial ecosystems to climate change. *Global Change Biology*, *24*, 4095-4106. https://doi.org/10.1111/gcb.14327
Li, G., Wilschut, R. A., Luo, S., Chen, H., Wang, X., Du, G., & Geisen, S. (2023c). Nematode biomass changes along an elevational gradient are trophic group dependent but independent of body size. *Global Change Biology*, *29*, 4898-4909. https://doi.org/10.1111/gcb.16814
Li, H., Van den Bulcke, J., Mendoza, O., Deroo, H., Haesaert, G., Dewitte, K., De Neve, S., & Sleutel, S. (2022b). Soil texture controls added organic matter mineralization by regulating soil moisture—evidence from a field experiment in a maritime climate. *Geoderma*, *410*, 115690. https://doi.org/10.1016/j.geoderma.2021.115690
Li, J., Bevacqua, E., Wang, Z., Sitch, S., Arora, V., Arneth, A., Jain, A. K., Goll, D., Tian, H., & Zscheischler, J. (2023b). Hydroclimatic extremes contribute to asymmetric trends in ecosystem productivity loss. *Communications Earth & Environment*, *4*, 197. https://doi.org/10.1038/s43247-023-00869-4
Li, X., Zhu, H., Geisen, S., Bellard, C., Hu, F., Li, H., Chen, X., & Liu, M. (2020). Agriculture erases climate constraints on soil nematode communities across large spatial scales. *Global Change Biology*, *26*, 919-930. https://doi.org/10.1111/gcb.14821
Li, Y., Fan, J., Hu, Z., Shao, Q., Zhang, L., & Yu, H. (2015). Influence of Land Use Patterns on Evapotranspiration and Its Components in a Temperate Grassland Ecosystem. *Advances in Meteorology*, *2015*, 452603. https://doi.org/10.1155/2015/452603
Li, Y., Li, K., Zhou, Q., Zhao, Y., Cai, L., & Yang, Z. (2024c). Spatiotemporal dynamics and similarity in soil moisture in shallow soils on karst slopes. *Journal of Hydrology*, *639*, 131655. https://doi.org/10.1016/j.jhydrol.2024.131655
Li, Y., Li, Y., Zhang, Q., Xu, G., Liang, G., Kim, D.-G., Carmona, C. R., Yang, M., Xue, J., Xiang, Y., Yao, B., & Shen, Y. (2024b). Enhancing soil carbon and nitrogen through grassland conversion from degraded croplands in China: Assessing magnitudes and identifying key drivers of phosphorus reduction. *Soil and Tillage Research*, *236*, 105943. https://doi.org/10.1016/j.still.2023.105943
Li, Z., Kravchenko, A. N., Cupples, A., Guber, A. K., Kuzyakov, Y., Philip Robertson, G., & Blagodatskaya, E. (2024a). Composition and metabolism of microbial communities in soil pores. *Nature Communications*, *15*, 3578. https://doi.org/10.1038/s41467-024-47755-x
Lian, X., Zhao, W., & Gentine, P. (2022). Recent global decline in rainfall interception loss due to altered rainfall regimes. *Nature Communications*, *13*, 7642. https://doi.org/10.1038/s41467-022-35414-y
Liang, G., Stefanski, A., Eddy, W. C., Bermudez, R., Montgomery, R. A., Hobbie, S. E., Rich, R. L., & Reich, P. B. (2024). Soil respiration response to decade-long warming modulated by soil moisture in a boreal forest. *Nature Geoscience, 17*, 905-911. https://doi.org/10.1038/s41561-024-01512-3
Liaw, A., & Wiener, M. (2002). Classification and Regression by randomForest. *R News*, *2*, 18-22.
Lin, M., Sadeghi, S. M. M., & Van Stan, J. T. (2020). Partitioning of Rainfall and Sprinkler-Irrigation by Crop Canopies: A Global Review and Evaluation of Available Research. *Hydrology*, *7*, 76. https://doi.org/10.3390/hydrology7040076
Linsler, D., Geisseler, D., Loges, R., Taube, F., & Ludwig, B. (2013). Temporal dynamics of soil organic matter composition and aggregate distribution in permanent grassland after a single tillage event in a temperate climate. *Soil and Tillage Research*, *126*, 90-99. https://doi.org/10.1016/j.still.2012.07.017
Liu, L., Qin, S., Richard Whalley, W., Zhou, H., Ren, T., & Gao, W. (2024). The pore-rhizosheath shapes maize root architecture by enhancing root distribution in macropores. *Plant Cell & Environment*, *47*, 2911-2922. https://doi.org/10.1111/pce.14915
Liu, S., Huang, X. J., Gan, L., Zhang, Z. B., Dong, Y., & Peng, X. H. (2024a). Drying-wetting cycles affect soil structure by impacting soil aggregate transformations and soil organic carbon fractions. *Catena*, *243*, 108188. https://doi.org/10.1016/j.catena.2024.108188
Liu, W., Zhang, Z. H. E., & Wan, S. (2009). Predominant role of water in regulating soil and microbial respiration and their responses to climate change in a semiarid grassland. *Global Change Biology*, *15*, 184-195. https://doi.org/10.1111/j.1365-2486.2008.01728.x

Liu, X.-t., Liang, S.-w., Tian, Y.-j., Wang, X., Liang, W.-j., & Zhang, X.-k. (2023). Effect of land use on soil nematode community composition and co-occurrence network relationship. *Journal of Integrative Agriculture*, *23*, 2807-2819. https://doi.org/10.1016/j.jia.2023.11.019

Liu, Y., He, N., Zhu, J., Xu, L., Yu, G., Niu, S., Sun, X., & Wen, X. (2017). Regional variation in the temperature sensitivity of soil organic matter decomposition in China's forests and grasslands. *Global Change Biology*, *23*, 3393-3402. https://doi.org/10.1111/gcb.13613

Liu, Y., Zhang, Y., Peñuelas, J., Kannenberg, S. A., Gong, H., Yuan, W., Wu, C., Zhou, S., & Piao, S. (2025a). Drought legacies delay spring green-up in northern ecosystems. *Nature Climate Change*, *15*, 444-451. https://doi.org/10.1038/s41558-025-02273-6

Long, X., Zhao, J., Li, J., Liao, X., Wang, J., Fu, Z., Zhang, W., Liu, X., & Wang, K. (2024). Disturbance intensity shapes the soil micro-food web compositions and energy fluxes during seven-year land use changes. *Soil Biology and Biochemistry*, *194*, 109424. https://doi.org/10.1016/j.soilbio.2024.109424

Lozano, Y. M., Aguilar-Trigueros, C. A., Ospina, J. M., & Rillig, M. C. (2022). Drought legacy effects on root morphological traits and plant biomass via soil biota feedback. *New Phytologist*, *236*, 222-234. https://doi.org/10.1111/nph.18327

Lu, L., Li, G., He, N., Li, H., Liu, T., Li, X., Whalen, J. K., Geisen, S., & Liu, M. (2023). Drought shifts soil nematodes to smaller size across biological scales. *Soil Biology and Biochemistry*, *184*, 109099. https://doi.org/10.1016/j.soilbio.2023.109099

Lucas, M. (2021). Perspectives from the Fritz-Scheffer Awardee 2020—The mutual interactions between roots and soil structure and how these affect rhizosphere processes#. *Journal of Plant Nutrition and Soil Science*, *185*, 8-18. https://doi.org/10.1002/jpln.202100385

Lucas, M., Nguyen, L. T. T., Guber, A., & Kravchenko, A. N. (2022). Cover crop influence on pore size distribution and biopore dynamics: Enumerating root and soil faunal effects. *Frontiers in Plant Science*, *13*, 928569. https://doi.org/10.3389/fpls.2022.928569

Lucas, M., Rohe, L., Apelt, B., Stange, C. F., Vogel, H. J., Well, R., & Schluter, S. (2024). The distribution of particulate organic matter in the heterogeneous soil matrix - Balancing between aerobic respiration and denitrification. *Science of the Total Environment*, *951*, 175383. https://doi.org/10.1016/j.scitotenv.2024.175383

Lucas, M., Santiago, J. P., Chen, J., Guber, A., & Kravchenko, A. (2023). The soil pore structure encountered by roots affects plant-derived carbon inputs and fate. *New Phytologist*, *240*, 515-528. https://doi.org/10.1111/nph.19159

Lucas, M., Schlüter, S., Vogel, H.-J., & Vetterlein, D. (2019). Soil structure formation along an agricultural chronosequence. *Geoderma*, *350*, 61-72. https://doi.org/10.1016/j.geoderma.2019.04.041

Lucas, M., Vetterlein, D., Vogel, H. J., & Schlüter, S. (2020). Revealing pore connectivity across scales and resolutions with X-ray CT. *European Journal of Soil Science*, *72*, 546-560. https://doi.org/10.1111/ejss.12961

Luo, Y., Wang, X., Cui, M., Wang, J., & Gao, Y. (2021). Mowing increases fine root production and root turnover in an artificially restored Songnen grassland. *Plant and Soil*, *465*, 549-561. https://doi.org/10.1007/s11104-021-05017-5

Lutz, S., Bodenhausen, N., Hess, J., Valzano-Held, A., Waelchli, J., Deslandes-Herold, G., Schlaeppi, K., & van der Heijden, M. G. A. (2023). Soil microbiome indicators can predict crop growth response to large-scale inoculation with arbuscular mycorrhizal fungi. *Nature Microbiology*, *8*, 2277-2289. https://doi.org/10.1038/s41564-023-01520-w

Lynch, J. P. (2013). Steep, cheap and deep: an ideotype to optimize water and N acquisition by maize root systems. *Annals of Botany*, *112*, 347-357. https://doi.org/10.1093/aob/mcs293

Lynch, J. P. (2018). Rightsizing root phenotypes for drought resistance. *Journal of Experimental Botany*, *69*, 3279-3292. https://doi.org/10.1093/jxb/ery048

Lynch, J. P. (2019). Root phenotypes for improved nutrient capture: an underexploited opportunity for global agriculture. *New Phytologist*, *223*, 548-564. https://doi.org/10.1111/nph.15738

Lyu, M., Homyak, P. M., Xie, J. S., Penuelas, J., Ryan, M. G., Xiong, X. L., Sardans, J., Lin, W. S., Wang,

M. H., Chen, G. S., & Yang, Y. S. (2023). Litter quality controls tradeoffs in soil carbon decomposition and replenishment in a subtropical forest. *Journal of Ecology*, *111*, 2181-2193. https://doi.org/10.1111/1365-2745.14167

Madsen, H., Lawrence, D., Lang, M., Martinkova, M., & Kjeldsen, T. R. (2014). Review of trend analysis and climate change projections of extreme precipitation and floods in Europe. *Journal of Hydrology*, *519*, 3634-3650. https://doi.org/10.1016/j.jhydrol.2014.11.003

Maestre, F. T., Eldridge, D. J., Soliveres, S., Kefi, S., Delgado-Baquerizo, M., Bowker, M. A., Garcia-Palacios, P., Gaitan, J., Gallardo, A., Lazaro, R., & Berdugo, M. (2016). Structure and functioning of dryland ecosystems in a changing world. *Annual review of ecology, evolution, and systematics*, *47*, 215-237. https://doi.org/10.1146/annurev-ecolsys-121415-032311

Malik, A. A., Puissant, J., Buckeridge, K. M., Goodall, T., Jehmlich, N., Chowdhury, S., Gweon, H. S., Peyton, J. M., Mason, K. E., van Agtmaal, M., Blaud, A., Clark, I. M., Whitaker, J., Pywell, R. F., Ostle, N., Gleixner, G., & Griffiths, R. I. (2018). Land use driven change in soil pH affects microbial carbon cycling processes. *Nature Communications*, *9*, 3591. https://doi.org/10.1038/s41467-018-05980-1

Martin, T., & Sprunger, C. D. (2023). Nematodes require space: The relationship between nematode community assemblage and soil carbon across varying aggregate fractions. *Geoderma*, *436*, 116536. https://doi.org/10.1016/j.geoderma.2023.116536

Matter, J. M., Stute, M., Snaebjornsdottir, S. O., Oelkers, E. H., Gislason, S. R., Aradottir, E. S., Sigfusson, B., Gunnarsson, I., Sigurdardottir, H., Gunnlaugsson, E., Axelsson, G., Alfredsson, H. A., Wolff-Boenisch, D., Mesfin, K., Fernandez de la Reguera Taya, D., Hall, J., Dideriksen, K., & Broecker, W. S. (2016). Rapid carbon mineralization for permanent disposal of anthropogenic carbon dioxide emissions. *Science*, *352*, 1312-1314. https://doi.org/10.1126/science.aad8132

Maurel, C., & Nacry, P. (2020). Root architecture and hydraulics converge for acclimation to changing water availability. *Nature Plants*, *6*, 744-749. https://doi.org/10.1038/s41477-020-0684-5

McFarlane, K. J., Cusack, D. F., Dietterich, L. H., Hedgpeth, A. L., Finstad, K. M., & Nottingham, A. T. (2024). Experimental warming and drying increase older carbon contributions to soil respiration in lowland tropical forests. *Nature Communications*, *15*, 7084. https://doi.org/10.1038/s41467-024-51422-6

McKee, K. L. (2002). Root proliferation in decaying roots and old root channels: a nutrient conservation mechanism in oligotrophic mangrove forests? *Journal of Ecology*, *89*, 876-887. https://doi.org/10.1046/j.0022-0477.2001.00606.x

Meurer, K., Barron, J., Chenu, C., Coucheney, E., Fielding, M., Hallett, P., Herrmann, A. M., Keller, T., Koestel, J., Larsbo, M., Lewan, E., Or, D., Parsons, D., Parvin, N., Taylor, A., Vereecken, H., & Jarvis, N. (2020). A framework for modelling soil structure dynamics induced by biological activity. *Global Change Biology*, *26*, 5382-5403. https://doi.org/10.1111/gcb.15289

Minnich, M. (1993). *Behavior and Determination of Volatile Organic Compunds in Soil: A Literature Review*.

Mordhorst, A., Peth, S., & Horn, R. (2014). Influence of mechanical loading on static and dynamic CO_2 efflux on differently textured and managed Luvisols. *Geoderma*, *219*, 1-13. https://doi.org/10.1016/j.geoderma.2013.12.020

Mueller, C. W., Baumert, V., Carminati, A., Germon, A., Holz, M., Kögel-Knabner, I., Peth, S., Schlüter, S., Uteau, D., Vetterlein, D., Teixeira, P., & Vidal, A. (2024). From rhizosphere to detritusphere – Soil structure formation driven by plant roots and the interactions with soil biota. *Soil Biology and Biochemistry*, *193*, 109396. https://doi.org/10.1016/j.soilbio.2024.109396

Mueller, K. E., Blumenthal, D. M., Carrillo, Y., Cesarz, S., Ciobanu, M., Hines, J., Pabst, S., Pendall, E., de Tomasel, C. M., Wall, D. H., & Eisenhauer, N. (2016). Elevated CO_2 and warming shift the functional composition of soil nematode communities in a semiarid grassland. *Soil Biology and Biochemistry*, *103*, 46-51. https://doi.org/10.1016/j.soilbio.2016.08.005

Mulder, C., Boit, A., Bonkowski, M., De Ruiter, P. C., Mancinelli, G., Van der Heijden, M. G. A., Van Wijnen, H. J., Vonk, J. A., & Rutgers, M. (2011). A Belowground Perspective on Dutch

Agroecosystems: How Soil Organisms Interact to Support Ecosystem Services. In *Advances in ecological research* (Vol. 44, pp. 277-357). https://doi.org/10.1016/b978-0-12-374794-5.00005-5

Mulder, C., & Vonk, J. A. (2011). Nematode traits and environmental constraints in 200 soil systems: scaling within the 60–6000 μm body size range. *Ecology*, *92*, 2004-2004. https://doi.org/10.1890/11-0546.1

Muller, L. M., & Bahn, M. (2022). Drought legacies and ecosystem responses to subsequent drought. *Global Change Biology*, *28*, 5086-5103. https://doi.org/10.1111/gcb.16270

Murphy, J., & Riley, J., P. (1962). A modified single solution method for the determination of phosphate in natural waters. *Analytica Chimica Acta*, *27*, 31-36. https://doi.org/10.1016/S0003-2670(00)88444-5

Nannipieri, P., Hannula, S. E., Pietramellara, G., Schloter, M., Sizmur, T., & Pathan, S. I. (2023). Legacy effects of rhizodeposits on soil microbiomes: A perspective. *Soil Biology and Biochemistry*, *184*, 109107. https://doi.org/10.1016/j.soilbio.2023.109107

Negassa, W. C., Guber, A. K., Kravchenko, A. N., Marsh, T. L., Hildebrandt, B., & Rivers, M. L. (2015). Properties of soil pore space regulate pathways of plant residue decomposition and community structure of associated bacteria. *PLoS One*, *10*, e0123999. https://doi.org/10.1371/journal.pone.0123999

Neher, D. A. (2010). Ecology of plant and free-living nematodes in natural and agricultural soil. *Annual review of phytopathology*, *48*, 371-394. https://doi.org/10.1146/annurev-phyto-073009-114439

Neher, D. A., Weicht, T. R., Savin, M., Görres, J. H., & Amador, J. A. (1999). Grazing in a porous environment.: 2.: Nematode community structure. *Plant and Soil*, *212*, 85-99. https://doi.org/10.1023/A:1004665120360

Neina, D. (2019). The Role of Soil pH in Plant Nutrition and Soil Remediation. *Applied and Environmental Soil Science*, *2019*, 1-9. https://doi.org/10.1155/2019/5794869

Nemecek, T., Huguenin-Elie, O., Dubois, D., Gaillard, G., Schaller, B., & Chervet, A. (2011). Life cycle assessment of Swiss farming systems: II. Extensive and intensive production. *Agricultural Systems*, *104*, 233-245. https://doi.org/10.1016/j.agsy.2010.07.007

Newcomb, C. J., Qafoku, N. P., Grate, J. W., Bailey, V. L., & De Yoreo, J. J. (2017). Developing a molecular picture of soil organic matter-mineral interactions by quantifying organo-mineral binding. *Nature Communications*, *8*, 396. https://doi.org/10.1038/s41467-017-00407-9

Nguyen, T. T., Grote, U., Neubacher, F., Rahut, D. B., Do, M. H., & Paudel, G. P. (2023). Security risks from climate change and environmental degradation: implications for sustainable land use transformation in the Global South. *Current Opinion in Environmental Sustainability*, *63*, 101322. https://doi.org/10.1016/j.cosust.2023.101322

Nunan, N., Leloup, J., Ruamps, L. S., Pouteau, V., & Chenu, C. (2017). Effects of habitat constraints on soil microbial community function. *Scientific Reports*, *7*, 4280. https://doi.org/10.1038/s41598-017-04485-z

Or, D., Keller, T., & Schlesinger, W. H. (2021). Natural and managed soil structure: On the fragile scaffolding for soil functioning. *Soil and Tillage Research*, *208*, 104912. https://doi.org/10.1016/j.still.2020.104912

Otobe, K., Itou, K., & Mizukubo, T. (2004). Micro-moulded substrates for the analysis of structure-dependent behaviour of nematodes. *Nematology*, *6*, 73-77. https://doi.org/10.1163/156854104323072946

Pajor, R., Falconer, R., Hapca, S., & Otten, W. (2010). Modelling and quantifying the effect of heterogeneity in soil physical conditions on fungal growth. *Biogeosciences*, *7*, 3731-3740. https://doi.org/10.5194/bg-7-3731-2010

Palta, J. A., & Turner, N. C. (2018). Crop root system traits cannot be seen as a silver bullet delivering drought resistance. *Plant and Soil*, *439*, 31-43. https://doi.org/10.1007/s11104-018-3864-6

Pandey, B. K., Huang, G. Q., Bhosale, R., Hartman, S., Sturrock, C. J., Jose, L., Martin, O. C., Karady, M., Voesenek, L. A. C. J., Ljung, K., Lynch, J. P., Brown, K. M., Whalley, W. R., Mooney, S. J., Zhang, D. B., & Bennett, M. J. (2021). Plant roots sense soil compaction through restricted ethylene

diffusion. *Science*, *371*, 276-280. https://doi.org/10.1126/science.abf3013

Papatheodorou, E. M., Argyropoulou, M. D., & Stamou, G. P. (2004). The effects of large- and small-scale differences in soil temperature and moisture on bacterial functional diversity and the community of bacterivorous nematodes. *Applied Soil Ecology*, *25*, 37-49. https://doi.org/10.1016/s0929-1393(03)00100-8

Patah, S. F. A., & Othman, N. M. I. (2024). Influence of Soil Temperature on Root Development and Microbial Diversity in Paddy Fields: A Comprehensive Review. *Trends in Ecological and Indoor Environmental Engineering*, *2*, 1-9. https://doi.org/10.62622/teiee.024.2.4.01-09

Patel, K. F., Smith, A. P., Bond-Lamberty, B., Fansler, S. J., Tfaily, M. M., Bramer, L., Varga, T., & Bailey, V. L. (2021). Spatial access and resource limitations control carbon mineralization in soils. *Soil Biology and Biochemistry*, *162*, 108427. https://doi.org/10.1016/j.soilbio.2021.108427

Paterson, E., & Sim, A. (2013). Soil-specific response functions of organic matter mineralization to the availability of labile carbon. *Global Change Biology*, *19*, 1562-1571. https://doi.org/10.1111/gcb.12140

Pecl, G. T., Araujo, M. B., Bell, J. D., Blanchard, J., Bonebrake, T. C., Chen, I. C., Clark, T. D., Colwell, R. K., Danielsen, F., Evengard, B., Falconi, L., Ferrier, S., Frusher, S., Garcia, R. A., Griffis, R. B., Hobday, A. J., Janion-Scheepers, C., Jarzyna, M. A., Jennings, S., . . . Williams, S. E. (2017). Biodiversity redistribution under climate change: Impacts on ecosystems and human well-being. *Science*, *355*, eaai9214. https://doi.org/10.1126/science.aai9214

Peng, J., Wu, X., Ni, S., Wang, J., Song, Y., & Cai, C. (2022). Investigating intra-aggregate microstructure characteristics and influencing factors of six soil types along a climatic gradient. *Catena*, *210*, 105867. https://doi.org/10.1016/j.catena.2021.105867

Peng, J., Yang, Q., Zhang, C., Ni, S., Wang, J., & Cai, C. (2023). Aggregate pore structure, stability characteristics, and biochemical properties induced by different cultivation durations in the Mollisol region of Northeast China. *Soil and Tillage Research*, *233*, 105797. https://doi.org/10.1016/j.still.2023.105797

Peng, Z., van der Heijden, M. G. A., Liu, Y., Li, X., Pan, H., An, Y., Gao, H., Qi, J., Gao, J., Qian, X., Tiedje, J. M., Wei, G., & Jiao, S. (2025). Agricultural subsoil microbiomes and functions exhibit lower resistance to global change than topsoils in Chinese agroecosystems. *Nature Food*, *6*, 375-388. https://doi.org/10.1038/s43016-024-01106-7

Pereira, T. J., De Santiago, A., & Bik, H. M. (2024). Soil properties predict below-ground community structure, but not nematode microbiome patterns in semi-arid habitats. *Molecular Ecology*, *33*, e17501. https://doi.org/10.1111/mec.17501

Peterson, G. A., & Westfall, D. G. (2005). Managing precipitation use in sustainable dryland agroecosystems. *Annals of Applied Biology*, *144*, 127-138. https://doi.org/10.1111/j.1744-7348.2004.tb00326.x

Peth, S., Horn, R., Beckmann, F., Donath, T., Fischer, J., & Smucker, A. J. M. (2008). Three-Dimensional Quantification of Intra-Aggregate Pore-Space Features using Synchrotron-Radiation-Based Microtomography. *Soil Science Society of America Journal*, *72*, 897-907. https://doi.org/10.2136/sssaj2007.0130

Phalempin, M., Jentzsch, N., Köhne, J. M., Schreiter, S., Gründling, R., Vetterlein, D., & Schlüter, S. (2025b). Soil structure development in a five-year chronosequence of maize cropping on two contrasting soil textures. *Soil and Tillage Research*, *251*, 106561. https://doi.org/10.1016/j.still.2025.106561

Phalempin, M., Krämer, L., Geers-Lucas, M., Isensee, F., & Schlüter, S. (2025). Deep learning segmentation of soil constituents in 3D X-ray CT images. *Geoderma*, *458*, 117321. https://doi.org/10.1016/j.geoderma.2025.117321

Phalempin, M., Lippold, E., Vetterlein, D., & Schluter, S. (2021). An improved method for the segmentation of roots from X-ray computed tomography 3D images: Rootine v.2. *Plant Methods*, *17*, 39. https://doi.org/10.1186/s13007-021-00735-4

Philippot, L., Chenu, C., Kappler, A., Rillig, M. C., & Fierer, N. (2024). The interplay between microbial

communities and soil properties. *Nature Review Microbiology*, *22*, 226-239. https://doi.org/10.1038/s41579-023-00980-5

Pierret, A., Maeght, J. L., Clement, C., Montoroi, J. P., Hartmann, C., & Gonkhamdee, S. (2016). Understanding deep roots and their functions in ecosystems: an advocacy for more unconventional research. *Annals of Botany*, *118*, 621-635. https://doi.org/10.1093/aob/mcw130

Pires, L. F., Auler, A. C., Roque, W. L., & Mooney, S. J. (2020). X-ray microtomography analysis of soil pore structure dynamics under wetting and drying cycles. *Geoderma*, *362*, 114103. https://doi.org/10.1016/j.geoderma.2019.114103

Pires, L. F., Borges, J. A. R., Rosa, J. A., Cooper, M., Heck, R. J., Passoni, S., & Roque, W. L. (2017). Soil structure changes induced by tillage systems. *Soil and Tillage Research*, *165*, 66-79. https://doi.org/10.1016/j.still.2016.07.010

Poeplau, C., Don, A., Vesterdal, L., Leifeld, J., Van Wesemael, B. A. S., Schumacher, J., & Gensior, A. (2011). Temporal dynamics of soil organic carbon after land-use change in the temperate zone - carbon response functions as a model approach. *Global Change Biology*, *17*, 2415-2427. https://doi.org/10.1111/j.1365-2486.2011.02408.x

Ponton, S., Flanagan, L. B., Alstad, K. P., Johnson, B. G., Morgenstern, K. A. I., Kljun, N., Black, T. A., & Barr, A. G. (2006). Comparison of ecosystem water-use efficiency among Douglas-fir forest, aspen forest and grassland using eddy covariance and carbon isotope techniques. *Global Change Biology*, *12*, 294-310. https://doi.org/10.1111/j.1365-2486.2005.01103.x

Poppe Terán, C., Naz, B. S., Graf, A., Qu, Y., Hendricks Franssen, H.-J., Baatz, R., Ciais, P., & Vereecken, H. (2023). Rising water-use efficiency in European grasslands is driven by increased primary production. *Communications Earth & Environment*, *4*, 95. https://doi.org/10.1038/s43247-023-00757-x

Porazinska, D. L., Duncan, L. W., McSorley, R., & Graham, J. H. (1999). Nematode communities as indicators of status and processes of a soil ecosystem influenced by agricultural management practices. *Applied Soil Ecology*, *13*(1), 69-86. https://doi.org/10.1016/S0929-1393(99)00018-9

Postma, J. A., Kuppe, C., Owen, M. R., Mellor, N., Griffiths, M., Bennett, M. J., Lynch, J. P., & Watt, M. (2017). OpenSimRoot: widening the scope and application of root architectural models. *New Phytologist*, *215*, 1274-1286. https://doi.org/10.1111/nph.14641

Prechsl, U. E., Burri, S., Gilgen, A. K., Kahmen, A., & Buchmann, N. (2015). No shift to a deeper water uptake depth in response to summer drought of two lowland and sub-alpine C(3)-grasslands in Switzerland. *Oecologia*, *177*, 97-111. https://doi.org/10.1007/s00442-014-3092-6

Pugh, T. A., Muller, C., Elliott, J., Deryng, D., Folberth, C., Olin, S., Schmid, E., & Arneth, A. (2016). Climate analogues suggest limited potential for intensification of production on current croplands under climate change. *Nature Communications*, *7*, 12608. https://doi.org/10.1038/ncomms12608

Qi, J., Markewitz, D., & Radcliffe, D. (2018). Modelling the effect of changing precipitation inputs on deep soil water utilization. *Hydrological Processes*, *32*, 672-686. https://doi.org/10.1002/hyp.11452

Qi, Q., Ning, S., Guo, X., Zhao, J., Tian, R., Gui, H., He, J. S., Wang, H., Zhang, Z., Konstantinidis, K. T., Gao, Q., Wang, Y., Li, S., Zhao, W., Yang, Y., & Zhou, J. (2024). More sensitive microbial responses to the interactive effects of warming and altered precipitation in subsoil than topsoil of an alpine grassland ecosystem. *Global Change Biology*, *30*, e17487. https://doi.org/10.1111/gcb.17487

Quigley, M. Y., & Kravchenko, A. N. (2022). Inputs of root-derived carbon into soil and its losses are associated with pore-size distributions. *Geoderma*, *410*, 115667. https://doi.org/10.1016/j.geoderma.2021.115667

Quigley, M. Y., Negassa, W. C., Guber, A. K., Rivers, M. L., & Kravchenko, A. N. (2018). Influence of Pore Characteristics on the Fate and Distribution of Newly Added Carbon. *Frontiers in Environmental Science*, *6*, 51. https://doi.org/10.3389/fenvs.2018.00051

Quist, C. W., Gort, G., Mooijman, P., Brus, D. J., van den Elsen, S., Kostenko, O., Vervoort, M., Bakker, J., van der Putten, W. H., & Helder, J. (2019). Spatial distribution of soil nematodes relates to soil organic matter and life strategy. *Soil Biology and Biochemistry*, *136*, 107542. https://doi.org/10.1016/j.soilbio.2019.107542

Rabbi, S. M. F., Warren, C. R., Swarbrick, B., Minasny, B., McBratney, A. B., & Young, I. M. (2024). Microbial decomposition of organic matter and wetting–drying promotes aggregation in artificial soil but porosity increases only in wet-dry condition. *Geoderma*, *447*, 116924. https://doi.org/10.1016/j.geoderma.2024.116924

Rabot, E., Wiesmeier, M., Schlüter, S., & Vogel, H. J. (2018). Soil structure as an indicator of soil functions: A review. *Geoderma*, *314*, 122-137. https://doi.org/10.1016/j.geoderma.2017.11.009

Rahmati, M., Or, D., Amelung, W., Bauke, S. L., Bol, R., Hendricks Franssen, H.-J., Montzka, C., Vanderborght, J., & Vereecken, H. (2023). Soil is a living archive of the Earth system. *Nature Reviews Earth & Environment*, *4*, 421-423. https://doi.org/10.1038/s43017-023-00454-5

Rajan, N., Maas, S. J., & Cui, S. (2014). Extreme drought effects on summer evapotranspiration and energy balance of a grassland in the Southern Great Plains. *Ecohydrology*, *8*, 1194-1204. https://doi.org/10.1002/eco.1574

Rasmussen, C. R., Thorup-Kristensen, K., & Dresbøll, D. B. (2019). Uptake of subsoil water below 2 m fails to alleviate drought response in deep-rooted Chicory (Cichorium intybus L.). *Plant and Soil*, *446*, 275-290. https://doi.org/10.1007/s11104-019-04349-7

Ren, L. D., Yao, S. H., Sun, J. W., & Zhou, H. (2024b). Assessment of soil aggregate pore structure after 8 years of cultivation from the parent material of a Mollisol. *Catena*, *235*, 107699. https://doi.org/10.1016/j.catena.2023.107699

Ren, S., Wang, C., & Zhou, Z. (2024a). Global Distributions of Reactive Iron and Aluminum Influence the Spatial Variation of Soil Organic Carbon. *Global Change Biology*, *30*, e17576. https://doi.org/10.1111/gcb.17576

Revelle, W. (2024). Psych: Procedures for Psychological, Psychometric, and Personality Research.

Rickard, W., Hossain, I., Zhang, X., Cooper, H. V., Mooney, S. J., Hawkesford, M. J., & Whalley, W. R. (2025). Field plants strategically regulate water uptake from different soil depths by spatiotemporally adjusting their radial root hydraulic conductivity. *New Phytologist*, *247*, 546-561. https://doi.org/10.1111/nph.70013

Ritz, K., & Young, I. M. (2004). Interactions between soil structure and fungi. *Mycologist*, *18*, 52-59. https://doi.org/10.1017/S0269-915X(04)00201-0

Robinson, D. A., Hopmans, J. W., Filipovic, V., van der Ploeg, M., Lebron, I., Jones, S. B., Reinsch, S., Jarvis, N., & Tuller, M. (2019). Global environmental changes impact soil hydraulic functions through biophysical feedbacks. *Global Change Biology*, *25*, 1895-1904. https://doi.org/10.1111/gcb.14626

Rocci, K. S., Lavallee, J. M., Stewart, C. E., & Cotrufo, M. F. (2021). Soil organic carbon response to global environmental change depends on its distribution between mineral-associated and particulate organic matter: A meta-analysis. *Science of the Total Environment*, *793*, 148569. https://doi.org/10.1016/j.scitotenv.2021.148569

Rockel, B., Will, A., & Hense, A. (2008). The Regional Climate Model COSMO-CLM (CCLM). *Meteorologische Zeitschrift*, *17*, 347-348. https://doi.org/10.1127/0941-2948/2008/0309

Rodriguez-Iturbe, I., Porporato, A., Laio, F., & Ridolfi, L. (2001). Intensive or extensive use of soil moisture: Plant strategies to cope with stochastic water availability. *Geophysical Research Letters*, *28*, 4495-4497. https://doi.org/10.1029/2001gl012905

Romero-Ruiz, A., Linde, N., Keller, T., & Or, D. (2018). A Review of Geophysical Methods for Soil Structure Characterization. *Reviews of Geophysics*, *56*, 672-697. https://doi.org/10.1029/2018rg000611

Rose, L., Coners, H., & Leuschner, C. (2011). Effects of fertilization and cutting frequency on the water balance of a temperate grassland. *Ecohydrology*, *5*, 64-72. https://doi.org/10.1002/eco.201

Rosseel, Y. (2012). lavaan: An R Package for Structural Equation Modeling. *Journal of Statistical Software*, *48*, 1 - 36. https://doi.org/10.18637/jss.v048.i02

Ruamps, L. S., Nunan, N., & Chenu, C. (2011). Microbial biogeography at the soil pore scale. *Soil Biology and Biochemistry*, *43*, 280-286. https://doi.org/10.1016/j.soilbio.2010.10.010

Rui, Y., Jackson, R. D., Cotrufo, M. F., Sanford, G. R., Spiesman, B. J., Deiss, L., Culman, S. W., Liang,

C., & Ruark, M. D. (2022). Persistent soil carbon enhanced in Mollisols by well-managed grasslands but not annual grain or dairy forage cropping systems. *Proceedings of the National Academy of Sciences*, *119*, e2118931119. https://doi.org/10.1073/pnas.2118931119

Rutherford, P. M., & Juma, N. G. (1992). Influence of Texture on Habitable Pore-Space and Bacterial-Protozoan Populations in Soil. *Biology and Fertility of Soils*, *12*, 221-227. https://doi.org/10.1007/Bf00336036

Samson, M.-E., Chantigny, M. H., Vanasse, A., Menasseri-Aubry, S., Royer, I., & Angers, D. A. (2020). Management practices differently affect particulate and mineral-associated organic matter and their precursors in arable soils. *Soil Biology and Biochemistry*, *148*, 107867. https://doi.org/10.1016/j.soilbio.2020.107867

Sánchez-Moreno, S., & Ferris, H. (2007). Suppressive service of the soil food web: Effects of environmental management. *Agriculture, Ecosystems & Environment*, *119*, 75-87. https://doi.org/10.1016/j.agee.2006.06.012

Schädler, M., Buscot, F., Klotz, S., Reitz, T., Durka, W., Bumberger, J., Merbach, I., Michalski, S. G., Kirsch, K., Remmler, P., Schulz, E., & Auge, H. (2019). Investigating the consequences of climate change under different land-use regimes: a novel experimental infrastructure. *Ecosphere*, *10*, e02635. https://doi.org/10.1002/ecs2.2635

Scherzinger, F., Schadler, M., Reitz, T., Yin, R., Auge, H., Merbach, I., Roscher, C., Harpole, W. S., Blagodatskaya, E., Siebert, J., Ciobanu, M., Marder, F., Eisenhauer, N., & Quaas, M. (2024). Sustainable land management enhances ecological and economic multifunctionality under ambient and future climate. *Nature Communications*, *15*, 4930. https://doi.org/10.1038/s41467-024-48830-z

Schimel, D. S., & Carroll, D. (2024). Carbon Cycle–Climate Feedbacks in the Post-Paris World. *Annual Review of Earth and Planetary Sciences*, *52*, 467-493. https://doi.org/10.1146/annurev-earth-031621-081700

Schimel, J. P. (2018). Life in Dry Soils: Effects of Drought on Soil Microbial Communities and Processes. *Annual Review of Ecology, Evolution, and Systematics*, *49*, 409-432. https://doi.org/10.1146/annurev-ecolsys-110617-062614

Schindelin, J., Rueden, C. T., Hiner, M. C., & Eliceiri, K. W. (2015). The ImageJ ecosystem: An open platform for biomedical image analysis. *Molecular reproduction and development*, *82*, 518-529. https://doi.org/10.1002/mrd.22489

Schlaepfer, D. R., Bradford, J. B., Lauenroth, W. K., Munson, S. M., Tietjen, B., Hall, S. A., Wilson, S. D., Duniway, M. C., Jia, G., Pyke, D. A., Lkhagva, A., & Jamiyansharav, K. (2017). Climate change reduces extent of temperate drylands and intensifies drought in deep soils. *Nature Communications*, *8*, 14196. https://doi.org/10.1038/ncomms14196

Schlüter, S., Eickhorst, T., & Mueller, C. W. (2019). Correlative Imaging Reveals Holistic View of Soil Microenvironments. *Environmental science & technology*, *53*, 829-837. https://doi.org/10.1021/acs.est.8b05245

Schlüter, S., Gil, E., Doniger, T., Applebaum, I., & Steinberger, Y. (2022a). Abundance and community composition of free-living nematodes as a function of soil structure under different vineyard managements. *Applied Soil Ecology*, *170*, 104291. https://doi.org/10.1016/j.apsoil.2021.104291

Schlüter, S., Leuther, F., Albrecht, L., Hoeschen, C., Kilian, R., Surey, R., Mikutta, R., Kaiser, K., Mueller, C. W., & Vogel, H. J. (2022). Microscale carbon distribution around pores and particulate organic matter varies with soil moisture regime. *Nature Communications*, *13*, 2098. https://doi.org/10.1038/s41467-022-29605-w

Schlüter, S., Roussety, T., Rohe, L., Guliyev, V., Blagodatskaya, E., & Reitz, T. (2022b). Land use impact on carbon mineralization in well aerated soils is mainly explained by variations of particulate organic matter rather than of soil structure. *Soil*, *8*, 253-267. https://doi.org/10.5194/soil-8-253-2022

Schlüter, S., Sammartino, S., & Koestel, J. (2020a). Exploring the relationship between soil structure and soil functions via pore-scale imaging. *Geoderma*, *370*, 114370.

https://doi.org/10.1016/j.geoderma.2020.114370

Schlüter, S., Vogel, H.-J., Ippisch, O., Bastian, P., Roth, K., Schelle, H., Durner, W., Kasteel, R., & Vanderborght, J. (2012). Virtual Soils: Assessment of the Effects of Soil Structure on the Hydraulic Behavior of Cultivated Soils. *Vadose Zone Journal*, *11*, vzj2011-0174. https://doi.org/10.2136/vzj2011.0174

Schlüter, S., Vogel, H.-J., Ippisch, O., & Vanderborght, J. (2013). Combined Impact of Soil Heterogeneity and Vegetation Type on the Annual Water Balance at the Field Scale. *Vadose Zone Journal*, *12*, vzj2013-03, 1-17. https://doi.org/10.2136/vzj2013.03.0053

Schmidt, J. E., & Gaudin, A. C. M. (2017). Toward an Integrated Root Ideotype for Irrigated Systems. *Trends in Plant Science*, *22*, 433-443. https://doi.org/10.1016/j.tplants.2017.02.001

Schmidt, M. W., Torn, M. S., Abiven, S., Dittmar, T., Guggenberger, G., Janssens, I. A., Kleber, M., Kogel-Knabner, I., Lehmann, J., Manning, D. A., Nannipieri, P., Rasse, D. P., Weiner, S., & Trumbore, S. E. (2011). Persistence of soil organic matter as an ecosystem property. *Nature*, *478*, 49-56. https://doi.org/10.1038/nature10386

Schnabel, F., Purrucker, S., Schmitt, L., Engelmann, R. A., Kahl, A., Richter, R., Seele-Dilbat, C., Skiadaresis, G., & Wirth, C. (2022). Cumulative growth and stress responses to the 2018-2019 drought in a European floodplain forest. *Global Change Biology*, *28*, 1870-1883. https://doi.org/10.1111/gcb.16028

Segal, E., Kushnir, T., Mualem, Y., & Shani, U. (2008). Water Uptake and Hydraulics of the Root Hair Rhizosphere. *Vadose Zone Journal*, *7*, 1027-1034. https://doi.org/10.2136/vzj2007.0122

Sequeira, C. H., & Alley, M. M. (2011). Soil Organic Matter Fractions as Indices of Soil Quality Changes. *Soil Science Society of America Journal*, *75*, 1766-1773. https://doi.org/10.2136/sssaj2011.0067

Shaheb, M. R., Venkatesh, R., & Shearer, S. A. (2021). A Review on the Effect of Soil Compaction and its Management for Sustainable Crop Production. *Journal of Biosystems Engineering*, *46*, 417-439. https://doi.org/10.1007/s42853-021-00117-7

Shao, Y., Bao, W., Chen, D., Eisenhauer, N., Zhang, W., Pang, X., Xu, G., & Fu, S. (2015). Using structural equation modeling to test established theory and develop novel hypotheses for the structuring forces in soil food webs. *Pedobiologia*, *58*, 137-145. https://doi.org/10.1016/j.pedobi.2015.06.001

Shen, J., Li, C., Mi, G., Li, L., Yuan, L., Jiang, R., & Zhang, F. (2013). Maximizing root/rhizosphere efficiency to improve crop productivity and nutrient use efficiency in intensive agriculture of China. *Journal of Experimental Botany*, *64*, 1181-1192. https://doi.org/10.1093/jxb/ers342

Shen, W., Jenerette, G. D., Hui, D., Phillips, R. P., & Ren, H. (2008). Effects of changing precipitation regimes on dryland soil respiration and C pool dynamics at rainfall event, seasonal and interannual scales. *Journal of Geophysical Research: Biogeosciences*, *113*, G03024. https://doi.org/10.1029/2008jg000685

Shi, X., Qin, T., Yan, D., Tian, F., & Wang, H. (2021). A meta-analysis on effects of root development on soil hydraulic properties. *Geoderma*, *403*, 115363. https://doi.org/10.1016/j.geoderma.2021.115363

Shi, Y., Zhang, L., Mu, Y., Ma, W., Kong, X., & Yang, C. (2024). Dynamic characteristics of soil pore structure and water-heat variations during freeze-thaw process. *Engineering Geology*, *343*, 107785. https://doi.org/10.1016/j.enggeo.2024.107785

Shipley, B. (2009). Confirmatory path analysis in a generalized multilevel context. *Ecology*, *90*, 363-368. https://doi.org/10.1890/08-1034.1

Siebert, J., Ciobanu, M., Schadler, M., & Eisenhauer, N. (2020). Climate change and land use induce functional shifts in soil nematode communities. *Oecologia*, *192*, 281-294. https://doi.org/10.1007/s00442-019-04560-4

Sieriebriennikov, B., Ferris, H., & de Goede, R. G. M. (2014). NINJA: An automated calculation system for nematode-based biological monitoring. *European Journal of Soil Biology*, *61*, 90-93. https://doi.org/10.1016/j.ejsobi.2014.02.004

Sierra, C. A., Ahrens, B., Bolinder, M. A., Braakhekke, M. C., von Fromm, S., Katterer, T., Luo, Z., Parvin, N., & Wang, G. (2024). Carbon sequestration in the subsoil and the time required to stabilize carbon

for climate change mitigation. *Global Change Biology*, *30*, e17153. https://doi.org/10.1111/gcb.17153

Singh, A., & Verdi, A. (2024). Estimating the soil water retention curve by the HYPROP-WP4C system, HYPROP-based PCNN-PTF and inverse modeling using HYDRUS-1D. *Journal of Hydrology*, *639*, 131657. https://doi.org/10.1016/j.jhydrol.2024.131657

Smith, A. P., Bond-Lamberty, B., Benscoter, B. W., Tfaily, M. M., Hinkle, C. R., Liu, C., & Bailey, V. L. (2017). Shifts in pore connectivity from precipitation versus groundwater rewetting increases soil carbon loss after drought. *Nature Communications*, *8*, 1335. https://doi.org/10.1038/s41467-017-01320-x

Smith, P., House, J. I., Bustamante, M., Sobocka, J., Harper, R., Pan, G., West, P. C., Clark, J. M., Adhya, T., Rumpel, C., Paustian, K., Kuikman, P., Cotrufo, M. F., Elliott, J. A., McDowell, R., Griffiths, R. I., Asakawa, S., Bondeau, A., Jain, A. K., . . . Pugh, T. A. (2016). Global change pressures on soils from land use and management. *Global Change Biology*, *22*, 1008-1028. https://doi.org/10.1111/gcb.13068

Soufan, R., Delaunay, Y., Gonod, L. V., Shor, L. M., Garnier, P., Otten, W., & Baveye, P. C. (2018). Pore-Scale Monitoring of the Effect of Microarchitecture on Fungal Growth in a Two-Dimensional Soil-Like Micromodel. *Frontiers in Environmental Science*, *6*, 68. https://doi.org/10.3389/fenvs.2018.00068

Spera, S. A., Galford, G. L., Coe, M. T., Macedo, M. N., & Mustard, J. F. (2016). Land-use change affects water recycling in Brazil's last agricultural frontier. *Global Change Biology*, *22*, 3405-3413. https://doi.org/10.1111/gcb.13298

Spinoni, J., Vogt, J. V., Naumann, G., Barbosa, P., & Dosio, A. (2017). Will drought events become more frequent and severe in Europe? *International Journal of Climatology*, *38*, 1718-1736. https://doi.org/10.1002/joc.5291

Stolze, K., Barnes, A. D., Eisenhauer, N., & Totsche, K. U. (2022). Depth-differentiated, multivariate control of biopore number under different land-use practices. *Geoderma*, *418*. https://doi.org/10.1016/j.geoderma.2022.115852

Strong, D. T., Wever, H. D., Merckx, R., & Recous, S. (2004). Spatial location of carbon decomposition in the soil pore system. *European Journal of Soil Science*, *55*, 739-750. https://doi.org/10.1111/j.1365-2389.2004.00639.x

Sun, H., Shen, Y., Yu, Q., Flerchinger, G. N., Zhang, Y., Liu, C., & Zhang, X. (2010). Effect of precipitation change on water balance and WUE of the winter wheat–summer maize rotation in the North China Plain. *Agricultural Water Management*, *97*, 1139-1145. https://doi.org/10.1016/j.agwat.2009.06.004

Sun, J., Liu, W., Pan, Q., Zhang, B., Lv, Y., Huang, J., & Han, X. (2022). Positive legacies of severe droughts in the Inner Mongolia grassland. *Science Advances*, *8*, eadd6249. https://doi.org/10.1126/sciadv.add6249

Sun, L., Wang, R., Li, J., Wang, Q., Lyu, W., Wang, X., Cheng, K., Mao, H., & Zhang, X. (2019). Reasonable fertilization improves the conservation tillage benefit for soil water use and yield of rain-fed winter wheat: A case study from the Loess Plateau, China. *Field Crops Research*, *242*, 107589. https://doi.org/10.1016/j.fcr.2019.107589

Sun, L., Wang, S., Zhang, Y., Li, J., Wang, X., Wang, R., Lyu, W., Chen, N., & Wang, Q. (2018). Conservation agriculture based on crop rotation and tillage in the semi-arid Loess Plateau, China: Effects on crop yield and soil water use. *Agriculture, Ecosystems & Environment*, *251*, 67-77. https://doi.org/10.1016/j.agee.2017.09.011

Sun, W., Zhou, S., Yu, B., Zhang, Y., Keenan, T., & Fu, B. (2025). Soil moisture-atmosphere interactions drive terrestrial carbon-water trade-offs. *Communications Earth & Environment*, *6*, 169. https://doi.org/10.1038/s43247-025-02145-z

Sünnemann, M., Alt, C., Kostin, J. E., Lochner, A., Reitz, T., Siebert, J., Schädler, M., & Eisenhauer, N. (2021). Low-intensity land-use enhances soil microbial activity, biomass and fungal-to-bacterial ratio in current and future climates. *Journal of Applied Ecology*, *58*, 2614-2625.

https://doi.org/10.1111/1365-2664.14004
Swindon, J. G., Burke, I. C., & Lauenroth, W. K. (2019). Seasonal Patterns of Root Production with Water and Nitrogen Additions Across Three Dryland Ecosystems. *Ecosystems*, *22*, 1664-1675. https://doi.org/10.1007/s10021-019-00364-y
Thorup-Kristensen, K., Halberg, N., Nicolaisen, M., Olesen, J. E., Crews, T. E., Hinsinger, P., Kirkegaard, J., Pierret, A., & Dresboll, D. B. (2020). Digging Deeper for Agricultural Resources, the Value of Deep Rooting. *Trends in Plant Science*, *25*, 406-417. https://doi.org/10.1016/j.tplants.2019.12.007
Tissink, M., Radolinski, J., Reinthaler, D., Venier, S., Potsch, E. M., Schaumberger, A., & Bahn, M. (2025). Individual Versus Combined Effects of Warming, Elevated CO_2 and Drought on Grassland Water Uptake and Fine Root Traits. *Plant Cell & Environment*, *48*, 2083-2098. https://doi.org/10.1111/pce.15274
Totsche, K. U., Ray, N., & Kögel-Knabner, I. (2024). Structure–function co-evolution during pedogenesis—Microaggregate development and turnover in soils. *Journal of Plant Nutrition and Soil Science*, *187*, 5-16. https://doi.org/10.1002/jpln.202400012
Tracy, S. R., Black, C. R., Roberts, J. A., Sturrock, C., Mairhofer, S., Craigon, J., & Mooney, S. J. (2012). Quantifying the impact of soil compaction on root system architecture in tomato (Solanum lycopersicum) by X-ray micro-computed tomography. *Annals of Botany*, *110*, 511-519. https://doi.org/10.1093/aob/mcs031
Tracy, S. R., Nagel, K. A., Postma, J. A., Fassbender, H., Wasson, A., & Watt, M. (2020). Crop Improvement from Phenotyping Roots: Highlights Reveal Expanding Opportunities. *Trends in Plant Science*, *25*, 105-118. https://doi.org/10.1016/j.tplants.2019.10.015
Trenberth, K. E. (2011). Changes in precipitation with climate change. *Climate Research*, *47*, 123-138. https://doi.org/10.3354/cr00953
Treonis, A. M., Sutton, K. A., Unangst, S. K., Wren, J. E., Dragan, E. S., & McQueen, J. P. (2019). Soil organic matter determines the distribution and abundance of nematodes on alluvial fans in Death Valley, California. *Ecosphere*, *10*, e02659. https://doi.org/10.1002/ecs2.2659
Tsiafouli, M. A., Thebault, E., Sgardelis, S. P., de Ruiter, P. C., van der Putten, W. H., Birkhofer, K., Hemerik, L., de Vries, F. T., Bardgett, R. D., Brady, M. V., Bjornlund, L., Jorgensen, H. B., Christensen, S., Hertefeldt, T. D., Hotes, S., Gera Hol, W. H., Frouz, J., Liiri, M., Mortimer, S. R., . . . Hedlund, K. (2015). Intensive agriculture reduces soil biodiversity across Europe. *Global Change Biology*, *21*, 973-985. https://doi.org/10.1111/gcb.12752
Turner, N. C. (2004). Agronomic options for improving rainfall-use efficiency of crops in dryland farming systems. *Journal of Experimental Botany*, *55*, 2413-2425. https://doi.org/10.1093/jxb/erh154
van Bommel, M., Arndt, K., Endress, M.-G., Dehghani, F., Wirsching, J., Blagodatskaya, E., Blagodatsky, S., Kandeler, E., Marhan, S., Poll, C., & Ruess, L. (2024). Under the lens: Carbon and energy channels in the soil micro-food web. *Soil Biology and Biochemistry*, *199*, 109575. https://doi.org/10.1016/j.soilbio.2024.109575
van den Hoogen, J., Geisen, S., Routh, D., Ferris, H., Traunspurger, W., Wardle, D. A., de Goede, R. G. M., Adams, B. J., Ahmad, W., Andriuzzi, W. S., Bardgett, R. D., Bonkowski, M., Campos-Herrera, R., Cares, J. E., Caruso, T., de Brito Caixeta, L., Chen, X., Costa, S. R., Creamer, R., . . . Crowther, T. W. (2019). Soil nematode abundance and functional group composition at a global scale. *Nature*, *572*, 194-198. https://doi.org/10.1038/s41586-019-1418-6
van der Bom, F. J. T., Williams, A., & Bell, M. J. (2020). Root architecture for improved resource capture: trade-offs in complex environments. *Journal of Experimental Botany*, *71*, 5752-5763. https://doi.org/10.1093/jxb/eraa324
van der Putten, W. H., Bardgett, R. D., Bever, J. D., Bezemer, T. M., Casper, B. B., Fukami, T., Kardol, P., Klironomos, J. N., Kulmatiski, A., Schweitzer, J. A., Suding, K. N., Van de Voorde, T. F. J., Wardle, D. A., & Hutchings, M. (2013). Plant–soil feedbacks: the past, the present and future challenges. *Journal of Ecology*, *101*, 265-276. https://doi.org/10.1111/1365-2745.12054
van der Putten, W. H., Bradford, M. A., Pernilla Brinkman, E., van de Voorde, T. F. J., Veen, G. F., & Bailey, J. K. (2016). Where, when and how plant–soil feedback matters in a changing world. *Functional*

Ecology, *30*, 1109-1121. https://doi.org/10.1111/1365-2435.12657

Van Sundert, K., Arfin Khan, M. A. S., Bharath, S., Buckley, Y. M., Caldeira, M. C., Donohue, I., Dubbert, M., Ebeling, A., Eisenhauer, N., Eskelinen, A., Finn, A., Gebauer, T., Haider, S., Hansart, A., Jentsch, A., Kubert, A., Nijs, I., Nock, C. A., Nogueira, C., . . . Vicca, S. (2021). Fertilized graminoids intensify negative drought effects on grassland productivity. *Global Change Biology*, *27*, 2441-2457. https://doi.org/10.1111/gcb.15583

van Veelen, A., Koebernick, N., Scotson, C. S., McKay-Fletcher, D., Huthwelker, T., Borca, C. N., Mosselmans, J. F. W., & Roose, T. (2020). Root-induced soil deformation influences Fe, S and P: rhizosphere chemistry investigated using synchrotron XRF and XANES. *New Phytologistt*, *225*, 1476-1490. https://doi.org/10.1111/nph.16242

Vargas, R., & Hattori, T. (1986). Protozoan Predation of Bacterial-Cells in Soil Aggregates. *Fems Microbiology Ecology*, *38*, 233-242. https://doi.org/10.1016/0378-1097(86)90031-5

Vaz, C. M. P., Manieri, J. M., de Maria, I. C., & Tuller, M. (2011). Modeling and correction of soil penetration resistance for varying soil water content. *Geoderma*, *166*, 92-101. https://doi.org/10.1016/j.geoderma.2011.07.016

Vereecken, H., Amelung, W., Bauke, S. L., Bogena, H., Brüggemann, N., Montzka, C., Vanderborght, J., Bechtold, M., Blöschl, G., Carminati, A., Javaux, M., Konings, A. G., Kusche, J., Neuweiler, I., Or, D., Steele-Dunne, S., Verhoef, A., Young, M., & Zhang, Y. (2022). Soil hydrology in the Earth system. *Nature Reviews Earth & Environment*, *3*, 573-587. https://doi.org/10.1038/s43017-022-00324-6

Vervoort, M. T., Vonk, J. A., Mooijman, P. J., Van den Elsen, S. J., Van Megen, H. H., Veenhuizen, P., Landeweert, R., Bakker, J., Mulder, C., & Helder, J. (2012). SSU ribosomal DNA-based monitoring of nematode assemblages reveals distinct seasonal fluctuations within evolutionary heterogeneous feeding guilds. *PLoS One*, *7*, e47555. https://doi.org/10.1371/journal.pone.0047555

Vicente-Serrano, S. M., Beguería, S., & López-Moreno, J. I. (2010). A Multiscalar Drought Index Sensitive to Global Warming: The Standardized Precipitation Evapotranspiration Index. *Journal of Climate*, *23*, 1696-1718. https://doi.org/10.1175/2009jcli2909.1

Vicente-Serrano, S. M., Domínguez-Castro, F., Beguería, S., El Kenawy, A., Gimeno-Sotelo, L., Franquesa, M., Azorin-Molina, C., Andres-Martin, M., & Halifa-Marín, A. (2025). Atmospheric drought indices in future projections. *Nature Water*, *3*, 374-387. https://doi.org/10.1038/s44221-025-00416-9

Vogel, H. J. (2008). A numerical experiment on pore size, pore connectivity, water retention, permeability, and solute transport using network models. *European Journal of Soil Science*, *51*, 99-105. https://doi.org/10.1046/j.1365-2389.2000.00275.x

Volaire, F. (2018). A unified framework of plant adaptive strategies to drought: Crossing scales and disciplines. *Global Change Biology*, *24*, 2929-2938. https://doi.org/10.1111/gcb.14062

von Haden, A. C., & Dornbush, M. E. (2014). Patterns of root decomposition in response to soil moisture best explain high soil organic carbon heterogeneity within a mesic, restored prairie. *Agriculture, Ecosystems & Environment*, *185*, 188-196. https://doi.org/10.1016/j.agee.2013.12.027

Vonk, J. A., Breure, A. M., & Mulder, C. (2013). Environmentally-driven dissimilarity of trait-based indices of nematodes under different agricultural management and soil types. *Agriculture, Ecosystems & Environment*, *179*, 133-138. https://doi.org/10.1016/j.agee.2013.08.007

Wagai, R., Kishimoto-Mo, A. W., Yonemura, S., Shirato, Y., Hiradate, S., & Yagasaki, Y. (2013). Linking temperature sensitivity of soil organic matter decomposition to its molecular structure, accessibility, and microbial physiology. *Global Change Biology*, *19*, 1114-1125. https://doi.org/10.1111/gcb.12112

Waldo, B. D., Shahoveisi, F., & Carroll, M. J. (2024). Long-term fertilization and cultivation impacts on nematode abundance and community structure in tall fescue turfgrass. *Ecology and Evolution*, *14*, e10905. https://doi.org/10.1002/ece3.10905

Wan, B., Hu, Z., Liu, T., Yang, Q., Li, D., Zhang, C., Chen, X., Hu, F., Kardol, P., Griffiths, B. S., & Liu, M. (2022b). Organic amendments increase the flow uniformity of energy across nematode food

webs. *Soil Biology and Biochemistry*, *170*, 108695. https://doi.org/10.1016/j.soilbio.2022.108695

Wan, B., Liu, T., Gong, X., Zhang, Y., Li, C., Chen, X., Hu, F., Griffiths, B. S., & Liu, M. (2022a). Energy flux across multitrophic levels drives ecosystem multifunctionality: Evidence from nematode food webs. *Soil Biology and Biochemistry*, *169*, 108656. https://doi.org/10.1016/j.soilbio.2022.108656

Wander, M. M., & Bidart, M. G. (2000). Tillage practice influences on the physical protection, bioavailability and composition of particulate organic matter. *Biology and Fertility of Soils*, *32*, 360-367. https://doi.org/10.1007/s003740000260

Wang-Erlandsson, L., Tobian, A., van der Ent, R. J., Fetzer, I., te Wierik, S., Porkka, M., Staal, A., Jaramillo, F., Dahlmann, H., Singh, C., Greve, P., Gerten, D., Keys, P. W., Gleeson, T., Cornell, S. E., Steffen, W., Bai, X., & Rockström, J. (2022). A planetary boundary for green water. *Nature Reviews Earth & Environment*, *3*, 380-392. https://doi.org/10.1038/s43017-022-00287-8

Wang, C., & Kuzyakov, Y. (2024). Soil organic matter priming: The pH effects. *Global Change Biology*, *30*, e17349. https://doi.org/10.1111/gcb.17349

Wang, J., Sun, J., Yu, Z., Li, Y., Tian, D., Wang, B., Li, Z., Niu, S., & Enquist, B. (2019e). Vegetation type controls root turnover in global grasslands. *Global Ecology and Biogeography*, *28*, 442-455. https://doi.org/10.1111/geb.12866

Wang, S., Fu, B. J., Gao, G. Y., Yao, X. L., & Zhou, J. (2012). Soil moisture and evapotranspiration of different land cover types in the Loess Plateau, China. *Hydrology and Earth System Sciences*, *16*, 2883-2892. https://doi.org/10.5194/hess-16-2883-2012

Wang, Y., Guo, D., Xu, J., Liu, Z., Wang, L., & Chen, C. (2025). Quantitatively analyzed root system architecture influence on root-soil mechanical interactions using 3D printing models. *Plant and Soil*, 1-18. https://doi.org/10.1007/s11104-025-07333-6

Wang, Y., Hu, W., Sun, H., Zhao, Y., Zhang, P., Li, Z., Zhou, Z., Tong, Y., Liu, S., Zhou, J., Huang, M., Jia, X., Clothier, B., Shao, M., Zhou, W., & An, Z. (2024b). Soil moisture decline in China's monsoon loess critical zone: More a result of land-use conversion than climate change. *Proceedings of the National Academy of Sciences*, *121*, e2322127121. https://doi.org/10.1073/pnas.2322127121

Wang, Z., Ma, L., Liu, X., Xue, Z., Wu, J., & Wen, X. (2024a). Grass (Poa annua L.) cover for eight years as an effective strategy for recovering soil moisture. *Geoderma*, *449*, 117010. https://doi.org/10.1016/j.geoderma.2024.117010

Wardle, D. A., Verhoef, H. A., & Clarholm, M. (2004). Trophic relationships in the soil microfood-web: predicting the responses to a changing global environment. *Global Change Biology*, *4*, 713-727. https://doi.org/10.1046/j.1365-2486.1998.00206.x

Warter, M. M., Singer, M. B., Cuthbert, M. O., Roberts, D., Caylor, K. K., Sabathier, R., & Stella, J. (2021). Drought onset and propagation into soil moisture and grassland vegetation responses during the 2012–2019 major drought in Southern California. *Hydrology and Earth System Sciences*, *25*, 3713-3729. https://doi.org/10.5194/hess-25-3713-2021

Weides, S. E., Hajek, T., Liancourt, P., Herberich, M. M., Kramp, R. E., Tomiolo, S., Pacheco-Riano, L. C., Tielborger, K., & Majekova, M. (2024). Belowground niche partitioning is maintained under extreme drought. *Ecology*, *105*, e4198. https://doi.org/10.1002/ecy.4198

Weller, U., Albrecht, L., Schlüter, S., & Vogel, H.-J. (2022). An open Soil Structure Library based on X-ray CT data. *Soil*, *8*, 507-515. https://doi.org/10.5194/soil-8-507-2022

Wendel, A. S., Bauke, S. L., Amelung, W., & Knief, C. (2022). Root-rhizosphere-soil interactions in biopores. *Plant and Soil*, *475*(1-2), 253-277. https://doi.org/10.1007/s11104-022-05406-4

White, R. G., & Kirkegaard, J. A. (2010). The distribution and abundance of wheat roots in a dense, structured subsoil--implications for water uptake. *Plant Cell & Environment*, *33*, 133-148. https://doi.org/10.1111/j.1365-3040.2009.02059.x

Whitmore, A. P., & Whalley, W. R. (2009). Physical effects of soil drying on roots and crop growth. *Journal of Experimental Botany*, *60*, 2845-2857. https://doi.org/10.1093/jxb/erp200

Wickham, H. (2011). ggplot2. *Wiley interdisciplinary reviews: computational statistics*, *3*, 180-185. https://doi.org/10.1002/wics.147

Wickham, H., Chang, W., & Wickham, M. H. (2016). Package 'ggplot2': An implementation of the

Grammar of Graphics. *Journal of Statistical Software*, *1*(2), 189.

Wiesel, L., Daniell, T. J., King, D., & Neilson, R. (2015). Determination of the optimal soil sample size to accurately characterise nematode communities in soil. *Soil Biology and Biochemistry*, *80*, 89-91. https://doi.org/10.1016/j.soilbio.2014.09.026

Wilcox, K. R., Shi, Z., Gherardi, L. A., Lemoine, N. P., Koerner, S. E., Hoover, D. L., Bork, E., Byrne, K. M., Cahill, J., Jr., Collins, S. L., Evans, S., Gilgen, A. K., Holub, P., Jiang, L., Knapp, A. K., LeCain, D., Liang, J., Garcia-Palacios, P., Penuelas, J., . . . Luo, Y. (2017). Asymmetric responses of primary productivity to precipitation extremes: A synthesis of grassland precipitation manipulation experiments. *Global Change Biology*, *23*, 4376-4385. https://doi.org/10.1111/gcb.13706

Witzgall, K., Steiner, F. A., Hesse, B. D., Riveras-Muñoz, N., Rodríguez, V., Teixeira, P. P. C., Li, M., Oses, R., Seguel, O., Seitz, S., Wagner, D., Scholten, T., Buegger, F., Angst, G., & Mueller, C. W. (2024). Living and decaying roots as regulators of soil aggregation and organic matter formation—from the rhizosphere to the detritusphere. *Soil Biology and Biochemistry*, *197*, 109503. https://doi.org/10.1016/j.soilbio.2024.109503

Wong, K. M., Griffiths, M., Moran, A., Johnston, A., Liu, A. E., Sellers, M. A., & Topp, C. N. (2023). Cover crop cultivars and species differ in root traits potentially impacting their selection for ecosystem services. *Plant and Soil*, *500*, 279-296. https://doi.org/10.1007/s11104-023-06431-7

Wu, J., Joergensen, R. G., Pommerening, B., Chaussod, R., & Brookes, P. C. (1990). Measurement of Soil Microbial Biomass C by Fumigation Extraction - an Automated Procedure. *Soil Biology & Biochemistry*, *22*, 1167-1169. https://doi.org/10.1016/0038-0717(90)90046-3

Wu, T. Y., Wichern, F., Wiesmeier, M., Buegger, F., Shi, L. L., Dippold, M. A., Höschen, C., & Mueller, C. W. (2024). Organic carbon loading of soils determines the fate of added fresh plant-derived organic matter. *Geoderma*, *443*, 116816. https://doi.org/10.1016/j.geoderma.2024.116816

Wu, X., Liu, H., Li, X., Ciais, P., Babst, F., Guo, W., Zhang, C., Magliulo, V., Pavelka, M., Liu, S., Huang, Y., Wang, P., Shi, C., & Ma, Y. (2018). Differentiating drought legacy effects on vegetation growth over the temperate Northern Hemisphere. *Global Change Biology*, *24*, 504-516. https://doi.org/10.1111/gcb.13920

Wu, Z., Behzad, H. M., He, Q., Wu, C., Bai, Y., & Jiang, Y. (2021). Seasonal transpiration dynamics of evergreen Ligustrum lucidum linked with water source and water-use strategy in a limestone karst area, southwest China. *Journal of Hydrology*, *597*, 126199. https://doi.org/10.1016/j.jhydrol.2021.126199

Wunsch, A., Liesch, T., & Broda, S. (2022). Deep learning shows declining groundwater levels in Germany until 2100 due to climate change. *Nature Communications*, *13*, 1221. https://doi.org/10.1038/s41467-022-28770-2

Xie, N., An, T., Liang, X., Schaeffer, S., Sun, L., Fu, S., & Wang, J. (2024b). Interaction between maize residues and initial soil carbon status on soil labile organic carbon pools. *Applied Soil Ecology*, *202*, 105482. https://doi.org/10.1016/j.apsoil.2024.105482

Xiong, D., Wei, C., Wubs, E. R. J., Veen, G. F., Liang, W., Wang, X., Li, Q., Van der Putten, W. H., Han, X., & Ordonez, A. (2019a). Nonlinear responses of soil nematode community composition to increasing aridity. *Global Ecology and Biogeography*, *29*, 117-126. https://doi.org/10.1111/geb.13013

Xiong, M., Sun, R., & Chen, L. (2019b). A global comparison of soil erosion associated with land use and climate type. *Geoderma*, *343*, 31-39. https://doi.org/10.1016/j.geoderma.2019.02.013

Xiong, P., Zhang, Z., Guo, Z., & Peng, X. (2022b). Macropores in a compacted soil impact maize growth at the seedling stage: Effects of pore diameter and density. *Soil and Tillage Research*, *220*, 105370. https://doi.org/10.1016/j.still.2022.105370

Xiong, P., Zhang, Z., & Peng, X. (2022a). Root and root-derived biopore interactions in soils: A review. *Journal of Plant Nutrition and Soil Science*, *185*, 643-655. https://doi.org/10.1002/jpln.202200003

Xu, M., & Shang, H. (2016). Contribution of soil respiration to the global carbon equation. *Journal of Plant Physiology*, *203*, 16-28. https://doi.org/10.1016/j.jplph.2016.08.007

Yaffar, D., Lugli, L. F., Wong, M. Y., Norby, R. J., Addo-Danso, S. D., Arnaud, M., Cordeiro, A. L.,

Dietterich, L. H., Diaz-Toribio, M. H., Lee, M. Y., Ghimire, O. P., Smith-Martin, C. M., Toro, L., Andersen, K., McCulloch, L. A., Meier, I. C., Powers, J. S., Sanchez-Julia, M., Soper, F. M., & Cusack, D. F. (2024). Tropical root responses to global changes: A synthesis. *Global Change Biology*, *30*, e17420. https://doi.org/10.1111/gcb.17420

Yan, D., Yan, D., Song, X., Yu, Z., Peng, D., Ting, X., & Weng, B. (2018). Community structure of soil nematodes under different drought conditions. *Geoderma*, *325*, 110-116. https://doi.org/10.1016/j.geoderma.2018.03.028

Yang, Q., Fan, J., & Luo, Z. (2024b). Response of soil moisture and vegetation growth to precipitation under different land uses in the Northern Loess Plateau, China. *Catena*, *236*, 107728. https://doi.org/10.1016/j.catena.2023.107728

Yang, Y., Tilman, D., Jin, Z., Smith, P., Barrett, C. B., Zhu, Y. G., Burney, J., D'Odorico, P., Fantke, P., Fargione, J., Finlay, J. C., Rulli, M. C., Sloat, L., Jan van Groenigen, K., West, P. C., Ziska, L., Michalak, A. M., Clim-Ag, T., Lobell, D. B., . . . Zhuang, M. (2024a). Climate change exacerbates the environmental impacts of agriculture. *Science*, *385*, eadn3747. https://doi.org/10.1126/science.adn3747

Yeates, G. W. (2003). Nematodes as soil indicators: functional and biodiversity aspects. *Biology and Fertility of Soils*, *37*, 199-210. https://doi.org/10.1007/s00374-003-0586-5

Yeates, G. W., Bongers, T., De Goede, R. G., Freckman, D. W., & Georgieva, S. S. (1993). Feeding habits in soil nematode families and genera-an outline for soil ecologists. *Journal of Nematology*, *25*, 315-331. https://www.ncbi.nlm.nih.gov/pubmed/19279775

Yin, H., Li, Y., Xiao, J., Xu, Z., Cheng, X., & Liu, Q. (2013). Enhanced root exudation stimulates soil nitrogen transformations in a subalpine coniferous forest under experimental warming. *Global Change Biology*, *19*, 2158-2167. https://doi.org/10.1111/gcb.12161

Yoshimura, C., Gessner, M. O., Tockner, K., & Furumai, H. (2008). Chemical properties, microbial respiration, and decomposition of coarse and fine particulate organic matter. *Journal of the North American Benthological Society*, *27*, 664-673. https://doi.org/10.1899/07-106.1

Young, I. M., & Crawford, J. W. (2004). Interactions and self-organization in the soil-microbe complex. *Science*, *304*, 1634-1637. https://doi.org/10.1126/science.1097394

Yu, L., Leng, G., Tang, Q., Lu, C., Gao, Y., Yao, L., Fan, S., Dong, J., Tu, H., Ai, Z., & Liao, X. (2025). Land-atmosphere interactions mitigate the direct surface-drying effects of land use and cover change. *One Earth*, *8*, 101210. https://doi.org/10.1016/j.oneear.2025.101210

Yu, X., Qi, D., Zhou, H., & Lu, S. (2024a). Variation of soil pore structure and predication of the related functions following land-use conversion identified by multi-scale X-ray tomography. *Land Degradation & Development*, *35*, 4875-4886. https://doi.org/10.1002/ldr.5264

Yvan, C., Stéphane, S., Stéphane, C., Pierre, B., Guy, R., & Hubert, B. (2012). Role of earthworms in regenerating soil structure after compaction in reduced tillage systems. *Soil Biology and Biochemistry*, *55*, 93-103. https://doi.org/10.1016/j.soilbio.2012.06.013

Zeleke, K. T., & Wade, L. J. (2012). Evapotranspiration Estimation Using Soil Water Balance, Weather and Crop Data. In A. Irmak (Ed.), *Evapotranspiration – Remote Sensing and Modeling*. InTech. https://doi.org/https://doi.org/10.5772/17489

Zeng, Z., Wu, W., Ge, Q., Li, Z., Wang, X., Zhou, Y., Zhang, Z., Li, Y., Huang, H., Liu, G., & Peñuelas, J. (2021). Legacy effects of spring phenology on vegetation growth under preseason meteorological drought in the Northern Hemisphere. *Agricultural and Forest Meteorology*, *310*, 108630. https://doi.org/10.1016/j.agrformet.2021.108630

Zhalnina, K., Louie, K. B., Hao, Z., Mansoori, N., da Rocha, U. N., Shi, S., Cho, H., Karaoz, U., Loque, D., Bowen, B. P., Firestone, M. K., Northen, T. R., & Brodie, E. L. (2018). Dynamic root exudate chemistry and microbial substrate preferences drive patterns in rhizosphere microbial community assembly. *Nature Microbiology*, *3*, 470-480. https://doi.org/10.1038/s41564-018-0129-3

Zhang, G., Zhang, Y., Zhao, D., Liu, S., Wen, X., Han, J., & Liao, Y. (2023). Quantifying the impacts of agricultural management practices on the water use efficiency for sustainable production in the Loess Plateau region: A meta-analysis. *Field Crops Research*, *291*, 108787.

https://doi.org/10.1016/j.fcr.2022.108787

Zhang, W., Munkholm, L. J., Heck, R. J., Watts, C. W., & Jensen, J. L. (2025). Aggregate pore and shape properties were more strongly correlated to soil organic carbon in large aggregates: Evidence from a long-term management-induced soil carbon gradient. *Geoderma*, *459*, 117357. https://doi.org/10.1016/j.geoderma.2025.117357

Zhang, Z.-y., Zhang, X.-k., Jhao, J.-s., Zhang, X.-p., & Liang, W.-j. (2015). Tillage and rotation effects on community composition and metabolic footprints of soil nematodes in a black soil. *European Journal of Soil Biology*, *66*, 40-48. https://doi.org/10.1016/j.ejsobi.2014.11.006

Zhao, C., Jia, X., Zhu, Y., & Shao, M. a. (2017b). Long-term temporal variations of soil water content under different vegetation types in the Loess Plateau, China. *Catena*, *158*, 55-62. https://doi.org/10.1016/j.catena.2017.06.006

Zhao, D., Xu, M. X., Liu, G. B., Ma, L. Y., Zhang, S. M., Xiao, T. Q., & Peng, G. Y. (2017a). Effect of vegetation type on microstructure of soil aggregates on the Loess Plateau, China. *Agriculture Ecosystems & Environment*, *242*, 1-8. https://doi.org/10.1016/j.agee.2017.03.014

Zhao, Q., Freschet, G. T., Tao, T., Smith, G. R., Wang, P., Hu, L., Ma, M., Johnson, D., Crowther, T. W., & Hu, S. (2024). Resolving the Intricate Effects of Multiple Global Change Drivers on Root Litter Decomposition. *Global Change Biology*, *30*, e17547. https://doi.org/10.1111/gcb.17547

Zheng, L., Wu, S., Lu, L., Li, T., Liu, Z., Li, X., & Li, H. (2023). Unraveling the interaction effects of soil temperature and moisture on soil nematode community: A laboratory study. *European Journal of Soil Biology*, *118*, 103537. https://doi.org/10.1016/j.ejsobi.2023.103537

Zheng, Z.-M., Yu, G.-R., Fu, Y.-L., Wang, Y.-S., Sun, X.-M., & Wang, Y.-H. (2009). Temperature sensitivity of soil respiration is affected by prevailing climatic conditions and soil organic carbon content: A trans-China based case study. *Soil Biology and Biochemistry*, *41*, 1531-1540. https://doi.org/10.1016/j.soilbio.2009.04.013

Zhou, J., Wu, J., Huang, J., Sheng, X., Dou, X., & Lu, M. (2022). A synthesis of soil nematode responses to global change factors. *Soil Biology and Biochemistry*, *165*, 108538. https://doi.org/10.1016/j.soilbio.2021.108538

Zuo, F.-L., Li, X.-Y., Yang, X.-F., Ma, Y.-J., Shi, F.-Z., Liao, Q.-W., Li, D.-S., Wang, Y., & Wang, R.-D. (2021). Linking root traits and soil moisture redistribution under Achnatherum splendens using electrical resistivity tomography and dye experiments. *Geoderma*, *386*, 114908. https://doi.org/10.1016/j.geoderma.2020.114908

Zuo, Q., Shi, J., Li, Y., & Zhang, R. (2006). Root length density and water uptake distributions of winter wheat under sub-irrigation. *Plant and Soil*, *285*, 45-55. https://doi.org/10.1007/s11104-005-4827-2

Zuo, Y., Wang, K., Dou, Z., Wang, N., Liu, T., & Lu, Q. (2020). A review of soil nematodes as biological indicators for the assessment of soil health. *Frontiers of Agricultural Science and Engineering*, *7*, 275-281. https://doi.org/10.15302/j-fase-2020327

Zwicke, M., Picon-Cochard, C., Morvan-Bertrand, A., Prud'homme, M. P., & Volaire, F. (2015). What functional strategies drive drought survival and recovery of perennial species from upland grassland? *Annals of Botany*, *116*, 1001-1015. https://doi.org/10.1093/aob/mcv037

List of publications

Submitted:

Mengqi Wu, Maxime Phalempin, Thomas Reitz, Evgenia Blagodatskaya, Steffen Schlüter. Links between soil microstructure dynamics and carbon cycling in response to land use and climate change (Soil biology & Biochemistry, under review).

Mengqi Wu, Christiane Roscher, Martin Schädler, Mika Tarkka, Doris Vetterlein, Steffen Schlüter. Legacy effects of climate extremes on deep soil water storage and water use efficiency across different land-use systems (Communications Earth & Environment, under review).

Xiaoli Yang, Martin Schädler, Nico Eisenhauer, Steffen Schlüter, **Mengqi Wu**, Evgenia Blagodatskaya, Xiangtai Wang. Trait-based responses of soil nematode communities to land use and climate change (Journal of Applied Ecology, under review)

Accepted:

Wu, M.[#], Yang, X.[#], Reitz, T., Blagodatskaya, E., Eisenhauer, N., Schädler, M., & Schlüter, S. (2025). Microhabitat properties explain variations in soil nematode communities across climate conditions in cropland, but not in grassland. ***Soil Biology and Biochemistry***, 201, 109657.

Schlüter, S., **Wu, M.**, Phalempin, M., Philipp, L., Blagodatskaya, E., Reitz, T., ... & Merbach, I. (2025). Divergence in physical, chemical, and biological soil properties caused by different long-term bare fallow management and natural succession. ***Geoderma***, *459*, 11736.

Curriculum vitae

Mengqi Wu

EDUCATION BACKGROUND

- **Helmholtz Centre for Environment Research - UFZ** Aug 2022 – Dec 2025
  Department of Soil System Science Halle, Germany
- **China Agricultural University** Sep 2020 – Jun 2022
  Department of Plant Nutrition Beijing, China
- **Yangtze University** Sep 2016 – Jun 2020
  Department of Agricultural Resources and Environment Jingzhou, Hubei, China

PROFESSIONAL EXPERIENCE

- **Doctoral Candidate** Aug 2022 – Jul 2025
  Supervised by Steffen Schlüter, Mika Tarkka, and Doris Vetterlein, funded by UFZ
  Project: Impact of land use and water regime on root-soil interactions as mediated through plant communities, the project 3 in GLIMPSE program "*Global change impacts on microbiota-plant-soil processes relevant for water and matter cycling in agricultural ecosystems*"
- **Master of Agriculture** Sep 2020 – Jun 2022
  Supervised by Kemo Jin and Jianbo Shen, in China Agricultural University
  Project: The mechanism of rhizosphere pore structure regulated by root-secreted organic acids affecting phosphorus uptake of maize under soil compaction in Rhizobiont program
- **Internship** Mar 2019 – Sep 2019
  Supervised by Jia Liu, in Jiangxi Academy of Agricultural Sciences
  Project: Effect of biogas residue used as substrate for seedlings, a province-level project
- **Bachelor of Agriculture** Sep 2017 – Nov 2018
  Supervised by Yanli Li, in Yangtze University
  Project: Hyperspectral monitoring of wheat growth parameters under water stress, a university-level project

Date: Signature:

Acknowledgement

How time flies! It feels like just yesterday that I was packing my bags and preparing to begin my doctoral journey in Germany. Arriving alone in a foreign country, I was full of curiosity but also somewhat naive, facing language barriers, unfamiliar food and customs, and a challenging research topic that brought one surprise and trouble after another. At that time, I could hardly have imagined completing my PhD project and the writing of dissertation within three years. Yet, through perseverance and with the support of many, I have come this far. This doctoral journey would not have been possible without the encouragement, support, and guidance of many individuals and institutions to whom I am deeply grateful.

First and foremost, I would like to express my sincere and heartfelt gratitude to my supervisor, Dr. Steffen Schlüter. Thank you for giving me the chance as your PhD student at UFZ and for your continuous guidance, constructive criticism, and unwavering support throughout every stage of this period. I feel very lucky to be your PhD student and I enjoyed the discussion and solving the problems with you. Your scientific expertise, insightful and timely feedback, and thoughtful encouragement have not only shaped this dissertation but also profoundly influenced my development as an independent researcher. I am equally grateful to my co-supervisors Prof. Doris Vetterlein and Prof. Mika Tarkka and all co-authors Xiaoli Yang, Maxime Phalempin, Thomas Reitz, Evgenia Blagodatskaya, Christiane Roscher, Martin Schädler, and Nico Eisenhauer for their critical contributions, methodological advice, and generous mentorship, which enriched the quality and depth of this work.

I would like to acknowledge Department of Soil System Science department for providing the necessary resources, facilities, a stimulating academic environment, and supporting me to join international conferences. I am grateful to all my colleagues for providing me with a friendly work environment, especially colleagues Lucas Kanagarajah, Asha Nambiar Puthussseri Valiyaveettil, Sophie Wachter, Mathew-John Mancha, Abebaw Misganaw Ambaw, Veronic Topfer, Eva Lippold, Sara Konig, Julius Ansorge, Judith Rüschhoff, Susanne Schreiter, Ulrich Weller, Hans-Jorg Vogel and previous colleagues Maik Lucas and Sebastian Blaser. Moreover, I acknowledge the support of the technical staff, especially Ralf Gründling, Max Koehne, and Eric Braatz, for

their invaluable support in fieldwork and laboratory analyses. This research was conducted within the framework of the Global Change Experimental Facility (GCEF), and I extend my gratitude to the entire GCEF management team and the staff of the Bad Laushstädt for maintaining the experimental infrastructure and providing logistical support. I also acknowledge the support of Higrade and HIAD for supporting the course of statistical analysis and data management.

During the period when I first arrived in Germany, everything was very strange and unfamiliar. Thanks for Guoting Shen, Xiaoli Yang, Qijun Yang, Shiyue Yang, Qun Liu, Negar Ghaderi Golezani, Fathmeh Dehghani, Maria Martin Roldan for helping me quickly familiarize the work and life in Halle. Most importantly, I would like to thank my father Shuquan Wu, mother Meixiang Yue, grandma Lianying Wang, and my brother Zhengming Wu for their patience, trust, and support. Thank you Jianhao Wei for your presence, company, love, understanding and support. Your encouragement has brought me joy, comfort and new perspectives on life. Lastly, I would like to thank myself, who learnt to try to remain calm in the face if difficulties and consistently endeavored to solve all the problems in study and life.

To everyone who has been a part of this academic journey, whether mentioned here or not, thank you for your contributions, big or small. Your impact is deeply appreciated and will forever be a part of this achievement.

Eidesstattliche Erklärung / *Declaration under Oath*

Ich erkläre an Eides statt, dass ich die Arbeit selbstständig und ohne fremde Hilfe verfasst, keine anderen als die von mir angegebenen Quellen und Hilfsmittel benutzt und die den benutzten Werken wörtlich oder inhaltlich entnommenen Stellen als solche kenntlich gemacht habe.
I declare under penalty of perjury that this thesis is my own work entirely and has been written without any help from other people. I used only the sources mentioned and included all the citations correctly both in word or content.

_____ _____

Datum / Date Unterschrift des Antragstellers / *Signature of the applicant*